PLAXIS 2D 2025.1

Materials Models Manual



Last Updated: September 24, 2025



UNDERSTAND THE UNDERGROUND

Table of Contents

1 lı	ntroduction	7
	1.1 Material Models and Licencing levels	7
	1.2 On the use of different models	
	1.3 Limitations	11
2 F	Preliminaries on material modelling	14
	2.1 General definitions of stress	
	2.2 General definitions of strain	
	2.3 Elastic strains	
	2.4 Undrained effective stress analysis (effective stiffness parameters)	
	2.4.1 Skempton B-parameter	
	2.4.2 Biot pore pressure coefficient α_{Biot} [ULT]	
	2.5 Undrained effective stress analysis with effective strength parameters (Undrained	
	A)	
	2.6 Undrained effective stress analysis with undrained strength parameters	
	(Undrained B)	25
	2.7 Undrained total stress analysis with undrained parameters (Undrained C)	
	2.8 The initial pre-consolidation stress in advanced models	
	2.9 On the initial stresses	29
3 I	inear Elastic Perfectly Plastic Model (Mohr-Coulomb	
	Model)	21
•	3.1 Linear Elastic Perfectly - Plastic behaviour	
	3.2 Formulation of the Mohr-Coulomb model	
	3.3 Parameters of the Mohr-Coulomb model	
	3.4 Depth-dependency	
	3.5 On the use of the Mohr-Coulomb model in dynamics calculations [ULT]	
4 -	The Hoek-Brown model (rock behaviour)	42
	4.1 Formulation of the Hoek-Brown model	
	4.2 Conversion of Hoek-Brown to Mohr-Coulomb	
	4.3 Parameters of the Hoek-Brown model	
	4.4 On the use of the Hoek-Brown model in dynamics calculations	
	·	
5 7	The Jointed Rock model (anisotropy)	51
J		
	5.1 Anisotropic elastic material stiffness matrix	
	5.3 Parameters of the Jointed Rock model	
	5.4 On the use of the Jointed Rock model in dynamics calculations	
	5.7 On the use of the confice flock model in dynamics calculations	00
6 7	The Hardening Sail model (Isotropic bardening)	65
O	The Hardening Soil model (Isotropic hardening)	
	6.1 Hyperbolic relationship for standard drained triaxial test	
	6.2 Approximation of hyperbola by the Hardening Soil model	თშ

	6.3 Plastic volumetric strain for triaxial states of stress	69
	6.4 Parameters of the Hardening Soil Model	
	6.5 On the cap yield surface in the Hardening Soil model	
	6.6 State parameters in the Hardening Soil model	
	6.7 On the use of the Hardening Soil model in dynamics calculations	79
7 T	he Hardening Soil model with small-strain stiffness	
(HSsmall)	
	7.1 Describing small-strain stiffness with a Simple Hyperbolic Law	81
	7.2 Applying the Hardin-Drnevich relationship in the HS Model	
	7.3 Virgin (initial) loading vs unloading/reloading	
	7.4 Model Parameters	
	7.5 On the parameters G_0 and $\gamma_{0.7}$	
	7.6 Model Initialisation	
	7.8 On the use of the Hardening Soil model with small-strain stiffness in dynamics	90
	calculations	91
	7.9 Other differences to the Hardening Soil model	91
0 N	Andified Com Clay model	02
O IV	Modified Cam-Clay model	
	8.1 Formulation of the Modified Cam-Clay model	
	8.3 State parameters in the Modified Cam-Clay model	
	8.4 On the use of the Modified Cam-Clay model in dynamics calculations	
	8.5 Warning	
αт	he NGI-ADP model (anisotropic undrained shear strength)	97
J I	9.1 Formulation of the NGI-ADP model	
	9.1.1 1D model presentation	
	9.1.2 The NGI-ADP model in plane strain	
	9.1.3 The NGI-ADP model in 3D stress space	
	9.1.4 The NGI-ADP model traction criterion for interfaces in 2D	102
	9.2 Parameters of the NGI-ADP model	
	9.3 State parameters in the NGI-ADP model	106
10	The Soft soil model [ADV]	.108
	10.1 Isotropic states of stress and strain ($\sigma'_1 = \sigma'_2 = \sigma'_3$)	
	10.2 Yield function	
	10.3 Parameters of the Soft Soil model	112
	10.4 State parameters in the Soft Soil model	116
	10.5 On the use of the Soft Soil model in dynamics calculations	116
11 5	Soft Soil Creep model (time dependent behaviour) [ADV]	117
	•	
	11.1 Introduction	117
	11.1 Introduction	
	11.2 Basics of one-dimensional creep	118
		118 119
	11.2 Basics of one-dimensional creep	118 119 121 123
	11.2 Basics of one-dimensional creep	118 119 121 123

	11.8 Parameters of the Soft Soil Creep model	126
	11.9 State parameters in the Soft Soil Creep model	
	11.10 On the use of the Soft Soil Creep model in dynamics calculations	130
	11.11 On the use of the Soft Soil Creep model in practical applications	
12	The Sekiguchi-Ohta model [ADV]	132
	12.1 Formulation of the Sekiguchi-Ohta model	
	12.1.1 Isotropic states of stress and strain ($\sigma'_1 = \sigma'_2 = \sigma'_3$)	
	12.1.2 Inviscid (time-independent) formulation	
	12.1.3 Viscid (time-dependent) formulation	
	12.2 Parameters of the Sekiguchi-Ohta model	
	12.2.1 Model parameters of the inviscid model	
	12.2.2 Model parameters of the viscid model	137
	12.3 State parameters in the Sekiguchi-Ohta model	138
13	The UDCAM-S model [ADV]	140
	13.1 Parameters of the UDCAM-S model	
	13.2 State parameters in the UDCAM-S model	
	13.3 On the use of the UDCAM-S model in dynamics calculations	
14	The Concrete model [ADV]	146
	14.1 Formulation of the Concrete model	
	14.2 Strain hardening and softening	
	14.2.1 Compression	
	14.2.2 Tension	
	14.3 Time-dependency of the Concrete model	
	14.3.1 Strength and Stiffness	
	14.3.2 Plastic Deformability	152
	14.3.3 Fracture energy	
	14.3.4 Viscoelastic Creep	
	14.3.5 Shrinkage	
	14.4 Parameters of the Concrete model	
	14.4.1 Recommended values for the parameters of the Concrete model	
	14.4.2 Summary of recommended parameters for Concrete model	
	14.5 State parameters in the Concrete model	
	14.6 On the use of the Concrete model in dynamics calculations 14.7 Warning	
45	TI UDOOD DIM I I []	400
15	The UBC3D-PLM model [ULT]	
	15.1 Elasto-plastic behaviour and hardening rule	
	15.2 Flow rule	
	15.3 Load state during liquefaction	
	15.4 Post-liquefaction rule and cyclic mobility	168
	15.5 Parameters of the UBC3D-PLM model	
	15.6 State parameters in the UBC3D-PLM model	
10	Hear defined eath medals [ADV/1/[HT] - [OCT]	470
10	User-defined soil models [ADV]/[ULT] + [GSE]	
	16.1 Introduction	
	16.2 Implementation of User Defined (UD) soil Models in calculations program	
	16.2.1 Main Functionalities UD Models	I/ /

16.2.2 Using predefined subroutines from the source code	183
16.2.3 Definition of user-interface functions	
16.2.4 UDSM additional information	185
16.2.5 Compiling the user subroutine	186
16.2.6 Debugging possibilities	
16.3 Input of UD model parameters via user-interface	187
17 Application of advanced soil models	190
17.1 Hardening Soil model: Response in drained and undrained triaxial tests	
17.1 Hardening Soil Hodel. Response in drained and drid affect triaxial tests	
17.2.1 Triaxial Test	
17.2.2 Oedometer test	
17.2.3 Pressiometer test	
17.2.4 Conclusions of the Application of the Hardening Soil model on real soi tests	
17.3 Application of the Hardening Soil model with small-strain stiffness on real soil tests	
17.4 Soft Soil Creep model : Undrained triaxial tests at different loading rates	
17.4 Soft Soil Creep model: Response in one-dimensional compression test	
17.6 Soft Soil model: Response in isotropic compression test	
17.7 Hardening Soil model and Hardening Soil model with small-strain stiffness:	
Excavation in Berlin sand	21/
18 Structural Behaviour	. 220
18.1 Anchors	220
18.2 2D Geogrids	220
18.3 2D plates	
18.4 2D Embedded beams	224
19 Hydraulic Models	228
19.1 Van Genuchten model	
19.2 Approximate Van Genuchten model	
20 References	234
20 1(010101000	. 20-
21 Appendices	240
A Symbols	
A.1 General symbols	241
A.2 Concrete Model symbols	
B Applicability of the material models	
B.1 Aplicability material models: Based on different materials	246
B.2 Aplicability material models: Based on different applications	
B.3 Aplicability material models: Based on different applications	24/
material	249
	270
C Modelling of embedded structures	
right of chinenter and alternication for the contraction of the contra	

C.1 Applicability of modelling techniques for embedded structures	251
D Fortran subroutines for User-defined soil models	
D.1 Subroutines	
D.Z Turicuoris	200
E Soil Models and License levels	
E.1 Overview Soil Models and Licese Levels	256

Introduction

The mechanical behaviour of soils and rocks may be modelled at various degrees of accuracy. Hooke's law of linear, isotropic elasticity, for example, may be thought of as the simplest available stress-strain relationship. As it involves only two input parameters, i.e. Young's modulus, *E*, and Poisson's ratio,v, it is generally too crude to capture essential features of soil and rock behaviour. The linear elastic perfectly plastic model (Mohr-Coulomb) may be considered as a first order approximation of soil or rock behaviour. However, PLAXIS includes more advanced material models involving specific features such as stress-dependency of stiffness, strain-hardening /softening, memory of pre-consolidation, critical state, anisotropy, creep, swelling and shrinkage. Users are encouraged to employ the advanced models in an attempt to simulate the behaviour of soils and rocks more realistically, thereby obtaining more accurate results from their PLAXIS calculations. The use of the *SoilTest* facility may help in calibrating the corresponding model parameters. An overview of the applicability of the material models is given in B Applicability of the material models (p. 246).

1.1 Material Models and Licencing levels

Soil/material models in PLAXIS 2D are offered for different licence levels (See <u>General Information Manual</u>). In this manual, soil models available for each licence level can be identified as follows:

- Material models with no identification generally available for PLAXIS 2D licence.
- [ADV] Material models available only for users with PLAXIS 2D/PLAXIS 3D Advanced licence.
- [ULT] Material models available only for users with PLAXIS 2D/PLAXIS 3D Ultimate licence.
- [GSE] Material models available only for users with Geotechnical SELECT subscription.

A compilation of the different soil models offered by PLAXIS 2D with their associated licence can be check in E Soil Models and License levels (p. 256).

1.2 On the use of different models

1.2.1 Linear Elastic model (LE)

The Linear Elastic model is based on Hooke's law of isotropic elasticity. It involves two basic elastic parameters, i.e. Young's modulus E and Poisson's ratio v. Although the Linear Elastic model is not suitable to model soil, it may be used to model stiff volumes in the soil, like concrete walls, or intact rock formations.

1.2.2 Mohr-Coulomb model (MC)

The linear elastic perfectly-plastic Mohr-Coulomb model involves five input parameters, i.e. E and v for soil elasticity: ω and c for soil plasticity and ψ as an angle of dilatancy. This Mohr-Coulomb model represents a 'first-order' approximation of soil or rock behaviour. It is recommended to use this model for a first analysis of the problem considered. For each layer one estimates a constant average stiffness or a stiffness that increases linearly with depth. Due to this constant stiffness, computations tend to be relatively fast and one obtains a first estimate of deformations.

1.2.3 Hoek-Brown model (HB)

The Hoek-Brown model is an isotropic elastic perfectly-plastic model for weathered rock based on the 2002 edition of the Hoek-Brown failure criterion. This non-linear stress-dependent criterion describes shear failure and tensile failure by a continuous function, and is familiar to most geologists and rock engineers. Besides the elastic parameters (E and ν), the model involves practical rock parameters such as the uni-axial compressive strength of the intact rock (σ_{ci}), the Geological Strength Index (GSI), and the disturbance factor (D).

1.2.4 Jointed Rock model (JR)

The Jointed Rock model is an anisotropic elastic-plastic model, especially meant to simulate the behaviour of rock layers involving stratification and particular fault directions. Plasticity can only occur in a maximum of three shear directions (shear planes). Each plane has its own strength parameters φ and c. The intact rock is considered to behave fully elastic with constant stiffness properties E and ν . Reduced elastic properties may be defined for the stratification direction.

1.2.5 Hardening Soil model (HS)

The Hardening Soil model is an advanced model for the simulation of soil behaviour. As for the Mohr-Coulomb model, limiting states of stress are described by means of the friction angle, φ , the cohesion, c, and the dilatancy angle, ψ . However, soil stiffness is described much more accurately by using three different input stiffnesses: the triaxial loading stiffness, E_{50} , the triaxial unloading stiffness, E_{ur} , and the oedometer loading stiffness, E_{oed} . As average values for various soil types, $E_{ur} pprox 3E_{50}$ and $E_{oed} pprox E_{50}$ are suggested as default settings, but both very soft and very stiff soils tend to give other ratios of E_{oed}/E_{50} , which can be entered by the user.

In contrast to the Mohr-Coulomb model, the Hardening Soil model also accounts for stressdependency of stiffness moduli. This means that all stiffnesses increase with pressure. Hence, all three input stiffnesses relate to a reference stress, usually taken as 100 kPa (1 bar).

Besides the model parameters mentioned above, initial soil conditions, such as preconsolidation, play an essential role in most soil deformation problems. This can be taken into account in the initial stress generation.

1.2.6 Hardening Soil model with small-strain stiffness (HSsmall)

The Hardening Soil model with small-strain stiffness (HSsmall) is a modification of the above Hardening Soil model that accounts for the increased stiffness of soils at small strains. At low strain levels most soils exhibit a higher stiffness than at engineering strain levels, and this stiffness varies non-linearly with strain. This behaviour is described in the HSsmall model using an additional strain-history parameter and two additional material parameters, i.e. G_0^{ref} and $\gamma_{0.7}$.

 G_0^{ref} is the small-strain shear modulus and $\gamma_{0.7}$ is the strain level at which the shear modulus has reduced to about 70% of the small-strain shear modulus. The advanced features of the HSsmall model are most apparent in working load conditions. Here, the model gives more reliable displacements than the HS model. When used in dynamic applications, the Hardening Soil model with small-strain stiffness also introduces hysteretic material damping.

1.2.7 Modified Cam-Clay model (MCC)

The Modified Cam-Clay model is a well known model from international soil modelling literature; see for example Muir Wood (1990). It is meant primarily for the modelling of near normallyconsolidated clay-type soils. This model has been added to PLAXIS to allow for a comparison with other codes.

1.2.8 NGI-ADP model

The NGI-ADP model is an anisotropic undrained shear strength model. The soil shear strength is defined by means of S_u values for active, passive and direct simple shear stress states. The model may be used for onshore and offshore applications in undrained clays and silts.

1.2.9 Soft Soil model (SS) - [ADV]

The Soft Soil model is a Cam-Clay type model especially meant for primary compression of near normally-consolidated clay-type soils. Although the modelling capabilities of this model are generally superseded by the Hardening Soil model, the Soft Soil model is better capable to model the compression behaviour of very soft soils.

1.2.10 Soft Soil Creep model (SSC) - [ADV]

The Hardening Soil model is generally suitable for all soils, but it does not account for viscous effects, i.e. creep and stress relaxation. In fact, all soils exhibit some creep and primary compression is thus followed by a certain amount of secondary compression.

The latter is most dominant in soft soils, i.e. normally consolidated clays, silts and peat, and PLAXIS thus implemented a model under the name Soft Soil Creep model. The Soft Soil Creep model has been developed primarily for application to settlement problems of foundations, embankments, etc. For unloading problems, as normally encountered in tunnelling and other excavation problems, the Soft Soil Creep model hardly supersedes the simple Mohr-Coulomb model. As for the Hardening Soil model, proper initial soil conditions are also essential when using the Soft Soil Creep model. This also includes data on the pre-consolidation stress, as the model accounts for the effect of overconsolidation. Note that the initial overconsolidation ratio also determines the initial creep rate.

1.2.11 Sekiguchi-Ohta model - [ADV]

The Sekiguchi-Ohta model is a Cam-Clay type of model with anisotropic yield contour defined by K_{nc}^0 . Two versions of the model exist: The inviscid model is a time independent model which has similarities with the Soft Soil model. The viscid model is time-dependent and has similarities with the Soft Soil Creep model. Both models have been developed in Japan. These models were previously available as user-defined models, but have become standard models in PLAXIS nowadays.

1.2.12 | UDCAM-S model - [ADV]

The Simplified UnDrained Cyclic Accumulation Model (UDCAM-S) is an advanced model to deal with undrained soil behaviour and degradation of the strength and stiffness in cyclic loading of clay or very low permeable silty soils. The UDCAM-S model is derived from the complex UDCAM model by NGI (Andersen & Jostad, 2009) with simplifications in order to be more suitable for engineering practice. The material model is based on the NGI-ADP model for the undrained behaviour of clays, implementing a pre-processing procedure called cyclic accumulation tool (See the Reference Manual - Chapter 6 - Cyclic accumulation and optimisation tool) to obtain the degraded parameter set based on the type of analysis the user has to perform.

1.2.13 Concrete model - [ADV]

The Concrete model is an advanced elastoplastic model for concrete and shotcrete structures. It simulates the time-dependent strength and stiffness of concrete, strain hardening-softening in compression and tension as well as creep and shrinkage. The failure criterion involves a Mohr-Coulomb yield surface for deviatoric loading, which is combined with a Rankine yield surface in the tensile regime. The Concrete model employs 25 input parameters, but most of them can be derived from standard uniaxial tensile and compression tests and are generally familiar to structural engineers.

1.2.14 UBC3D-PLM model - [ULT]

The UBC3D-PLM model is an advanced model for the simulation of liquefaction behaviour in dynamic applications. The UBC3D-PLM model employs two yield surfaces to guarantee a smooth transition near the mobilised friction angle. The UBC3D-PLM model uses the Mohr-Coulomb yield condition with an hardening law similar to the Hardening Soil model. For the secondary state, the UBC3D-PLM model incorporates a densification law through a second yield surface with a kinematic hardening rule based on the number of loading cycles. This correlation improves the precision of the evolution of the excess pore pressure.

The dynamic applications require a deep and extended investigation of the soil deposit. However, the UBC3D-PLM model implements a specific formulation with input parameters based on the most common tests: drained triaxial tests (CD TxC) or standard penetration tests (SPT).

1.2.15 Calibration of model parameters using the SoilTest facility - [GSE]

The SoilTest facility may be used to check the performance of material models and the chosen model parameters in well defined soil lab test conditions as well as in arbitrary stress-strain conditions. In this way, users can compare the model response with real lab test data and get a feel for the accuracy at which real soil behaviour is approximated by the model. Even if a perfect match is obtained, it is good to realise that using calibrated material models in practical applications (where conditions are different than in the lab) may still lead to differences between the finite element model and reality. Nevertheless, the use of the SoilTest facility can help in understanding the capabilities and limitations of the material model and the influence of the model parameters.

1.3 | Limitations

The PLAXIS code and its soil models have been developed to perform calculations of realistic geotechnical problems. In this respect PLAXIS can be considered as a geotechnical simulation tool. The soil models can be regarded as a qualitative representation of soil behaviour whereas the model parameters are used to quantify the soil characteristics. Although much care has been taken for the development of the PLAXIS code and its soil models, the simulation of reality remains an approximation, which implicitly involves some inevitable numerical and modelling errors. Moreover, the accuracy at which reality is approximated depends highly on the expertise of the user regarding the modelling of the problem, the understanding of the soil models and their limitations, the selection of model parameters, and the ability to judge the reliability of the computational results.

Some of the limitations in the currently available models are listed below:

1.3.1 Linear Elastic model

Linear Elastic model Soil behaviour is highly non-linear and irreversible. The linear elastic model is insufficient to capture the essential features of soil. The use of the linear elastic model may, however, be considered to model strong massive structures in the soil or bedrock layers. Stress states in the linear elastic model are not limited in any way, which means that the model shows infinite strength. Be careful using this model for materials that are loaded up to their material strength.

1.3.2 Mohr-Coulomb model

The linear elastic perfectly-plastic Mohr-Coulomb model is a first order model that includes only a limited number of features that soil behaviour shows in reality. Although the increase of stiffness with depth can be taken into account, the Mohr-Coulomb model does neither include stress-dependency nor stress-path dependency nor strain dependency of stiffness or anisotropic stiffness. In general, effective stress states at failure are quite well described using the Mohr-Coulomb failure criterion with effective strength parameters φ' and c'. For undrained materials, the Mohr-Coulomb model may be used with the friction angle φ set to 0° and the cohesion c set to $c_u(S_u)$, to enable a direct control of undrained shear strength. In that case note that the model does not automatically include the increase of shear strength with consolidation.

1.3.3 Hoek-Brown model

The Hoek-Brown model is an isotropic continuum model particularly meant to model weathered rock. Hence, the model is not suitable for stratified or jointed rock sections with a significant anisotropic stiffness or with one or more dominant sliding directions. For such behaviour, the Jointed Rock model is available.

1.3.4 Hardening Soil model

Although the Hardening Soil model can be regarded as an advanced soil model, there are a number of features of real soil behaviour the model does not include. It is a hardening model that does not account for softening due to soil dilatancy and de-bonding effects. In fact, it is an isotropic hardening model so that it models neither hysteretic and cyclic loading nor cyclic mobility. Moreover, the model does not distinguish between large stiffness at small strains and reduced stiffness at engineering strain levels. The user has to select the stiffness parameters in accordance with the dominant strain levels in the application. Last but not least, the use of the Hardening Soil model generally results in longer calculation times, since the material stiffness matrix is formed and decomposed in each calculation step.

1.3.5 | Hardening Soil model with small-strain stiffness

As the Hardening Soil model with small-strain stiffness (HSsmall) incorporates the loading history of the soil and a strain-dependent stiffness, it can, to some extent, be used to model cyclic loading. However, it does not incorporate a gradual softening during cyclic loading, so is not suitable for cyclic loading problems in which softening plays a role. In fact, just as in the Hardening Soil model, softening due to soil dilatancy and debonding effects are not taken into account. Moreover, the HSsmall does not incorporate the accumulation of irreversible volumetric straining nor liquefaction behaviour with cyclic loading. The use of the HSsmall will generally result in calculation times that are even longer than those of the Hardening Soil model.

1.3.6 Jointed Rock model

The Jointed Rock model is a first order anisotropic model that includes a limited number of features that rock behaviour shows in reality. Plasticity can only occur in a maximum of three shear directions (shear planes). Each plane has its own shear strength parameters φ_i and c_i and tensile strengtht_i. Hence, the maximum shear stress is linearly dependent on the normal stress, and not curved as in reality. The intact rock is considered to behave fully elastic with constant stiffness properties E and ν . Reduced elastic properties may be defined for the stratification direction. Note that failure is limited to the predefined shear plane directions. It is possible that realistic potential failure mechanisms are not captured by the model because of the elastic behaviour in any other direction than the three shear planes.

1.3.7 Modified Cam-Clay model

The same limitations (including those in the Soft Soil Creep model) hold in the Modified Cam-Clay model. Moreover, the Modified Cam-Clay model may allow for unrealistically high shear stresses. This is particularly the case for overconsolidated stress states where the stress path crosses the critical state line. Furthermore, the Modified Cam-Clay model may give softening behaviour for such stress paths. Without special regularization techniques, softening behaviour may lead to mesh dependency and convergence problems of iterative procedures. Moreover, the Modified Cam-Clay model cannot be used in combination with Safety analysis by means of phi-c reduction.

1.3.8 NGI-ADP model

The NGI-ADP model is an undrained shear strength model particularly meant to model undrained clays and silts. It can be used in a drained or effective stress analysis, but note that the shear strength is not automatically updated with changes of effective stresses. Also note that the NGI-ADP model does not include a tension cut-off.

1.3.9 Soft Soil model-[ADV]

The same limitations (including the ones for the Soft Soil Creep model) hold in the Soft Soil model. The utilization of the Soft Soil model should be limited to the situations that are dominated by compression. It is not recommended for use in excavation problems, since the model hardly supercedes the Mohr-Coulomb model in unloading problems.

1.3.10 Soft Soil Creep model-[ADV]

All above limitations also hold true for the Soft Soil Creep model. In addition this model tends to over-predict the range of elastic soil behaviour. This is especially the case for excavation problems, including tunnelling. Care must also be taken with the generation of initial stresses for normally consolidated soils. Although it would seem logical to use OCR = 1.0 for normally consolidated soils, such use would generally lead to an over-prediction of deformations in

problems where the stress level is dominated by the initial self-weight stresses. Therefore, for such problems it is recommended to use a slightly increased OCR-value to generate the initial stress state. In fact, in reality most soils tend to show a slightly increased pre-consolidation stress in comparison with the initial effective stress. Before starting an analysis with external loading it is suggested to perform a single calculation phase with a short time interval and without loading to verify the surface settlement rate based on common practice.

1.3.11 UDCAM-S model-[ADV]

The UDCAM-S model is an undrained shear strength model particularly meant to model undrained clays and silts under design storms. It can be used in a drained or effective stress analysis, but note that the shear strength is not automatically updated with changes of effective stress. Also note that the NGI-ADP model does not include a tension cut-off.

1.3.12 Concrete model-[ADV]

The Concrete model is an elastoplastic time-dependent model particularly meant to model shotcrete or concrete structures. The design approach is separately implemented in the model through two safety factor parameters in order to avoid inconsistency between the different aspects computed by the Concrete model. The user should be careful in dynamics analysis because of the time interval difference between dynamic input and shotcrete hardening. The model is not suitable for failure involving low fracture energy.

1.3.13 Interfaces

Interface elements are generally modelled by means of the bi-linear Mohr-Coulomb model. When a more advanced model is used for the corresponding cluster material data set, the interface element will only pick up the relevant data (c, φ, ψ, E, v) for the Mohr-Coulomb model, as described in the Reference Manual. In such cases the interface stiffness is set equal to the elastic soil stiffness. Hence, $E=E_{ur}$ where E_{ur} is stress level dependent, following a power law with E_{ur} proportional to σ_m . For the Soft Soil model, Soft Soil Creep model and Modified Cam-Clay model the power m is equal to 1 and E_{ur} is largely determined by the swelling constant κ^* .

1.3.14 Undrained behaviour

In general, care must be taken in undrained conditions, since the effective stress path that is followed in any of the models may deviate significantly from reality. Although PLAXIS has options to deal with undrained behaviour in an effective stress analysis, the use of undrained shear strength (c_{ij} or Su) may be preferred over the use of effective strength properties (φ) and c') in such cases. Please note that direct input on undrained shear strength does not automatically include the increase of shear strength with consolidation. If, for any reason, the user decides to use effective strength properties in undrained conditions, it is strongly recommended to check the resulting mobilised shear strength using the corresponding option in the PLAXIS Output program.

Preliminaries on material modelling

A material model is described by a set of mathematical equations that give a relationship between stress and strain. Material models are often expressed in a form in which infinitesimal increments of stress (or 'stress rates') are related to infinitesimal increments of strain (or 'strain rates'). All material models implemented in PLAXIS are based on a relationship between the effective stress rates, $\dot{\sigma}'$, and the strain rates, $\dot{\epsilon}'$. In the following section it is described how stresses and strains are defined in PLAXIS. In subsequent sections the basic stress-strain relationship is formulated and the influence of pore pressures in undrained materials is described. Later sections focus on initial conditions for advanced material models.

This Material Models Manual is a general manual for all PLAXIS programs and uses the coordinate system as used in most programs (Figure 2–1 (p. 15)). Please note that the PLAXIS 3D uses a different coordinate system where z is the vertical axis. Users should realize this when reading this manual.

2.1 General definitions of stress

Stress is a tensor which can be represented by a matrix in Cartesian coordinates:

Figure 2-1: General three-dimensional coordinate system and sign convention for stresses

In the standard deformation theory, the stress tensor is symmetric such that $\sigma_{xy} = \sigma_{yx}$, $\sigma_{yz} = \sigma_{zy}$ and $\sigma_{zx} = \sigma_{xz}$. In this situation, stresses are often written in vector notation, which involves only six different components:

$$\underline{\sigma} = \left(\sigma_{xx}\,\sigma_{yy}\sigma_{zz}\,\sigma_{xy}\sigma_{yz}\sigma_{zx}\right)^T\tag{2-2}$$

According to Terzaghi's principle, stresses in the soil are divided into effective stresses, $\underline{\sigma}'$, and pore pressures, $\underline{\sigma}_w$:

$$\underline{\sigma} = \underline{\sigma}' + \underline{\sigma}_w$$
 (2–3)

Pore pressures are generally provided by water in the pores. Water is considered not to sustain any shear stresses. As a result, effective shear stresses are equal to total shear stresses. Positive normal stress components are considered to represent tension, whereas negative normal stress components indicate pressure (or compression). Moreover, water is considered to be fully isotropic, so all pore pressure components are equal. Hence, pore pressure can be represented by a single value, p_w :

$$\underline{\sigma}_w = (p_w \ p_w \ p_w \ 0 \ 0 \ 0)^T \tag{2-4}$$

Material models for soil and rock are generally expressed as a relationship between infinitesimal increments of effective stress and infinitesimal increments of strain. In such a relationship, infinitesimal increments of effective stress are represented by stress rates (with a dot above the stress symbol):

$$\underline{\dot{\sigma}}' = \left(\dot{\sigma}'_{xx} \ \dot{\sigma}'_{yy} \ \dot{\sigma}'_{zz} \ \dot{\sigma}_{xy} \ \dot{\sigma}_{yz} \ \dot{\sigma}_{zx}\right)^{T} \tag{2-5}$$

It is often useful to apply principal stresses rather than Cartesian stress components when formulating material models. Principal stresses are the stresses in such a coordinate system direction that all shear stress components are zero. Principal stresses are, in fact, the eigenvalues of the stress tensor. Principal effective stresses can be determined in the following wav:

$$\det(\boldsymbol{\sigma} - \boldsymbol{\sigma} \boldsymbol{I}) = 0 \tag{2-6}$$

where I is the identity matrix. This equation gives three solutions for σ' , i.e. the principal effective stresses (σ'_{1} , σ'_{2} , σ'_{3}). In PLAXIS the principal effective stresses are arranged in algebraic order:

$$\sigma_1' \le \sigma_2' \le \sigma_3' \tag{2-7}$$

Hence, σ'_{1} is the largest compressive principal stress and σ'_{3} is the smallest compressive principal stress. In this manual, models are often presented with reference to the principal stress space, as indicated in Figure 2.

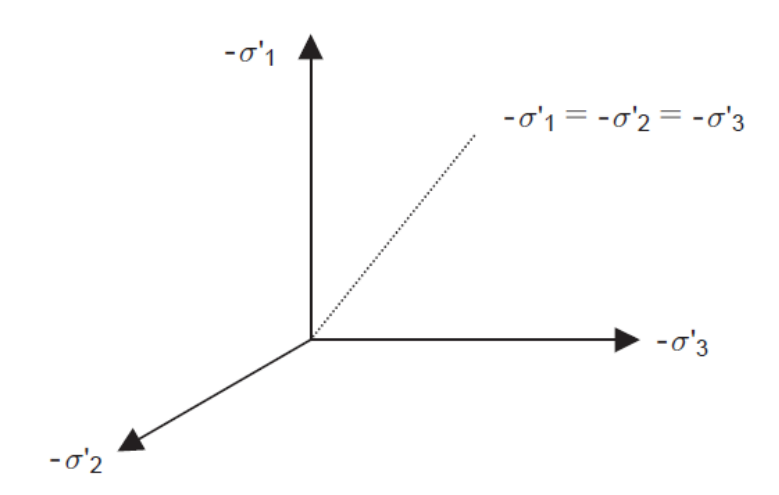


Figure 2-2: Principal stress space

In addition to principal stresses it is also useful to define invariants of stress, which are stress measures that are independent of the orientation of the coordinate system. Two useful stress invariants are:

$$p' = \frac{1}{3} \left(\sigma'_{xx} + \sigma'_{yy} + \sigma'_{zz} \right)$$

$$q = \sqrt{\frac{1}{2} \left(\left(\sigma'_{xx} - \sigma'_{yy} \right)^2 + \left(\sigma'_{yy} - \sigma'_{zz} \right)^2 + \left(\sigma'_{zz} - \sigma'_{xx} \right)^2 + 6 \left(\sigma^2_{xy} + \sigma^2_{yz} + \sigma^2_{zx} \right) \right)}$$
(2-8)

$$q = \sqrt{rac{1}{2} \Big(ig(\sigma'_{xx} - \sigma'_{yy} ig)^2 + ig(\sigma'_{yy} - \sigma'_{zz} ig)^2 + ig(\sigma'_{zz} - \sigma'_{xx} ig)^2 + 6 \Big(\sigma^2_{xy} + \sigma^2_{yz} + \sigma^2_{zx} ig) \Big)}$$
 (2-9)

p'Isotropic effective stress, or mean effective stress.

Equivalent shear stress. It has the important property that it reduces to $q=|\sigma_1'-\sigma_3'|$ for triaxial stress states with $\sigma_2'=\sigma_3'$.

Principal effective stresses can be written in terms of the invariants:

$$\sigma_1'=p'+rac{2}{3}q\sinigg(heta-rac{2}{3}\piigg)$$
 (2–10)

$$\sigma_2'=p'+rac{2}{3}q\sin\left(heta
ight)$$
 (2–11)

$$\sigma_3'=p'+rac{2}{3}q\sin\left(heta+rac{2}{3}\pi
ight)$$
 (2–12)

in which θ is referred to as Lode 's angle (a third invariant), which is defined as:

$$\theta = \frac{1}{3}\arcsin\left(\frac{27}{2}\frac{J_3}{a^3}\right) \tag{2-13}$$

with

$$J_{3} = \left(\sigma'_{xx} - p'\right)\left(\sigma'_{yy} - p'\right)\left(\sigma'_{zz} - p'\right) - \left(\sigma'_{yy} - p'\right)\sigma_{zx}^{2} \\ - \left(\sigma'_{xx} - p'\right)\sigma_{yz}^{2} - \left(\sigma'_{zz} - p'\right)\sigma_{xy}^{2} + 2\sigma_{xy}\sigma_{yz}\sigma_{zx}$$
 (2-14)

2.2 General definitions of strain

Strain is a tensor which can be represented by a matrix with Cartesian coordinates as:

$$\boldsymbol{\varepsilon} = \begin{bmatrix} \varepsilon_{xx} & \varepsilon_{xy} & \varepsilon_{xz} \\ \varepsilon_{yx} & \varepsilon_{yy} & \varepsilon_{yz} \\ \varepsilon_{zx} & \varepsilon_{zy} & \varepsilon_{zz} \end{bmatrix}$$
(2-15)

Strains are the derivatives of the displacement components, i.e. $arepsilon_{ij}=rac{1}{2}\Big(rac{\partial u_i}{\partial j}+rac{\partial u_j}{\partial i}\Big)$

where i and i are either x, y or z.

According to the small deformation theory, only the sum of complementing Cartesian shear strain components ε_{ii} and ε_{ii} result in shear stress. This sum is denoted as the shear strain γ . Hence, instead of ε_{xy} , ε_{yx} , ε_{yz} , ε_{zy} , ε_{zx} and ε_{xz} the shear strain components γ_{xy} , γ_{yz} and γ_{zx} are used respectively. Under the above conditions, strains are often written in vector notation, which involves only six different components:

$$\underline{\varepsilon} = (\varepsilon_{xx} \ \varepsilon_{yy} \ \varepsilon_{zz} \ \gamma_{xy} \ \gamma_{yz} \ \gamma_{zx})^T \tag{2-16}$$

$$arepsilon_{xx} = rac{\partial}{\partial x} u_x$$
 (2–17)

$$arepsilon_{yy} = rac{\partial}{\partial y} u_y$$
 (2–18)

$$arepsilon_{zz}=rac{\partial}{\partial z}u_z$$
 (2–19)

$$\gamma_{xy} = \varepsilon_{xy} + \varepsilon_{yx} = \frac{\partial}{\partial y} u_x + \frac{\partial}{\partial x} u_y$$
 (2-20)

$$\gamma_{yz}=arepsilon_{yz}+arepsilon_{zy}=rac{\partial}{\partial z}u_y+rac{\partial}{\partial y}u_z$$
 (2–21)

$$\gamma_{zx}=arepsilon_{zx}+arepsilon_{xz}=rac{\partial}{\partial x}u_z+rac{\partial}{\partial z}u_x$$
 (2-22)

Similarly as for stresses, positive normal strain components refer to extension, whereas negative normal strain components indicate compression.

In the formulation of material models, where infinitesimal increments of strain are considered, these increments are represented by strain rates (with a dot above the strain symbol). notation

$$\underline{\dot{\varepsilon}} = \left(\dot{\varepsilon}_{xx} \ \dot{\varepsilon}_{yy} \ \dot{\varepsilon}_{zz} \ \dot{\gamma}_{xy} \ \dot{\gamma}_{yz} \ \dot{\gamma}_{zx}\right)^{T} \tag{2-23}$$

In analogy to the invariants of stress, it is also useful to define invariants of strain. A strain invariant that is often used is the volumetric strain, ε_{v} , which is defined as the sum of all normal strain components in a standard calculation according to small deformation theory:

$$\varepsilon_v = \varepsilon_{xx} + \varepsilon_{yy} + \varepsilon_{zz} = \varepsilon_1 + \varepsilon_2 + \varepsilon_3$$
 (2–24)

In Updated mesh calculations the volumetric strain is calculated as:

$$\varepsilon_v = \varepsilon_{xx} + \varepsilon_{yy} + \varepsilon_{zz} + \varepsilon_{xx}\varepsilon_{yy} + \varepsilon_{xx}\varepsilon_{zz} + \varepsilon_{yy}\varepsilon_{zz} + \varepsilon_{xx}\varepsilon_{yy}\varepsilon_{zz}$$
 (2-25)

The volumetric strain is defined as negative for compaction and as positive for dilatancy.

Another invariant is the deviatoric strain (ε_a), which is calculated as:

$$arepsilon_{q} = \sqrt{rac{2}{9}} \left[(arepsilon_{xx} - arepsilon_{yy})^{2} + (arepsilon_{yy} - arepsilon_{zz})^{2} + (arepsilon_{zz} - arepsilon_{xx})^{2}
ight] + rac{1}{3} \left(\gamma^{2}_{xy} + \gamma^{2}_{yz} + \gamma^{2}_{zx}
ight)$$
 (2-26)

For triaxial conditions i.e. $\varepsilon_2 = \varepsilon_3$ the deviatoric strain, reduces to:

$$arepsilon_q = rac{2}{3}|arepsilon_1 - arepsilon_3|$$
 (2–27)

where ε_1 and ε_3 are the major and minor principal strains components respectively. Furthermore, when volumetric strains are negligible ($\varepsilon_v = 0$), then $\varepsilon_3 = -1/2\varepsilon_1$, so $\varepsilon_q = |\varepsilon_1|$

For elastoplastic models, as used in PLAXIS, strains are decomposed into elastic and plastic components:

$$\underline{\varepsilon} = \underline{\varepsilon}^e + \underline{\varepsilon}^p$$
 (2–28)

Throughout this manual, the superscript e will be used to denote elastic strains and the superscript p will be used to denote plastic strains.

2.3 Elastic strains

Material models for soil and rock are generally expressed as a relationship between infinitesimal increments of effective stress ('effective stress rates') and infinitesimal increments of strain ('strain rates'). This relationship may be expressed in the form:

$$\underline{\dot{\sigma}}' = M\underline{\dot{\varepsilon}}$$
 (2–29)

where M is a material stiffness matrix. Note that in this type of approach, pore-pressures are explicitly excluded from the stress-strain relationship.

The simplest material model in PLAXIS is based on Hooke's law for isotropic linear elastic behaviour. This model is available under the name Linear Elastic model, but it is also the basis of other models. Hooke's law can be given by the equation:

$$\begin{bmatrix} \dot{\sigma}_{xx}' \\ \sigma_{yy}' \\ \dot{\sigma}_{zz}' \\ \dot{\sigma}_{xy}' \\ \dot{\sigma}_{zz}' \\ \dot{\sigma}_{xy}' \\ \dot{\sigma}_{yz}' \\ \dot{\sigma}_{zx}' \end{bmatrix} = \frac{E'}{(1-2\nu')(1+\nu')} \begin{bmatrix} 1-\nu' & \nu' & \nu' & 0 & 0 & 0 \\ \nu' & 1-\nu' & \nu' & 0 & 0 & 0 \\ \nu' & \nu' & 1-\nu' & 0 & 0 & 0 \\ 0 & 0 & 0 & \frac{1}{2}-\nu' & 0 & 0 \\ 0 & 0 & 0 & 0 & \frac{1}{2}-\nu' & 0 \\ 0 & 0 & 0 & 0 & 0 & \frac{1}{2}-\nu' \end{bmatrix} \begin{bmatrix} \dot{\varepsilon}_{xx}' \\ \dot{\varepsilon}_{xy}' \\ \dot{\varepsilon}_{zz}' \\ \dot{\varepsilon}_{xy}' \\ \dot{\varepsilon}_{yz}' \\ \dot{\varepsilon}_{zx}' \end{bmatrix}$$

$$(2-30)$$

The elastic material stiffness matrix is often denoted as \mathbf{D}^e . Two parameters are used in this model, the effective Young's modulus, E', and the effective Poisson's ratio, v'. In the remaining part of this manual effective parameters are denoted without dash ('), unless a different meaning is explicitly stated. The symbols E and v are sometimes used in this manual in combination with the subscript ur to emphasize that the parameter is explicitly meant for unloading and reloading. A stiffness modulus may also be indicated with the subscript ref to emphasize that it refers to a particular reference level (y_{ref}) .

According to Hooke's law, the relationship between Young's modulus E and other stiffness moduli, such as the shear modulus G, the bulk modulus K, and the oedometer modulus E_{oed} , is given by:

$$G=rac{E}{2(1+
u)}$$
 a) $K=rac{E}{3(1-2
u)}$ b) $E_{oed}=rac{(1-
u)E}{(1-2
u)(1+
u)}$ c)

Using these auxiliary stiffness parameters, Hooke's law can be presented in an alternative form

During the input of material parameters for the Linear Elastic model or the Mohr-Coulomb model the values of G and E_{oed} are presented as auxiliary parameters (alternatives), calculated from Eqn. 2-31 (p. 18). Note that the alternatives are influenced by the input values of E and v. Entering a particular value for one of the alternatives G or E_{oed} results in a change of the E modulus, while v remains the same.

It is possible for the Linear Elastic model and the Mohr-Coulomb model to specify a stiffness that varies linearly with depth. This can be done by entering a value for E_{inc} which is the increment of stiffness per unit of depth, as indicated in Eqn. 2-33 (p. 19)

Together with the input of E_{inc} the input of y_{ref} becomes relevant. Above y_{ref} the stiffness is equal to E_{ref} . Below the stiffness is given by:

$$E(y) = E_{ref} + (y_{ref} - y)E_{inc}$$
 $y < y_{ref}$ (2-33)



Note:

The Linear Elastic model is usually inappropriate to model the highly non-linear behaviour of soil, but it is of interest to simulate structural behaviour, such as thick concrete walls or plates, for which strength properties are usually very high compared with those of soil. For these applications, the Linear Elastic model will often be selected together with Non-porous drainage type in order to exclude pore pressures from these structural elements.

2.4 Undrained effective stress analysis (effective stiffness parameters)

In PLAXIS it is possible to specify undrained behaviour in an effective stress analysis using effective model parameters. This is achieved by identifying the type of material behaviour (Drainage type) of a soil layer as Undrained A or Undrained B (2.5 Undrained effective stress analysis with effective strength parameters (Undrained A) (p. 24) and 2.6 Undrained effective stress analysis with undrained strength parameters (Undrained B) (p. 25)). In this section, it is explained how PLAXIS deals with this special option.

The presence of pore pressures in a soil body, usually caused by water, contributes to the total stress level. According to Terzaghi's principle, total stresses vector notation σ can be divided into effective stresses $\underline{\sigma}'$, active pore pressure p_{active} and pore water pressures p_w (see also Eqn. 2-3 (p. 15)). However, water is supposed not to sustain any shear stress, and therefore the effective shear stresses are equal to the total shear stresses:

$$\underline{\sigma} = \underline{\sigma}' + mp_{active}$$
 (2–34)

where,

$$m=egin{bmatrix}1\1\1\0\0\0\end{bmatrix}$$
 and $p_{active}=lpha_{Biot}S_{eff}p_w$ (2–35)

$$\sigma_{xx} = \sigma_{xx}^{\prime} + \alpha_{Biot} S_{eff} p_w$$
 (2–36)

$$\sigma_{yy} = \sigma'_{yy} + lpha_{Biot} S_{eff} p_w$$
 (2–37)

$$\sigma_{zz} = \sigma'_{zz} + \alpha_{Biot} S_{eff} p_w$$
 (2–38)

$$\sigma_{xy} = \sigma'_{xy}$$

$$\sigma_{yz} = \sigma'_{yz}$$
 $\sigma_{zx} = \sigma'_{zx}$
(2–39)

where

 α_{Biot} = Biot's pore pressure coefficient.

Effective degree of saturation.

Considering incompressible grains, Biot's coefficient α_{Biot} is equal to unity (α_{Biot} = 1). The situation of compressible grains or compressible solid material (α_{Biot} < 1) is explained in more detail at the end of this section.

Note that, similar to the total and the effective stress components, p_w is considered negative for pressure.

The product $\alpha_{Biot} S_{eff} p_w$ is termed 'Active pore pressure', p_{active} in PLAXIS. A further distinction is made between steady state pore stress, p_{steady} , and excess pore stress, p_{excess} :

$$p_w = p_{steady} + p_{excess}$$
 (2–40)

Steady state pore pressures are considered to be input data, i.e. generated on the basis of phreatic levels or by means of a groundwater flow calculation. Excess pore pressures are generated during plastic calculations for the case of undrained A or B material behaviour or during a consolidation analysis. Undrained material behaviour and the corresponding calculation of excess pore pressures are described below.

Since the time derivative of the steady state component equals zero, it follows:

$$\dot{p}_w = \dot{p}_{excess}$$
 (2–41)

Hooke's law can be inverted to obtain:

$$\begin{bmatrix} \dot{\varepsilon}^{e}_{xx} \\ \dot{\varepsilon}^{e}_{yy} \\ \dot{\varepsilon}^{e}_{zz} \\ \dot{\gamma}^{e}_{yz} \\ \dot{\gamma}^{e}_{zx} \end{bmatrix} = \frac{1}{E'} \begin{bmatrix} 1 & -v' & -v' & 0 & 0 & 0 \\ -v' & 1 & -v' & 0 & 0 & 0 \\ -v' & -v' & 1 & 0 & 0 & 0 \\ 0 & 0 & 0 & 2 + 2v' & 0 & 0 \\ 0 & 0 & 0 & 0 & 2 + 2v' & 0 \\ 0 & 0 & 0 & 0 & 0 & 2 + 2v' \end{bmatrix} \begin{bmatrix} \dot{\sigma}'_{xx} \\ \dot{\sigma}'_{yy} \\ \dot{\sigma}'_{zz} \\ \dot{\sigma}'_{xy} \\ \dot{\sigma}'_{yz} \\ \dot{\sigma}'_{zx} \end{bmatrix}$$
(2-42)

Substituting Eqn. 2–39 (p. 20) gives:

$$\begin{bmatrix} \dot{\varepsilon}^{e}_{xx} \\ \dot{\varepsilon}^{e}_{yy} \\ \dot{\varepsilon}^{e}_{zz} \\ \dot{\gamma}^{e}_{xy} \\ \dot{\gamma}^{e}_{zz} \\ \dot{\gamma}^{e}_{zx} \end{bmatrix} = \frac{1}{E'} \begin{bmatrix} 1 & -v' & -v' & 0 & 0 & 0 \\ -v' & 1 & -v' & 0 & 0 & 0 \\ -v' & -v' & 1 & 0 & 0 & 0 \\ 0 & 0 & 0 & 2 + 2v' & 0 & 0 \\ 0 & 0 & 0 & 0 & 2 + 2v' & 0 \\ 0 & 0 & 0 & 0 & 0 & 2 + 2v' \end{bmatrix} \begin{bmatrix} \dot{\sigma}_{xx} - \alpha_{Biot} \dot{p}_{w} \\ \dot{\sigma}_{yy} - \alpha_{Biot} \dot{p}_{w} \\ \dot{\sigma}_{zz} - \alpha_{Biot} \dot{p}_{w} \\ \dot{\sigma}'_{xy} \\ \dot{\sigma}'_{xy} \\ \dot{\sigma}'_{yz} \\ \dot{\sigma}'_{zx} \end{bmatrix}$$
 (2-43)

Considering slightly compressible water, the rate of excess pore pressure is written as:

$$\dot{p}_{excess} = rac{lpha_{biot} \dot{arepsilon}_v}{nC_w + (lpha_{biot} - n)C_s}$$
 (2-44)

$$C_w = \frac{1}{k_w} \tag{2-45}$$

$$C_s = \frac{1}{k_s} \tag{2-46}$$

in which K_w is the bulk modulus of the water, K_s is the bulk modulus of the solid material, C_w is the compressibility of the water, C_s is the compressibility of the solid material and n is the soil porosity.

$$n = \frac{e_0}{1 + e_0} \tag{2-47}$$

where e_0 is the initial void ratio as specified in the general soil properties.

The inverted form of Hooke's law may be written in terms of the total stress rates and the undrained parameters E_u and v_u :

$$\begin{bmatrix} \dot{\varepsilon}_{xx}^{e} \\ \dot{\varepsilon}_{yy}^{e} \\ \dot{\varepsilon}_{yz}^{e} \\ \dot{\gamma}_{xy}^{e} \\ \dot{\gamma}_{zx}^{e} \end{bmatrix} = \frac{1}{E_{u}} \begin{bmatrix} 1 & -v_{u} & -v_{u} & 0 & 0 & 0 \\ -v_{u} & 1 & -v_{u} & 0 & 0 & 0 \\ -v_{u} & -v_{u} & 1 & 0 & 0 & 0 \\ 0 & 0 & 0 & 2 + 2v_{u} & 0 & 0 \\ 0 & 0 & 0 & 0 & 2 + 2v_{u} & 0 \\ 0 & 0 & 0 & 0 & 0 & 2 + 2v_{u} \end{bmatrix} \begin{bmatrix} \dot{\sigma}'_{xx} \\ \dot{\sigma}'_{yy} \\ \dot{\sigma}'_{yz} \\ \dot{\sigma}'_{xy} \\ \dot{\sigma}'_{yz} \\ \dot{\sigma}'_{yz} \\ \dot{\sigma}'_{xy} \end{bmatrix}$$
(2-48)

where:

$$egin{align} E_u &= 2G(1+v_u); \ v_u &= rac{3v'+lpha_{Biot}B(1-2v')}{3-lpha_{Biot}B(1-2v')} \ B &= rac{lpha_{Biot}+n\left(rac{K'}{K_w}+lpha_{Biot}-1
ight)}{lpha_{Biot}+n\left(rac{K'}{K_w}+lpha_{Biot}-1
ight)} \end{align}$$

where B is Skempton's B-parameter.

Hence, the special option for undrained behaviour in PLAXIS (Undrained A or Undrained B) is such that the effective parameters G and v' are transformed into undrained parameters E_u and v_u according to Eqn. 2-49 (p. 21) . Note that the index u is used to indicate auxiliary parameters for undrained soil. Hence, E_u and v_u should not be confused with E_{ur} and v_{ur} as used to denote unloading / reloading.

Fully incompressible behaviour is obtained for $v_u = 0.5$. However, taking $v_u = 0.5$ leads to singularity of the stiffness matrix. In fact, water is not fully incompressible, but a realistic bulk modulus for water is very large. In order to avoid numerical problems caused by an extremely low compressibility, v_u is, by default, taken as 0.495, which makes the undrained soil body

slightly compressible. In order to ensure realistic computational results, the bulk modulus of the water must be high compared with the bulk modulus of the soil skeleton, i.e. $K_w >> n K'$. This condition is sufficiently ensured by requiring $v' \le 0.35$.

Consequently, for material behaviour *Undrained A* or *Undrained B*, a bulk modulus for water is automatically added to the stiffness matrix. The bulk modulus of water is obtained in three ways: automatically from Eqn. 2-50 (p. 22) (v-undrained definition - Direct), automatically but by specifying the Skempton's B-parameter (v-undrained definition - Skempton B based) and manually by directly specifying K_w and α_{Biot} (Biot effective stress concept).

$$rac{K_w}{n} = rac{3(v_u - v')}{(1 - 2v_u)(1 + v')} \quad K' = rac{0.495 - v'}{1 + v'} 300 K' \geq 30 K' \quad (For \, lpha_{Biot} = 1)$$
 (2–50)

? Note: In the UBC3D-PLM model, the implicit Poisson's ratio (v') is defined based on the elastic bulk modulus K and the elastic shear modulus G at the current stress state, v'= (3K - 2G)/(6K + 2G). For this reason, the value follows the evolution of the stiffnesses and it is not constant.

Hence, K_W/n is larger than 30K', at least for $v' \le 0.35$ and $\alpha_{Biot} = 1$. The bulk stiffness of water K_{w} , calculated in this way, is a numerical value related to the soil stiffness. It is lower than or equal to the real bulk stiffness of pure water, K_w^0 (2·10⁶ kN/m²). In retrospect it is worth mentioning here a review about the Skempton B-parameter.

2.4.1 Skempton B-parameter

When the Drainage type is set to Undrained A or Undrained B, PLAXIS automatically assumes an implicit undrained bulk modulus, K_u , for the soil as a whole (soil skeleton + water) and distinguishes between total stress rates, effective stress rates and rates of excess pore pressure:

$$Excess\ pore\ pressure: \quad \dot{p}_{excess} = B\dot{p} = rac{lpha_{biot}\dot{arepsilon}_v}{nC_w + (lpha_{biot} - n)C_s}$$
 (2–52)

Effective stress:
$$\dot{p}' = (1 - \alpha_{Biot}B)\dot{p} = K'\dot{\varepsilon}_v$$
 (2-53)

Note that for *Undrained A* or *Undrained B* effective stiffness parameters should be entered in the material data set, i.e. E' and v' and not E_u and v_u , or the respective stiffness parameters in advanced models; the latter should be done for *Undrained C* behaviour in a total stress analysis (2.7 Undrained total stress analysis with undrained parameters (Undrained C) (p. 26)). The undrained bulk modulus is automatically calculated by PLAXIS using Hooke's law of elasticity:

$$K_u = rac{2G(1+v_u)}{3(1-2v_u)} \quad where \quad G = rac{E'}{2(1+v')}$$
 (2-54)

When using the *v*-undrained option with suboption Direct, by default $v_u = 0.495$ (but can be changed) and α_{Biot} = 1, whereas when using the *v*-undrained option with suboption Skempton B based with input of Skempton's B-parameter or the option Biot effective stress concept, v_{ij} is calculated as:

$$v_u = rac{3v' + lpha_{Biot}B(1 - 2v')}{3 - lpha_{Biot}B(1 - 2v')}$$
 (2–55)

If the soil is only partially saturated, the pores contain both air and water and the equivalent bulk modulus of the pore fluid K_w^{unsat} is expected to be much smaller compared to that of pure water, in the case of fully saturated soil K_w . PLAXIS assumes a constant gas pressure i.e. air is always drained, the drainage type of soil only relates to the drainage type of liquid water. Excess pore pressure change will therefore depend on the bulk modulus of liquid water and the surface tension (capillary effect). This assumption allows to establish the following rigorous relationship for the unsaturated bulk modulus of the pore fluid:

$$K_w^{unsat} = \frac{K_w}{1 + \frac{K_w}{S_w} \left(-\frac{\partial S_w}{\partial p_w} \right)} \tag{2-56}$$

where is the derivative of saturation w.r.t. pore water pressure (suction), i.e. the slope of water retention curve

The value of Skempton's B-parameter is calculated from the ratio of the bulk stiffnesses of the soil skeleton and the pore fluid, as already defined in Eqn. 2-50 (p. 22):

$$B = rac{lpha_{Biot}}{lpha_{Biot} + n \Big(rac{K'}{K_w} + lpha_{Biot} - 1\Big)}$$
 (2–57)

The rate of excess pore pressure is calculated from the (small) volumetric strain rate, according

$$\dot{p}_{excess} = \frac{\alpha_{Biot} \dot{\varepsilon}_v}{nC_w + (\alpha_{Biot} - n)C_s} \tag{2-58}$$

The types of elements used in PLAXIS are sufficiently adequate to avoid mesh locking effects for nearly incompressible materials.

This special option to model undrained material behaviour on the basis of effective model parameters is available for most material models in PLAXIS. This enables undrained calculations to be executed with effective stiffness parameters, with explicit distinction between effective stresses and (excess) pore pressures. However, shear induced (excess) pore pressure may not be sufficiently included.

Such an analysis requires effective soil parameters and is therefore highly convenient when such parameters are available. For soft soil projects, accurate data on effective parameters may not always be available. Instead, in situ tests and laboratory tests may have been performed to obtain undrained soil parameters. In such situations measured undrained Young's moduli can be easily converted into effective Young's moduli based on Hooke's law:

$$E' = \frac{2(1+v')}{3}E_u \tag{2-59}$$

For advanced models there is no such direct conversion possible. In that case it is recommended to estimate the required effective stiffness parameter from the measured undrained stiffness parameter, then perform a simple undrained test to check the resulting undrained stiffness and adapt the effective stiffness if needed. The Soil test facility (Reference Manual) may be used as a convenient tool to perform such test.

2.4.2 Biot pore pressure coefficient α_{Biot} [ULT]

In general, for geotechnical applications, the compressibility of the soil skeleton is much higher than the compressibility of the individual grains, so deformations of the grains themselves can be ignored. However, in the case of very deep soil layers at very high pressures, the stiffness of the soil or rock matrix comes close to the stiffness of the solid material of which the soil grains or the rock is composed of, and, therefore, the compressibility of the solid material cannot be ignored. This has consequences for the division of total stress into effective stress and pore pressure. Considering compressible solid material, Terzaghi's effective stress definition changes into:

$$\underline{\sigma}' = \underline{\sigma} - \alpha_{biot} S_{eff} \underline{m} p_w \tag{2-60}$$

Where α_{Biot} is Biot's pore pressure coefficient, S_{eff} is the effective degree of saturation, \underline{m} is a vector with unity values (1) for the normal components and 0-values for the shear components, and p_w is the pore water pressure. The alpha coefficient is defined as:

$$lpha_{biot} = 1 - rac{K'}{K_c}$$
 (2–61)

Where K' is the effective bulk modulus of the soil matrix and K_s is the bulk modulus of the solid material. Indeed, for incompressible solid material ($K_s = \infty$) Terzaghi's original stress definition is retained. A lower value of α_{Biot} implies that for a given value of total stress and pore water pressure, the resulting effective stress is higher than when considering incompressible solid material ($\alpha_{Biot} = 1$).

In the case of undrained soil behaviour (Undrained A or B in PLAXIS 2D), Biot's pore pressure coefficient also affects the undrained Poisson's ratio v_u that is automatically calculated by PLAXIS 2D based on a manual input of K_w parameter (see Eq. Eqn. 2-49 (p. 21)).

The default value of Biot's pore pressure coefficient is 1.0 (v-undrained definition option), but users may change this value in the range of [0.001, 1.0] for the Biot effective stress concept option.

2.5 Undrained effective stress analysis with effective strength parameters (Undrained A)

In principle, undrained effective stress analysis as described in 2.4 Undrained effective stress analysis (effective stiffness parameters) (p. 19) can be used in combination with effective strength parameters φ' and c' to model the material's undrained shear strength (*Undrained A*). In this case, the development of the pore pressure plays a crucial role in providing the right effective stress path that leads to failure at a realistic value of undrained shear strength (c_u or s_{ij}). However, note that most soil models are not capable of providing the right effective stress path in undrained loading. As a result, they will produce the wrong undrained shear strength if the material strength has been specified on the basis of effective strength parameters. Another problem is that for undrained materials effective strength parameters are usually not available from soil investigation data. In order to overcome these problems, some models allow for a direct input of undrained shear strength. This approach is described in 2.6 Undrained effective stress analysis with undrained strength parameters (Undrained B) (p. 25).

If the user wants to model the material strength of undrained materials using the effective strength parameters φ' and c', this can be done in PLAXIS in the same way as for drained materials. However, in this case the *Drainage type* must be set to *Undrained A*. As a result, PLAXIS will automatically add the stiffness of water to the stiffness matrix (see 2.4 Undrained effective stress analysis (effective stiffness parameters) (p. 19)) in order to distinguish between effective stresses and (excess) pore pressures (= effective stress analysis). The advantage of using effective strength parameters in undrained loading conditions is that after consolidation a qualitatively increased shear strength is obtained, although this increased shear strength could also be quantitatively wrong, for the same reason as explained before.

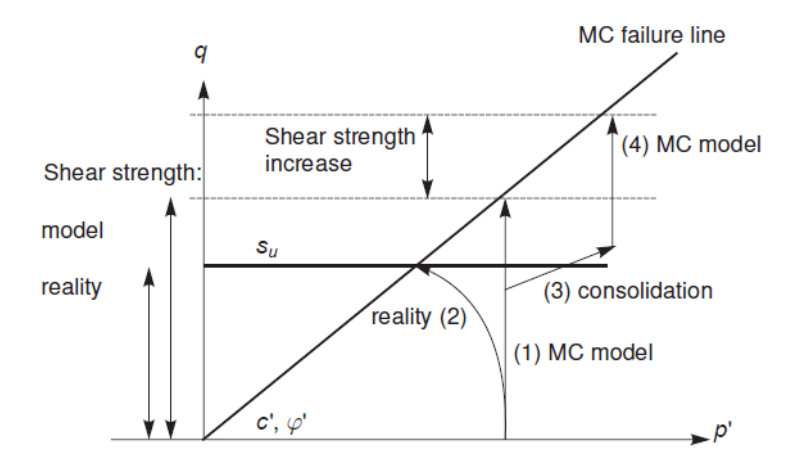


Figure 2-3: Illustration of stress paths; reality vs Mohr-Coulomb model

2.4 Undrained effective stress analysis (effective stiffness parameters) (p. 19) illustrates an example using the Mohr-Coulomb model. When the Drainage type is set to Undrained A, the model will follow an effective stress path where the mean effective stress, p', remains constant all the way up to failure (1). It is known that especially soft soils, like normally consolidated clays and peat, will follow an effective stress path in undrained loading where p' reduces significantly as a result of shear induced pore pressure (2). As a result, the maximum deviatoric stress that can be reached in the model is over-estimated in the Mohr-Coulomb model. In other words, the mobilised shear strength in the model supersedes the available undrained shear strength.

If, at some stress state, the soil is consolidated, the mean effective stress will increase (3). Upon further undrained loading with the Mohr-Coulomb model, the observed shear strength will be increased (4) compared to the previous shear strength, but this increased shear strength may again be unrealistic, especially for soft soils.

On the other hand, advanced models do include, to some extent, the reduction of mean effective stress in undrained loading, but even when using advanced models it is generally advised to check the mobilised shear strength in the Output program against the available (undrained) shear strength when this approach is followed.

Note that whenever the *Drainage type* parameter is set to *Undrained A*, effective values must be entered for the stiffness parameters (Young's modulus E' and Poisson ratio v' in case of the Mohr-Coulomb model or the respective stiffness parameters in the advanced models).

Care must be taken when using Undrained A together with a non-zero dilatancy angle ψ . The use of a positive dilatancy angle may lead to unrealistically large tensile pore stresses and, as a result, an unrealistically large shear strength. The use of a negative dilatancy angle may lead to unrealistically high pore pressure and unrealistic liquefaction type of behaviour. Hence, for *Undrained* A it is recommended to use $\psi = 0$.

2.6 Undrained effective stress analysis with undrained strength parameters (Undrained B)

For undrained soil layers with a known undrained shear strength profile, PLAXIS offers for some models the possibility of an undrained effective stress analysis, as described in 2.4 Undrained effective stress analysis (effective stiffness parameters) (p. 19), with direct input of the

undrained shear strength, i.e. setting the friction angle to zero and the cohesion equal to the undrained shear strength ($\varphi = \varphi_{ij} = 0^{\circ}$; $c = s_{ij}$) (Drainage type = Undrained B). Also in this case, distinction is made between pore pressures and effective stresses. Although the pore pressures and effective stress path may not be fully correct, the resulting undrained shear strength is not affected, since it is directly specified as an input parameter.

The option to perform an undrained effective stress analysis with undrained strength properties is only available for the Mohr-Coulomb model, the Hardening Soil model, the Hardening Soil model with small-strain stiffness and the NGI-ADP model. Since most soils show an increasing shear strength with depth, it is possible to specify the increase per unit of depth in PLAXIS in the Stress dependency blocks on the Mechanical tabsheet of the Soil window.

Note that if the Hardening Soil model or the Hardening Soil model with small-strain stiffness is used with $\varphi = 0^{\circ}$, the stiffness moduli in the model are no longer stress-dependent and the model exhibits no compression hardening, although the model retains its separate unloadingreloading modulus and shear hardening. Also note that a direct input of undrained shear strength does not automatically give the increase of shear strength with consolidation.

Further note that whenever the *Drainage type* parameter is set to *Undrained B*, effective values must be entered for the stiffness parameters (Young's modulus E' and Poisson ratio v' in case of the Mohr-Coulomb model or the respective stiffness parameters in the advanced models).

2.7 Undrained total stress analysis with undrained parameters (Undrained C)

If, for any reason, it is desired not to use the Undrained A or Undrained B options in PLAXIS to perform an undrained effective stress analysis, one may simulate undrained behaviour using a conventional total stress analysis with all parameters specified as undrained. In that case, stiffness is modelled using an undrained Young's modulus E_u and an undrained Poisson ratio v_u , and strength is modelled using an undrained shear strength s_{ij} and $\varphi = \varphi_{ij} = 0^{\circ}$. Typically, for the undrained Poisson ratio a value close to 0.5 is selected (between 0.495 and 0.499). A value of 0.5 exactly is not possible, since this would lead to singularity of the stiffness matrix.

In PLAXIS it is possible to perform a total stress analysis with undrained parameters if the Mohr-Coulomb model or the NGI-ADP model is used. In this case, one should select Undrained C as the *Drainage type*. The disadvantage of the undrained total stress analysis is that no distinction is made between effective stresses and pore pressures. Hence, all output referring to effective stresses should now be interpreted as total stresses and all pore pressures are equal to zero.

Note that a direct input of undrained shear strength does not automatically give the increase of shear strength with consolidation. In fact, it does not make sense to perform a consolidation analysis since there are no pore pressures to consolidate. Also note that the K_0 -value to generate initial stresses refers to total stresses rather than effective stresses in this case. This type of approach is not possible for most advanced models.

2.7.1 Overview of models and allowable drainage types

Material model	Drainage type
Linear Elastic model	Drained, Undrained A, Undrained C, Non-porous
Mohr-Coulomb model	Drained, Undrained A, Undrained B, Undrained C, Non-porous
Hardening Soil model	Drained, Undrained A, Undrained B

Material model	Drainage type
Hardening Soil model with small- strain stiffness	Drained, Undrained A, Undrained B
UBC3D-PLM model	Drained, Undrained A
Soft Soil model	Drained, Undrained A
Soft Soil Creep model	Drained, Undrained A
Jointed Rock model	Drained, Non-porous
Modified Cam- Clay model	Drained, Undrained A
NGI-ADP model	Drained, Undrained C
UDCAM-S model	Undrained C
Hoek-Brown model	Drained, Non-porous
Sekiguchi-Ohta model	Drained, Undrained A
Concrete model	Drained, Non-porous
User-defined soil models	Drained, Undrained A, Non-porous

2.8 The initial pre-consolidation stress in advanced models

When using advanced models in PLAXIS an initial pre-consolidation stress has to be determined. In the engineering practice it is common to use a vertical pre-consolidation stress, σ_p , but

PLAXIS needs an equivalent isotropic pre-consolidation stress, p_p^{eq} to determine the initial position of a cap-type yield surface. If a material is overconsolidated, information is required about the overconsolidation Ratio (OCR), i.e. the ratio of the greatest effective vertical stress previously reached, σ_p (see Figure 2–4 (p. 28)), and the in-situ effective vertical stress, σ'_{vv} (note that in PLAXIS 3D the vertical (effective) stress is σ_{zz}^{0}).

$$OCR = \frac{\sigma_p}{\sigma_{nn}^{\prime 0}}$$
 (2–62)

The two ways of specifying the vertical pre-consolidation stress are illustrated in Figure 2-4 (p. 28).

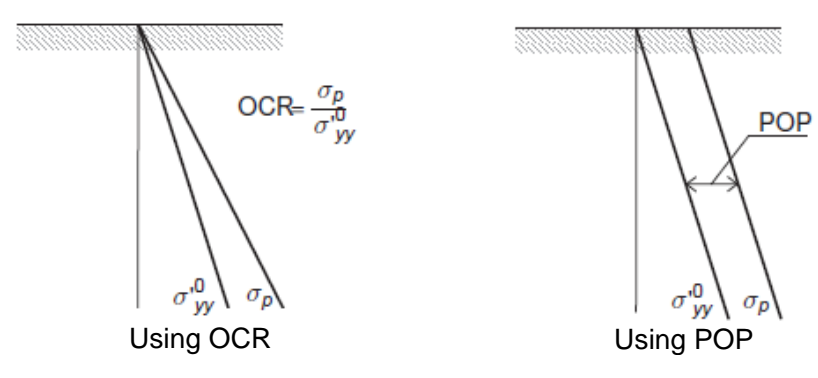


Figure 2-4: Illustration of vertical pre-consolidation stress in relation to the in-situ vertical stress

It is also possible to specify the initial stress state using the Pre-Overburden Pressure (POP) as an alternative to prescribing the overconsolidation ratio. The Pre-Overburden Pressure is defined by:

$$POP = \left| \sigma_p - \sigma_{yy}^{\prime 0} \right| \tag{2-63}$$

The pre-consolidation stress σ_p is used to compute the equivalent pre-consolidation pressure p_p eq which determines the initial position of a cap-type yield surface in the advanced soil models. The calculation of p_p^{eq} is based on the principal stress history ($\sigma'_{1,max}$, σ'_{2} , σ'_{3}). The actual determination of p_n^{eq} depends on the constitutive model being used. The principal stress history is initialised in the Initial phase (KO-procedure or Gravity loading) based on the Cartesian effective stress components and the pre-overburden pressure (POP) or overconsolidation ratio (OCR) defined in the boreholes or data set. From this, Cartesian pre-consolidation stress levels are calculated based on the following equations:

$$\begin{split} \sigma'_{xx,c} &= K_0^{nc} \, OCR \, \sigma'_{yy} \\ \sigma'_{xx,c} &= OCR \, \sigma'_{yy} \\ \sigma'_{zz,c} &= K_0^{nc} \, OCR \sigma'_{yy} \\ \sigma_{xy,c} &= \sigma_{xy} \end{split} \tag{2-64}$$

 $K_0^{nc} = K_0 - value \ associated \ with \ normally \ consolidated \ states \ of \ stress.$

Note:

- ullet K_0^{nc} is a model parameter in advanced constitutive models and estimated in simple models $(K_0^{nc} = 1 - \sin \varphi)$.
- Models that do not have φ as input parameter use K_0^{nc} =0.5 (φ =30°).

For the Modified Cam-Clay model, K_0^{nc} is automatically determined based on the parameter M as entered by the user. The exact relationship between M and K_0 can be formulated as (Bringreve, 1994):

$$M=3\sqrt{rac{\left(1-K_{0}^{nc}
ight)^{2}}{\left(1+2K_{0}^{nc}
ight)^{2}}+rac{\left(1-K_{0}^{nc}
ight)\left(1-2v_{ur}
ight)\left(\lambda^{*}/k^{*}-1
ight)}{\left(1+2K_{0}^{nc}
ight)\left(1-2v_{ur}
ight)\lambda^{*}/k-\left(1-K_{0}^{nc}
ight)\left(1+v_{ur}
ight)}}$$
 (2–65)

For more details see 8 Modified Cam-Clay model (p. 93).

The Cartesian stress components ($\sigma'_{xx,c}$, $\sigma'_{yy,c}$, $\sigma'_{zz,c}$, $\sigma'_{xy,c}$) are transformed to principal stress components ($\sigma'_{1,max_1}, \sigma'_{2_1}, \sigma'_{3_2}$) and the maximum major principal stress, σ'_{1,max_1} is kept as a general state parameter which is available for succeeding phases. In subsequent phases, $\sigma'_{1\,max}$ is updated if the major principal stress is larger than the current one.

If, in later calculation phases, the soil behaviour is changed to an(other) advanced material model, the equivalent pre-consolidation pressure p_n^{eq} is initialised according to the current (updated) principal stress history (σ'_{1max} , σ'_{2} , σ'_{3}).

The stress state at pre-consolidation stress level is expressed in (p, q):

$$p' = -rac{1}{3}igg(1 + 2K_0^{nc}igg)\sigma_p \quad ext{and} \quad ext{q=}(1\text{-}\ K_0^{nc})\sigma_p$$
 (2-66)

The equivalent isotropic pre-consolidation stress is calculated depending on the model used.

Note that OCR and POP are only taken into account in the K_0 -procedure (initial calculation phase). Gravity loading does not consider OCR or POP, and always gives a normallyconsolidated stress state. If an advanced soil model (involving pre-consolidation stress) is activated in a later calculation phase, i.e.

- The corresponding soil cluster is activated for the first time, or
- The material data of a soil is changed from a 'simple'soil model without pre-consolidation stress to an 'advanced'soil model with the pre-consolidation stress as a state parameter

then the stress state at the beginning of that phase is assumed to be normally-consolidated, i.e. the pre-consolidation stress is initiated in accordance with the current stress state. If, in such a case, an overconsolidated stress state is to be modelled, the overconsolidation has to be simulated by applying and removing an overburden load.

2.9 On the initial stresses

In overconsolidated soils the coefficient of lateral earth pressure for the initial stress state is larger than for normally consolidated soils. This effect is automatically taken into account for advanced soil models when generating the initial stresses using the K_0 -procedure. The procedure that is followed here is described below. The procedure is described for the lateral stress in x-direction (σ'_{xx} based on $K_{0,x}$), but a similar procedure is followed for the lateral stress in z-direction (σ'_{zz} based on $K_{0,z}$).

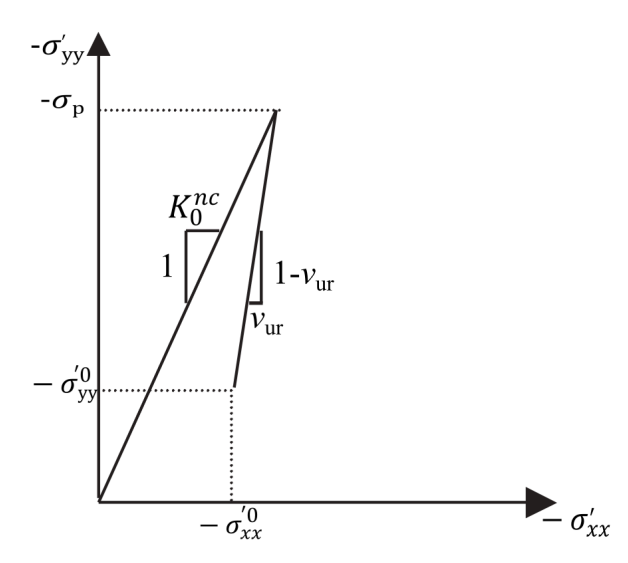


Figure 2-5: Overconsolidated stress state obtained from primary loading and subsequent unloading

Consider a one-dimensional compression test, preloaded to $\sigma'_{yy} = \sigma_p$ and subsequently unloaded to $\sigma'_{yy} = \sigma'_{yy}^{0}$. During unloading the sample behaves elastically and the incremental stress ratio is, according to Hooke's law, given by (see <u>Figure 2–5 (p. 30)</u>):

$$\frac{\Delta \sigma'_{xx}}{\Delta \sigma'_{yy}} = \frac{K_0^{nc} \sigma_p - \sigma'^0_{xx}}{\sigma_p - \sigma'^0_{yy}} = \frac{K_0^{nc} OCR \sigma'^0_{yy} - \sigma'^0_{xx}}{(OCR - 1)\sigma'^0_{yy}} = \frac{v_{ur}}{1 - v_{ur}}$$
(2-67)

where K_0^{nc} is the stress ratio in the normally consolidated state. Hence, the default stress ratio of the overconsolidated soil sample is given by:

$$K_{0,x} = rac{\sigma_{xx}^{\prime 0}}{\sigma_{yy}^{\prime 0}} = K_0^{nc}OCR - rac{v_{ur}}{1 - v_{ur}} igg(OCR - 1 igg)$$
 (2–68)

When using POP as an alternative way to define overconsolidation, the default initial horizontal stress is defined by:

$$\sigma_{xx}^{\prime 0} = K_0^{nc} \sigma_p - \frac{v_{ur}}{1 - v_{ur}} POP$$
 (2–69)

The use of a small Poisson's ratio will lead to a relatively large ratio of lateral stress and vertical stress, as generally observed in overconsolidated soils. Note that Egn. 2-68 (p. 30) and Egn. 2-69 (p. 30) are only valid in the elastic domain, because the formulas are derived from Hooke's law of elasticity. If a soil sample is unloaded by a large amount, resulting in a high degree of overconsolidation, the stress ratio will be limited by the Mohr-Coulomb failure condition.

Note that the above initial stress ratio's are only suggested (default) values, and may be overruled by the user if more precise data are available or if other values seem more appropriate.



Linear Elastic Perfectly Plastic Model (Mohr-Coulomb Model)

Soils behave rather non-linear when subjected to changes of stress or strain. In reality, the stiffness of soil depends at least on the stress level, the stress path and the strain level. Some such features are included in the advanced soil models in PLAXIS. The Mohr-Coulomb model, however, is a simple and well-known linear elastic perfectly plastic model, which can be used as a first approximation of soil behaviour. The linear elastic part of the Mohr-Coulomb model is based on Hooke's law of isotropic elasticity (3.1 Linear Elastic Perfectly - Plastic behaviour (p. 31)). The perfectly plastic part is based on the Mohr-Coulomb failure criterion, formulated in a non-associated plasticity framework.

Plasticity involves the development of irreversible strains. In order to evaluate whether or not plasticity occurs in a calculation, a yield function, f, is introduced as a function of stress and strain. Plastic yielding is related with the condition f=0. This condition can often be presented as a surface in principal stress space. A perfectly-plastic model is a constitutive model with a fixed yield surface, i.e. a yield surface that is fully defined by model parameters and not affected by (plastic) straining. For stress states represented by points within the yield surface, the behaviour is purely elastic and all strains are reversible.

3.1 Linear Elastic Perfectly - Plastic behaviour

The basic principle of elastoplasticity is that strains and strain rates are decomposed into an elastic part and a plastic part:

$$\underline{\varepsilon} = \underline{\varepsilon}^e + \underline{\varepsilon}^p \qquad \qquad \underline{\dot{\varepsilon}} = \underline{\dot{\varepsilon}}^e + \underline{\dot{\varepsilon}}^p$$
 (3-1)

Hooke's law is used to relate the stress rates to the elastic strain rates. Substitution of Eqn. 3-1 (p. 32) into Hooke's law Eqn. 2-30 (p. 18) leads to:

$$\underline{\dot{\sigma}}' = \mathbf{D}^e \, \underline{\dot{\varepsilon}}^e = \, \mathbf{D}^e \big(\underline{\dot{\varepsilon}} - \underline{\dot{\varepsilon}}^p\big)$$
 (3-2)

According to the classical theory of plasticity, plastic strain rates are proportional to the derivative of the yield function with respect to the stresses. This means that the plastic strain rates can be represented as vectors perpendicular to the yield surface. This classical form of the theory is referred to as associated plasticity. However, for Mohr-Coulomb type yield functions, the theory of associated plasticity overestimates dilatancy. Therefore, in addition to the yield function, a plastic potential function q is introduced. The case $q \neq f$ is denoted as nonassociated plasticity. In general, the plastic strain rates are written as:

$$\underline{\dot{\varepsilon}}^p = \lambda \frac{\partial g}{\partial \underline{\sigma}'}$$
 (3–3)

in which λ is the plastic multiplier. For purely elastic behaviour λ is zero, whereas in the case of plastic behaviour λ is positive:

$$\lambda = 0 \ for: \ f < 0 \ or: \ \frac{\partial f^T}{\partial \underline{\sigma}'} \mathbf{D}^e \, \underline{\dot{\varepsilon}} \le 0 \qquad \left(Elasticity\right)$$

$$\lambda > 0 \ for: \ f = 0 \ and: \ \frac{\partial f^T}{\partial \underline{\sigma}'} \mathbf{D}^e \, \underline{\dot{\varepsilon}} > 0 \quad \left(Plasticity\right)$$
(3-4)
$$(3-5)$$

$$\lambda > 0 \; for: \; f = 0 \; \; and: \; \; \; rac{\partial f^T}{\partial \sigma'} oldsymbol{D}^e \, \dot{\underline{arepsilon}} > 0 \; \; \; \left(Plasticity
ight)$$
 (3–5)

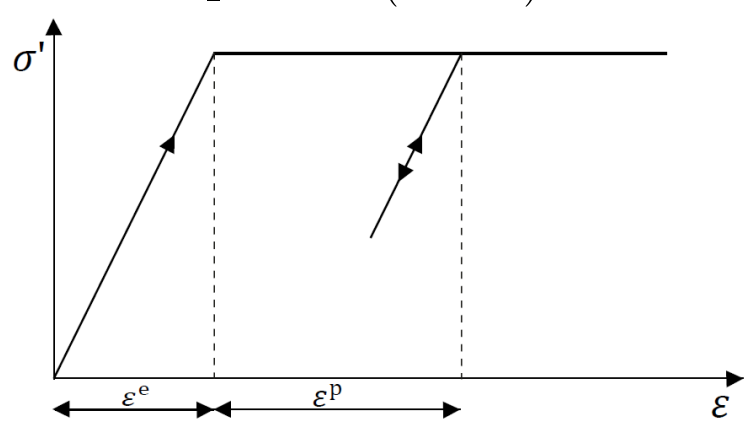


Figure 3-1: Basic idea of an elastic perfectly plastic model

These equations may be used to obtain the following relationship between the effective stress rates and strain rates for elastic perfectly-plastic behaviour (Smith & Griffiths [1982]; Vermeer & Borst [1984]):

$$\underline{\dot{\sigma}}' = \left(\mathbf{D}^e - \frac{\alpha}{d} \mathbf{D}^e \frac{\partial g}{\partial \underline{\sigma}'} \frac{\partial f^T}{\partial \underline{\sigma}'} \mathbf{D}^e \right) \underline{\dot{\varepsilon}}$$
 (3-6)

where:

$$d = \left(rac{\partial f^T}{\partial \underline{\sigma}'} oldsymbol{D}^e rac{\partial g}{\partial \underline{\sigma}'}
ight)$$
 (3–7)

The parameter α is used as a switch. If the material behaviour is elastic, as defined by Eqn. 3-4 (p. 32), the value of α is equal to zero, whilst for plasticity, as defined by Eqn. 3–5 (p. 32), the value of α is equal to unity.

The above theory of plasticity is restricted to smooth yield surfaces and does not cover a multi surface yield contour as present in the full Mohr-Coulomb model. For such a yield surface the theory of plasticity has been extended by Koiter (1960) and others to account for flow vertices involving two or more plastic potential functions:

$$\underline{\dot{\varepsilon}}^p = \lambda_1 \frac{\partial g_1}{\partial \sigma'} + \lambda_2 \frac{\partial g_2}{\partial \sigma'} + \dots \tag{3-8}$$

Similarly, several quasi independent yield functions $(f_1, f_2, ...)$ are used to determine the magnitude of the multipliers ($\lambda_1, \lambda_2, ...$).

3.2 Formulation of the Mohr-Coulomb model

The Mohr-Coulomb yield condition is an extension of Coulomb's friction law to general states of stress. In fact, this condition ensures that Coulomb's friction law is obeyed in any plane within a material element.

The full Mohr-Coulomb yield condition consists of six yield functions when formulated in terms of principal stresses (see for instance Smith & Griffiths, 1982):

$$f_{1a} = \frac{1}{2} (\sigma'_{2} - \sigma'_{3}) + \frac{1}{2} (\sigma'_{2} + \sigma'_{3}) \sin(\phi) - c\cos(\phi) \leq 0 \qquad a)$$

$$f_{1b} = \frac{1}{2} (\sigma'_{3} - \sigma'_{2}) + \frac{1}{2} (\sigma'_{3} + \sigma'_{2}) \sin(\phi) - c\cos(\phi) \leq 0 \qquad b)$$

$$f_{2a} = \frac{1}{2} (\sigma'_{3} - \sigma'_{1}) + \frac{1}{2} (\sigma'_{3} + \sigma'_{1}) \sin(\phi) - c\cos(\phi) \leq 0 \qquad c)$$

$$f_{2b} = \frac{1}{2} (\sigma'_{1} - \sigma'_{3}) + \frac{1}{2} (\sigma'_{1} + \sigma'_{3}) \sin(\phi) - c\cos(\phi) \leq 0 \qquad d)$$

$$f_{3a} = \frac{1}{2} (\sigma'_{1} - \sigma'_{2}) + \frac{1}{2} (\sigma'_{1} + \sigma'_{2}) \sin(\phi) - c\cos(\phi) \leq 0 \qquad e)$$

$$f_{3b} = \frac{1}{2} (\sigma'_{2} - \sigma'_{1}) + \frac{1}{2} (\sigma'_{2} + \sigma'_{1}) \sin(\phi) - c\cos(\phi) \leq 0 \qquad f)$$

The two plastic model parameters appearing in the yield functions are the well-known friction angle φ and the cohesion c. The condition $f_i = 0$ for all yield functions together (where f_i is used to denote each individual yield function) represents a fixed hexagonal cone in principal stress space as shown in Figure 3-2 (p. 33).

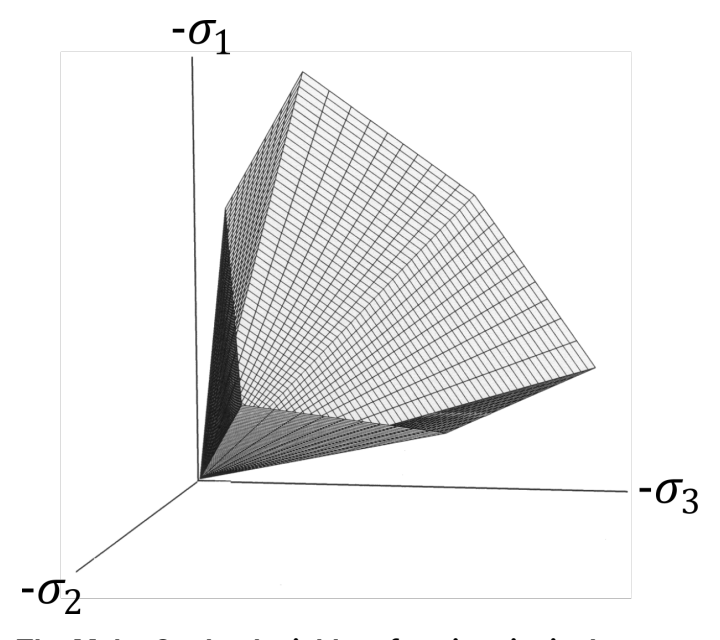


Figure 3–2: The Mohr-Coulomb yield surface in principal stress space (c = 0)

In addition to the yield functions, six plastic potential functions are defined for the Mohr-Coulomb model:

$$\begin{split} g_{1a} &= \frac{1}{2} \left(\sigma'_2 - \sigma'_3 \right) + \frac{1}{2} \left(\sigma'_2 + \sigma'_3 \right) \sin \left(\psi \right) \leq 0 \qquad a) \\ g_{1b} &= \frac{1}{2} \left(\sigma'_3 - \sigma'_2 \right) + \frac{1}{2} \left(\sigma'_3 + \sigma'_2 \right) \sin \left(\psi \right) \leq 0 \qquad b) \\ g_{2a} &= \frac{1}{2} \left(\sigma'_3 - \sigma'_1 \right) + \frac{1}{2} \left(\sigma'_3 + \sigma'_1 \right) \sin \left(\psi \right) \leq 0 \qquad c) \\ g_{2b} &= \frac{1}{2} \left(\sigma'_1 - \sigma'_3 \right) + \frac{1}{2} \left(\sigma'_1 + \sigma'_3 \right) \sin \left(\psi \right) \leq 0 \qquad d) \\ g_{3a} &= \frac{1}{2} \left(\sigma'_1 - \sigma'_2 \right) + \frac{1}{2} \left(\sigma'_1 + \sigma'_2 \right) \sin \left(\psi \right) \leq 0 \qquad e) \\ g_{3b} &= \frac{1}{2} \left(\sigma'_2 - \sigma'_1 \right) + \frac{1}{2} \left(\sigma'_2 + \sigma'_1 \right) \sin \left(\psi \right) \leq 0 \qquad f) \end{split}$$

The plastic potential functions contain a third plasticity parameter, the dilatancy angle ψ . This parameter is required to model positive plastic volumetric strain increments (dilatancy) as actually observed for dense soils. A discussion of all of the model parameters used in the Mohr-Coulomb model is given in the next section.

When implementing the Mohr-Coulomb model for general stress states, special treatment is required for the intersection of two yield surfaces. Some programs use a smooth transition from one yield surface to another, i.e. the rounding-off of the corners (see for example Smith & Griffiths, 1982). In PLAXIS, however, the exact form of the full Mohr-Coulomb model is implemented, using a sharp transition from one yield surface to another. For a detailed description of the corner treatment the reader is referred to the literature (Koiter, 1960; van Langen & Vermeer, 1990).

For c > 0, the standard Mohr-Coulomb criterion allows for tension. In fact, allowable tensile stresses increase with cohesion. In reality, soil can sustain none or only very small tensile stresses. This behaviour can be included in a PLAXIS analysis by specifying a tension cut-off. In this case, Mohr circles with positive principal stresses are not allowed. The tension cut-off introduces three additional yield functions, defined as:

$$egin{align} f_4 &= {\sigma'}_1 - \sigma_t \leq 0 & a) \ f_5 &= {\sigma'}_2 - \sigma_t \leq 0 & b) \ f_6 &= {\sigma'}_3 - \sigma_t \leq 0 & c) \ \end{array}$$

When this tension cut-off procedure is used, the allowable tensile stress, σ_t , is, by default, taken equal to zero, but this value can be changed by the user. For these three yield functions an associated flow rule is adopted.

For stress states within the yield surface, the behaviour is elastic and obeys Hooke's law for isotropic linear elasticity, as discussed in . Hence, besides the plasticity parameters c, φ , and ψ , input is required on the elastic Young's modulus E and Poisson's ratio v. The model described here is officially called the linear elastic perfectly plastic model with Mohr-Coulomb failure criterion. For simplicity, this model is called the Mohr-Coulomb model in PLAXIS.

3.3 Parameters of the Mohr-Coulomb model

The linear elastic perfectly-plastic Mohr-Coulomb model requires a total of five parameters, 2 stiffness parameters and 3 strength parameters, which are generally familiar to most geotechnical engineers and which can be obtained from basic tests on soil samples. The stiffness parameters with their standard units are:

E _{ref}	Young's modulus	[kN/m ²]
V	Poisson's ratio	[-]

Instead of using the Young's modulus as a stiffness parameter, alternative stiffness parameters can be entered. These parameters with their standard units are listed below:

G	Shear modulus	[kN/m ²]
E _{oed}	Oedometer modulus	[kN/m ²]

The strength parameters of the Mohr-Coulomb model are:

С	Cohesion	[kN/m ²]
φ	Friction angle	[°]
Ψ	Dilatancy angle	[°]
σ_t	Tension cut-off and tensile strength	[kN/m ²]

Parameters can either be effective parameters (indicated by a prime sign (')) or undrained parameters (indicated by a subscript u), depending on the selected drainage type.

[ULT] In the case of dynamic applications, alternative and/or additional parameters may be used to define stiffness based on wave velocities. These parameters are listed below:

V _P	Compression wave velocity	[m/s]
V _S	Shear wave velocity	[m/s]

3.3.1 Young's modulus (E)

PLAXIS uses the Young's modulus as the basic stiffness modulus in the elastic model and the Mohr-Coulomb model, but some alternative stiffness moduli are displayed as well. A stiffness modulus has the dimension of stress. The values of the stiffness parameter adopted in a calculation require special attention as many geomaterials show a non-linear behaviour from the very beginning of loading. In triaxial testing of soil samples the initial slope of the stress-strain curve (tangent modulus) is usually indicated as E_0 and the secant modulus at 50% strength is denoted as E_{50} (see Figure 3-3 (p. 36)). For materials with a large linear elastic range it is realistic to use E_0 , but for loading of soils one generally uses E_{50} . Considering unloading problems, as in the case of tunnelling and excavations, one needs an unload-reload modulus (E_{ur}) instead of E_{50} .

For soils, both the unloading modulus, E_{ur} , and the first loading modulus, E_{50} , tend to increase with the confining pressure. Hence, deep soil layers tend to have greater stiffness than shallow layers. Moreover, the observed stiffness depends on the stress path that is followed. The stiffness is much higher for unloading and reloading than for primary loading. Also, the observed soil stiffness in terms of a Young's modulus may be lower for (drained) compression than for shearing. Hence, when using a constant stiffness modulus to represent soil behaviour one should choose a value that is consistent with the stress level and the stress path development. Note that some stress-dependency of soil behaviour is taken into account in the advanced models in PLAXIS which are described in subsequent chapters. For the Mohr-Coulomb model, PLAXIS offers a special option for the input of a stiffness increasing with depth (see 3.4 Depthdependency (p. 40)). Note that for material data sets where the drainage type is set to Undrained (A) or Undrained (B), Young's modulus has the meaning of an effective Young's modulus, whilst PLAXIS automatically takes care of the incompressibility (2.4 Undrained effective stress analysis (effective stiffness parameters) (p. 19)).

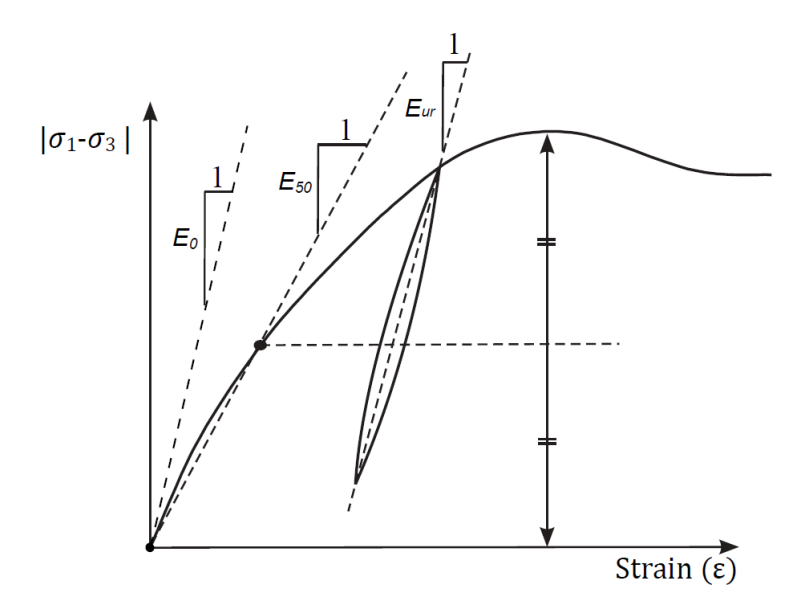


Figure 3–3: Definition of E_{0} , E_{50} and E_{ur} for drained triaxial test results

3.3.2 Poisson's ratio (v)

Standard drained triaxial tests may yield a significant rate of volume decrease at the very beginning of axial loading and, consequently, a low initial value of Poisson's ratio (v_0) . For some cases, such as particular unloading problems, it may be realistic to use such a low initial value, but in general when using the Mohr-Coulomb model the use of a higher value is recommended.

The selection of a Poisson's ratio is particularly simple when the elastic model or Mohr-Coulomb model is used for gravity loading under conditions of one-dimensional compression. For this type of loading PLAXIS should give realistic ratios of $K_0 = \sigma'_h / \sigma'_v$.

As both models will give the well-known ratio of $\sigma'_h / \sigma'_v = v / (1 - v)$ for one-dimensional compression it is easy to select a Poisson's ratio that gives a realistic value of K_0 . Hence, v is evaluated by matching K_0 . In many cases one will obtain ν values in the range between 0.3 and 0.4. In general, such values can also be used for loading conditions other than one-dimensional compression. Please note that in this way it is not possible to create K_0 values larger than 1, as may be observed in highly overconsolidated stress states. For unloading conditions, however, it is more appropriate to use values in the range between 0.15 and 0.25.

Further note that for material data sets where the drainage type is set to *Undrained (A)* or Undrained (B), Poisson's ratio has the meaning of an effective Poisson's ratio, whilst PLAXIS automatically takes care of the incompressibility (2.4 Undrained effective stress analysis (effective stiffness parameters) (p. 19)). To ensure that the soil skeleton is much more compressible than the pore water, the effective Poisson's ratio should be smaller than 0.35 for Undrained (A) or Undrained (B) materials.

3.3.3 Shear modulus (G)

The shear modulus, G, has the dimension of stress. According to Hooke's law, the relationship between Young's modulus E and the shear modulus is given by (see Egn. 2-31 (p. 18) a)):

$$G=rac{E}{2(1+v)}$$
 (3–12)

Entering a particular value for one of the alternatives G or E_{oed} results in a change of the E modulus whilst v remains the same.

3.3.4 Oedometer modulus (E_{oed})

The oedometer modulus, E_{oed} , or constrained modulus, has the dimension of stress. According to Hooke's law, the relationship between Young's modulus E and the oedometer modulus is given by (see Eqn. 2-31 (p. 18) c)).

$$E_{oed} = rac{(1-v)E}{(1-2v)(1+v)}$$
 (3–13)

Entering a particular value for one of the alternatives G or E_{oed} results in a change of the Emodulus whilst v remains the same.

3.3.5 Compression wave velocity V_n [ULT]

The compression wave velocity, V_D , in a confined one-dimensional soil is a function of stiffness, E_{oed} , and the mass density, ρ , as:

in which γ_{unsat} is the total unsaturated unit weight and g is the gravity acceleration (9.8 m/s²).}

3.3.6 Shear wave velocity V_s [ULT]

The shear wave velocity, V_s , in a confined one-dimensional soil is a function of shear stiffness, G, and the mass density, ρ , as:

in which γ_{unsat} is the total unsaturated unit weight and g is the gravity acceleration (9.8 m/s²).

3.3.7 Cohesion (c) or undrained shear strength (s_{ij})

The cohesive strength has the dimension of stress. In the Mohr-Coulomb model, the cohesion parameter may be used to model the effective cohesion c' of the soil (cohesion intercept), in combination with a realistic effective friction angle φ' (see Figure 3-4 (p. 38) (a)). This may not only be done for drained soil behaviour, but also if the type of material behaviour is set to Undrained (A), as in both cases PLAXIS will perform an effective stress analysis. Alternatively, the cohesion parameter may be used to model the undrained shear strength s_u of the soil, in combination with $\varphi = \varphi_u = 0$ when the Drainage type is set to Undrained (B) or Undrained (C) In that case the Mohr-Coulomb failure criterion reduces to the well-known Tresca criterion. PLAXIS allows for an increase of shear strength with depth using the $s_{u,inc}$ parameter (3.4) Depth-dependency (p. 40)).

The disadvantage of using effective strength parameters c' and ϕ' in combination with the drainage type being set to Undrained (A) is that the undrained shear strength as obtained from the model may deviate from the undrained shear strength in reality because of differences in the actual stress path being followed. In this respect, advanced soil models generally perform better than the Mohr-Coulomb model, but in all cases it is recommended to compare the resulting stress state in all calculation phases with the present shear strength in reality $(|\sigma_1 - \sigma_3| \le 2 s_u)$.

On the other hand, the advantage of using effective strength parameters is that the change in shear strength with consolidation is obtained automatically, although it is still recommended to check the resulting stress state after consolidation.

The advantage of using the cohesion parameter to model undrained shear strength in combination with $\varphi = 0$ (Undrained (B) or Undrained (C)) is that the user has direct control over the shear strength, independent of the actual stress state and stress path followed. Please note that this option may not be appropriate when using advanced soil models.

PLAXIS can handle cohesionless sands (c = 0), but some options may not perform well. To avoid complications, non-experienced users are advised to enter at least a small value in soil layers near the ground surface (use c > 0.2 kPa). Please note that a positive value for the cohesion may lead to a tensile strength, which may be unrealistic for soils. By default, the Tension cut-off option is used to reduce the tensile strength.

PLAXIS offers a special option for the input of layers in which the cohesion increases with depth (see 3.4 Depth-dependency (p. 40)).

3.3.8 Friction angle (φ)

The friction angle φ (phi) is entered in degrees. In general the friction angle is used to model the effective friction of the soil, in combination with an effective cohesion c' (Figure 3-4 (p. 38) (a)). This may not only be done for drained soil behaviour, but also if the type of material behaviour is set to Undrained (A), since in both cases PLAXIS will perform an effective stress analysis. Alternatively, the soil strength is modelled by setting the cohesion parameter equal to the undrained shear strength of the soil, in combination with $\varphi = 0$ (Undrained (B) or Undrained (C)) (Figure 3-4 (p. 38) (b)). In that case the Mohr-Coulomb failure criterion reduces to the well-known Tresca criterion.

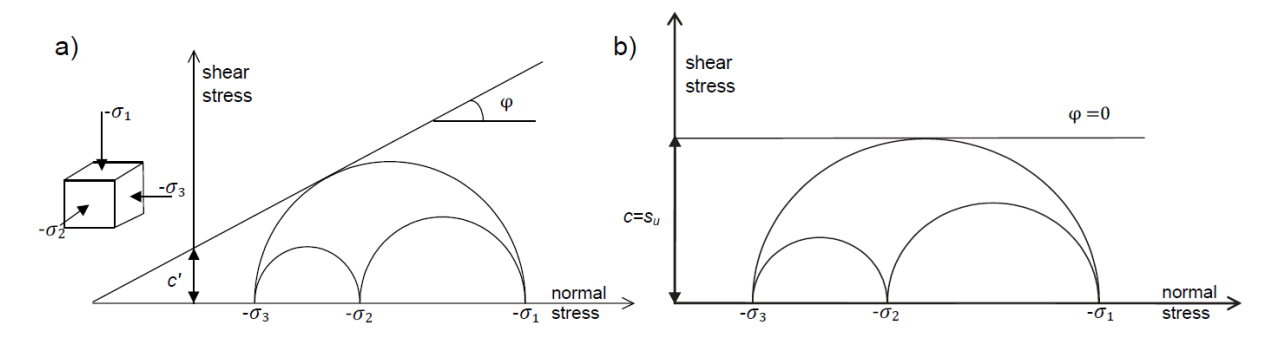


Figure 3-4: Stress circles at yield; one touches Coulomb's envelope. a) Using effective strength parameters (Mohr-Coulomb) - b) Using undrained strength parameters (Tresca).

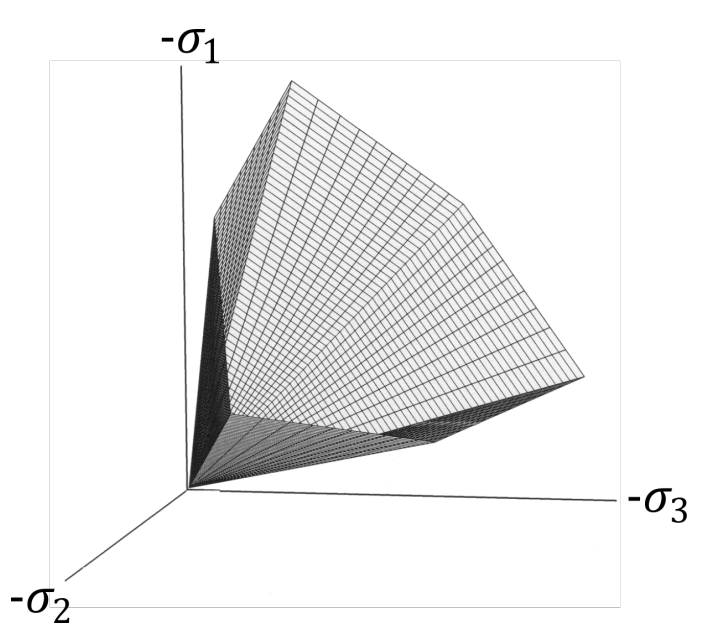


Figure 3-5: Failure surface in principal stress space for cohesionless soil

High friction angles, as sometimes obtained for dense sands, will substantially increase plastic computational effort. Moreover, high friction may be subjected to strain-softening behaviour, which means that such high friction angles are not sustainable under (large) deformation. Hence, high friction angles should be avoided when performing preliminary computations for a particular project*. The friction angle largely determines the shear strength as shown in Figure 3-4 (p. 38) by means of Mohr's stress circles. A more general representation of the yield criterion is shown in Figure 3-5 (p. 39). The Mohr-Coulomb failure criterion proves to be better for describing soil strength for general stress states than the Drucker-Prager approximation.

1 Note: *The friction angles are in the order of 20 - 30 degrees for clay and silt (the more plastic the clay, the lower the friction), and 30 - 40 degrees for sand and gravel (the denser the sand, the higher the friction).

3.3.9 Dilatancy angle (ψ)

The dilatancy angle, ψ (psi), is specified in degrees. Apart from heavily overconsolidated layers, clay soils tend to show little dilatancy ($\psi \approx 0$). The dilatancy of sand depends on both the density and the friction angle. In general the dilatancy angle of soils is much smaller than the friction angle. For quartz sands the order of magnitude is $\psi \approx \varphi - 30^\circ$. For φ -values of less than 30°, however, the angle of dilatancy is mostly zero. A small negative value for ψ is only realistic for extremely loose sands. In the Hardening Soil model or Hardening Soil model with small-strain stiffness the end of dilatancy, as generally observed when the soil reaches the critical state, can be modelled using the Dilatancy cut-off. However, this option is not available for the Mohr-Coulomb model. For further information about the link between the friction angle and dilatancy, see Bolton (1986)..

A positive dilatancy angle implies that in drained conditions the soil will continue to dilate as long as shear deformation occurs. This is clearly unrealistic, as most soils will reach a critical state at some point and further shear deformation will occur without volume changes. In undrained conditions a positive dilatancy angle, combined with the restriction on volume changes, leads to a generation of tensile pore stresses. In an undrained effective stress analysis therefore the strength of the soil may be overestimated.

When the soil strength is modelled as undrained shear strength, s_u , and $\varphi = 0$, (Undrained (B) or Undrained (C)) the dilatancy angle is automatially set to zero. Great care must be taken when using a positive value of dilatancy in combination with drainage type set to Undrained (A). In that case the model will show unlimited soil strength due to tensile pore stresses. These tensile pore stresses can be limited by setting the cavitation cut-off.

3.3.10 Tension cut-off

In some practical problems an area with tensile stresses may develop. According to the Coulomb envelope shown in Figure 3-4 (p. 38) this is allowed when the shear stress (radius of Mohr circle) is sufficiently small. However, the soil surface near a trench in clay sometimes shows tensile cracks. This indicates that soil may also fail in tension instead of in shear. Such behaviour can be included in a PLAXIS analysis by selecting the tension cut-off. In this case Mohr circles with positive principal stresses are not allowed. When selecting the tension cut-off the allowable tensile strength may be entered. For the Mohr-Coulomb model the tension cut-off is, by default, selected with a tensile strength of zero.

3.4 Depth-dependency

The advanced features comprise the increase of stiffness and cohesive strength with depth and the use of a tension cut-off. In fact, the latter option is used by default, but it may be deactivated here, if desired. These parameters are defined in the Depth-dependency blocks on the Mechanical tabsheet of the Soil window.

3.4.1 Increase of stiffness (E_{inc})

In real soils, the stiffness depends significantly on the stress level, which means that the stiffness generally increases with depth. When using the Mohr-Coulomb model, the stiffness is a constant value. In order to account for the increase of the stiffness with depth the E_{inc} -value may be used, which is the increase of the Young's modulus per unit of depth (expressed in the unit of stress per unit depth). At the level given by the y_{ref} parameter, and above, the stiffness is equal to the reference Young's modulus, E_{ref} , as entered on the **Mechanical** tabsheet. Below, the stiffness is given by:

$$E(y) = E_{ref} + (y_{ref} - y)E_{inc}$$
 $(y < y_{ref})$ (3–16)

where y represents the vertical direction. The actual value of Young's modulus in the stress points is obtained from the reference value and E_{inc} . Note that during calculations a stiffness increasing with depth does not change as a function of the stress state.

Note: Note that in PLAXIS 3D the vertical coordinate is z instead of y.

3.4.2 Increase of cohesion or shear strength with depth (c_{inc} or $s_{u.inc}$)

PLAXIS offers an advanced option for the input of clay layers in which the cohesion, c, (or undrained shear strength, s_u) increases with depth. In order to account for the increase of the cohesion with depth the cinc-value may be used, which is the increase of cohesion per unit of depth (expressed in the unit of stress per unit depth). At the level given by the y_{ref} parameter, and above, the cohesion is equal to the (reference) cohesion, c_{ref} , as entered on the **Mechanical** tabsheet. Below, the cohesive strength is given by:

$$c(y) = c_{ref} + (y_{ref} - y)c_{inc} \quad (y < y_{ref}) \quad a)$$
 $s_u(y) = s_{u,ref} + (y_{ref} - y)s_{u,inc} \quad (y < y_{ref}) \quad b)$ (3-17)

where v represents the vertical direction. Note that when using effective strength properties $(\varphi'>0)$ it is generally not necessary to use an increase of cohesion with depth, since the friction together with the initial effective stress will result in an increasing shear strength with depth.

3.5 On the use of the Mohr-Coulomb model in dynamics calculations [ULT]

When using the Mohr-Coulomb model in dynamics calculations, the stiffness parameters need to be selected such that the model correctly predicts wave velocities in the soil (Eqn. 3-14 (p. 37) and Eqn. 3-15 (p. 37)). This generally requires a much larger small strain stiffness rather than a stiffness at engineering strain levels. When subjected to dynamic or cyclic loading, the Mohr-Coulomb model may generate plastic strains if stress points reach the Mohr-Coulomb failure criterion, which will lead to damping in dynamics calculations. However, it should be noted that the stress cycles within the Mohr-Coulomb failure contour will only generate elastic strains and no (hysteretic) damping, nor accumulation of strains or pore pressure or liquefaction. In order to simulate the soil's damping characteristics in cyclic loading, Rayleigh damping may be defined.

The Hoek-Brown model (rock behaviour)

The material behaviour of rock differs from the behaviour of soils in the sense that it is generally stiffer and stronger. The dependency of the stiffness on the stress level is almost negligible, so stiffness of rocks can be considered constant. On the other hand, the dependency of the (shear) strength on the stress level is significant. In this respect, heavily jointed or weathered rock can be regarded a frictional material. A first approach is to model the shear strength of rock by means of the Mohr-Coulomb failure criterion. However, considering the large range of stress levels where rock may be subjected to, a linear stress-dependency, as obtained from the Mohr-Coulomb model, is generally not sufficient. Furthermore, rock may also show a significant tensile strength. The Hoek-Brown failure criterion is a better non-linear approximation of the strength of rocks. It involves shear strength as well as tensile strength in a continuous formulation. Together with Hooke's law of isotropic linear elastic behaviour it forms the Hoek-Brown model for rock behaviour. The 2002 edition of this model (Hoek, Carranza-Torres & Corkum, 2002) has been implemented in PLAXIS 2D to simulate the isotropic behaviour of rock-type materials. The implementation of the model, including the material strength factorization, is based on Bentz, Schwab, Vermeer &Kauther, (2007). More background information on the Hoek-Brown model and the selection of model parameters can be found in Hoek, 2006. For anisotropic behaviour of stratified rock reference is made to 5 The Jointed Rock model (anisotropy) (p. 54).

4.1 Formulation of the Hoek-Brown model

The generalised Hoek-Brown failure criterion can be formulated as a non-linear relationship between the major and minor effective principal stresses (considering tension positive and compression negative):

$$\sigma_1'=\sigma_3'-|\sigma_{ci}|igg(m_brac{\sigma_3'}{\sigma_{ci}}+sigg)^a$$
 (4–1)

where m_b is a reduced value of the intact rock parameter m_i , which also depends on the Geological Strength Index (GSI) and the Disturbance Factor (D):

$$m_b = m_i \exp\left(\frac{GSI - 100}{28 - 14D}\right)$$
 (4-2)

s and a are auxiliary material constants for the rock mass, that can be expressed as:

$$s = \exp\left(\frac{GSI - 100}{9 - 3D}\right) \tag{4-3}$$

$$a = \frac{1}{2} + \frac{1}{6} \left[\exp\left(\frac{-GSI}{15}\right) - \exp\left(\frac{-20}{3}\right) \right] \tag{4-4}$$

 σ_{ci} is the uni-axial compressive strength of the intact rock material (defined as a positive value). From this value, the uni-axial compressive strength of the specific rock under consideration, σ_c , can be obtained by:

$$\sigma_c = -|\sigma_{ci}|s^a \tag{4-5}$$

The tensile strength of the specific rock under consideration, σ_t , can be obtained by:

$$\sigma_t = \frac{s \left| \sigma_{ci} \right|}{m_b} \tag{4-6}$$

The Hoek-Brown failure criterion is illustrated in Figure 4-1 (p. 43).

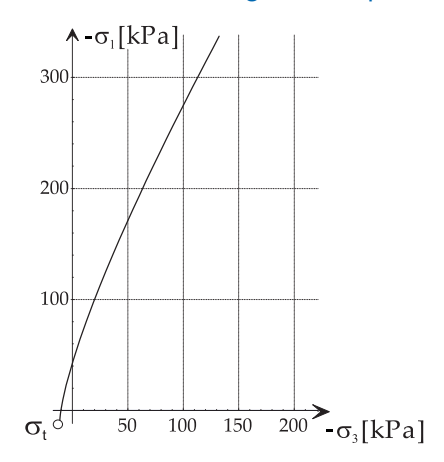


Figure 4-1: Hoek-Brown failure criterion in principal stresses

In the framework of plasticity theory, the Hoek-Brown failure criterion is reformulated into the following yield function:

$$f_{HB}=\sigma_1'-\sigma_3'+ar{f}ig(\sigma_3'ig)\quad where \quad ar{f}ig(\sigma_3'ig)=|\sigma_{ci}|igg(m_brac{-\sigma_3'}{|\sigma_{ci}|}+sigg)^a$$
 (4–7)

For general three-dimensional stress states, more than one yield function is required to deal with the corners of the yield contour, similar to the full Mohr-Coulomb criterion. Defining compression as negative and considering ordering of principal stresses such that $\sigma'_{1} \leq \sigma'_{2} \leq \sigma'_{3}$, the full criterion can be captured by two yield functions:

$$f_{HB,13} = \sigma_1' - \sigma_3' + ar{f}(\sigma_3') \quad where \quad ar{f}(\sigma_3') = |\sigma_{ci}| igg(m_b rac{-\sigma_3'}{|\sigma_{ci}|} + sigg)^a$$
 (4–8)

$$f_{HB,12} = \sigma_1' - \sigma_3' + \overset{-}{f}(\sigma_2') \quad where \quad \overset{-}{f}(\sigma_2') = |\sigma_{ci}| igg(m_b rac{-\sigma_2'}{|\sigma_{ci}|} + sigg)^a$$
 (4–9)

The full Hoek-Brown failure contour ($f_i = 0$) in principal stress space is illustrated in Figure 4–2 (p. 44).

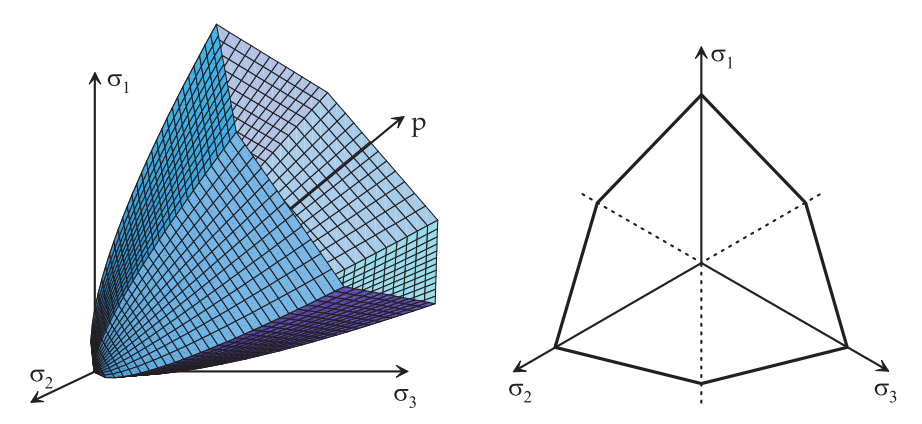


Figure 4-2: The Hoek-Brown failure contour in principal stress space

In addition to the two yield functions, two corresponding plastic potential functions are defined for the Hoek-Brown model:

$$g_{HB,13}=S_1-\left(rac{1+\sin\left(\psi_{mob}
ight)}{1-\sin\left(\psi_{mob}
ight)}
ight)S_3$$
 (4–10)

$$g_{HB,12}=S_1-\left(rac{1+\sin\left(\psi_{mob}
ight)}{1-\sin\left(\psi_{mob}
ight)}
ight)S_2$$
 (4–11)

where S_i are the transformed stresses, defined as:

$$S_i = \left(rac{-\sigma_i}{m_b|\sigma_{ci}|} + rac{s}{m_b^2}
ight) ~~~ for~~~~i=1,2,3$$
 (4–12)

 ψ_{mob} is the mobilised dilatancy angle, varying with σ'_3 from its input value at (σ'_3 = 0) down to zero at $-\sigma'_3 = \sigma_{\psi}$ and beyond:

$$\psi_{mob}=rac{\sigma_{\psi}+\sigma_{3}'}{\sigma_{\psi}}\psi\geq0 \ \left(0\geq-\sigma_{3}'\geq\sigma_{\psi}
ight)$$
 (4–13)

Moreover, in order to allow for plastic expansion in the tensile zone, an increased artificial value of the mobilised dilatancy is used:

$$\psi_{mob}=\psi+rac{\sigma_3'}{\sigma_t}(90^o-\psi) \qquad \left(\sigma_t'\geq\sigma_3'\geq0
ight)$$
 (4–14)

The evolution of the mobilised dilatancy angle as a function of σ'_3 is visualized in Figure 4–3 (p. 45).

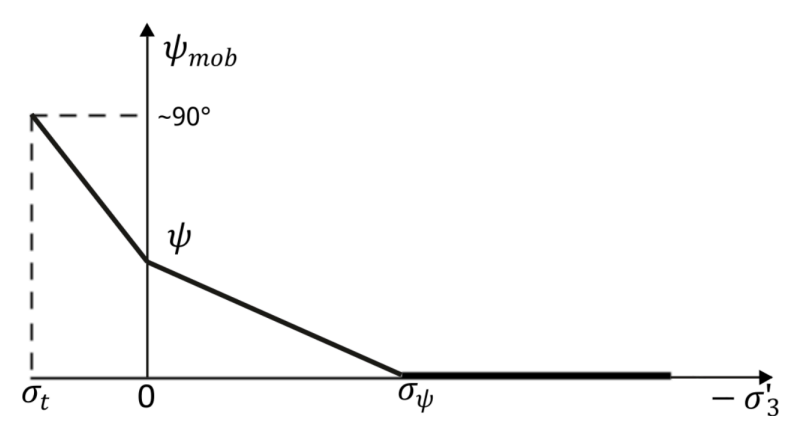


Figure 4-3: Evolution of mobilised dilatancy angle

Regarding the elastic behaviour of the Hoek-Brown model, Hooke's law of isotropic linear elastic behaviour, as described in 2.3 Elastic strains (p. 18), is adopted. This part of the model involves Young's modulus, E, representing the in-situ stiffness of the jointed rock mass before failure, and Poisson's ratio, v, describing transverse straining.

4.2 Conversion of Hoek-Brown to Mohr-Coulomb

In order to compare the Hoek-Brown failure criterion with the well-known Mohr-Coulomb failure criterion for practical applications involving a particular stress range, a balanced fit can be made for confining stresses in the range (considering tension positive and compression negative):

$$-\sigma_t < \sigma_3' < -\sigma_{3\max}'$$

This gives the following expressions for the Mohr-Coulomb effective strength parameters φ' and c' (Hoek, E., C. Carranza-Torres, B. Corkum, et al(2002)).

$$\sin(\phi t) = rac{6am_b(s + m_b\sigma_{3n}')^{a-1}}{2(1+a)(2+a) + 6am_b(s + m_b\sigma_{3n}')^{a-1}}$$
 (4-15)

$$\sin(\phi') = \frac{6am_b(s + m_b\sigma'_{3n})^{a-1}}{2(1+a)(2+a) + 6am_b(s + m_b\sigma'_{3n})^{a-1}}
c' = \frac{|\sigma_{ci}|[(1+2a)s + (1-a)m_b\sigma'_{3n}](s + m_b\sigma'_{3n})^{a-1}}{(1+a)(2+a)\sqrt{1 + \frac{(6am_b(s + m_b\sigma'_{3n})^{a-1})}{((1+a)(2+a))}}}$$
(4-15)

where $\sigma'_{3n} = -\sigma'_{3max}/|\sigma_{ci}|$ The upper limit of the confining stress, σ'_{3max} , depends on the application.

4.3 Parameters of the Hoek-Brown model

The Hoek-Brown model involves a total of 8 parameters, which are generally familiar to geologists and mining engineers. These parameters with their standard units are listed below:

E _{rm}	The rock mass Young's modulus	[kN/m ²]
ν	Poisson's ratio	[-]
$ \sigma_{ci} $	Uni-axial compressive strength of the intact rock (>0)	[kN/m ²]

m _i	Intact rock parameter	[-]
GSI	Geological Strength Index	[-]
D	Disturbance factor	[-]
Ψ _{max}	Dilatancy angle (at $\sigma'_3 = 0$)	[°]
σ ψ	Absolute value of confining pressure σ'_3 at which ψ = 0°	[kN/m ²]

On the Mechanical tabsheet the rock mass intrinsic parameters are also displayed:

m _b	Rock mass parameter	[-]
s	Rock mass parameter	[-]
а	Rock mass parameter	[-]
σ_t	Rock mass tensile strength	[kN/m ²]
$\sigma_{\scriptscriptstyle C}$	Rock mass uni-axial compressive strength	[kN/m ²]

Note: Note that it is common in rock mechanics to express E, σ_{ci} and σ_{tli} ; in the unit MPa (megaPascal = MN/m²), whereas the input values in PLAXIS are given in standard units as defined in the project properties.

The Hoek-Brown model is the most used failure criterion for rock masses, nevertheless there are some uncertainties regarding the input parameters that require a consolidated experience. For this reason, PLAXIS implements in the side panel of the Mechanical tabsheet of the Hoek-Brown model a pre-processing tool to guide the user in the determination of the rock mass strength and stiffness parameters.

- Analysis: shows the Hoek-Brown failure envelope in the plane of principal effective stresses σ'_3 - σ'_4 , in order to visualise the effects of changing of rock mass parameters on the failure
- The second tabsheet is specific to determine the parameter $|\sigma_{ci}|$, m_i , GSI and D. More details are given below.

4.3.1 The rock mass Young's modulus E_{rm}

In principle, Young's modulus can be measured from axial compression tests or direct shear tests on rock samples. However, this modulus is more applicable to the intact rock material, and should be reduced to obtain a representative stiffness of the in-situ rock mass. The rock mass Young's modulus E_{rm} is assumed to be a constant value for the considered rock layer. The rock mass stiffness E_{rm} can be estimated through one of the suggested empirical correlations.

• Generalised Hoek & Diederichs (2006):

$$E_{rm} = E_i igg(0.02 + rac{1 - D/2}{1 + e^{(60 + 15D - GSI)/11}} igg)$$
 (4–17)

where

 E_i The intact rock modulus. GSI Geological strength Index.

DDisturbance factor.

When no direct values of the intact rock modulus E_i are available or where undisturbed sampling for measurement of E_i is difficult, it is possible to estimate the intact rock modulus from the following relationship:

$$E_i = MR\sigma_{ci}$$
 (4–18)

where

MRThe Modulus Ratio originally proposed by <u>Deere, 1968</u> and reported in <u>Table</u> 4–1 (p. 47) and σ_{ci} is the uni-axial compressive strength.

Table 4-1: Guidelines for the selection of modulus ratio (MR) values (Hoek & Diederichs (2006))

Name	Rock type	Texture	MR	MR±
Agglomerate	Igneous	Coarse	500	100
Amphibolites	Metamorphic	Medium	450	50
Andesite	Igneous	Medium	400	100
Anhydrite	Sedimentary	Fine	350	0
Basalt	Igneous	Fine	350	100
Breccia	Igneous	Medium	500	0
Breccia	Sedimentary	Coarse	290	60
Chalk	Sedimentary	Very fine	1000	0
Claystones	Sedimentary	Very fine	250	50
Conglomerates	Sedimentary	Coarse	350	50
Crystalline limestone	Sedimentary	Coarse	500	100
Dacite	Igneous	Fine	400	50
Diabase	Igneous	Fine	325	25
Diorite	Igneous	Medium	325	25
Dolerite	Igneous	Medium	350	50
Dolomites	Sedimentary	Very fine	425	75
Gabbro	Igneous	Coarse	450	50
Gneiss	Metamorphic	Fine	525	225
Granite	Igneous	Coarse	425	125
Granodiorite	Igneous	Coarse, Medium	425	25
Greywackes	Sedimentary	Fine	350	0
Gypsum	Sedimentary	Medium	350	0

Name	Rock type	Texture	MR	MR±
Hornfels	Metamorphic	Medium	550	150
Marble	Metamorphic	Coarse	850	150
Marls	Sedimentary	Very fine	175	25
Metasandstone	Metamorphic	Medium	250	50
Mictric limestones	Sedimentary	Fine	900	100
Migmatite	Metamorhpic	Coarse	375	25
Norite	Igneous	Coarse, Medium	375	25
Peridotite	Igneous	Very fine	275	25
Phyllites	Metamorhpic	Fine	550	250
Porphyries	Igneous	Coarse, Medium	400	0
Quartzites	Metamorhpic	Fine	375	75
Rhyolite	Igneous	Medium	400	100
Sandstones	Sedimentary	Medium	275	75
Schists	Metamorhpic	Medium	675	425
Shales	Sedimentary	Very fine	200	50
Siltstones	Sedimentary	Fine	375	25
Slates	Metamorhpic	Very fine	500	100
Sparitic limestones	Sedimentary	Medium	700	100
Tuff	Igneous	Fine	300	100

Simplified Hoek & Diederichs (2006) that depends only in GSI and D:

$$E_{rm}(MPa) = 100000 igg(rac{1 - D/2}{1 + e^{((75 + 25D - GSI)/11)}} igg)$$
 (4–19)

Note that the input of Young's modulus in PLAXIS is generally in kN/m^2 (= $kPa = 10^{-3} MPa$), which means that the value obtained from the above formula must be multiplied by 10^3 .

4.3.2 Poisson's ratio v

Poisson's ratio, v, is generally in the range of 0.1 - 0.4. Typical values for particular rock types are listed in Figure 4-4 (p. 49).

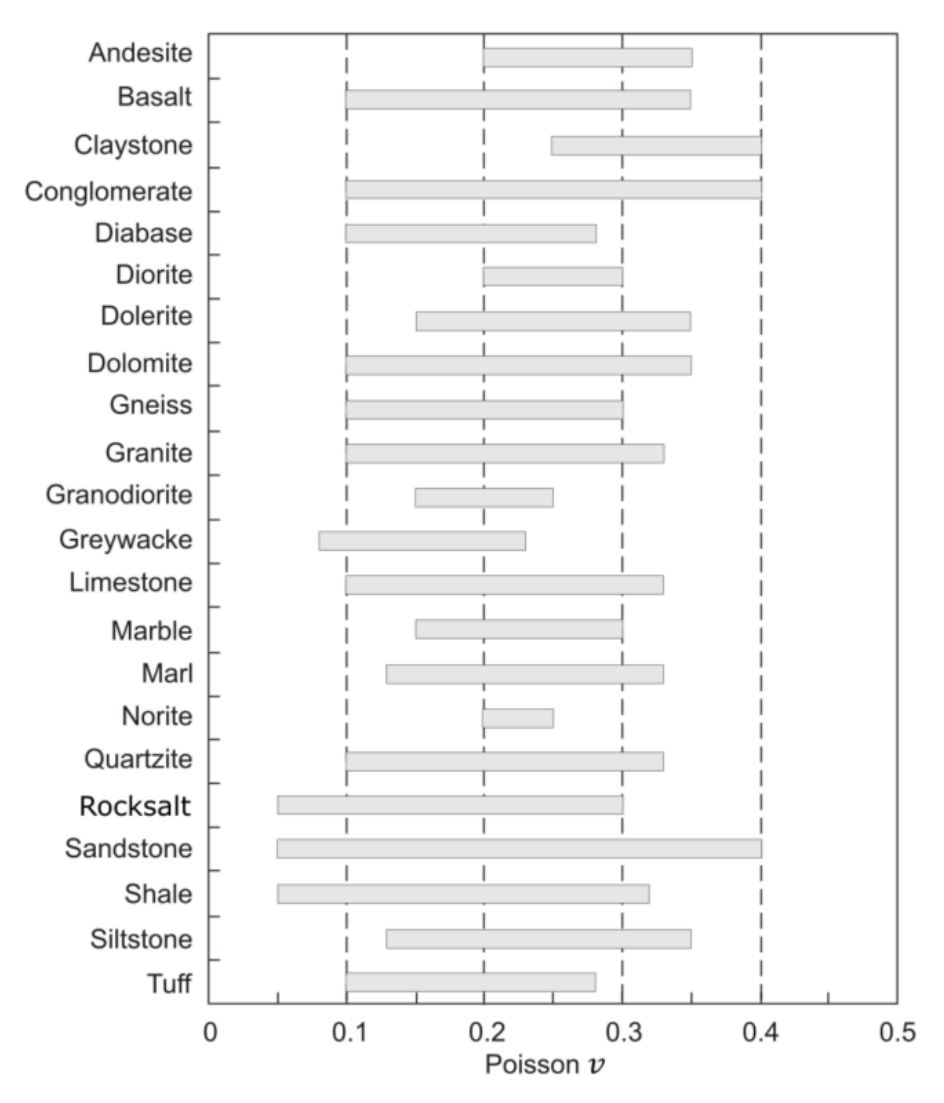


Figure 4-4: Typical Poisson's ratio values

4.3.3 Uni-axial compressive strength of intact rock $|\sigma_{ci}|$

The uni-axial strength of intact rock $|\sigma_{ci}|$ can be determined in laboratory testing, e.g. axial compression. Laboratory testing is often conducted on intact rock so that GSI = 100 and D = 0. In accordance with estimation methods generally executed in the field (i.e. geological hammer, pocket knife), typical values are reported in the side panel of the pre-processing tool.

4.3.4 Intact rock parameter m_i

The intact rock parameter m_i is an empirical model parameter. Typical values are given in the side panel of the pre-processing tool which are based on the rock type as reported by Marinos & Hoek (2001) and Wyllie & Mah (2004) (see also Reference Manual - Chapter 6 - Hoek-Brown pre-processing tool - Table: Values of the constant m_i for intact rock.)

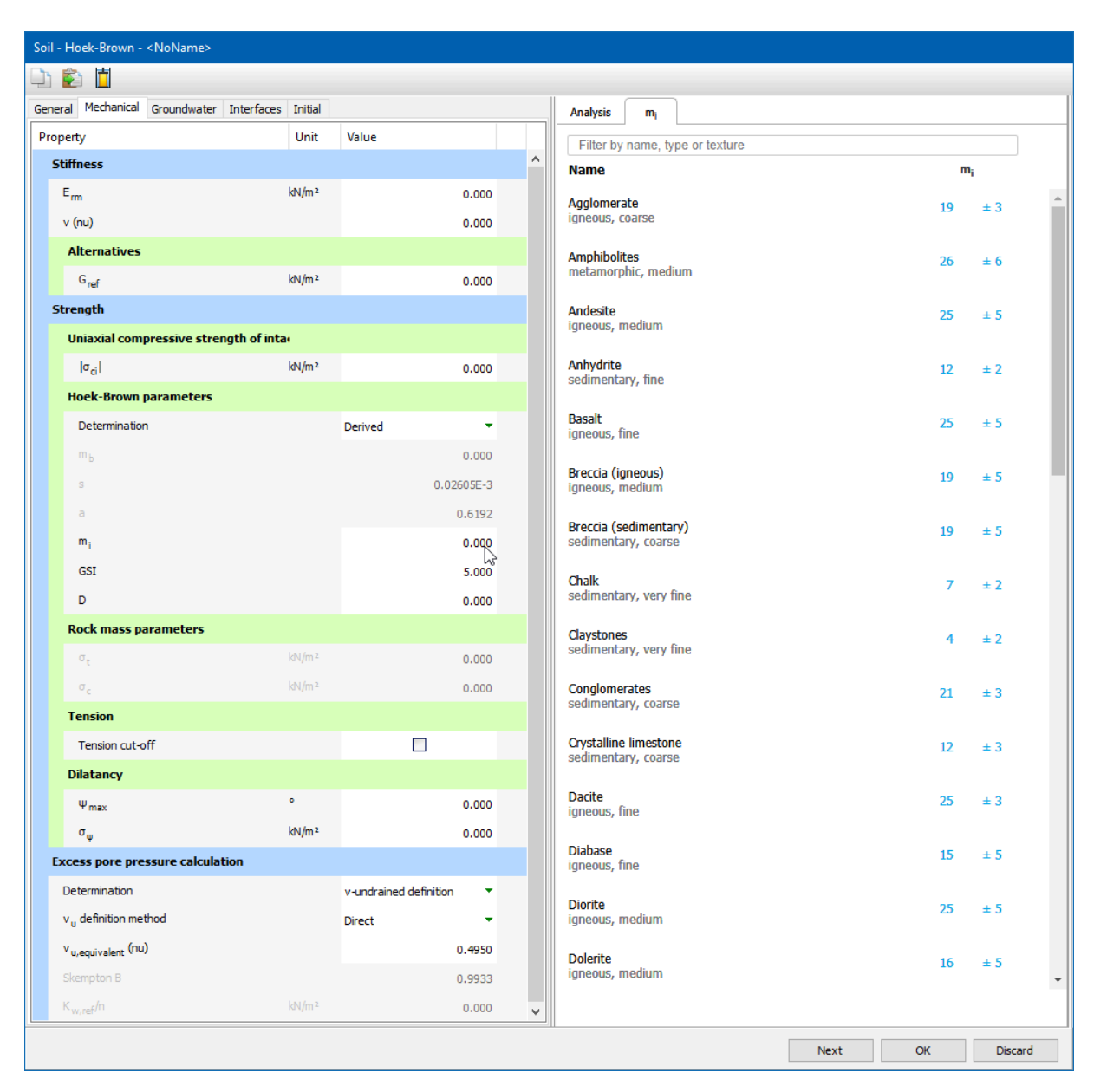


Figure 4–5: Intact rock parameter m_i for Hoek-Brown model

4.3.5 Geological Strength Index GSI

The GSI parameter can be computed thanks to the side panel of the pre-processing tool. The GSI tabsheet allows to choose between two rock types: General and Flysch. An intact rock is equivalent to GSI = 100, whereas a soil structure is in proximity to GSI = 0. Based on the selected rock type, the GSI can be chosen taking the structure and the surface conditions of the rock mass into account.

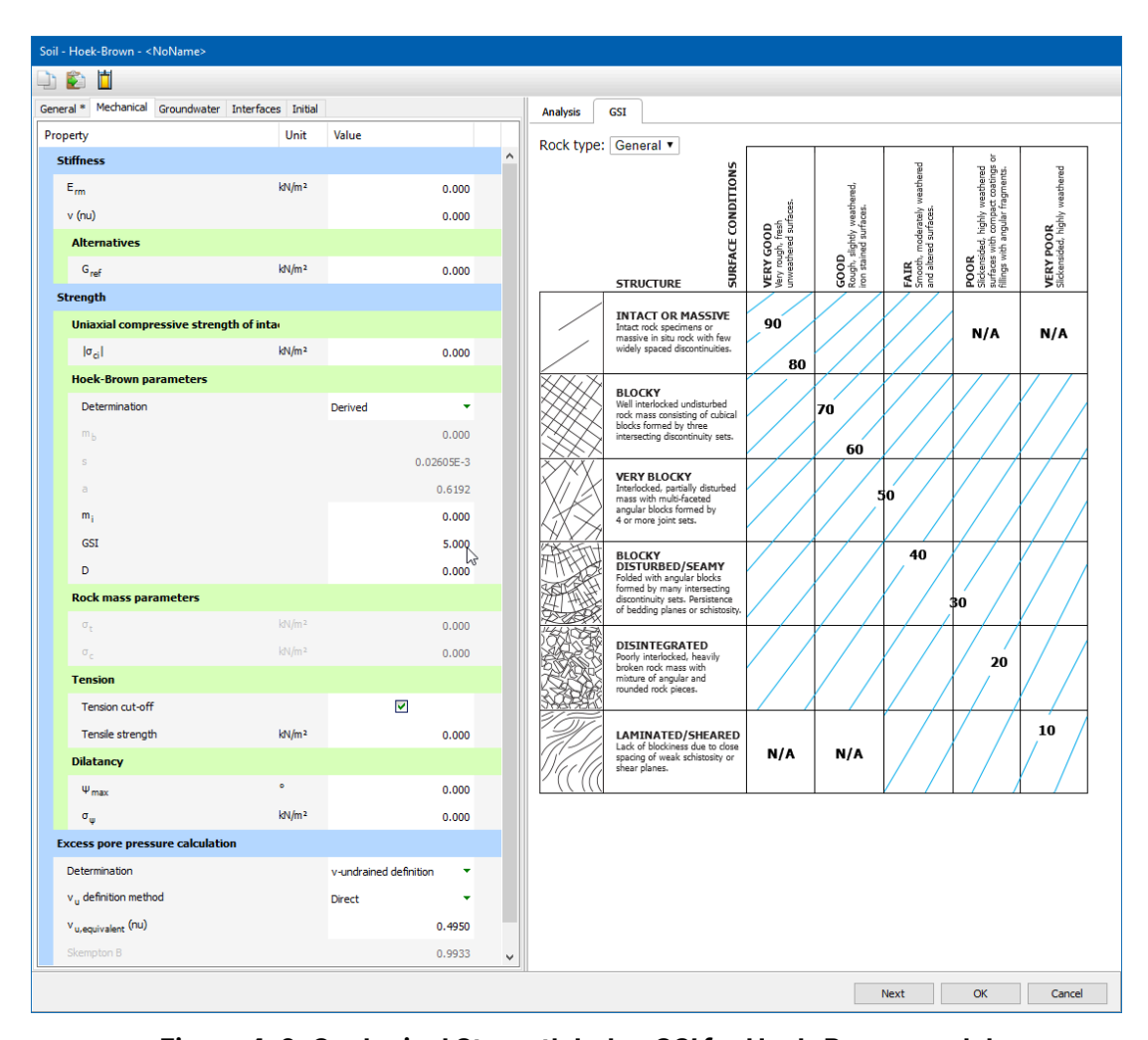


Figure 4-6: Geological Strength Index GSI for Hoek-Brown model

4.3.6 Disturbance factor D

The Disturbance factor, D, is a parameter that depends on the amount of disturbance of the rock as a result of mechanical processes in open excavations, tunnels or mines, such as blasting, tunnel boring, machine driven or manual excavation. No disturbance is equivalent to D = 0, whereas severe disturbance is equivalent to D = 1. For more information see Hoek (2006). Typical values are given in the side panel of the pre-processing tool.

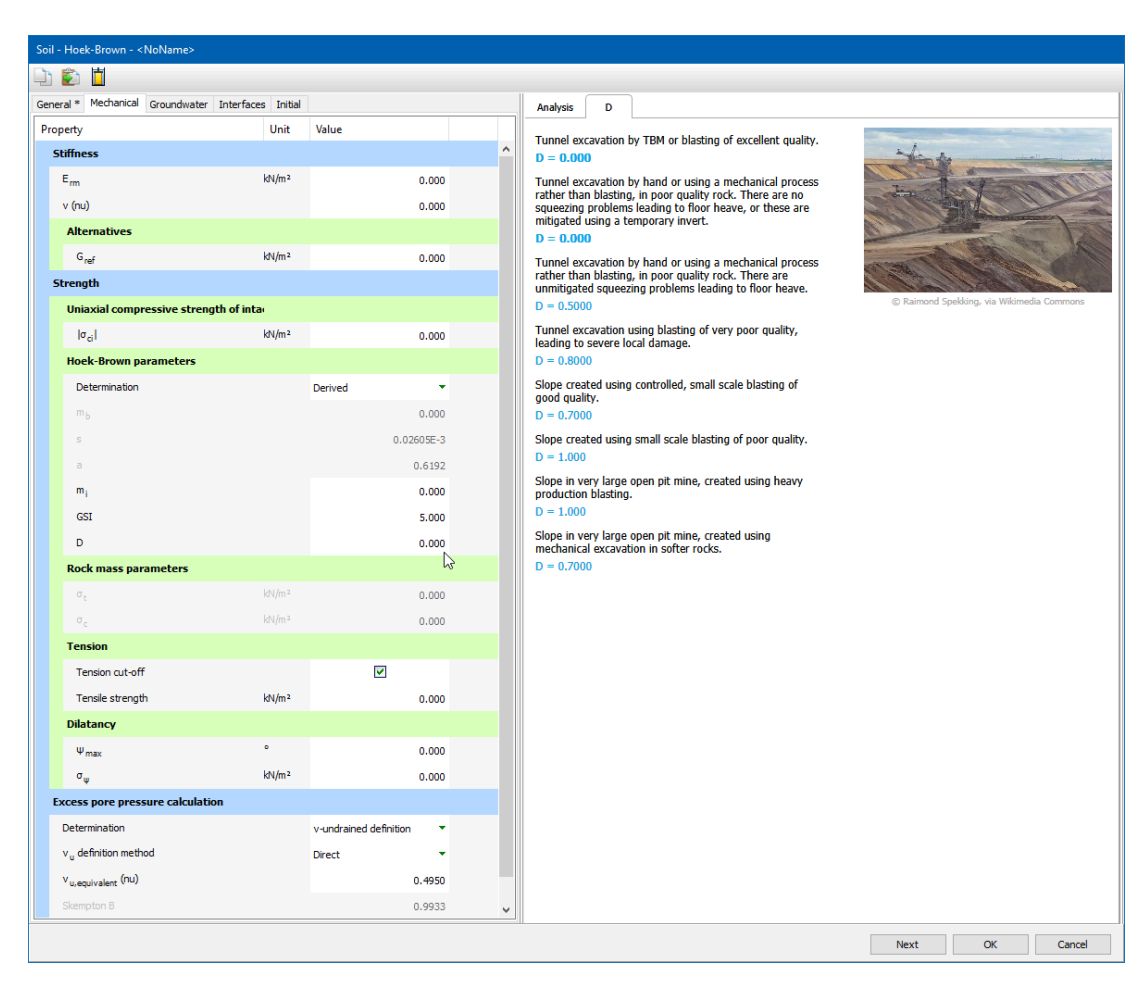


Figure 4–7: Disturbance factor D for Hoek-Brown model

1 Note: The disturbance factor D should only be applied to the actual zone of damaged rock in order to avoid greatly underestimation of the strength and overall stability. The thickness T of the blast damaged zone depends upon the design of the blast (Reference Manual- Chapter 6- Hoek-Brown preprocessing tool).

4.3.7 Tension cut-off

The Hoek-Brown model simulates the *Tensile strength* of the rock mass via the $|\sigma_{ci}|$ parameter, calculated from rock properties σ_{C} , s and m_{b} . To enhance modelling capabilities and flexibility, PLAXIS 2D allows to calibrate separately the rock tensile strength using tension cut-off facility. By default the tension cut-off option is disabled. When enabled, users can put a tensile strength value, and if that value is lower than σ_t , the tensile capacity will be cut-off at that value. This feature can be helpful in some situations, for instance in Safety analysis where this tension cutoff value (but not the σ_t parameter) is reduced with the safety factor.

4.3.8 Dilatancy ψ and σ_{ψ}

Rocks may show dilatant material behaviour when subjected to shear under relatively low confining stress. At larger confining stress, dilatancy is suppressed. This behaviour is modelled by means of a specified value of ψ for $\sigma_3 = 0$, with a linear decrease down to zero for $\sigma'_3 = \sigma_{\psi}$, where σ_{ψ} is an additional input parameter (Figure 4–3 (p. 45)).

4.4 On the use of the Hoek-Brown model in dynamics calculations

When using the Hoek-Brown model in dynamics calculations, the stiffness need to be selected such that the model correctly predicts wave velocities in the soil (Eqn. 3-15 (p. 37)). When subjected to dynamic or cyclic loading, the Hoek-Brown model may generate plastic strains if stress points reach the Hoek-Brown failure criterion, which will lead to damping in dynamics calculations. However, the stress cycles within the Hoek-Brown failure contour will only generate elastic strains and no (hysteretic) damping, nor accumulation of strains or pore pressure or liquefaction. In order to simulate the rock's damping characteristics in cyclic loading, Rayleigh damping may be defined.

The Jointed Rock model (anisotropy)

Materials may have different properties in different directions. As a result, they may respond differently when subjected to particular conditions in one direction or another. This aspect of material behaviour is called anisotropy. When modelling anisotropy, distinction can be made between elastic anisotropy and plastic anisotropy. Elastic anisotropy refers to the use of different elastic stiffness properties in different directions. Plastic anisotropy may involve the use of different strength properties in different directions, as considered in the Jointed Rock model. Another form of plastic anisotropy is kinematic hardening. The latter is not considered in PLAXIS.

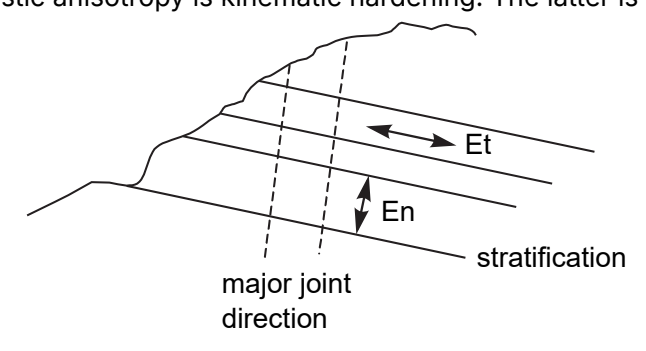


Figure 5–1: Visualization of concept behind the Jointed Rock model

The Jointed Rock model is an anisotropic elastic perfectly-plastic model, especially meant to simulate the behaviour of stratified and jointed rock layers. In this model it is assumed that there is intact rock with an optional stratification direction and major joint directions. The intact rock is considered to behave as a transversely anisotropic elastic material, quantified by five parameters and a direction. The anisotropy may result from stratification or from other phenomena. In the major joint directions it is assumed that shear stresses are limited according to Coulomb's criterion. Upon reaching the maximum shear stress in such a direction, plastic

sliding will occur. A maximum of three sliding directions ('planes') can be defined, of which the first plane is assumed to coincide with the direction of elastic anisotropy. Each plane may have different shear strength properties. In addition to plastic shearing, the tensile stresses perpendicular to the three planes are limited according to a predefined tensile strength (tension cut-off).

The application of the Jointed Rock model is justified when families of joints or joint sets are present. These joint sets have to be parallel, not filled with fault gouge, and their spacing has to be small compared to the characteristic dimension of the structure.

Some basic characteristics of the Jointed Rock model are:

- Anisotropic elastic behaviour for intact rock: Parameters E_t , $E_{nt}v_{nt}v_{ts}$, G_{nt}
- Shear failure according to Coulomb in 3 directions: Parameters c_i , φ_i and ψ_i
- Limited tensile strength in three directions: Parameters $\sigma_{t,i}$

5.1 Anisotropic elastic material stiffness matrix

The elastic material behaviour in the Jointed Rock model is described by an elastic material stiffness matrix, \mathbf{D}^* . In contrast to Hooke's law, the \mathbf{D}^* -matrix as used in the Jointed Rock model is transversely anisotropic. Different stiffnesses can be used normal to and in a predefined direction ('plane 1'). This direction may correspond to the stratification direction or to any other direction with significantly different elastic stiffness properties.

Consider, for example, a horizontal stratification, where the stiffness in z- direction, E_n , is different from the stiffness in the rock as a continuum, E_t . In this case the 'plane 1' direction is parallel to the xy-plane and the following constitutive relations exist (See: Zienkiewicz & Taylor: The Finite Element Method, 4th Ed.):

$$\dot{\varepsilon}_{xx} = \frac{\dot{\sigma}_{xx}}{E_t} - \frac{v_{nt}\dot{\sigma}_{yy}}{E_t} - \frac{v_{ts}\dot{\sigma}_{zz}}{E_n} \quad a)$$

$$\dot{\varepsilon}_{yy} = -\frac{v_{nt}\dot{\sigma}_{xx}}{E_t} + \frac{\dot{\sigma}_{yy}}{E_t} - \frac{v_{ts}\dot{\sigma}_{zz}}{E_n} \quad b)$$

$$\dot{\varepsilon}_{zz} = -\frac{v_{ts}\dot{\sigma}_{xx}}{E_n} - \frac{v_{ts}\dot{\sigma}_{yy}}{E_n} + \frac{\dot{\sigma}_{zz}}{E_n} \quad c)$$

$$\dot{\gamma}_{xy} = \frac{2(1+v_{nt})}{E_t}\sigma_{xy} \qquad d)$$

$$\dot{\gamma}_{yz} = \frac{\dot{\sigma}_{yz}}{G_{nt}} \qquad e)$$

$$\dot{\gamma}_{zx} = \frac{\dot{\sigma}_{zx}}{G_{rx}} \qquad f)$$

The inverse of the anisotropic elastic material stiffness matrix, (\boldsymbol{D}^*) $^{-1}$, follows from the above relations. This matrix is symmetric. The regular material stiffness matrix \mathbf{p}^* can only be obtained by numerical inversion.

In order for the \boldsymbol{D}^* to remain positive definite, the following requirement has to be obeyed:

$$v_{ts} < \sqrt{rac{E_n}{E_t} igg(rac{1-v_{nt}}{2}igg)}$$
 (5–2)

In general, the stratification plane will not be parallel to the global xy-plane, but the above relations will generally hold for a local (n,s,t) coordinate system where the stratification plane is parallel to the st-plane. The orientation of this plane is defined by the dip angle (or shortly dip) and strike (see 5.3 Parameters of the Jointed Rock model (p. 59)). As a consequence,

the local material stiffness matrix has to be transformed from the local to the global coordinate system. Therefore we consider first a transformation of stresses and strains:

$$\underline{\underline{\sigma}}_{nst} = \mathbf{R}_{\underline{\sigma}}\underline{\underline{\sigma}}_{xyz} \qquad \underline{\underline{\sigma}}_{xyz} = \mathbf{R}_{\underline{\sigma}}^{-1}\underline{\underline{\sigma}}_{nst}$$

$$\underline{\underline{\varepsilon}}_{nst} = \mathbf{R}_{\underline{\varepsilon}}\underline{\underline{\varepsilon}}_{xyz} \qquad \underline{\underline{\varepsilon}}_{xyz} = \mathbf{R}_{\underline{\varepsilon}}^{-1}\underline{\underline{\varepsilon}}_{nst}$$

$$(5-3)$$

$$\underline{arepsilon}_{nst} = oldsymbol{R}_{arepsilon} \underline{arepsilon}_{xyz} = oldsymbol{R}_{arepsilon}^{-1} \underline{arepsilon}_{nst}$$
 (5–4)

where

$$m{R}_{\sigma} = egin{bmatrix} n_{x}^{2} & n_{y}^{2} & n_{z}^{2} & 2n_{x}n_{y} & 2n_{y}n_{z} & 2n_{x}n_{z} \ s_{x}^{2} & s_{y}^{2} & s_{z}^{2} & 2s_{x}s_{y} & 2s_{y}s_{z} & 2s_{x}s_{z} \ t_{x}^{2} & t_{y}^{2} & t_{z}^{2} & 2t_{x}t_{y} & 2t_{y}t_{z} & 2t_{x}t_{z} \ n_{x}s_{x} & n_{y}s_{y} & n_{z}s_{z} & n_{x}s_{y} + n_{y}s_{x} & n_{y}s_{z} + n_{z}s_{y} & n_{z}s_{x} + n_{x}s_{z} \ s_{x}t_{x} & s_{y}t_{y} & s_{z}t_{z} & s_{x}t_{y} + s_{y}t_{x} & s_{y}t_{z} + s_{z}t_{y} & s_{x}t_{z} + s_{z}t_{x} \ n_{x}t_{x} & n_{y}t_{y} & n_{z}t_{z} & n_{x}t_{y} + n_{y}t_{x} & n_{y}t_{z} + n_{z}t_{y} & n_{z}t_{x} + n_{x}s_{z} \end{bmatrix}$$

and

$$m{R}_{arepsilon} = egin{bmatrix} n_{x}^{2} & n_{y}^{2} & n_{z}^{2} & n_{x}n_{y} & n_{y}n_{z} & n_{x}n_{z} \ s_{x}^{2} & s_{y}^{2} & s_{z}^{2} & s_{x}s_{y} & s_{y}s_{z} & s_{x}s_{z} \ t_{x}^{2} & t_{y}^{2} & t_{z}^{2} & t_{x}t_{y} & t_{y}t_{z} & t_{x}t_{z} \ 2n_{x}s_{x} & 2n_{y}s_{y} & 2n_{z}s_{z} & n_{x}s_{y} + n_{y}s_{x} & n_{y}s_{z} + n_{z}s_{y} & n_{z}s_{x} + n_{x}s_{z} \ 2s_{x}t_{x} & 2s_{y}t_{y} & 2s_{z}t_{z} & s_{x}t_{y} + s_{y}t_{x} & s_{y}t_{z} + s_{z}t_{y} & s_{x}t_{z} + s_{z}t_{x} \ 2n_{x}t_{x} & 2n_{y}t_{y} & 2n_{z}t_{z} & n_{x}t_{y} + n_{y}t_{x} & n_{y}t_{z} + n_{z}t_{y} & n_{z}t_{x} + n_{x}s_{z} \end{bmatrix}$$

 n_{x_1} , n_{y_1} , n_{z_1} , s_{x_1} , s_{y_2} , s_{z_3} , t_{x_4} , t_{y_3} and t_{z_4} are the components of the normalised n_{z_4} , s_{z_4} and t_{z_5} are the components of the normalised n_{z_5} , s_{z_5} (x,y,z)-coordinates (i.e. 'sines' and 'cosines'; see <u>5.3 Parameters of the Jointed Rock model (p.</u> <u>59</u>). For plane strain condition $n_z = s_z = t_x = t_y = 0$ and $t_z = 1$.

It further holds that:

$$oldsymbol{R}_{arepsilon}^T = oldsymbol{R}_{\sigma}^{-1} \qquad \qquad oldsymbol{R}_{\sigma}^T = oldsymbol{R}_{arepsilon}^{-1} \qquad \qquad ext{(5-7)}$$

A local stress-strain relationship in (n,s,t)-coordinates can be transformed to a global relationship in (x,y,z)-coordinates in the following way:

$$\frac{\underline{\sigma}_{nst} = \boldsymbol{D}_{nst}^* \underline{\varepsilon}_{nst}}{\underline{\sigma}_{nst} = \boldsymbol{R}_{nst}^* \underline{\sigma}_{xyz}} \right\} \Rightarrow \boldsymbol{R}_{\sigma} \underline{\sigma}_{xyz} = \boldsymbol{D}_{nst}^* \boldsymbol{R}_{\varepsilon} \underline{\varepsilon}_{xyz}$$

$$\underline{\varepsilon}_{nst} = \boldsymbol{R}_{nst}^* \underline{\varepsilon}_{xyz}$$

$$(5-8)$$

Hence,

$$\underline{\sigma}_{xyz} = \boldsymbol{R}_{\sigma}^{-1} \, \mathbf{D}_{\mathbf{nst}}^* \mathbf{R}_{\varepsilon} \underline{\varepsilon}_{xyz} \tag{5-9}$$

Using to above condition (Eqn. 5-7 (p. 56))

to above condition (
$$\underline{\mathbf{Eqn. 5-7 (p. 56)}}$$
)
$$\underline{\sigma}_{xyz} = \mathbf{R}_{\varepsilon}^T \mathbf{D}_{nst}^* \mathbf{R}_{\varepsilon} \underline{\varepsilon}_{xyz} = \mathbf{D}_{xyz}^* \underline{\varepsilon}_{xyz} \quad or \quad \mathbf{D}_{xyz}^* = \mathbf{R}_{\varepsilon}^T \mathbf{D}_{nst}^* \mathbf{R}_{\varepsilon}$$
 (5-10)

Actually, not the D^* -matrix is given in local coordinates but the inverse matrix (D^{*-1}).

$$\frac{\underline{\varepsilon}_{nst} = \boldsymbol{D}_{nst}^* \underline{\sigma}_{nst}}{\underline{\sigma}_{nst} = \boldsymbol{R}_{\sigma}^* \underline{\sigma}_{xyz}} \right\} \Rightarrow \underline{\varepsilon}_{xyz} = \boldsymbol{R}_{\varepsilon}^{-1} \ \mathbf{D}_{nst}^{*}^{-1} \boldsymbol{R}_{\sigma} \underline{\sigma}_{xyz} = \boldsymbol{R}_{\varepsilon}^{T} \ \mathbf{D}_{nst}^{*}^{-1} \boldsymbol{R}_{\sigma} \underline{\sigma}_{xyz}$$

$$\underline{\varepsilon}_{nst} = \boldsymbol{R}_{\varepsilon}^* \underline{\varepsilon}_{xyz}$$

$$(5-11)$$

Hence,

$$\mathbf{D}_{\mathbf{x}\mathbf{y}\mathbf{z}}^{*} = \mathbf{R}_{\sigma}^{T} \mathbf{D}_{\mathbf{n}\mathbf{s}\mathbf{t}}^{*} \mathbf{R}_{\sigma} \quad or \quad \mathbf{D}_{xyz}^{*} = \left[\mathbf{R}_{\sigma}^{T} \mathbf{D}_{\mathbf{n}\mathbf{s}\mathbf{t}}^{*}^{-1} \mathbf{R}_{\sigma}\right]^{-1}$$
 (5–12)

Instead of inverting the (D_{nst}^* ⁻¹)-matrix in the first place, the transformation is considered first, after which the total is numerically inverted to obtain the global material stiffness matrix D_{xyz}^* .

5.2 Plastic behaviour in three directions

A maximum of 3 sliding directions (sliding planes) can be defined in the Jointed Rock model. The first sliding plane corresponds to the direction of elastic anisotropy. In addition, a maximum of two other sliding directions may be defined. However, the formulation of plasticity on all planes is similar. On each plane a local Coulomb condition applies to limit the shear stress, |\tau| Moreover, a tension cut-off criterion is used to limit the tensile stress on a plane. Each plane, i, has its own strength parameters c_i , φ_i , ψ_i and $\sigma_{t,i}$.

In order to check the plasticity conditions for a plane with local (n, s, t)-coordinates it is necessary to calculate the local stresses from the Cartesian stresses. The local stresses involve three components, i.e. a normal stress component, σ_n , and two independent shear stress components, τ_s and τ_t .

$$\underline{\sigma}_i = \mathbf{T_i^T}\underline{\sigma}$$
 (5–13)

where

$$\underline{\sigma} = (\sigma_n \ \tau_s \ \tau_t)^T$$

$$\underline{\sigma} = (\sigma_{xx} \ \sigma_{yy} \ \sigma_{zz} \ \sigma_{xy} \ \sigma_{yz} \ \sigma_{zx})^T$$

$$(b)$$

$$T_i^T = transformation matrix (3x6), for plane i$$

As usual in PLAXIS, tensile (normal) stresses are defined as positive whereas compression is defined as negative.

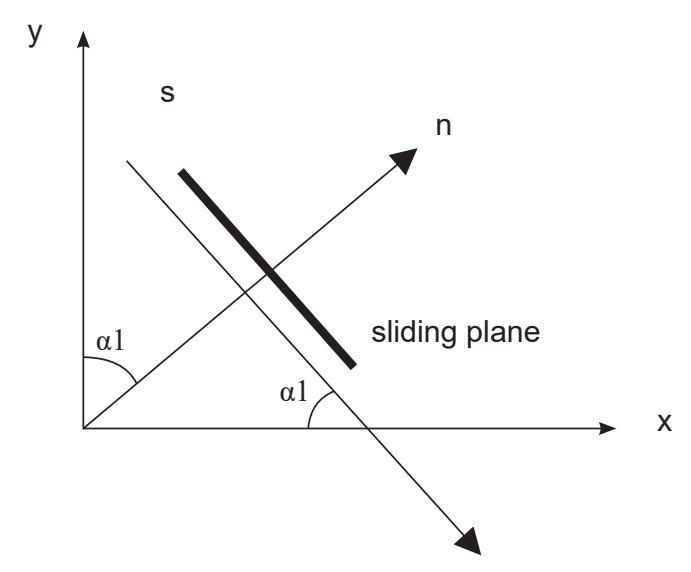


Figure 5-2: Plane strain situation with a single sliding plane and vectors n, s

Consider a plane strain situation as visualised in Figure 5–2 (p. 57). Here a sliding plane is considered under an angle α_1 (= dip) with respect to the x-axis. In this case the transformation matrix T^T becomes:

$$m{T}^T = egin{bmatrix} s^2 & c^2 & 0 & -2sc & 0 & 0 \ sc & -sc & 0 & -s^2+c^2 & 0 & 0 \ 0 & 0 & 0 & -c & -c \ \end{bmatrix}$$
 (5–15)

where:

$$s = \sin{(\alpha_1)}$$
 $c = \cos{(\alpha_1)}$

In the general three-dimensional case the transformation matrix is more complex, since it involves both dip and strike (see 5.3 Parameters of the Jointed Rock model (p. 59)):

$$m{T}^T = egin{bmatrix} n_x^2 & n_y^2 & n_z^2 & 2n_x n_y & 2n_y n_z & 2n_z n_x \ n_x s_x & n_y s_y & n_z s_z & n_x s_y + n_y s_x & n_z s_y + n_y s_z & n_z s_x + n_x s_z \ n_x t_x & n_y t_y & n_z t_z & n_y t_x + n_x t_y & n_y t_z + n_z t_y & n_z t_x + n_x t_z \end{bmatrix}$$
 (5-16)

Note that the general transformation matrix, T, for the calculation of local stresses corresponds to rows 1, 4 and 6 of R_{σ} (see Eqn. 5–5 (p. 56)).

After having determined the local stress components, the plasticity conditions can be checked on the basis of yield functions. The yield functions for plane *i* are defined as:

$$egin{aligned} f_i^c &= | au_s| + \sigma_n an{(lpha_i)} - c_i & (Coulomb) \ f_i^c &= \sigma_n - \sigma_{t,i} (\sigma_{t,i} \leq c_i \cot{(\phi_i)}) & (Tension \ cut - off) \end{aligned}$$

Figure 5-3 (p. 58) visualizes the full yield criterion on a single plane.

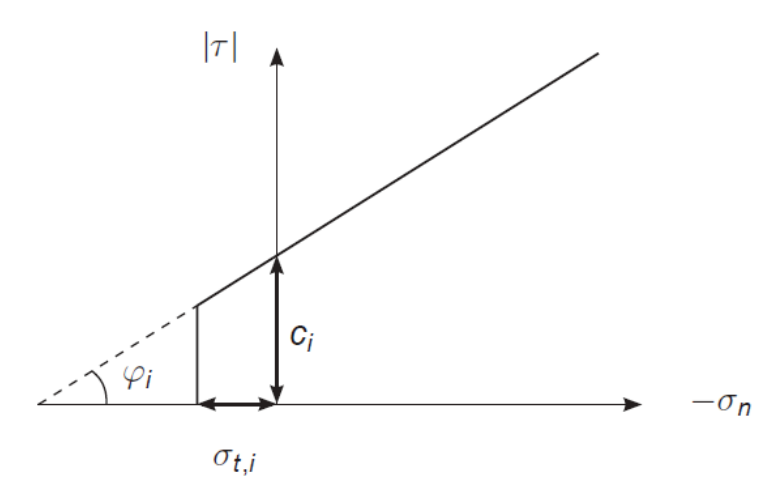


Figure 5-3: Yield criterion for individual plane

The local plastic strains are defined by:

$$\Delta \underline{arepsilon}_{j}^{p} = \lambda_{j} rac{\partial g_{j}^{c}}{\partial \underline{\sigma}_{j}}$$
 (5–18)

where g_i is the local plastic potential function for plane j:

$$egin{aligned} g_i^c &= | au_j| + \sigma_n an(\psi_i) - c_i & (Coulomb) \ g_i^c &= \sigma_n - \sigma_{t,i} & (Tension\ cut - off) \end{aligned}$$
 (5–19)

The transformation matrix, T, is also used to transform the local plastic strain increments of plane j, $\Delta \underline{\varepsilon}_{j}^{p}$, into global plastic strain increments, $\Delta \underline{\varepsilon}^{p}$:

$$\Delta \underline{\varepsilon}^p = T_j \Delta \underline{\varepsilon}_j^p$$
 (5–20)

The consistency condition requires that at yielding the value of the yield function must remain zero for all active yield functions. For all planes together, a maximum of 6 yield functions exist, so up to 6 plastic multipliers must be found such that all yield functions are at most zero and the plastic multipliers are non-negative.

$$\begin{split} f_i^c &= f_i^{c(e)} - \sum_{j=1}^{np} <\lambda_j^c > \frac{\partial f_i^{c^T}}{\partial \sigma} T_i^T D T_j \frac{\partial g_j^c}{\partial \sigma} - \sum_{j=1}^{np} <\lambda_j^t > \frac{\partial f_i^{c^T}}{\partial \sigma} T_i^T D T_j \frac{\partial g_j^t}{\partial \sigma} \\ f_i^t &= f_i^{t(e)} - \sum_{j=1}^{np} <\lambda_j^c > \frac{\partial f_i^{t^T}}{\partial \sigma} T_i^T D T_j \frac{\partial g_j^c}{\partial \sigma} - \sum_{j=1}^{np} <\lambda_j^t > \frac{\partial f_i^{t^T}}{\partial \sigma} T_i^T D T_j \frac{\partial g_j^t}{\partial \sigma} \end{split}$$
 (5-21)

This means finding up to 6 values of $\lambda_i \ge 0$ such that all $f_i \le 0$ and $\lambda_i f_i = 0$.

When the maximum of 3 planes are used, there are $2^6 = 64$ possibilities of (combined) yielding. In the calculation process, all these possibilities are taken into account in order to provide an exact calculation of stresses.

5.3 Parameters of the Jointed Rock model

Most parameters of the Jointed Rock model coincide with those of the isotropic Mohr-Coulomb model. These are the basic elastic parameters and the basic strength parameters.

Elastic parameters as in Mohr-Coulomb model (see <u>3.3 Parameters of the Mohr-Coulomb model (p. 34)</u>)			
E _t	Young's modulus for rock as a continuum	[kN/m ²]	
v _{nt} Poisson's ratio for rock as a continuum [-]			

Anisotropic elastic parameters 'Plane 1' direction (e.g. stratification direction)			
En	Young's modulus perpendicular to 'Plane 1' direction	[kN/m ²]	
G _{nt}	Shear modulus perpendicular to 'Plane 1' direction	[kN/m ²]	
V _{ts}	Poisson's ratio perpendicular to 'Plane 1' direction $ u_{ts} < \sqrt{rac{E_n}{E_t} \left(rac{1- u_{nt}}{2} ight)}$	[-]	

Strength parameters in joint directions (Plane i=1, 2, 3):		
Ci	Cohesion	[kN/m ²]
φ_i	Friction angle	[°]
Ψ_i	Dilatancy angle	[°]
$\sigma_{t,i}$	Tensile strength	[kN/m ²]

Definition of joint directions (Plane i=1, 2, 3):			
Number of planes Number of joint directions ($1 \le n \le 3$) [-]			
α _{1,i}	$Dip\;(0 \leq \alpha_{1,i} \leq 90)$	[°]	
α _{2,i}	Strike (-180 $\leq \alpha_{2,i} \leq 180$) ($\alpha_{2,i} = 90$ in PLAXIS 2D)	[°]	

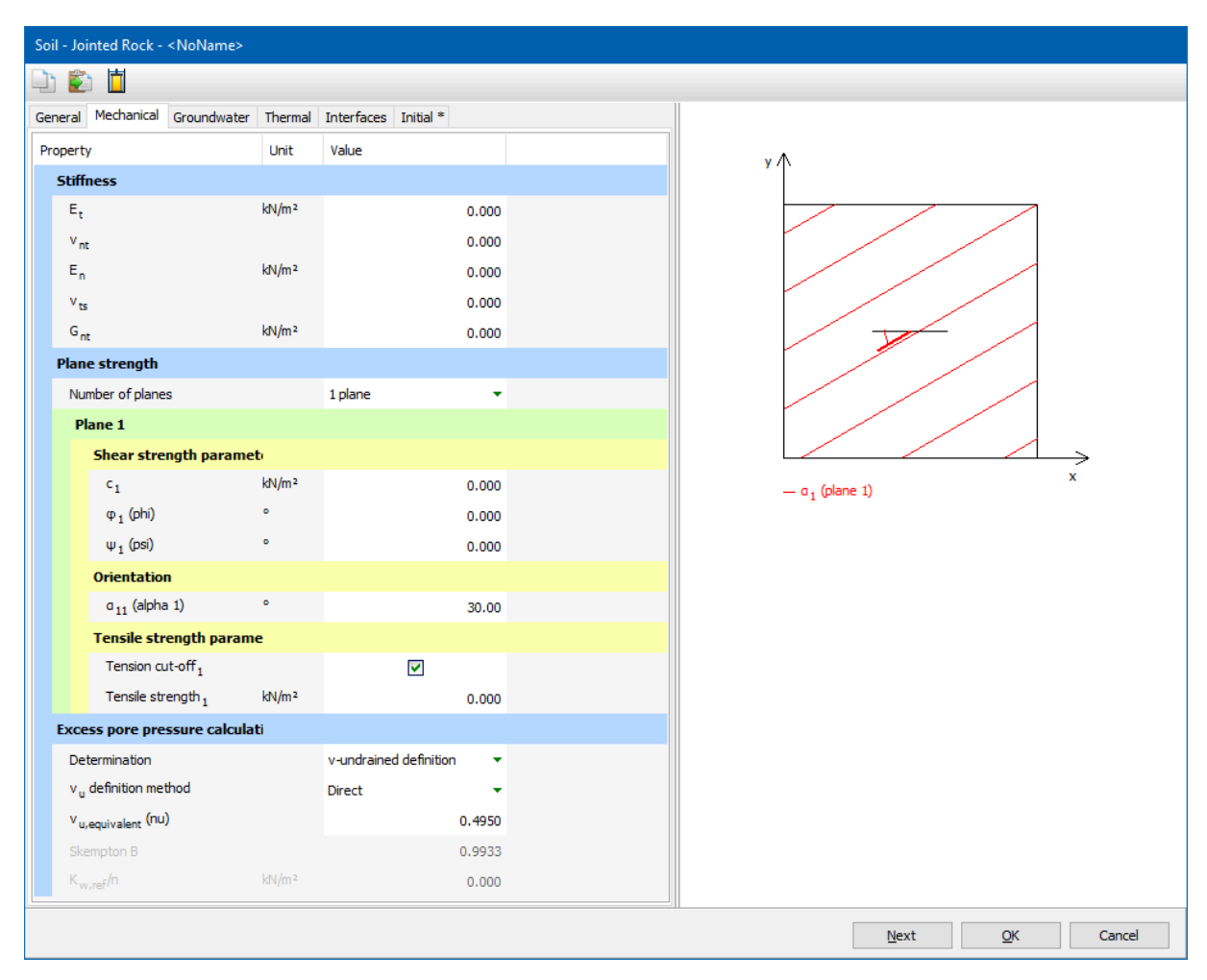


Figure 5-4: Parameters for the Jointed Rock model

5.3.1 Elastic parameters

The elastic parameters E_t and v_{nt} are the (constant) stiffness (Young's modulus) and Poisson's ratio of the rock as a continuum according to Hooke's law, i.e. as if it would not be anisotropic.

Elastic anisotropy in a rock formation may be introduced by stratification. The stiffness perpendicular to the stratification direction is usually reduced compared with the general stiffness. This reduced stiffness can be represented by the parameter E_n , together with a second Poisson's ratio, v_{ts}. In general, the elastic stiffness normal to the direction of elastic anisotropy is defined by the parameters E_n and v_{ts} . In order to avoid singularity of the material stiffness matrix, the input of v_{ts} is limited by:

$$v_{ts} < \sqrt{rac{E_n}{E_t}igg(rac{1-v_{nt}}{2}igg)}$$
 (5–22)

Elastic shearing in the stratification direction is also considered to be 'weaker' than elastic shearing in other directions. In general, the shear stiffness in the anisotropic direction can explicitly be defined by means of the elastic shear modulus G_{nt} . In contrast to Hooke's law of isotropic elasticity, G nt is a separate parameter and is not simply related to Young's modulus by means of Poisson's ratio (see Eqn. 5–1 (p. 55) (d) & (e)).

If the elastic behaviour of the rock is fully isotropic, then the parameters E_n and v_{ts} can be simply set equal to E_t and v_{nt} respectively, whereas G_{nt} should be set to $1/2E_t/(1+v_{nt})$.

5.3.2 Strength parameters

Each sliding direction (plane) has its own strength properties c_i , φ_i and $\sigma_{t,i}$ and dilatancy angle ψ_i . The strength properties c_i and φ_i determine the allowable shear strength according to Coulomb's criterion and σ_t determines the tensile strength according to the tension cut-off criterion. The latter is displayed after pressing Advanced button. By default, the tension cut-off is active and the tensile strength is set to zero. The dilatancy angle, ψ_i , is used in the plastic potential function q, and determines the plastic volume expansion due to shearing.

5.3.3 Definition of joint directions

It is assumed that the direction of elastic anisotropy corresponds with the first direction where plastic shearing may occur ('plane 1'). This direction must always be specified. In the case the rock formation is stratified without major joints, the number of sliding planes (= sliding directions) is still 1, and strength parameters must be specified for this direction anyway. A maximum of three sliding directions can be defined. These directions may correspond to the most critical directions of joints in the rock formation.

The sliding directions are defined by means of two parameters: The Dip angle (α_1) (or shortly Dip) and the Strike (α_2). The definition of both parameters is visualised in Figure 5–5 (p. 62).

Consider a sliding plane, as indicated in Figure 5–5 (p. 62). The sliding plane can be defined by the vectors (s,t), which are both normal to the vector n. The vector n is the 'normal' to the sliding plane, whereas the vector s is the 'line of maximum declination' of the sliding plane (dip) and the vector t is the "trace on the horizontal plane of the sliding plane" (strike). The sliding plane makes an angle α_1 with respect to the horizontal plane, where the horizontal plane can be defined by the vectors (s^*,t) , which are both normal to the vertical axis. The angle α_1 is the dip, which is defined as the positive 'downward' inclination angle between the horizontal plane and the sliding plane. Hence, α_1 is the positive angle between the vectors s^* and s, along the t-direction. The dip ought to be entered in the range [0°, 90°], but negative values as well as values larger than 90° can also be entered.

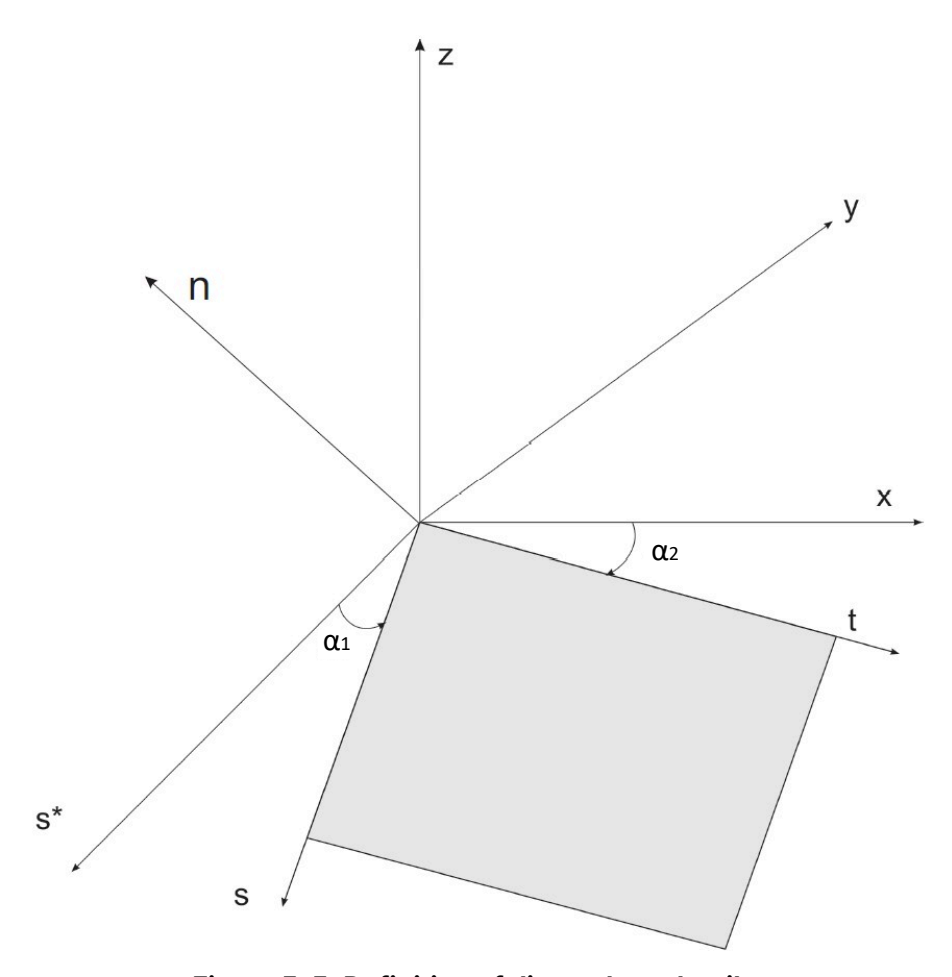


Figure 5-5: Definition of dip angle and strike

The orientation of the sliding plane is further defined by the *strike*, α_2 , which is defined in PLAXIS as the orientation of the vector t with respect to the x-direction. The strike is defined as the negative angle between the vectors x and t along the z-direction. The strike direction is entered in the range [-180°, 180°].

From the definitions as given above, it follows for PLAXIS 3D that:

$$\underline{n} = \begin{bmatrix} n_x \\ n_y \\ n_z \end{bmatrix} = \begin{bmatrix} -\sin(\alpha_1)\sin(\alpha_2) \\ -\sin(\alpha_1)\cos(\alpha_2) \\ \cos(\alpha_1) \end{bmatrix}$$

$$\underline{s} = \begin{bmatrix} s_x \\ s_y \\ s_z \end{bmatrix} = \begin{bmatrix} -\cos(\alpha_1)\sin(\alpha_2) \\ -\cos(\alpha_1)\cos(\alpha_2) \\ -\sin(\alpha_1) \end{bmatrix}$$

$$\underline{t} = \begin{bmatrix} t_x \\ t_y \\ t_z \end{bmatrix} = \begin{bmatrix} \cos(\alpha_2) \\ -\sin(\alpha_2) \\ 0 \end{bmatrix}$$
(5-24)

whereas for PLAXIS 2D α_2 is taken by definition as α_2 = 90°, such that:

$$\underline{n} = \begin{bmatrix} n_x \\ n_y \\ n_z \end{bmatrix} = \begin{bmatrix} -\sin(\alpha_1) \\ \cos(\alpha_1) \\ 0 \end{bmatrix}$$
 (5-26)

$$\underline{s} = \begin{bmatrix} s_x \\ s_y \\ s_z \end{bmatrix} = \begin{bmatrix} -\cos(\alpha_1) \\ -\sin(\alpha_2) \\ 0 \end{bmatrix}$$

$$\underline{t} = \begin{bmatrix} t_x \\ t_y \\ t_z \end{bmatrix} = \begin{bmatrix} 0 \\ 0 \\ 1 \end{bmatrix}$$
(5-27)

Figure 5-6 (p. 63) shows some examples of how sliding planes occur in a 3D models for different values of α_1 and α_2 . As it can be seen, for plane strain conditions (the cases considered in PLAXIS 2D) only α_1 is required. By default, α_2 is fixed at 90°.

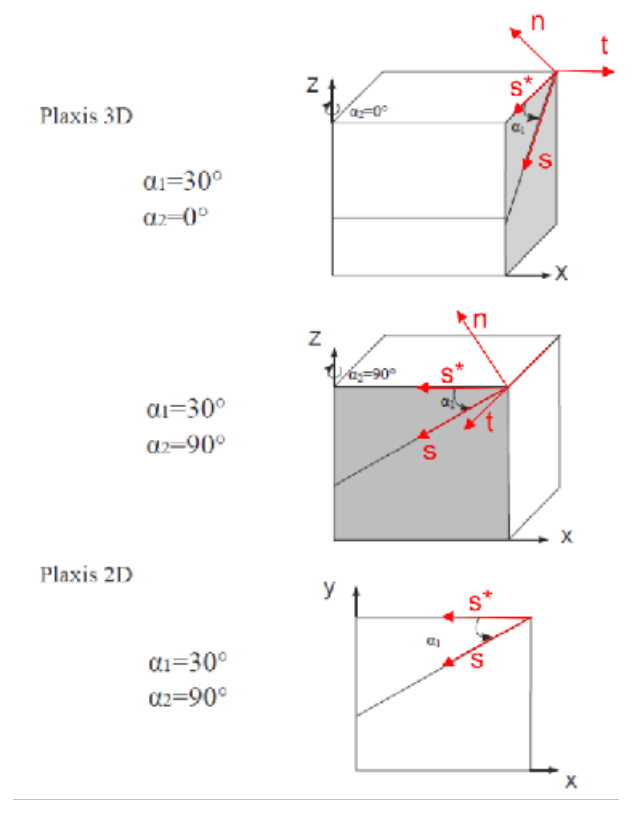


Figure 5-6: Examples of failure directions defined by α_1 and α_2

5.4 On the use of the Jointed Rock model in dynamics calculations

When using the Jointed Rock model in dynamics calculations, the stiffness need to be selected such that the model correctly predicts wave velocities in the soil (Equation Egn. 3-15 (p. 37)). When subjected to dynamic or cyclic loading, the Jointed Rock model may generate plastic strains if stress points reach the Coulomb failure criterion, which will lead to damping in dynamics calculations. However, it should be noted that stress cycles within the Coulomb failure contour will only generate elastic strains and no (hysteretic) damping, nor accumulation of strains or pore pressure or liquefaction. In order to simulate the rock's damping characteristics in cyclic loading, Rayleigh damping may be defined.

1 Note: A slightly modified version of the Jointed Rock model with generalised Mohr-Coulomb failure criterion in addition to the individual failure directions is available as user-defined soil model. Contact Plaxis for more information.

Note:

- In a geological context, strike is defined as the angle from the North to the strike of the dipping plane (positive towards East direction), whereas in PLAXIS definition strike is defined from the global x-direction to the strike of the dipping plane (with the same positive rotation direction). If we define the angle from the North direction to the x-direction of the PLAXIS model as declination, then strike in PLAXIS is the geological strike minus declination.
- Moreover, there might be confusion between true strike and its opposite direction (180° direction). Hence, care must be taken when translating strike from geological data into PLAXIS input.



The Hardening Soil model (Isotropic hardening)

In contrast to an elastic perfectly-plastic model, the yield surface of a hardening plasticity model is not fixed in principal stress space, but it can expand due to plastic straining. Distinction can be made between two main types of hardening, namely shear and compression hardening. Shear hardening is used to model irreversible strains due to primary deviatoric loading. Compression hardening is used to model irreversible plastic strains due to primary compression in oedometer loading and isotropic loading. Both types of hardening are contained in the present model.

The Hardening Soil model is an advanced model for simulating the behaviour of different types of soil, including soft and stiff soils, Shanz (1998). When subjected to primary deviatoric loading, soil shows a decreasing stiffness and simultaneously irreversible plastic strains develop. In the special case of a drained triaxial test, the observed relationship between the axial strain and the deviatoric stress can be well approximated by a hyperbola. Such a relationship was first formulated by Kondner (1963) and later used in the well-known hyperbolic model QDuncan & Chang, 1970). The Hardening Soil model, however, supersedes the hyperbolic model by far: Firstly by using the theory of plasticity rather than the theory of elasticity, secondly by including soil dilatancy and thirdly by introducing a yield cap. Some basic characteristics of the model are:

- Stress dependent stiffness according to a power law: Input parameter m
- Plastic straining due to primary deviatoric loading: Input parameter $E_{50}^{
 m ref}$
- ullet Plastic straining due to primary compression: Input parameter $E_{oed}^{
 m ref}$
- ullet Elastic unloading / reloading: Input parameters $E_{ur}^{
 m ref}$, ${
 m v}_{ur}$
- Failure according to the Mohr-Coulomb failure criterion: Parameters c, φ and ψ

A basic feature of the present Hardening Soil model is the stress dependency of soil stiffness. For oedometer conditions of stress and strain, the model implies for example the relationship

 $E_{oed} = E_{oed}^{ref} (\sigma / p^{ref})^m$. In the special case of soft soils it is realistic to use m = 1. In such situations there is also a simple relationship between the modified compression index λ^* , as used in models for soft soil and the oedometer loading modulus (see also Parameters of the Soft Soil model).

$$E_{oed}^{ref}=rac{p^{ref}}{\lambda^*} \qquad \qquad \lambda^*=rac{\lambda}{(1+e_0)}$$
 (6–1)

where p^{ref} is a reference pressure. Here we consider a tangent oedometer modulus at a particular reference pressure p^{ref} . Hence, the primary loading stiffness relates to the modified compression index λ^* or to the standard Cam-Clav compression index λ .

Similarly, the unloading-reloading modulus relates to the modified swelling index κ^* or to the standard Cam-Clay swelling index κ . There is the approximate relationship:

$$E_{ur}^{ref}pproxrac{2p^{ref}}{\kappa^*} \hspace{1cm} k^*=rac{k}{(1+e_0)}$$
 (6–2)

This relationship applies in combination with the input value m = 1.

6.1 Hyperbolic relationship for standard drained triaxial test

A basic idea for the formulation of the Hardening Soil model is the hyperbolic relationship between the vertical strain, ε_1 , and the deviatoric stress, q, in primary triaxial loading. Here standard drained triaxial tests tend to yield curves that can be described by:

$$-arepsilon_1 = rac{1}{E_i} rac{q}{1-q/q_a} \quad for: \ q < q_f$$
 (6–3)

where

 q_a = Asymptotic value of the shear strength.

= Initial stiffness. E_i

 E_i is related to E_{50} by:

$$E_i = \frac{2E_{50}}{2 - R_f} \tag{6-4}$$

This relationship is plotted in Figure 6–1 (p. 67). The parameter E_{50} is the confining stress dependent stiffness modulus for primary loading and is given by the equation:

$$E_{50} = E_{50}^{ref} igg(rac{c\cos{\left(arphi
ight)} - \sigma_3^\prime\sin{\left(arphi
ight)}}{c\cos{\left(arphi
ight)} + p^{ref}\sin{\left(arphi
ight)}}igg)^m$$
 (6–5)

where

 E_{50}^{ref} = Reference stiffness modulus corresponding to the reference confining pressure p^{ref} .

In PLAXIS, a default setting $p^{ref} = 100$ stress units is used. The actual stiffness depends on the minor principal stress, σ'_3 , which is the confining pressure in a triaxial test. Please note that σ'_3 is negative for compression. The non-linearity of stress dependency is defined by the power m. In order to simulate a logarithmic compression behaviour, as observed for soft clays, the power should be taken equal to 1.0:(i.e., linear dependency). Conversely, Janbu (1963) reports values of m around 0.5 for Norwegian sands and silts, whilst von Soos (1990) reports values in the range of 0.5 < m < 1.0.

The ultimate deviatoric stress, q_f , and the quantity q_a in Eqn. 6–3 (p. 66) are defined as:

$$q_f = (c\cot(\varphi)) - \sigma_3' \bigg) \frac{2\sin(\varphi)}{1 - \sin(\varphi)} \qquad and: \qquad q_a = \frac{q_f}{R_f}$$
 (6-6)

Again it is remarked that σ'_3 is negative in compression. The above relationship for q_f is derived from the Mohr-Coulomb failure criterion, which involves the strength parameters c and φ . As soon as $q = q_f$, the failure criterion is satisfied and perfectly plastic yielding occurs as described by the Mohr-Coulomb failure criterion.

The ratio between q_f and q_a is given by the failure ratio R_f , which should obviously be smaller than or equal to 1. In PLAXIS, $R_f = 0.9$ is chosen as a suitable default setting.

For unloading and reloading stress paths, another stress-dependent stiffness modulus is used:

$$E_{ur} = E_{ur}^{ref} \left(rac{c\cos\left(arphi
ight) - \sigma_{3}^{\prime}\sin\left(arphi
ight)}{c\cos\left(arphi
ight) + p^{ref}\sin\left(arphi
ight)}
ight)^{m}$$
 (6–7)

where

Unloading-reloading Young's modulus, corresponding to the reference pressure p^{ref}.

f 0 Note: In many practical cases it is appropriate to set E^{ref}_{ur} equal to 3 E^{ref}_{50} ; this is the default setting used in PLAXIS.

deviatoric stress

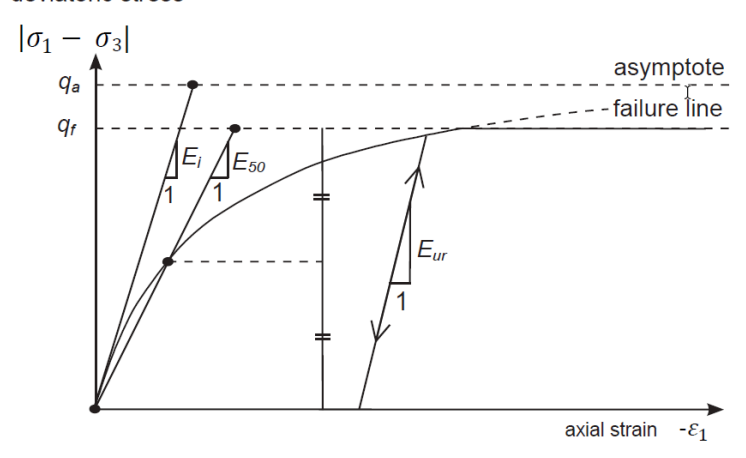


Figure 6-1: Hyperbolic stress-strain relation in primary loading for a standard drained triaxial test

6.2 Approximation of hyperbola by the Hardening Soil model

For the sake of convenience, restriction is made here to triaxial loading conditions with $\sigma'_2 = \sigma'_3$ being the intermediate and minor principal stresses and σ'_{1} being the major principal stress. It should also be noted that compressive stresses and strains are considered negative.

Moreover, it is assumed that $q < q_f$, as also indicated in Figure 24. For a more general presentation of the Hardening Soil model the reader is referred to Schanz, Vermeer & Bonnier (1999). In this section it will be shown that this model gives virtually the hyperbolic stress strain curve of Eqn. 6-3 (p. 66) when considering stress paths of standard drained triaxial tests. Let us first consider the corresponding plastic strains. This stems from a shear hardening yield function of the form:

$$f = \bar{f} - \gamma^p$$
 (6–8)

where

 \bar{f} = Function of stress

 γ^p = Plastic hardening parameter, which is a measure of the mobilised plastic shear

$$\overline{f}=rac{2}{E_i}rac{q}{1-q/q_a}-rac{2q}{E_{ur}}$$
 (6–9)

with q, q_a , E_i and E_{ur} as defined by Eqn. 6–3 (p. 66) to Eqn. 6–6 (p. 67), whilst the superscript p is used to denote plastic strains.

An essential feature of the above definitions for \bar{f} is that it matches the well-known hyperbolic law Eqn. 6-3 (p. 66). For checking this statement, one has to consider primary loading, as this implies the yield condition f = 0. Moreover, it is assumed that for hard soils, plastic volumetric strain changes (ε_{V}^{p}) tend to be relatively small and this leads to the approximation:

$$\gamma^p = -(2arepsilon_1^p - arepsilon_v^p) pprox -2arepsilon_1^p$$
 (6–10)

For primary loading, $y^p = \bar{f}$ and it follows from Eqn. 6–8 (p. 68) and Eqn. 6–10 (p. 68) that:

$$arepsilon_1^ppproxrac{1}{2}ar{f}=rac{1}{E_i}rac{q}{1-q/q_a}-rac{q}{E_{vr}}$$
 (6–11)

In addition to the plastic strains, the model accounts for elastic strains. Plastic strains develop in primary loading only, but elastic strains develop both in primary loading and unloading / reloading. For drained triaxial test stress paths with $\sigma'_2 = \sigma'_3 = \text{constant}$, the elastic Young's modulus E_{ur} remains constant and the elastic strains are given by the equations:

$$-arepsilon_1^e=rac{q}{E_{ur}}$$
 $-arepsilon_2^e=-arepsilon_3^e=-
u_{ur}rac{q}{E_{ur}}$ (6–12)

where v_{ur} is the unloading-reloading Poisson's ratio. Here it should be realised that restriction is made to strains that develop during shearing stage, whilst the strains that develop during the very first stage of the test (consolidation) are not considered.

For the shearing stage of the triaxial test, the axial strain is the sum of an elastic component given by Eqn. 6-12 (p. 68) and a plastic component according to Eqn. 6-11 (p. 68). Hence, it follows that:

$$-arepsilon_1=-arepsilon_1^e-arepsilon_1^ppproxrac{1}{E_i}rac{q}{1-q/q_a}$$
 (6–13)

Note again that this relationship holds true in the absence of plastic volumetric strains, i.e. when ε_{v}^{p} = 0. As highlighted before, plastic volumetric strains will never be precisely equal to zero, but for hard soils plastic volumetric strain changes tend to be small when compared with the axial strain.

For a given constant value of the hardening parameter, y^p , the yield condition f = 0, can be visualised in p' - q-plane by means of a yield locus. Hence, γ^p is associated with mobilised friction. When plotting such yield loci, one has to use Eqn. 6-9 (p. 68) as well as Eqn. <u>6-7 (p. 67)</u> and Eqn. 6-6 (p. 67) for E_{50} and E_{ur} respectively. Because of the latter expressions, the shape of the yield loci depends on the exponent m. For m = 1, straight lines are obtained, but slightly curved yield loci correspond to lower values of the exponent. Figure <u>6-2 (p. 69)</u> shows the shape of yield loci for increasing values of y^p considering m = 0.5, being typical for hard soils. Hence, v^p can be regarded as the plastic shear strain related to the mobilised shear resistance.

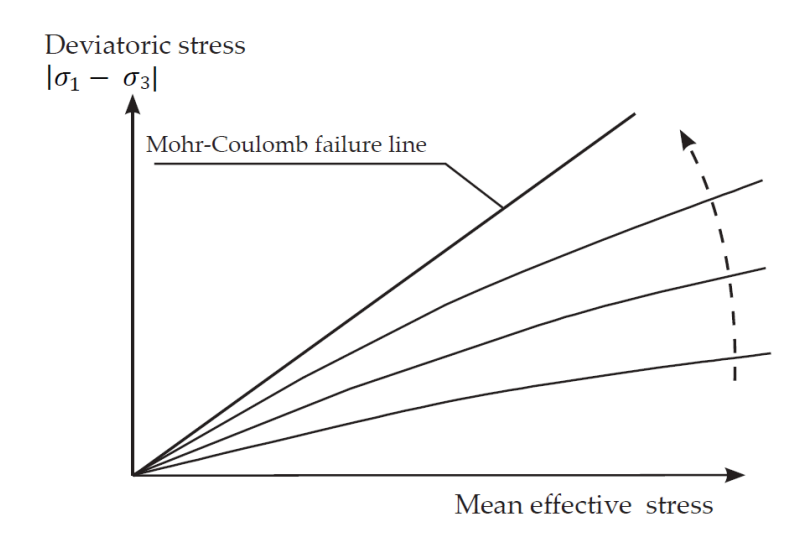


Figure 6-2: Successive yield loci for various constant values of the hardening parameter y^p

6.3 Plastic volumetric strain for triaxial states of stress

Having presented a relationship for the plastic shear strain, y^p , attention is now focused on the plastic volumetric strain, ε_{v}^{p} . As for all plasticity models, the Hardening Soil model involves a relationship between rates of plastic strain, i.e. a relationship between $\dot{\varepsilon}_{v}^{p}$ and $\dot{\gamma}^{p}$. This shear hardening flow rule has the linear form:

$$\dot{arepsilon}_v^p = \sin(\psi_m)\dot{\gamma}^p$$
 (6–14)

Clearly, further detail is needed by specifying the mobilised dilatancy angle ψ_m . For the present model, the following is considered (see also Figure 6-3 (p. 70)):

$$For \quad \sin\left(\varphi_{m}\right)<3/4\sin\left(\varphi\right): \qquad \qquad \psi_{m}=0$$

$$For \quad \sin\left(\varphi_{m}\right)\geq3/4\sin\left(\varphi\right) \quad and \quad \psi>0 \quad \sin\left(\psi_{m}\right)=\max\left(\frac{\sin(\varphi_{m})-\sin(\varphi_{cv})}{1-\sin(\varphi_{cv})},0\right)$$

$$For \quad \sin\left(\varphi_{m}\right)\geq3/4\sin\left(\varphi\right) \quad and \quad \psi\leq0 \qquad \qquad \psi_{m}=\psi$$

$$If \quad \varphi=0 \qquad \qquad \psi_{m}=0$$

where

Critical state friction angle, being a material constant independent of density.

 φ_m Mobilised friction angle:

$$\sin\left(arphi_{m}
ight) = rac{\sigma_{1}' - \sigma_{3}'}{\sigma_{1}' + \sigma_{3}' - 2c\cot\left(arphi
ight)}$$
 (6–16)

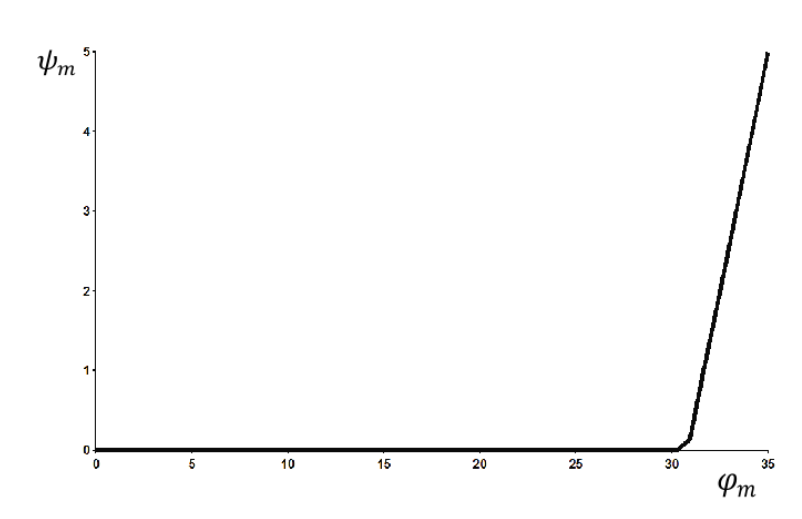


Figure 6-3: Plot of mobilized dilatancy angle ψ_m and mobilized friction angle ϕ_m for Hardening Soil model

The above equations are a small adaptation from the well-known stress-dilatancy theory by Rowe (1962), as explained by Schanz & Vermeer (1966). The mobilised dilatancy angle, ψ_m , follows Rowe's theory for larger values of the mobilised friction angle, as long as this results in a positive value of ψ_m . For small mobilised friction angles and for negative values of ψ_m , as computed by Rowe's formula (as long as the dilatancy angle ψ is positive), ψ_m is taken zero. Furthermore, in all cases when $\varphi = 0$, ψ_m is set equal to zero.

The essential property of the stress-dilatancy theory is that the material contracts for small stress ratios $\varphi_m < \varphi_{cv}$, whilst dilatancy occurs for high stress ratios $\varphi_m > \varphi_{cv}$. At failure, when the mobilised friction angle equals the failure angle, φ , it is found from Eqn. 6-15 (p. 70) that:

$$\sin\left(\psi\right) = \frac{\sin\left(\varphi\right) - \sin\left(\varphi_{cv}\right)}{1 - \sin\left(\varphi\right)\sin\left(\varphi_{cv}\right)} \tag{6-17}$$

or equivalently:

$$\sin\left(\varphi_{cv}\right) = \frac{\sin\left(\varphi\right) - \sin\left(\psi\right)}{1 - \sin\left(\varphi\right)\sin\left(\psi\right)} \tag{6-18}$$

Hence, the critical state angle can be computed from the failure angles φ and ψ . PLAXIS performs this computation automatically and therefore users do not need to specify a value for φ_{CV} . Instead, one has to provide input data on the peak friction angle, φ , and the peak dilatancy angle, ψ .

The shear hardening process will continue with the mobilization of the shear strength, until the maximum shear strength according to the Mohr-Coulomb model failure criterion is reached.

6.4 Parameters of the Hardening Soil Model

Some parameters of the present hardening model coincide with those of the non-hardening Mohr-Coulomb model. These are the failure parameters c, φ and ψ .



Figure 6-4: Parameters for the Hardening Soil model

Failure parameters as in Mohr-Coulomb model (see 3.3 Parameters of the Mohr-Coulomb model (p. 34))

С	(Effective) cohesion	[kN/m ²]
φ	(Effective) angle of internal friction	[°]
Ψ	Angle of dilatancy	[°]
σ_t	Tension cut-off and tensile strength	[kN/m ²]

Basic parameters for soil stiffness:

$E_{50}^{ m ref}$	Secant stiffness in standard drained triaxial test at the reference stress	[kN/m ²]
$E_{oed}^{ m ref}$	Tangent stiffness for primary oedometer loading at the reference stress	[kN/m ²]
$E_{ur}^{ m ref}$	Unloading / reloading stiffness at the reference stress (default $E_{ur}^{ref} = 3E_{50}^{ref}$)	[kN/m²]
m	Power for stress-level dependency of stiffness	[-]

Advanced parameters (it is advised to use the default setting):

V _{ur}	Poisson's ratio for unloading-reloading (default $v_{ur} = 0.2$)	[-]
p ^{ref}	Reference stress for stiffnesses (default $p^{ref} = 100 \text{ kN/m}^2$)	[kN/m²]
K_0^{nc}	K_0 -value for normal consolidation (default $K_0^{nc}=1$ - sin φ)	[-]
R_f	Failure ratio q_f / q_a (default R_f = 0.9) (see Figure 6–1 (p. 67)).	[-]
$\sigma_{tension}$	Tensile strength (default $\sigma_{tension} = 0$)	[kN/m ²]
C _{inc}	As in Mohr-Coulomb model (default $c_{inc} = 0$)	[kN/m ³]

Instead of entering the basic parameters for soil stiffness, alternative parameters can be entered. These parameters are listed below:

C_c	Compression index	[-]
C _s	Swelling index or reloading index	[-]
e _{init}	Initial void ratio	[-]

6.4.1| Stiffness moduli $E_{50}^{ m ref}$, $E_{oed}^{ m ref}$ & $E_{ur}^{ m ref}$ and power m

The advantage of the Hardening Soil model over the Mohr-Coulomb model is not only the use of a hyperbolic stress-strain curve instead of a bi-linear curve, but also the control of stress level dependency. When using the Mohr-Coulomb model, the user has to select a fixed value of Young's modulus whereas for real soils this stiffness depends on the stress level. It is therefore necessary to estimate the stress levels within the soil and use these to obtain suitable values

of stiffness. With the Hardening Soil model, however, this cumbersome selection of input parameters is not required.

Instead, a stiffness modulus $E_{50}^{
m ref}$ is defined for a reference minor principal effective stress of $-\sigma'_3 = p^{ref}$. This is the secant stiffness at 50 % of the maximum deviatoric stress, at a cell pressure equal to the reference stress p^{ref} (Figure 6–5 (p. 73)). As a default value, the program uses $p^{ref} = 100 \text{ kN/m}^2$.

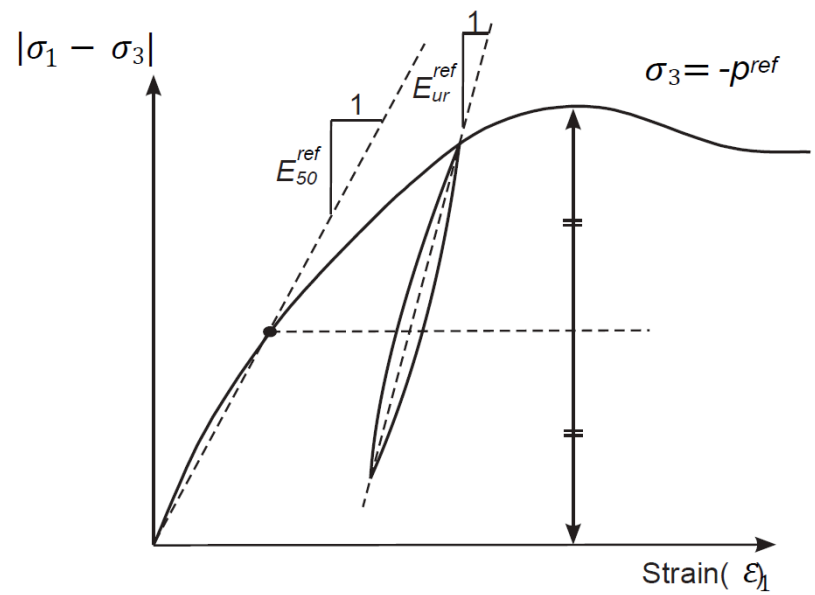


Figure 6–5: Definition of E_{50}^{ref} and E_{ux}^{ref} for drained triaxial test results

As some PLAXIS users are familiar with the input of shear moduli rather than the above stiffness moduli, shear moduli will now be discussed. Within Hooke's law of isotropic elasticity conversion between E and G goes by the equation E = 2(1+v)G. As E_{ur} is a real elastic stiffness, one may thus write $E_{ur}=2(1+v)G_{ur}$, where G_{ur} is an elastic shear modulus.

Note: PLAXIS allows for the input of E_{ur} and v_{ur} but not for a direct input of G_{ur} . In contrast to E_{ur} , the secant modulus E_{50} is not used within a concept of elasticity. As a consequence, there is no simple conversion from E_{50} to G_{50} .

In contrast to elasticity based models, the elastoplastic Hardening Soil model does not involve a fixed relationship between the (drained) triaxial stiffness E_{50} and the oedometer stiffness E_{oed} for one-dimensional compression. Instead, these stiffnesses can be inputted independently. Having defined E_{50} by Eqn. 6–5 (p. 66), it is now important to define the oedometer stiffness. Here we use the equation:

$$E_{oed} = E_{oed}^{ref} \left(rac{c\cos\left(arphi
ight) - rac{\sigma_3'}{K_0^{nc}}\sin\left(arphi
ight)}{c\cos(arphi) + p^{ref}\sin\left(arphi
ight)}
ight)^m$$
 (6–19)

where E_{oed} is a tangent stiffness modulus obtained from an oedometer test, as indicated in Figure 6-6 (p. 74).

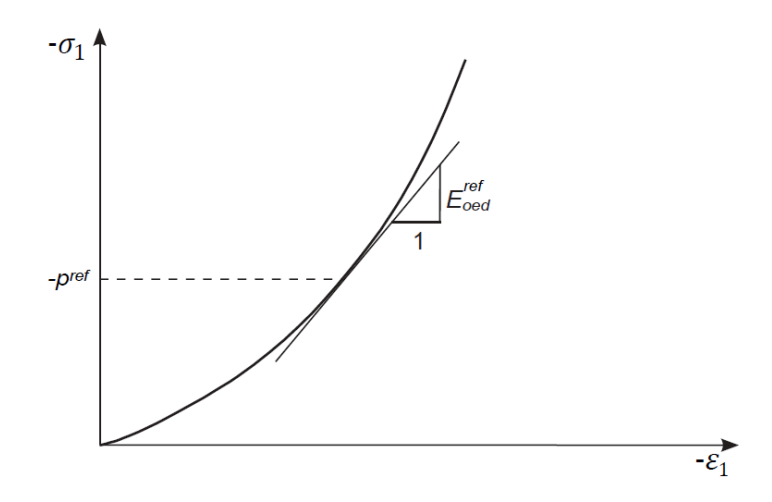


Figure 6–6: Definition of E_{oed}^{ref} and $E_{\mathit{ur}}^{\mathit{ref}}$ in oedometer test results

Hence, E_{oed}^{ref} is a tangent stiffness at a vertical stress of $-\sigma_1' = \frac{\sigma_3'}{K_0^{ne}} = p^{ref}$. Note that we basically use σ'_1 rather than σ'_3 and that we consider primary loading.

When undrained behaviour is considered in the Hardening Soil model the Drainage type should preferably be set to Undrained (A). Alternatively, Undrained (B) can be used in case the effective strength properties are not known or the undrained shear strength is not properly captured using Undrained (A). However, it should be noted that the material loses its stress-dependency of stiffness in that case. Undrained (C) is not possible since the model is essentially formulated as an effective stress model.

6.4.2 Alternative stiffness parameters

When soft soils are considered, the stiffness parameters can be calculated from the compression index, swelling index and the initial void ratio ¹. The relationship between these parameters and the compression index, C_c , is given by:

$$C_c = rac{2.3(1+e_{init})p_{ref}}{E_{oed}^{ref}}$$
 (6–20)

The relationship between the E_{ur}^{ref} and the swelling index, C_{s} , is given by:

$$C_s pprox rac{2.3(1+e_{init})(1+
u_{ur})(1-2
u_{ur})p_{ref}}{\left(1-
u_{ur}
ight)E_{ur}^{ref}K_0}$$
 (6–21)

f O Note: For the relation between $E_{ur}^{
m ref}$ and C_s PLAXIS assumes that the soil is only lightly overconsolidated, hence $K_0 = K_0^{nc}$ is used.

Regardless the previous value of E_{50} , a new value will be automatically assigned according to:

$$E_{50}^{ref} = 1.25 E_{oed}^{ref}$$
 (6–22)

¹ In the PLAXIS material database, these alternative parameters depend on the initial void ratio. In reality, these parameters depend on the actual void ratio, which is not a constant.

Although for Soft soils, $E_{50}^{\rm ref}$ could be as high as 2 $E_{oed}^{\rm ref}$, this high value could lead to a numerical instability; therefore a lower value is used. Changing the value of $C_{\rm s}$ will change the stiffness parameter E_{ur}^{ref} .

Note that the value of the power for stress-level dependency of stiffness (m) is automatically set to 1.

6.4.3 Advanced parameters

Realistic values of v_{ur} are about 0.2 and this value is thus used as a default setting, as indicated in Figure 6-4 (p. 71). Note that in the Hardening Soil model, v_{ur} is a pure elastic parameter.

In contrast to the isotropic elasticity, K_0^{nc} is not simply a function of Poisson's ratio, but an independent input parameter. As a default setting PLAXIS uses the correlation K_0^{nc} = 1-sin φ . It is suggested to maintain this value as the correlation is quite realistic. However, users do have the possibility to select different values. Not all possible input values for K_0^{nc} can be accommodated for. Depending on other parameters, such as $E_{50}^{
m ref}$, $E_{oed}^{
m ref}$ $E_{ur}^{
m ref}$ and ${
m v}_{ur}$, there happens to be a certain range of valid K_0^{nc} -values. K_0^{nc} values outside this range are rejected by PLAXIS. On inputting values, the program shows the nearest possible value that will be used in the computations.

6.4.4 Dilatancy cut-off

After extensive shearing, dilating materials may reach a state of critical density where dilatancy has come to an end, as indicated in Figure 6-7 (p. 76). This phenomenon of soil behaviour can be included in the Hardening Soil model by means of a dilatancy cut-off. In order to specify this cut-off limit, the initial void ratio, e_{init} , and the maximum void ratio, e_{max} , of the material must be entered as general parameters. As soon as the volume change results in a state of maximum void ratio, the mobilised dilatancy angle, ψ_m , is automatically set back to zero, as indicated in Figure 6-7 (p. 76).

$$for \ \ e < e_{\max} \ \ \sin\left(\psi_m\right) = \frac{\sin(\varphi_m) - \sin(\varphi_{cv})}{1 - \sin(\varphi_m)\sin(\varphi_{cv})}$$

$$where: \ \ \sin\left(\varphi_{cv}\right) = \frac{\sin(\varphi) - \sin(\psi)}{1 - \sin(\varphi)\sin(\psi)}$$

$$for \ \ e \ge e_{\max} \ \ \psi_m = 0$$

$$(6-24)$$

for
$$e \ge e_{\max}$$
 $\psi_m = 0$ (6-24)

The void ratio is related to the volumetric strain, ε_{v} by the relationship:

$$\left(arepsilon_v-arepsilon_v^{init}
ight)=\ln\!\left(rac{1+e}{1+e_{init}}
ight)$$
 (6–25)

where an increment of ε_{v} is positive for dilatancy.

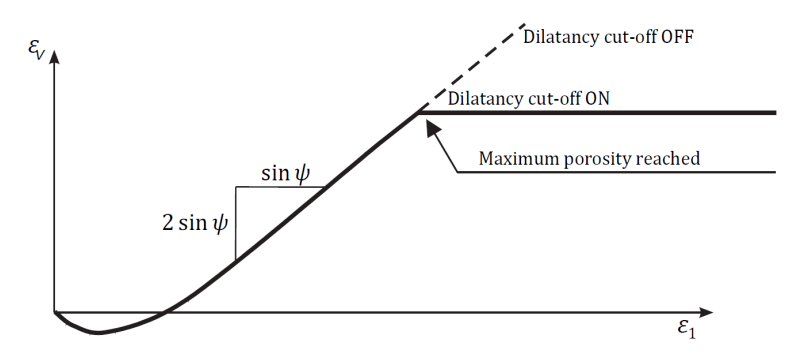


Figure 6-7: Resulting strain curve for a standard drained triaxial test when including dilatancy cut-off

The selection of the Dilatancy cut-off is only available when the Hardening Soil model or the Hardening Soil model with small-strain stiffness has been selected. By default, the Dilatancy cut-off is not active. Note that the dilatancy cut-off does not help in limiting the shear strength when using the Undrained A drainage type with a positive dilatancy angle. This is because the void ratio remains constant for undrained materials. Therefore, it is strongly recommended to set $\psi = 0$ for undrained material behaviour (*Undrained A*).

6.5 On the cap yield surface in the Hardening Soil model

Shear hardening yield surfaces as indicated in Figure 6-2 (p. 69) do not explain the plastic volume strain that is measured in isotropic compression which is mostly observed in softer types of soil. A second type of yield surface must therefore be introduced to close the elastic region for compressive (compaction hardening) stress paths. Without such a cap type yield surface it would not be possible to formulate a model with independent input of both E_{50}^{ref} and E_{oed}^{ref} . The triaxial modulus largely controls the shear yield surface and the oedometer modulus controls the cap yield surface. In fact, E_{50}^{ref} largely controls the magnitude of the plastic strains that are associated with the shear yield surface. Similarly, $E_{oed}^{\it ref}$ is used to control the magnitude of plastic strains that originate from the yield cap. In this section the yield cap will be described in detail. To this end we consider the definition of the cap yield surface:

$$f_c = rac{{ ilde q}^2}{M^2} + ig(p'ig)^2 - p_p^2$$
 (6–26)

where

Mauxiliary model parameter that relates to K_0^{nc} (discussed later in section).

Furthermore we have:

 $p'=(\sigma'_1+\sigma'_2+\sigma'_3)/3$ and $\tilde{q}=-\sigma'_1-(\alpha-1)\sigma'_2+\alpha\sigma'_3$ with $\alpha=(3+\sin\varphi)/(3-\sin\varphi)$. \tilde{q} is a special stress measure for deviatoric stresses.

In the special case of triaxial compression $(-\sigma'_1 > -\sigma'_2 = -\sigma'_3)$ it yields $\tilde{q} = -(\sigma'_1 - \sigma'_3)$ and for triaxial extension $(-\sigma'_1 = -\sigma'_2 > -\sigma'_3)$ \tilde{q} reduces to $\tilde{q} = -\alpha(\sigma'_1 - \sigma'_3)$. The magnitude of the yield cap is determined by the isotropic pre-consolidation stress p_p (i.e. the hardening parameter associated with this yield surface). In a (p', \tilde{q}) plane, the yield cap $(f_c = 0)$ is a part of an ellipse with its centre point in the origin (Figure 6–8 (p. 78)). The hardening law relating $\dot{p_p}$ to

volumetric cap strain $\dot{arepsilon}_v^{pc}$ in primary drained isotropic compression and assuming p_p as positive for compression can be described by:

$$\dot{\varepsilon}_{v}^{pc} = \frac{K_{s}/K_{c} - 1}{K_{s}^{ref}} \left[\left(\frac{p_{p} + c \cot{(\varphi)}}{p^{ref} + c \cot{(\varphi)}} \right)^{-m} \right] \dot{p}_{p}$$
 (6-27)

in which K_s^{ref} is the reference bulk modulus in unloading / reloading:

$$K_{s}^{ref} = rac{E_{ur}^{ref}}{3(1-2
u_{ur})}$$
 (6–28)

and K_s/K_c is the ratio of bulk moduli in isotropic swelling and primary isotropic compression.

The volumetric cap strain is the plastic volumetric strain in isotropic compression. In addition to the well known constants m and p^{ref} there is another model constant K_s/K_c . Both M (Eqn. 6-26 (p. 76)) and K_s/K_c (Eqn. 6–27 (p. 77)) are cap parameters, but these are not used as direct input parameters. Instead, there is a relationship of the form:

$$M\leftrightarrow K_0^{nc} \qquad (default: K_0^{nc}=1-\sin{(\varphi)})$$
 (6–29)

and the ratio K_s/K_c can be approximated as:

$$K_s/K_cpproxrac{E_{ur}^{ref}}{E_{oed}^{ref}}rac{K_0^{nc}}{\left(1+2K_0^{nc}
ight)\left(1-2
u_{ur}
ight)}$$
 (6–30)

such that K_0^{nc} , E_{ur}^{ref} and E_{oed}^{ref} can be used as input parameters that determine the magnitude of M and K_s/K_c respectively. M is determined by finding the correct steepness of the cap for the K_0^{nc} path in the similar way as is done for the Soft Soil model K 0 n c -parameter (p. 115), see Egn. 10-13 (p. 115).

The ellipse on which the yield cap is located has length p_p on the p-axis and $M p_p$ on the \tilde{q} -axis. Hence, p_p determines its magnitude and M its aspect ratio. High values of M lead to steep caps underneath the Mohr-Coulomb line and correspondingly small K_0^{nc} -values, whereas small \emph{M} values define caps that are much more pointed around the p-axis leading to large K_0^{nc} -values. The ellipse is used both as a yield surface and as a plastic potential (associated plasticity). Input data on initial p_p -values is provided by means of the PLAXIS procedure for initial stresses. Here, p_p is either computed from the input overconsolidation ratio (OCR) or the pre-overburden pressure (POP) (see 2.9 On the initial stresses (p. 29)).

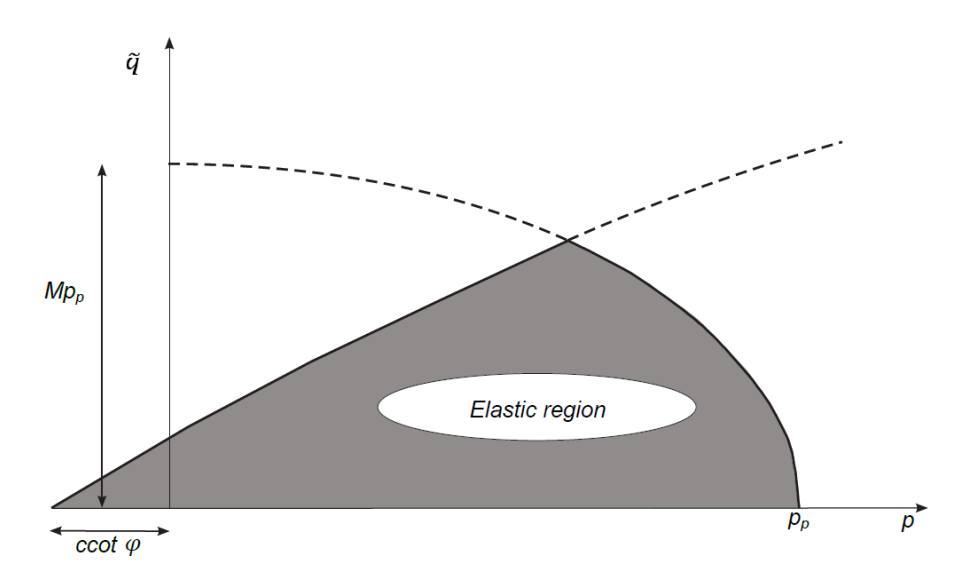


Figure 6–8: Yield surfaces of in p - \tilde{q} -plane. The elastic region can be further reduced by means of a tension cut-off

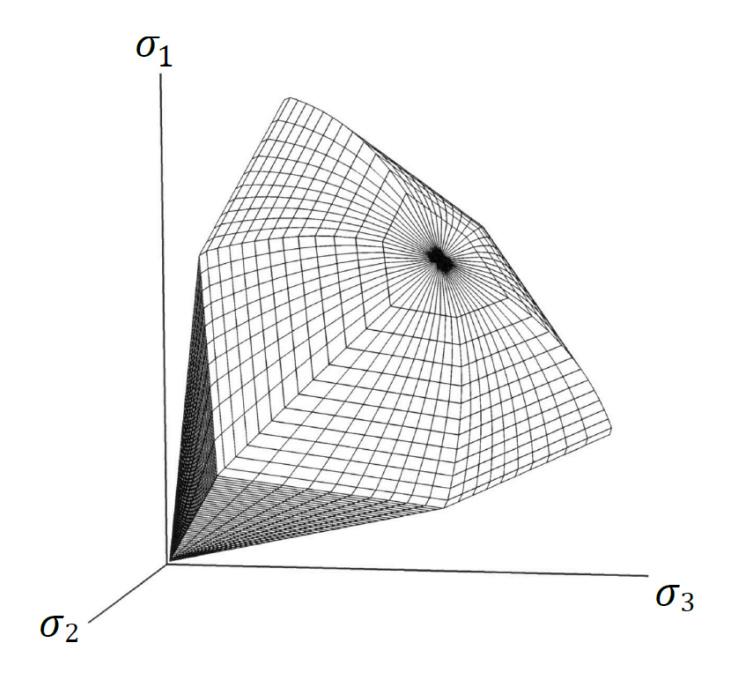


Figure 6-9: Representation of total yield contour of the Hardening Soil model in principal stress space for cohesionless soil

For understanding the yield surfaces in full detail, one should consider both Figure 6-8 (p. 78) and Figure 6-9 (p. 78). The first figure shows simple yield lines, whereas the second one depicts yield surfaces in principal stress space. Both the shear locus and the yield cap have the hexagonal shape of the classical Mohr-Coulomb failure criterion. In fact, the shear yield locus can expand up to the ultimate Mohr-Coulomb failure surface. The cap yield surface expands as a function of the pre-consolidation stress p_p .

6.6 State parameters in the Hardening Soil model

In addition to the output of standard stress and strain quantities, the Hardening Soil model provides output (when being used) on state variables such as the hardening parameters: equivalent mobilised plastic shear strain y^p and the isotropic pre-consolidation stress p_p . These parameters can be visualised by selecting the State parameters option from the stresses menu. An overview of available state parameters is given below:

	Equivalent isotropic stress	
P _{eq}	$p_{eq} = \sqrt{rac{ ilde{q}^2}{M^2} + \left(p\prime ight)^2}$	[kN/m ²]
p_p	Isotropic pre-consolidation stress	[kN/m ²]
OCR	Isotropic overconsolidation ratio ($OCR = p^p/p^{eq}$)	[-]
Υ ^p	Equivalent mobilised plastic shear strain	[-]
E _{ur}	Current stress-dependent elastic Young's modulus	[kN/m ²]
С	Current depth-dependent cohesion	[kN/m ²]

6.7 On the use of the Hardening Soil model in dynamics calculations

When using the Hardening Soil model in dynamics calculations, the elastic stiffness parameter E_{ur}^{ref} needs to be selected such that the model correctly predicts wave velocities in the soil. This generally requires an even larger small strain stiffness rather than just an unloading-reloading stiffness to be entered for E_{ur}^{ref} . When subjected to dynamic or cyclic loading, the Hardening Soil model will generate plastic strains when mobilizing the soil's material strength (shear hardening) or increasing the soil's preconsolidation stress (compaction hardening). However, it should be noted that stress cycles within the current hardening contours will only generate elastic strains and no (hysteretic) damping, nor accumulation of strains or pore pressure nor liquefaction. In order to simulate the soil's damping characteristics in cyclic loading, Rayleigh damping may be defined. Note that some of the limitations of the Hardening Soil model in dynamic applications can be overcome by using the Hardening Soil model with small-strain stiffness (7 The Hardening Soil model with small-strain stiffness (HSsmall) (p. 80)).

The Hardening Soil model with smallstrain stiffness (HSsmall)

The original Hardening Soil model assumes elastic material behaviour during unloading and reloading. However, the strain range in which soils can be considered truly elastic, i.e. where they recover from applied straining almost completely, is very small. With increasing strain amplitude, soil stiffness decays nonlinearly. Plotting soil stiffness against log(strain) yields characteristic S-shaped stiffness reduction curves. Figure 7–1 (p. 81) gives an example of such a stiffness reduction curve. It outlines also the characteristic shear strains that can be measured near geotechnical structures and the applicable strain ranges of laboratory tests. It turns out that at the minimum strain which can be reliably measured in classical laboratory tests, i.e. triaxial tests and oedometer tests without special instrumentation, soil stiffness is often decreased to less than half its initial value.

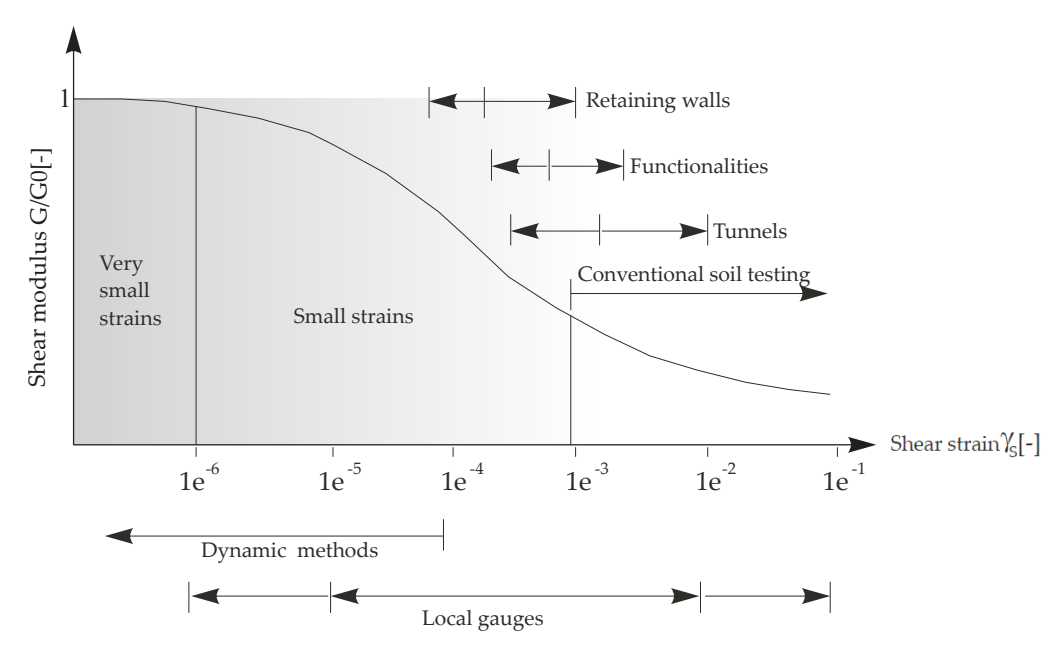


Figure 7-1: Characteristic stiffness-strain behaviour of soil with typical strain ranges for laboratory tests and structures (after Atkinson & Sallfors, 1991)

The soil stiffness that should be used in the analysis of geotechnical structures is not the one that relates to the strain range at the end of construction according to Figure 7-1 (p. 81). Instead, very small-strain soil stiffness and its non-linear dependency on strain amplitude should be properly taken into account. In addition to all features of the Hardening Soil model, the Hardening Soil model with small-strain stiffness offers the possibility to do so.

The Hardening Soil model with small-strain stiffness implemented in PLAXIS is based on the Hardening Soil model and uses almost entirely the same parameters (see 6.4 Parameters of the Hardening Soil Model (p. 71)). In fact, only two additional parameters are needed to describe the variation of stiffness with strain:

- the initial or very small-strain shear modulus G_0 .
- the shear strain level $y_{0.7}$ at which the secant shear modulus G_s is reduced to about 70% of G_0 .

7.1 Describing small-strain stiffness with a Simple Hyperbolic Law

In soil dynamics, small-strain stiffness has been a well known characteristic of soil behaviour for a long time. In static analysis, the findings from soil dynamics have long been considered not to be applicable.

Seeming differences between static and dynamic soil stiffness have been attributed to the nature of loading (e.g. inertia forces and strain rate effects) rather than to the magnitude of applied strain which is generally small in dynamic conditions (earthquakes excluded). As inertia forces and strain rate have only little influence on the initial soil stiffness, dynamic soil stiffness and small-strain stiffness can in fact be considered as synonyms.

Probably the most frequently used model in soil dynamics is the Hardin-Drnevich relationship. From test data, sufficient agreement is found that the stress-strain curve for small strains can be adequately described by a simple hyperbolic law. The following analogy to the hyperbolic law for larger strains by Konder (1963) (see 6 The Hardening Soil model (Isotropic hardening) (p. 65)) was proposed by Hardin & Drnevich(1972):

$$rac{G_s}{G_0}=rac{1}{1+\left|rac{\gamma}{\gamma_r}
ight|}$$
 (7–1)

where the threshold shear strain y_r is quantified as:

$$\gamma_r = rac{ au_{ ext{max}}}{G_0}$$
 (7–2)

with τ_{max} being the shear stress at failure. Essentially, Eqn. 7–1 (p. 82) and Eqn. 7–2 (p. 82) relate large (failure) strains to small-strain properties which often work well.

More straightforward and less prone to error is the use of a smaller threshold shear strain. Santos & Correia (2001), for example suggest to use the shear strain $\gamma_r = \gamma_{0.7}$ at which the secant shear modulus G_s is reduced to about 70 % of its initial value. Eqn. 7–1 (p. 82) can then be rewritten as:

In fact, using a = 0.385 and $y = y_{0.7}$ gives $G_s/G_0 = 0.722$. Hence, the formulation "about 70%" should be interpreted more accurately as 72.2%.

Figure 7–2 (p. 82) shows the fit of the modified Hardin-Drnevich relationship (Eqn. 7–3 (p. 82)) to normalised test data.

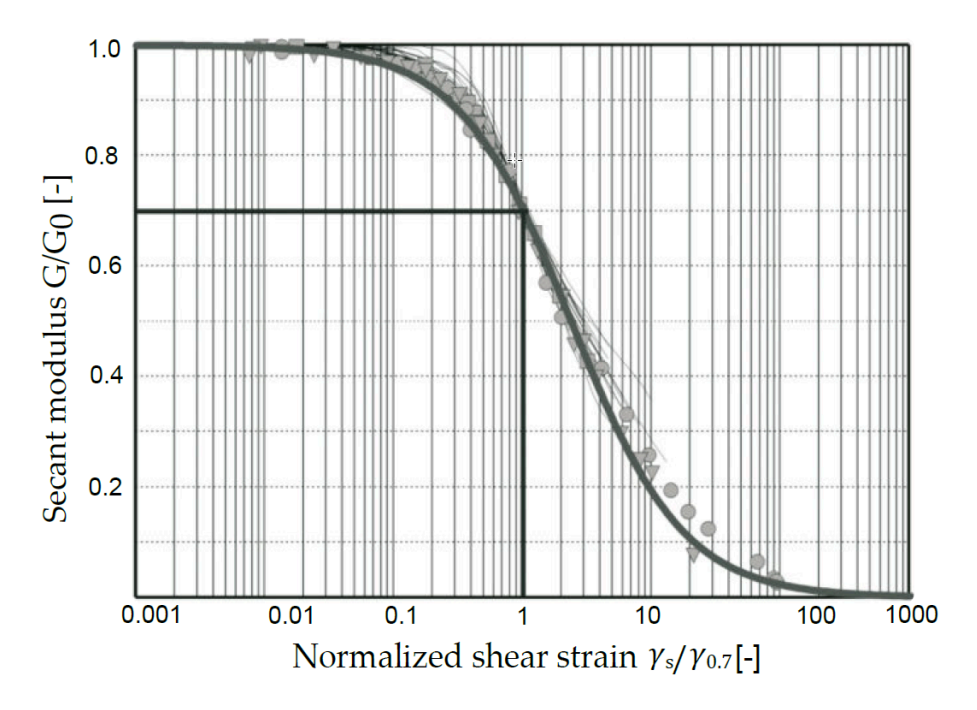


Figure 7-2: Results from the Hardin-Drnevich relationship compared to test data by Santos & Correia (2001)

7.2 Applying the Hardin-Drnevich relationship in the HS Model

The decay of soil stiffness from small strains to larger strains can be associated with loss of intermolecular and surface forces within the soil skeleton. Once the direction of loading is reversed, the stiffness regains a maximum recoverable value which is in the order of the initial soil stiffness. Then, while loading in the reversed direction is continued, the stiffness decreases again. A strain history dependent, multi-axial extension of the Hardin-Drnevich relationship is therefore needed in order to apply it in the Hardening Soil model. Such an extension has been proposed by Benz (2006) in the form of the small-strain overlay model. Benz derives a scalar valued shear strain y_{hist} by the following projection:

$$\gamma_{hist} = \sqrt{3} rac{\|oldsymbol{H} \Delta \underline{e}\|}{\|\Delta e\|}$$
 (7–4)

where

Actual deviatoric strain increment.

 \boldsymbol{H} Symmetric tensor that represents the deviatoric strain history of the material.

Whenever a strain reversal is detected the tensor H is partially or fully reset before the actual strain increment $\Delta \underline{e}$ is added.

As the criterion for strain reversals serves a criterion similar as in Simpson's brick model (1992): All three principal deviatoric strain directions are checked for strain reversals separately which resembles three independent brick models. When there is no principal strain rotation, the criterion reduces to two independent brick-models. For further details on the strain tensor Hand its transformation at changes in the load path it is referred to Benz (2006).

The scalar valued shear strain $\gamma = \gamma_{hist}$ calculated in Eqn. 7–4 (p. 83) is applied subsequently used in Eqn. 7-3 (p. 82). Note that in both, Eqn. 7-3 (p. 82) and Eqn. 7-4 (p. 83), the scalar valued shear strain is defined as:

$$\gamma = rac{3}{2}arepsilon_q$$
 (7–5)

where

Second deviatoric strain invariant General definitions of strain

In triaxial conditions y can therefore be expressed as:

$$\gamma = \varepsilon_{axial} - \varepsilon_{lateral}$$
 (7–6)

Within the Hardening Soil model with small-strain stiffness, the stress-strain relationship can be simply formulated from the secant shear modulus (Eqn. 7-3 (p. 82)) as:

$$au=G_s\gamma=rac{G_0\gamma}{1+0.385rac{\gamma}{\gamma_{0.7}}}$$
 (7–7)

Taking the derivative with respect to the shear strain gives the tangent shear modulus:

$$G_t = rac{G_0}{\left(1 + 0.385 rac{\gamma}{\gamma_{0.7}}
ight)^2}$$
 (7–8)

This stiffness reduction curve reaches far into the plastic material domain. In the Hardening Soil model and Hardening Soil model with small-strain stiffness, stiffness degradation due to plastic straining is simulated with strain hardening. In the Hardening Soil model with small-strain stiffness, the small-strain stiffness reduction curve is therefore bound by a certain lower limit, determined by conventional laboratory tests:

The lower cut-off of the tangent shear modulus G_t is introduced at the unloading reloading stiffness G_{ur} which is defined by the material parameters E_{ur} and v_{ur} :

$$G_t \geq G_{ur}$$
 where $G_{ur} = rac{E_{ur}}{2(1+v_{ur})}$ and $G_t = rac{E_t}{2(1+v_{ur})}$ (7–9)

The cut-off shear strain $\gamma_{cut-off}$ can be calculated as:

$$\gamma_{cut-off}=rac{1}{0.385}\left(\sqrt{rac{G_0}{G_{ur}}}-1
ight)\gamma_{0.7}$$
 (7–10)

Within the Hardening Soil model with small-strain stiffness, the quasi-elastic tangent shear modulus is calculated by integrating the secant stiffness modulus reduction curve over the actual shear strain increment. An example of a stiffness reduction curve used in the Hardening Soil model with small-strain stiffness is shown in Figure 7-3 (p. 84).

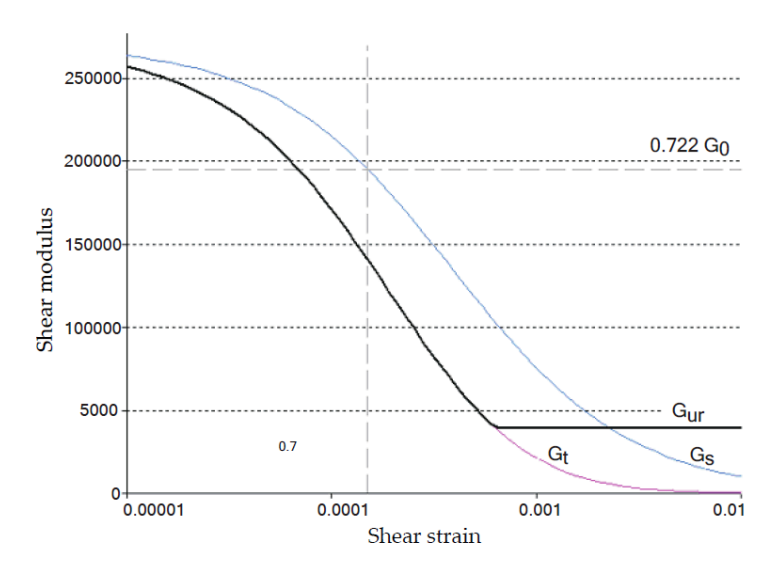


Figure 7–3: Secant and tangent shear modulus reduction curve

Moreover, the tangent shear modulus G_t and corresponding Young's modulus E_t (considering a constant Poisson's ratio v_{ur}), is stress-dependent, and follows the same power law as formulated in Egn. 6-7 (p. 67). For primary loading situations, the model uses the same hardening plasticity formulations as the Hardening Soil model, where E_{ur} is replaced by E_t as described above.

7.3 Virgin (initial) loading vs unloading/ reloading

Masing (1926) described the hysteretic behaviour of materials in unloading / reloading cycles in the form of the following rules:

The shear modulus in unloading is equal to the initial tangent modulus for the initial loading curve.

The shape of the unloading and reloading curves is equal to the initial loading curve, but twice stiffer. In terms of the above introduced threshold shear strain $\gamma_{0.7}$, Masing's rule can be fulfilled by the following setting in the Hardin-Drnevich relation:

$$\gamma_{0.7re-loading} = 2\gamma_{0.7virgin-loading}$$
 (7–11)

Figure 7-4 (p. 85) and Figure 7-5 (p. 86) illustrate Masing's rule and the secant stiffness reduction in virgin loading and unloading / reloading.

The Hardening Soil model with small-strain stiffness adopts Masing's rule. According to it, the threshold shear strain and the reloading curve are obtained by scaling the backbone curve (virgin loading) by a factor of 2. Note, however, that in this constitutive model, the hardening plasticity accounts for more rapidly decaying small-strain stiffness during virgin loading. Consequently, the unloading / reloading response - which will be, at least partly, purely elastic - will be naturally stiffer than virgin (i.e. elasto-plastic) loading. As such, the scaling factor for the threshold shear strain is assumed to be constant and equal to 2 (as presented in Eqn. 7-11 (p. 85)) throughout loading. This is different from what is often assumed by other constitutive models incorporating a small strain component, where the scaling factor is initialised to 1 and changed to 2 once a first strain reversal is detected. As mentioned earlier, this is not necessary in HS-small, as the modeled response will be generally elasto-plastic from the start of shearing, unless a deviatoric pre-loading is applied beforehand.

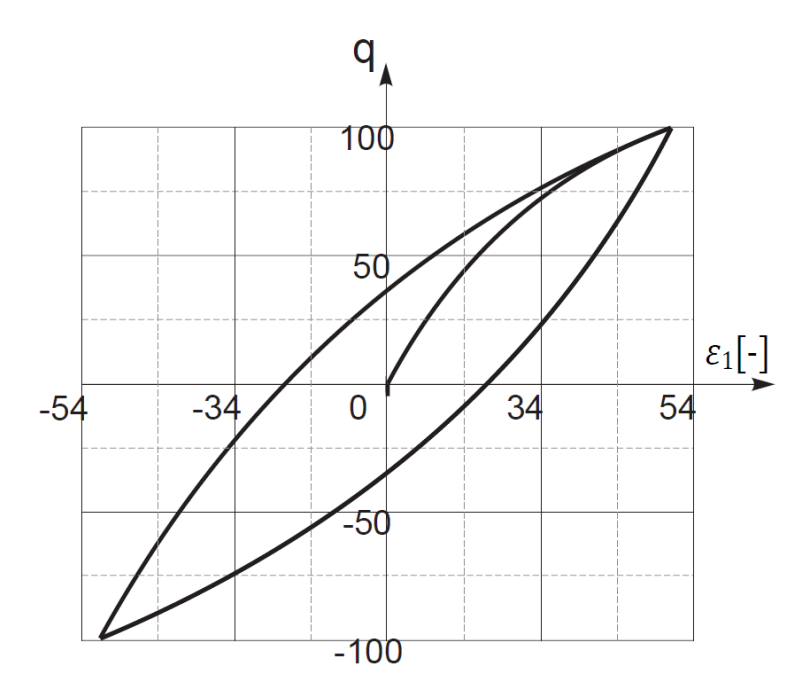


Figure 7-4: Hysteretic material behaviour

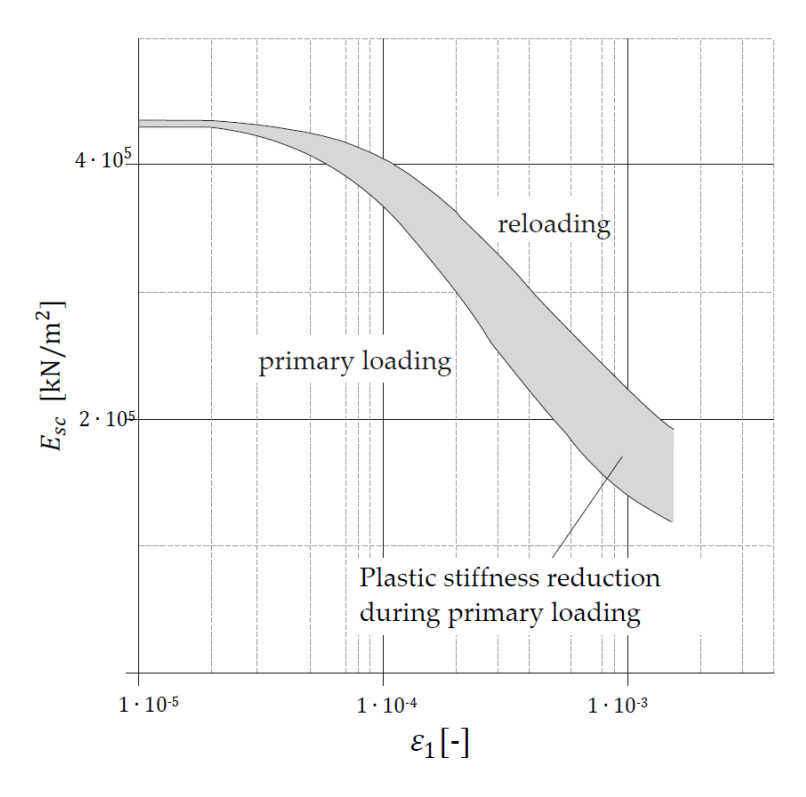


Figure 7-5: Stiffness reduction in initial -or primary loading and in unloading/reloading

7.4 | Model Parameters

Compared to the standard Hardening Soil model, the Hardening Soil model with smallstrain stiffness requires two additional stiffness parameters as input: G_0^{ref} and $\gamma_{0.7}$. All other parameters, including the alternative stiffness parameters, remain the same as in the standard Hardening Soil model. G_0^{ref} defines the shear modulus at very small strains e.g. ε < 10 $^{-6}$ at a reference minor principal stress of - $\sigma'_3 = p^{ref}$.

The Poisson's ratio v_{ur} is assumed a constant, so that the shear modulus G_0^{ref} can also be calculated from the very small strain Young's modulus as:

$$G_0^{ref}=E_0^{ref}/\Big(2\Big(1+
u_{ur}\Big)\Big)$$
 (7–12)

The threshold shear strain $\gamma_{0.7}$ is the shear strain at which the secant shear modulus G_s^{ref} is decayed to 0.722 G_0^{ref} . The threshold shear strain $\gamma_{0.7}$ is to be supplied for virgin loading. In summary, the input stiffness parameters of the Hardening Soil model with small-strain stiffness are listed below:

m	Power for stress-level dependency of stiffness	[-]
E_{50}^{ref}	Secant stiffness in standard drained triaxial test	[KN/m ²]
$E_{oed}^{\it ref}$	Reference tangent stiffness for primary oedometer loading	[KN/m ²]
E_{ur}^{ref}	Reference unloading / reloading stiffness from drained triaxial test	[KN/m ²]

V _{0.7}	Poisson's ratio for unloading-reloading	[-]
G_0^{ref}	Reference shear modulus at very small strains ($\varepsilon < 10^{-6}$)	[KN/m ²]
Y0.7	Threshold shear strain at which $G_s = 0.722G_0$	[-]

Figure 7-6 (p. 87) illustrates the model's stiffness parameters in a drained triaxial test: $\it E_{50}$, $\it E_{ur}$, and $\it E_0=2G_0(1+
u_{ur})$. For the order of strains at which $\it E_{ur}$ and $\it G_0$ are defined and determined, one may refer to e.g. Figure 7-1 (p. 81) and Figure 7-2 (p. 82).

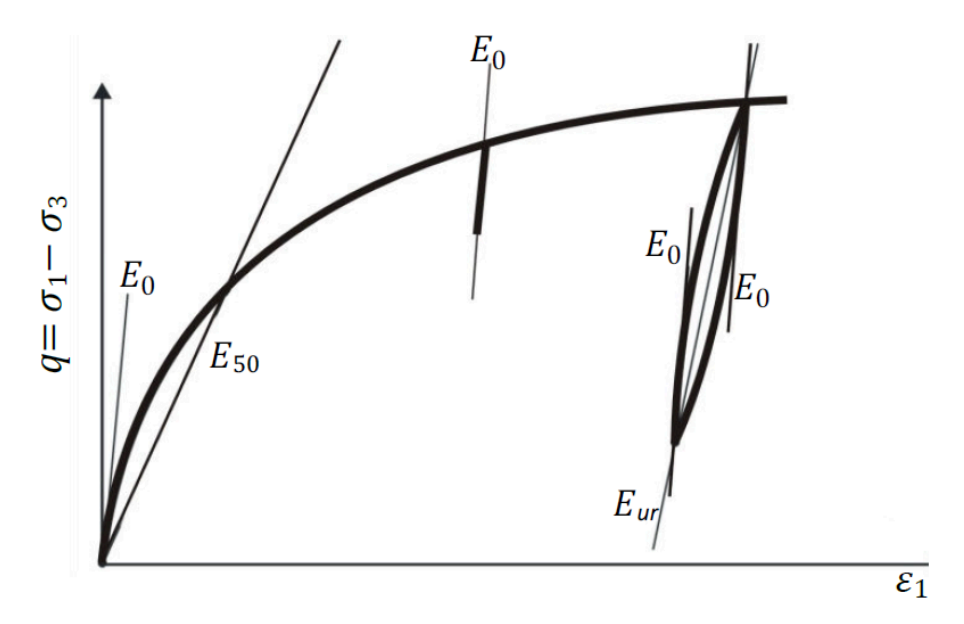


Figure 7–6: Stiffness parameters E_{50} , E_{ur} , and E_0 = $2G_0$ (1 + v_{ur}) of the Hardening Soil model with small-strain stiffness in a triaxial test

Figure 7-7 (p. 88) illustrates the model's stiffness parameters in a stress-controlled drained cyclic shear test.

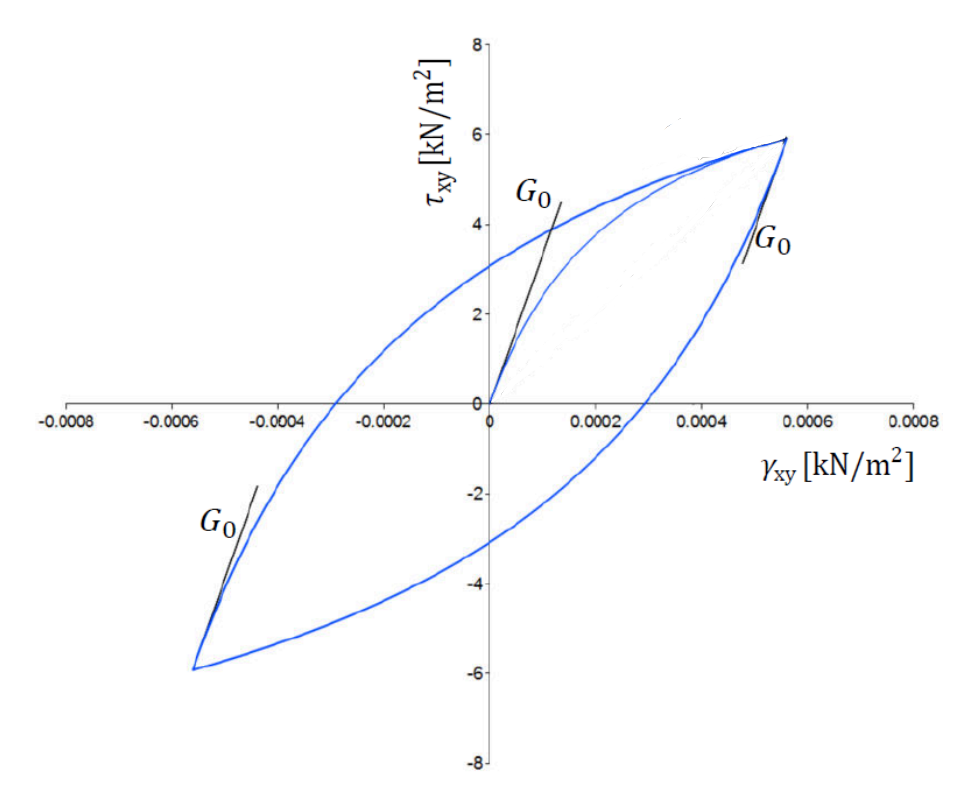


Figure 7-7: Stiffness parameters in cyclic shear test

For quartz sand, a first estimation of the HSsmall parameters is based on the relative density (RD) is given in Brinkgreve, Engin & Engin (2010).

7.5 On the parameters G_0 and $\gamma_{0.7}$

A number of factors influence the small-strain parameters G_0 and $\gamma_{0,7}$. Most importantly they are influenced by the material's actual state of stress and void ratio e. In the Hardening Soil model with small-strain stiffness, the stress dependency of the shear modulus G_0 is taken into account with the power law:

$$G_0 = G_0^{ref} igg(rac{c\cos{(arphi)} - \sigma_3'\sin{(arphi)}}{c\cos{(arphi)} + p^{ref}\sin{(arphi)}}igg)^m$$
 (7–13)

which resembles the ones used for the other stiffness parameters. The threshold shear strain $\gamma_{0.7}$ is taken independently of the mean stress.

Assuming that within a Hardening Soil model with small-strain stiffness (or HS) computation void ratio changes are rather small, the material parameters are not updated for changes in the void ratio. Knowledge of a material's initial void ratio can nevertheless be very helpful in deriving its small-strain shear stiffness G_0 . Many correlations are offered in the literature (Benz, 2006). A good estimation for many soils is for example the relation given by Hardin & Black (1969):

Alpan (1970) empirically related dynamic soil stiffness to static soil stiffness (Figure 7–8 (p. 89)). The dynamic soil stiffness in Alpan's chart is equivalent to the small-strain stiffness G_0 or E_0 . Considering that the static stiffness E_{static} defined by Alpan equals approximately the unloading / reloading stiffness Eur in the Hardening Soil model with small-strain stiffness, Alpan's chart can be used to guess a soil's small-strain stiffness entirely based on its unloading / reloading stiffness E_{ur} . Although Alpan suggests that the ratio E_0 / E_{ur} can exceed 10 for very soft clays, the maximum ratio E_0 / E_{ur} or G_0 / G_{ur} permitted in the HSsmall model is limited to 20.

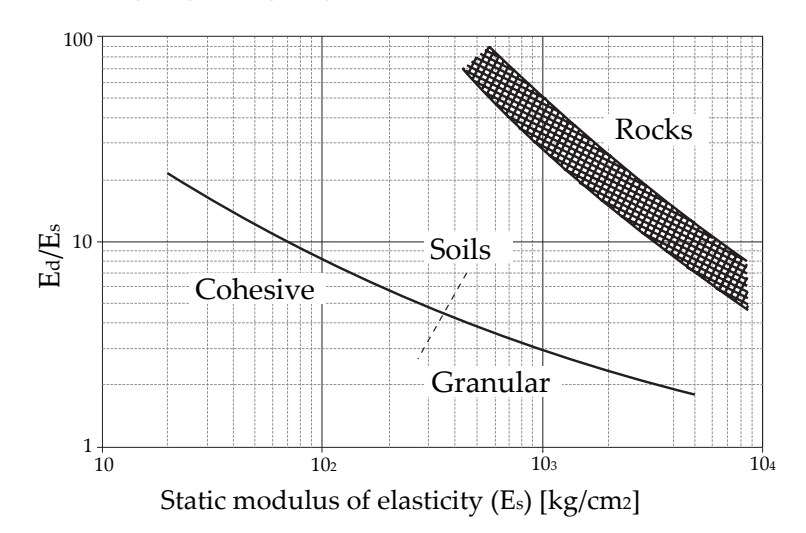


Figure 7–8: Relation between dynamic ($E_d = E_0$) and static soil stiffness ($E_s \approx E_{ur}$) after Alpan(1970)

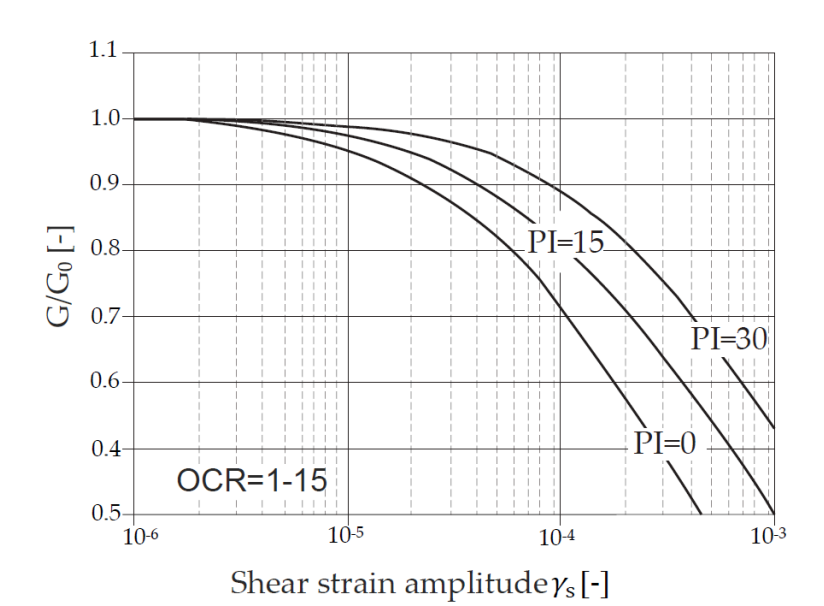


Figure 7-9: Influence of plasticity index (PI) on stiffness reduction after Vucetic & Dobry (1991)

In the absence of test data, correlations are also available for the threshold shear strain $\gamma_{0.7}$. Figure 7-9 (p. 89) for example gives a correlation between the threshold shear strain and the Plasticity Index. Using the original Hardin-Drnevich relationship, the threshold shear strain $\gamma_{0.7}$ might be also related to the model's failure parameters. Applying the Mohr-Coulomb failure criterion in Eqn. 7-2 (p. 82) and Eqn. 7-3 (p. 82) yields:

$$\gamma_{0.7}pproxrac{1}{9G_0}ig[2c'ig(1+\cosig(2arphi'ig)ig)-\sigma_1'ig(1+K_0ig)\sinig(2arphi'ig)ig]$$
 (7–15)

where

 K_{α} The earth pressure coefficient at rest.

 σ'_{1} The effective vertical stress (pressure negative).

7.6 | Model Initialisation

Stress relaxation erases soil's memory of previous applied stress. Soil aging in the form of particle (or assembly) reorganization during stress relaxation and formation of bonds between them can erase soil's strain history. Considering that the second process in a naturally deposited soil develops relatively fast, the strain history should start from zero (H) in most boundary value problems. This is the default setting in the Hardening Soil model with small-strain stiffness.

However, sometimes an initial strain history may be desired. In this case the strain history can be adjusted by applying an extra load step before starting the actual analysis. Such an additional load step might also be used to model overconsolidated soils. Usually the overconsolidation's cause has vanished long before the start of calculation, so that the strain history should be reset afterwards. Unfortunately, strain history is already triggered by adding and removing a surcharge. In this case the strain history can be reset manually, by using the Reset small strain option in the calculation phases window. Also, when resetting displacements to zero, the strain history tensor is reset and the influence of strains from previous calculation phases is ignored.

When using the Hardening Soil model with small-strain stiffness, caution should be given to nil-steps. The strain increments in nil-steps are purely derived from the small numerical unbalance in the system which is due to the accepted tolerated error in the computation. The strain increment direction in nil-steps is therefore arbitrary. Hence, a nil-step may function as randomly reverse load step which is in most cases not desired.

7.7 State parameters in the Hardening Soil model with small-strain stiffness

In addition to the output of standard stress and strain quantities, the Hardening Soil model with small-strain stiffness provides output on State variables. These parameters can be visualised by selecting the State parameters option from the stresses menu. An overview of available state parameters in addition to those listed for the Hardening Soil model is given below:

$arepsilon_{\chi\chi}$ - $arepsilon_{V}$	Strain history parameter used in strain-dependent stiffness formulation	[-]
$arepsilon_{yy}$ - $arepsilon_{v}$	Strain history parameter used in strain-dependent stiffness formulation	[-]
ε_{zz} - ε_{v}	Strain history parameter used in strain-dependent stiffness formulation	[-]
$arepsilon_{ extit{xy}}$	Strain history parameter used in strain-dependent stiffness formulation	[-]
$arepsilon_{yz}$	Strain history parameter used in strain-dependent stiffness formulation	[-]
$arepsilon_{ZX}$	Strain history parameter used in strain-dependent stiffness formulation	[-]

G _s ^{ref}	Secant shear modulus at reference stress level	[kN/m ²]
G/G _{ur}	Minimum ever registered value of the ratio of the primary shear stiffness modulus to the unloading-reloading shear stiffness modulus	[-]

7.8 On the use of the Hardening Soil model with small-strain stiffness in dynamics calculations

In contrast to the Hardening Soil model, the Hardening Soil model with small-strain stiffness shows hysteresis in cyclic loading (Figure 7-6 (p. 87)). The amount of hysteresis depends on the magnitude of the corresponding strain amplitude. However, note that due to the isotropic hardening nature of the plastic component, the model does not generate accumulated strains with multiple loading cycles, nor does it generate accumulated pore pressures with undrained behaviour. When the Hardening Soil model with small-strain stiffness is used wave velocities are not shown because they vary due to the stress-dependent stiffness.

When applied in dynamics calculations, the hysteretic behaviour of the Hardening Soil model with small-strain stiffness leads to damping. The amount of hysteretic damping depends on the applied load amplitude and corresponding strain amplitudes. The maximum amount of hysteretic damping obtained with the Hardening Soil model with small-strain stiffness depends on the ratio of G_0 to $G_{ur}=E_{ur}/2(1+v_{ur})$. A larger ratio leads to a larger maximum amount of hysteretic damping. For more information about the hysteretic damping in the Hardening Soil model with small-strain stiffness reference refer to Brinkgreve, Kappert & Bonnier (2007).

7.9 Other differences to the Hardening Soil model

7.9.1 The mobilised dilatancy angle

The shear hardening flow rule of both the Hardening Soil model and the Hardening Soil model with small-strain stiffness have the linear form:

$$\dot{arepsilon}_{v}^{p}=\sin{(\psi_{m})}\dot{\gamma}^{p}$$
 (7–16)

However, the mobilised dilatancy angle ψ_m in compression is defined differently. The HS model assumes the following:

$$For \ \sin\left(\varphi_m\right) < \frac{3}{4}\sin\left(\varphi\right) \qquad \psi_m = 0$$

$$For \ \sin\left(\varphi_m\right) < \frac{3}{4}\sin(\varphi) \ and \ \psi > 0 \qquad \sin\left(\psi_m\right) = \max\left(\frac{\sin(\varphi_m) - \sin(\varphi_{cv})}{1 - \sin(\varphi_m)\sin(\varphi_{cv})}, 0\right)$$

$$For \ \sin\left(\varphi_m\right) < \frac{3}{4}\sin(\varphi) \ and \ \psi \leq 0 \qquad \psi_m = \psi$$

$$If \ \varphi = 0 \qquad \psi_m = 0$$

$$(7-17)$$

 φ_{cv} Critical state friction angle, being a material constant independent of density. φ_m The mobilised friction angle.

$$\sin\left(\phi_{m}\right) = \frac{\sigma_{1}' - \sigma_{3}'}{\sigma_{1}' + \sigma_{3}' - 2c\cot\left(\phi\right)} \tag{7-18}$$

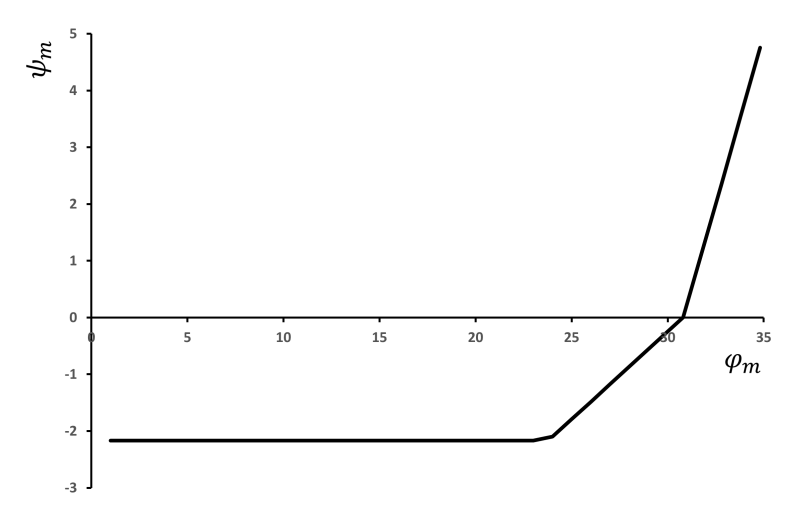


Figure 7–10: Plot of mobilised dilatancy angle ψ_m and mobilized friction angle φ_m for Hardening Soil model with small-strain stiffness

For small mobilised friction angles and for negative values of ψ_m , as computed by Rowe's formula, ψ_m in the Hardening Soil model is taken zero. Bounding the lower value of ψ_m may sometimes yield too little plastic volumetric strains though. Therefore, the Hardening Soil model with small-strain stiffness adapts an approach by Li & Dafalias (2000) whenever ψ_m , as computed by Rowe's formula, is negative. In that case, the mobilised dilatancy in the Hardening Soil model with small-strain stiffness is calculated by the following equation:

$$\sin\left(\psi_m
ight)=rac{1}{10}igg(-M_cexp\left[rac{1}{15} ext{ln}igg(rac{M_c}{M_d}rac{q}{q_a}igg)
ight]+M_digg)$$
 (7–19)

where:

$$M_c = rac{6\sin\left(arphi_{cv}
ight)}{3-\sin\left(arphi_{cv}
ight)}$$
 (7–20)

$$M_d = rac{6\sin\left(arphi_m
ight)}{3-\sin\left(arphi_m
ight)}$$
 (7–21)

$$\frac{q}{q_a} = \max\left(\frac{1 - \sin\left(\varphi_{cv}\right)}{\sin\left(\varphi_{cv}\right)} \cdot \frac{\sin\left(\varphi_m\right)}{1 - \sin\left(\varphi_m\right)}, 10^{-4}\right) \tag{7-22}$$

And the mobilised friction angle is limited to:

$$\sin\left(arphi_{m}
ight)\geqrac{\sin\left(arphi
ight)}{2-\sin\left(arphi
ight)}$$
 (7–23)

The mobilised dilatancy as a function of φ_m for the Hardening Soil model with small-strain stiffness is visualised in Figure 7–10 (p. 92) for the specific case of φ =35° and ψ =5°.



Modified Cam-Clay model

The Modified Cam-Clay model is described in several textbooks on critical state soil mechanics (for example Muir Wood (1990)). In this chapter a short overview is given of the basic equations.

8.1 Formulation of the Modified Cam-Clay model

In the Modified Cam-Clay model, a logarithmic relation is assumed between void ratio e and the mean effective stress p' in virgin isotropic compression, which can be formulated as:

$$e-e^0=-\lambda \ln \left(rac{p'}{p^0}
ight) \,\, {
m (virgin isotropic compression)}$$

The parameter λ is the Cam-Clay isotropic compression index, which determines the compressibility of the material in primary loading. When plotting relation (Eqn. 8–1 (p. 93)) in a e - $\ln p'$ diagram one obtains a straight line. During unloading and reloading, a different line is followed, which can be formulated as:

$$e - e^0 = -\kappa \ln\left(\frac{p'}{p^0}\right)$$
 (isotropic unloading and reloading) (8-2)

The parameter κ is the Cam-Clay isotropic swelling index, which determines the compressibility of material in unloading and reloading. In fact, an infinite number of unloading and reloading lines exists in p' - e-plane each corresponding to a particular value of the pre-consolidation stress p_p .

The yield function of the Modified Cam-Clay model is defined as:

$$f = rac{q^2}{M^2} + p' ig(p' - p_p ig)$$
 (8–3)

The yield surface (f = 0) represents an ellipse in p' - q-plane as indicated in Figure 8-1 (p. 94). The yield surface is the boundary of the elastic stress states. Stress paths within this boundary only give elastic strain increments, whereas stress paths that tend to cross the boundary generally give both elastic and plastic strain increments.

In p'-q - plane, the top of the ellipse intersects a line that we can be written as:

$$q = Mp' ag{8-4}$$

This line is called the critical state line (CSL) and gives the relation between p' and q in a state of failure (i.e. the critical state). The constant M is the tangent of the critical state line and determines the extent to which the ultimate deviatoric stress, q, depends on the mean effective stress, p'. Hence, M can be regarded as a friction constant. Moreover, M determines the shape of the yield surface (height of the ellipse) and influences the coefficient of lateral earth pressure K_0^{nc} in a normally consolidated stress state under conditions of one-dimensional compression.

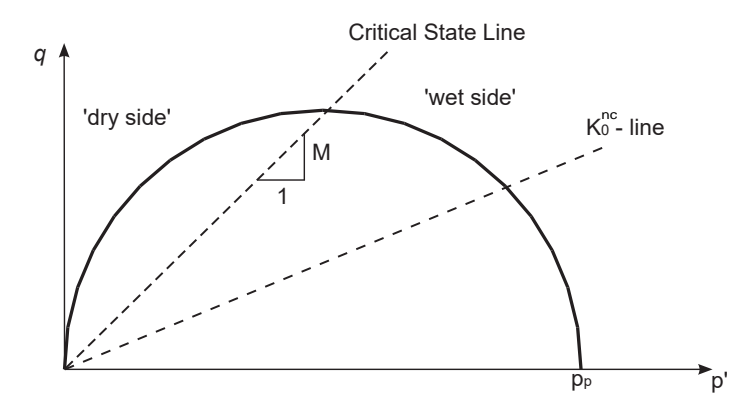


Figure 8-1: Yield surface of the of the Modified Cam-Clay model in p'-q - plane

The preconsolidation stress, p_p , determines the size of the ellipse. In fact, an infinite number of ellipses exist, each corresponding to a particular value of p_n .

The left hand side of the yield ellipse (often described as the 'dry side' of the critical state line) may be thought of as a failure surface. In this region plastic yielding is associated with softening. and therefore failure. The values of q can become unrealistically large in this region.

For more detailed information on Cam-Clay type models, the reader is referred to Muir Wood (1990).



Note:

Note that the Modified Cam-Clay model model as implemented in PLAXIS gives a Druger-Prager failure state instead of a Mohr-Coulomb model type of failure.

8.2 Parameters of the Modified Cam-Clay model

The Modified Cam-Clay model is based on the following parameters:

Parameters for stiffness:

λ	Cam-Clay compression index	[-]
К	Cam-Clay swelling index	[-]
V _{ur}	Poisson's ratio	[-]
e _{init}	Initial void ratio for loading/unloading	[-]

Parameters for strength:

М	Tangent of the critical state line	[-]
K_0^{nc}	Coefficient of lateral stress in normal consolidation derived from M . The relationship between M and K_0^{nc} is given in the Material Models Manual - Soft soil creep Model - Parameters of the soft soil creep model.	[-]

8.2.1 Compression index and swelling index

These parameters can be obtained from an isotropic compression test including isotropic unloading. When plotting the natural logarithm of the mean stress as a function of the void ratio for clay-type materials, the plot can be approximated by two straight lines. The slope of the primary loading line gives the compression index and the slope of the unloading line gives the swelling index. These parameters can be obtained from a one-dimensional compression test, as discussed in 10.3 Parameters of the Soft Soil model (p. 112).

8.2.2 Poisson's Ratio

Poisson's ratio v_{ur} is a real elastic parameter and not a pseudo-elasticity constant as used in the Mohr-Coulomb model. Its value will usually be in the range between 0.1 and 0.2.

8.2.3 Tangent of the critical state line

In order to obtain the correct shear strength, the parameter M should be based on the friction angle φ . The critical state line is comparable with the Drucker-Prager failure line, and represents a (circular) cone in principal stress space. Hence, the value of M can be obtained from φ :

$$M = \frac{6 sin \varphi}{3 - sin \varphi}$$
 (for initial compression stress states) $\left(\sigma_1' \le \sigma_2' = \sigma_3'\right)$ (8–5)

$$M=rac{6sinarphi}{3+sinarphi} ext{ (for initial compression stress states) } \left(\sigma_{1}^{'}=\sigma_{2}^{'}\leq\sigma_{3}^{'}
ight)$$
 (8–6)

$$M \approx \sqrt{3} \sin \varphi$$
 (for plane strain stress states) (8–7)

In addition to determining the shear strength, the parameter M has an important influence on the value of the coefficient of lateral earth pressure, K_0^{nc} , in a state of normal consolidation. In general, when M is chosen such that the model predicts the correct shearing strength, the resulting value of K_0^{nc} is too high.

8.3 State parameters in the Modified Cam-Clay model

In addition to the output of standard stress and strain, the Modified Cam-Clay model provides output (when being used) on state variables such as the isotropic pre-consolidation stress p_p

and the isotropic overconsolidation ration OCR. These parameters can be visualised by selecting the State parameters option from the Stresses menu. An overview of available state parameters is given below:

p _{eq}	Equivalent isotropic stress.	[kN/m ²]
	$P_{eq}=p'+rac{q^2}{M^2p'}$	
p _p	Isotropic preconsolidation stress	[kN/m ²]
OCR	Isotropic overconsolidation ratio ($OCR = p^p/p^{eq}$)	[-]

8.4 On the use of the Modified Cam-Clay model in dynamics calculations

When using the Modified Cam-Clay model in dynamics calculations, the swelling index κ needs to be selected such that the model correctly predicts wave velocities in the soil. This generally requires a smaller value than just an unloading-reloading index.

When subjected to dynamic or cyclic loading, the Modified Cam-Clay model will generate plastic strains when the preconsolidation stress is increased. However, it should be noted that stress cycles within the current creep contour will only generate elastic strains and no (hysteretic) damping, nor accumulation of strains or pore pressure, nor liquefaction. In order to account for the soil damping in cyclic loading, Rayleigh damping may be defined.

8.5 | Warning

The Modified Cam-Clay model may allow for extremely large shear stresses. This is particularly the case for stress paths that cross the critical state line. Furthermore, the Modified Cam-Clay model may give softening behaviour for particular stress paths. Without special regularization techniques, softening behaviour may lead to mesh dependency and convergence problems of iterative procedures. Moreover, the Modified Cam-Clay model cannot be used in combination with Safety analysis by means of phi-c reduction. The use of the Modified Cam-Clay model in practical applications is not recommended.



The NGI-ADP model (anisotropic undrained shear strength)

The NGI-ADP model may be used for capacity, deformation and soil-structure interaction analyses involving undrained loading of clay. The basis of the material model is:

- Input parameters for (undrained) shear strength for three different stress paths/ states (Active, Direct Simple Shear, Passive).
- A yield criterion based on a translated approximated Tresca criterion.
- Elliptical interpolation functions for plastic failure strains and for shear strengths in arbitrary stress paths.
- Isotropic elasticity, given by the unloading/reloading shear modulus, G_{ur} .

9.1 Formulation of the NGI-ADP model

The NGI-ADP model is formulated for a general stress state, matching both undrained failure shear strengths and strains to that of selected design profiles (Andresen & Jostad, 1999; Andresen, 2002; Grimstad, Andresen & Jostad, 2010). The model formulation is presented in steps, starting with 1D anisotropy in triaxial test condition. In The NGI-ADP model in plane strain a simplified expression for plane strain is presented. Thereafter the formulation is extended to full 3D stress state. In this formulation compressive stresses are positive.

In the NGI-ADP model the Tresca approximation after <u>Billington (1988)</u> together with a modified von Mises plastic potential function (<u>von Mises, 1913</u>) is used to circumvent the possible corner problems. The yield and plastic potential function are independent of the mean stress hence zero plastic volume strain develops.

9.1.1 1D model presentation

Under triaxial tests condition two undrained shear strengths can be determined, i.e. $s_u^{\ C}$ and s_{ij}^{E} . The test measures the response in vertical stress σ'_{ij} and horizontal stress σ'_{ij} for applied shear strain y. The Tresca yield criteria can be modified, Eqn. 9-1 (p. 98), to account for the difference in undrained shear strength in compression and extension:

$$f=\left(au-(1-\kappa) au_0-\kapparac{s_u^C-s_u^E}{2}
ight)-\kapparac{s_u^C+s_u^E}{2}=0$$
 (9–1)

where

= Shear stress defined as $\tau = 0.5(\sigma'_{v} - \sigma'_{h})$

Initial in situ maximum shear stress defined as τ_o $au_0 = 0.5(\sigma'_{v0} - \sigma'_{b0}) = 0.5(1 - K_0)$

To account for difference in failure shear strain a stress path dependent hardening parameter is introduced. The stress path dependent hardening is made possible by different plastic failure shear strain y_f^p in compression and extension. The hardening function is given by:

$$\kappa=2rac{\sqrt{\gamma^p/\gamma_f^p}}{1+\gamma^p/\gamma_f^p}; ext{ when } \gamma^p<\gamma_f^p; ext{ else } \kappa=1$$

 γ^p Plastic shear strain.

 γ_f^p Failure (peak) plastic shear strain.

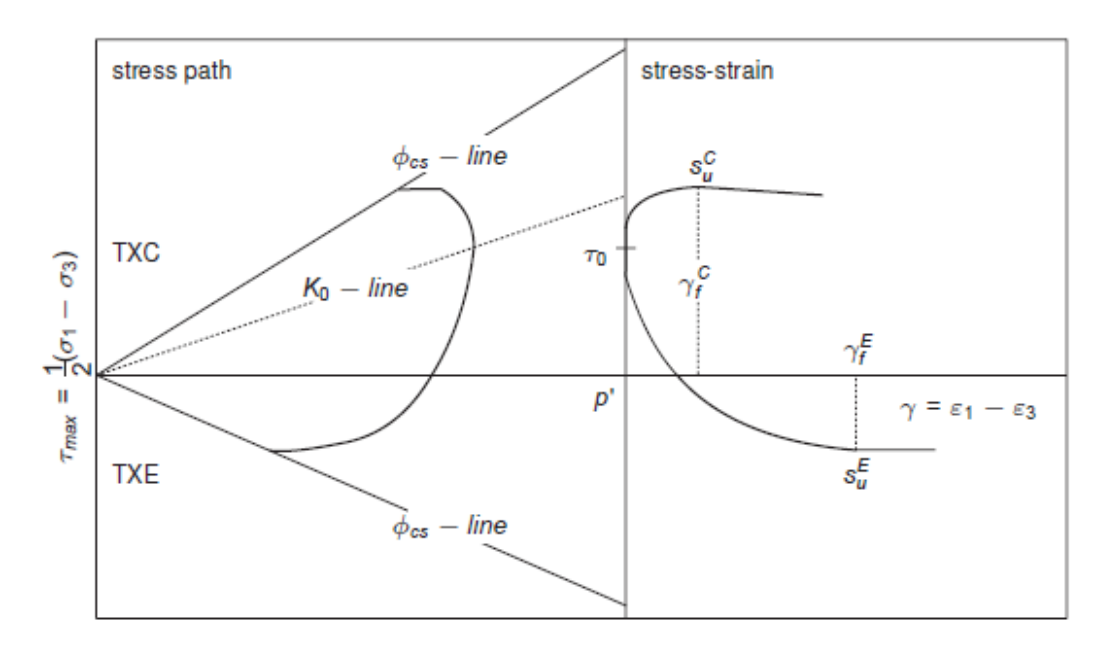


Figure 9–1: Typical stress paths and stress strain curves for triaxial compression and triaxial extension

9.1.2 The NGI-ADP model in plane strain

The yield criterion for the NGI-ADP model in plane strain is defined by:

$$f = \sqrt{\left(rac{\sigma_{yy} - \sigma_{xx}}{2} - (1 - \kappa) au_0 - \kapparac{s_u^A - s_u^P}{2}
ight)^2 + \left(au_{xy}rac{s_u^A + s_u^P}{2s_u^{DSS}}
ight)^2} - \kapparac{s_u^A + s_u^P}{2} = 0 \quad ag{9-3}$$

Restriction to clays with horizontal surfaces are made to simplify the presentation. Further y is taken as the vertical (depositional) direction. For isotropy in hardening (i.e. κ independent of stress orientation) plots as an elliptical shaped curve in a plane strain deviatoric stress plot. When κ equals 1.0, the criterion in Eqn. 9-3 (p. 99) reduces to the formulation given by Davis & Christian (1971). While hardening the yield curves are characterised by slightly distorted elliptical shapes. The shape is dependent on the interpolation function used and values of failure strain. The NGI-ADP model uses elliptical interpolation between failure strain in passive stress state, direct simple shear and active stress state. In the implementation of the NGI-ADP model the yield surface is ensured to remain convex by restricting the input.

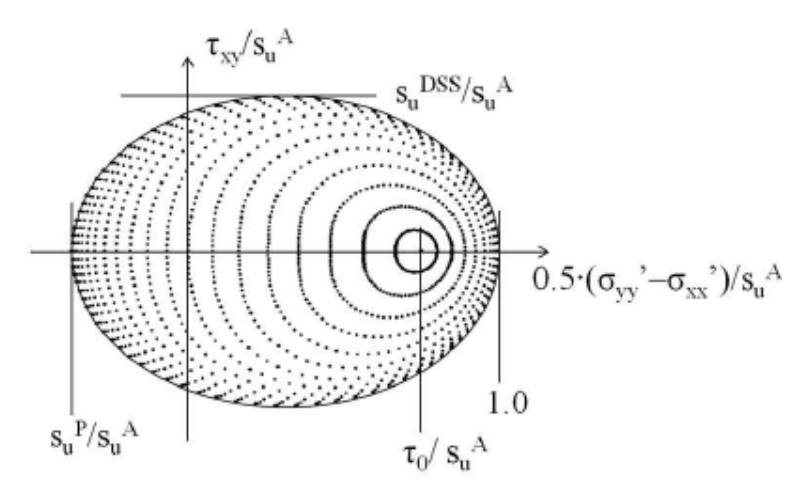


Figure 9-2: Typical deviatoric plane strain plot of equal shear strain contours for the NGI-ADP model

9.1.3 The NGI-ADP model in 3D stress space

This section describes the actual implementation of the NGI-ADP model in PLAXIS, whereas the previous sections should be regarded as an introduction using simplified formulation. For the general stress condition a modified deviatoric stress vector is defined as:

$$\begin{pmatrix}
\hat{s}_{xx} \\
\hat{s}_{yy} \\
\hat{s}_{zz} \\
\hat{s}_{xy} \\
\hat{s}_{yz}
\end{pmatrix} = \begin{pmatrix}
\sigma'_{xx} - \sigma'_{xx0}(1 - \kappa) + \kappa \frac{1}{3} \left(s_u^A - s_u^P\right) - \widehat{p} \\
\sigma'_{yy} - \sigma'_{yy0}(1 - \kappa) - \kappa \frac{2}{3} \left(s_u^A - s_u^P\right) - \widehat{p} \\
\sigma'_{zz} - \sigma'_{zz0}(1 - \kappa) + \kappa \frac{1}{3} \left(s_u^A - s_u^P\right) - \widehat{p} \\
\tau_{xy} s_u^A + \frac{s_u^P}{2s_u^{DSS}} \\
\tau_{xz} \\
\tau_{yz} \frac{s_u^A + s_u^P}{2s_u^{DSS}}
\end{pmatrix}$$
(9-4)

where

the modified mean stress. The modified mean stress is defined as:

$$\sigma'_{xx0},\sigma'_{m0},\sigma'_{zz0}=$$
 initial stresses

$$\widehat{p} = \frac{(\sigma'_{xx} - \sigma'_{xx0}(1-\kappa)) + (\sigma'_{yy} - \sigma'_{yy0}(1-\kappa)) + (\sigma'_{zz} - \sigma'_{zz0}(1-\kappa))}{3} \\
= p' - (1-\kappa)p'_{0}$$
(9-5)

where

$$p'$$
 = Mean stress

Modified second and third deviatoric invariants are defined accordingly in Eqn. 9-6 (p. 100) and Eqn. 9-7 (p. 100).

$$\widehat{J}_{2} = -\hat{s}_{xx}\hat{s}_{yy} - \hat{s}_{xx}\hat{s}_{zz} - \hat{s}_{yy}\hat{s}_{zz} + \hat{s}_{xz}^{2} + \hat{s}_{xz}^{2} + \hat{s}_{yz}^{2}$$

$$(9-6)$$

$$\widehat{J}_{3} = \hat{s}_{xx}\hat{s}_{yy}\hat{s}_{zz} + 2\hat{s}_{xy}\hat{s}_{yz}\hat{s}_{xz} - \hat{s}_{xx}\hat{s}_{yz}^{2} - \hat{s}_{yy}\hat{s}_{xz}^{2} - \hat{s}_{zz}\hat{s}_{xy}^{2}$$

$$\tag{9-7}$$

The vield criterion is expressed as:

$$f = \sqrt{H(\omega)\,\widehat{J}_2} - \kappa rac{s_u^A + s_u^P}{2} = 0$$
 (9–8)

where, to approximate the Tresca criterion, the term $H(\omega)$ is defined as:

$$H(\omega) = cos^2 \left(\frac{1}{6} arccos(1 - 2a_1\omega) \right) \quad \text{with} \quad \omega = \frac{27}{4} \frac{\widehat{J}_3^2}{\widehat{J}_3^2}$$
 (9-9)

By letting the value of a_1 go to 1.0 an exact Tresca criterion is obtained. The parameter a_1 can be directly linked to the rounding ratio s_u^{C}/s_u^{A} . This ratio takes typically a value just below 1.0 and a value of 0.99 is chosen as an appropriate default. Figure 9-3 (p. 100) shows the failure criterion of the NGI-ADP model in the \opin-plane (for Cartesian stresses) with default rounding ratio. This criterion is continuous and differentiable and it is described by a single function.

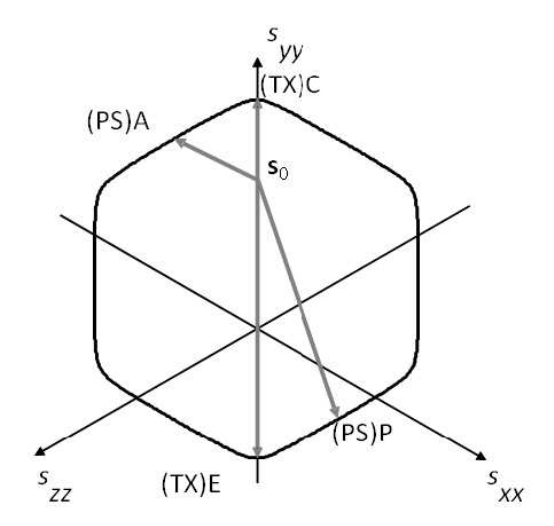


Figure 9-3: Failure criterion of the NGI-ADP model in the ω -plane

The combinations of strength ratios are limited by lower limit for combinations of s_u^C/s_u^A and s_{II}^{P}/s_{II}^{A} .

The value of γ_f^p is given by elliptical interpolation:

$$\gamma_{f}^{p}\!\left(\hat{ heta}
ight) = rac{\widehat{R}_{B}\widehat{R}_{D}\sqrt{\left(\widehat{R}_{D}^{2}-\widehat{R}_{C}^{2}
ight)\!\cos^{2}\!\hat{ heta}+\widehat{R}_{C}^{2}}-\widehat{R}_{D}^{2}\widehat{R}_{A}\!\cos\!\left(2\hat{ heta}
ight)}}{\widehat{R}_{B}^{2}-\left(\widehat{R}_{B}^{2}-\widehat{R}_{D}^{2}
ight)\!\cos^{2}\!\left(2\hat{ heta}
ight)}}$$
 (9–10)

where

$$\widehat{R}_A = rac{\gamma_{f,E}^p - \gamma_{f,C}^p}{2}$$
 (9–11)

$$\widehat{R}_B = rac{\gamma_{f,E}^p + \gamma_{f,C}^p}{2}$$
 (9–12)

$$\widehat{R}_{C}=\sqrt{\gamma_{f,E}^{p}\gamma_{f,C}^{p}}$$
 (9–13)

$$\widehat{R}_D = rac{\gamma_{f,DSS}^p \widehat{R}_B}{\widehat{R}_C}$$
 (9–14)

and , $\gamma_{f,C}^p$, $\gamma_{f,DSS}^p$ and $\gamma_{f,E}^p$ are the failure plastic maximum shear strain in triaxial compression, direct simple shear and triaxial extension respectively. Note that $\hat{\theta}$ is not the Lode angle, but is defined as:

$$cos\Bigl(2\hat{ heta}\Bigr)=rac{\sqrt{3}}{2}rac{\hat{s}_{yy}}{\sqrt{\widehat{J}_2}}$$
 (9–15)

A non-associated flow rule is used such that the derivative of the plastic potential α is:

$$\frac{\partial g}{\partial \boldsymbol{\sigma}'} = \frac{1}{2} \left(\widehat{I} + \frac{\partial p}{\partial \boldsymbol{\sigma}'} \left(\frac{\partial \widehat{s}}{\partial \widehat{p}} \right)^T \right) \frac{\partial \widehat{J}_2}{\partial \widehat{s}} \sqrt{\frac{1}{\widehat{J}_2}}$$
(9–16)

where \hat{i} is a modified unit vector:

The increment in plastic shear strain is defined as:

$$d\gamma^p = \sqrt{H(\omega)} \, egin{aligned} \left(rac{2}{3} \Big((darepsilon_{xx}^p - darepsilon_{yy}^p)^2 + (darepsilon_{xx}^p - darepsilon_{zz}^p)^2 + (darepsilon_{yy}^p - darepsilon_{zz}^p)^2 \Big) \ + (d\gamma_{xy}^p)^2 + (d\gamma_{xz}^p)^2 + (d\gamma_{yz}^p)^2 \end{aligned}
ight) \end{aligned}$$

where the plastic strains are defined as:

$$doldsymbol{arepsilon}^p = d\lambda rac{\partial g}{\partial oldsymbol{\sigma}'}$$
 (9–19)

with $d\lambda$ being the plastic multiplier. Hence, gives the relation between the hardening parameter γ^p and the plastic multiplier $d\lambda$.

9.1.4 The NGI-ADP model traction criterion for interfaces in 2D

For plane strain conditions a traction criterion, corresponding to the plane strain failure criterion is formulated. This criterion is intended to be used on interface elements in finite element calculations. The interface strength is controlled by a lower and upper limit, which are dependent on the direction of the interface, β .

Let a plane being oriented by the direction β to the horizontal. The plane has a tangential direction t and a normal direction n and the adjacent continuum defines the stresses σ_{nn} , σ_{tt} and τ_n by:

$$\begin{bmatrix} \sigma_{tt} \\ \sigma_{nn} \\ \tau_{nn} \end{bmatrix} = A \begin{bmatrix} \sigma_{xx} \\ \sigma_{yy} \\ \tau_{xy} \end{bmatrix} \tag{9-20}$$

where

Transformation matrix.

In a local coordinate system three strains ε_{nn} , ε_{tt} and γ_{tn} are defined in the plane strain condition. Due to the requirement of no volume change for a perfect plastic mechanism with shearing in tangential direction, will give that $\varepsilon_{nn} = \varepsilon_{tt} = 0$, resulting in:

$$rac{\partial f}{\partial (\sigma_{nn} - \sigma_{tt})} = 0$$
 (9–21)

The plane strain formulation for the NGI-ADP model is defined as follows:

$$f = \sqrt{ egin{pmatrix} \left(rac{\sigma_{nn} - \sigma_{tt}}{2} cos(2eta) - au_{tn} sin(2eta) - R_A
ight)^2 + \ \left(rac{R_B}{R_D} \left(rac{\sigma_{nn} - \sigma_{tt}}{2} sin(2eta) + au_{tn} cos(2eta)
ight)
ight)^2 } - R_B \end{cases}$$
 (9–22)

where

$$R_A = \frac{s_u^A - s_u^P}{2}$$
 (9–23)

$$R_B = \frac{s_u^A - s_u^P}{2}$$
 (9-24)

$$R_D = s_u^{DSS} ag{9-25}$$

9.2 Parameters of the NGI-ADP model

The NGI-ADP model requires a total of eleven parameters.

Parameters for stiffness:

G_{ur}/s_u^A	Ratio unloading/reloading shear modulus over (plane strain) active shear strength	[-]
γ_f^C	Shear strain in triaxial compression $\left(\left \gamma_f^C=3/2 \;\; arepsilon_1^C ight ight)$	[%]

	γ_f^E	Shear strain in triaxial extension	[%]
ſ	γ_f^{DSS}	Shear strain in direct simple shear	[%]

Parameters for strength:

$s_u^{A,ref}$	Reference (plane strain) active shear strength	[kN/ m ²]
$s_u^{C,TX}/s_u^A$	Ratio triaxial compressive shear strength over (plane strain) active shear strength(default = 0.99)	[-]
y_{ref}	Reference level	[m]
$s_{u,inc}^{\;A}$	Increase of shear strength with depth	[kN/ m²/m]
s_u^P/s_u^A	Ratio of (plane strain) passive shear strength over (plane strain) active shear strength	[-]
$ au_0/s_u^A$	Initial mobilization (default = 0.7)	[-]
s_u^{DSS}/s_u^A	Ratio of direct simple shear strength over (plane strain) active shear strength	[-]

Advanced parameters:

Undrained Poisson's ratio	[-]
---------------------------	-----

9.2.1 Ratio unloading / reloading shear modulus over plane strain active shear strength(G_{ur}/S_u^A)

Ratio unloading / reloading shear stiffness as a ratio of the plane strain active shear strength. If the shear strength is increasing with depth the constant ratio for G_{uv}/s_{uv}^{A} gives a shear stiffness increasing linearly with depth.

9.2.2 Shear strain at failure in triaxial compression (γ_f^c)

This parameter $\gamma_f^{\ C}$ (%) defines the shear strain at which failure is obtained in undrained triaxial compression mode of loading, i.e. $\gamma_f^C = 3/2 \varepsilon_1^C$ from triaxial testing.

9.2.3 Shear strain at failure in triaxial extension (y_f^E)

This parameter γ_f^E (%) defines the shear strain at which failure is obtained in undrained triaxial extension mode of loading, i.e. $\gamma_f^E = 3/2\varepsilon_1^E$ from triaxial testing.

9.2.4 Shear strain at failure in direct simple shear (γ_f^{DSS})

This parameter y_f^{DSS} (%) defines the shear strain at which failure is obtained in undrained direct simple shear mode of loading (DSS device).

For near normally consolidated clays, the failure strain in compression loading $\gamma_f^{\ \ C}$ is generally the lowest value and the failure strain in extension loading y_f^E is the highest value. The failure strain from direct simple shear loading takes an intermediate value, i.e. $\gamma_f^{\ C} < \gamma_f^{\ DSS} < \gamma_f^{\ E}$. From laboratory test results reported in literature one find typically γ_f^E in the range 3-8 %, γ_f^{DSS} in the range 2-8 % and v_f^C in the range 0.5 - 4%.

If stress-strain curves from undrained triaxial and/or DSS laboratory tests are available it is recommended to choose the elastic shear modulus and failure strains such that a good fit to the curves are obtained. This is in particular important for deformation and SLS assessments. However, for pure capacity and stability (e.g. factor of safety) analyses the values for shear strains at failure is not important and one may set all three values equal to e.g. 5 % for simplicity.

Note that it is the failure strains from triaxial loading that is input because they are the most readily available. When the NGI-ADP model is used for plane strain conditions the failure strains will automatically be slightly adjusted for that loading condition. See Grimstad, Andresen & Jostad (2010) for more details.

9.2.5 Reference active shear strength (suref A)

The reference active shear strength is the shear strength obtained in (plane strain) undrained active stress paths for the reference depth y_{ref} , expressed in the unit of stress.

9.2.6 Ratio triaxial compressive shear strength over active shear strength $(s_u^{C,TX}/s_u^A)$

This ratio $s_u^{C,TX}/s_u^A$ defines the shear strength in undrained triaxial compression mode of loading in relation to the shear strength in plane strain undrained active mode of loading. The value cannot be changed by the user and is predefined at 0.99 giving practically the same strengths in triaxial and plane strain conditions.

9.2.7 Reference depth (y_{ref})

This is the reference depth y_{ref} at which the reference active shear strength $s_{u,ref}^{A}$ is defined. Below this depth the shear strength and stiffness may increase linearly with increasing depth. Above the reference depth the shear strength is equal to $s_{u.ref}^A$.

9.2.8 Increase of shear strength with depth (s_{u.inc} A)

This parameter $s_{u,ref}^{A}$ defines the increase (positive) or decrease (negative) of the undrained active shear strength with depth, expressed in the unit of stress per unit of depth. Above the reference depth the shear strength is equal to $s_{u,ref}^{A}$, below the reference depth the shear strength is defined as:

$$s_u^A(y) = s_{u,ref}^A + (y_{ref} - y)s_{u,inc}^A$$
 (9–26)

9.2.9 Ratio of passive shear strength over active shear strength (s_u^p/s_u^A)

This ratio s_u^p/s_u^A defines the undrained shear strength for (plane strain) passive mode of loading.

9.2.10 Ratio of direct simple shear strength over active shear strength (s₁₁DSS) s..A)

This ratio s_u^{DSS}/s_u^A defines the undrained shear strength for direct simple shear mode of loading. Please note that active / passive strength input is defined for plane strain conditions. However, it is generally acceptable and only slightly conservative to use the strength obtained from a triaxial compression test as input for the active plane strain condition (i.e. $s_u^A = s_u^{C,TX}$) and the strength obtained from a triaxial extension test as input for the passive plane strain condition (i.e. $s_u^P = s_u^{E,TX}$). More control over the strength difference between triaxial and plane strain loading conditions can be obtained by using the advanced parameter $s_n^{C,TX}/s_n^A$.

For near normally consolidated clays, the passive strength s_u^P is generally the lowest strength value, while the direct simple shear strength takes an intermediate value, i.e. $s_u^P < s_u^{DSS} < s_u^A$. From laboratory results reported in literature one find typically s_u^P/s_u^A in the range 0.2 - 0.5 and s_u^{DSS}/s_u^A in the range 0.3 - 0.8. If direct simple shear strengths are not available s_u^{DSS} can be estimated from:

$$s_u^{DSS}/s_u^A = \left(1 + s_u^p/s_u^A\right)/2$$
 (9–27)

9.2.11 Initial mobilization (τ_0/s_0^A)

The initial mobilization au_0/s_u^A is clearly defined for nearly horizontally deposited normally consolidated or lightly overconsolidated clay layers where the vertical stress is the major principle stress σ'_1 . As defined in Figure 9–4 (p. 106), the initial mobilization can be calculated from the earth pressure coefficient at rest K_0 by the following equation:

$$au_0/s_u^A = -rac{0.5\,(1-K_0)\sigma_{yy0}'}{s_u^A}$$
 (9–28)

where

Initial (in situ) vertical effective stress (compression negative)

A default value 0.7 of τ_0/s_u^A is given which represent a typical value for a near normally consolidated clay deposit (e.g. K_0 = 0.55 and $-\sigma'_{yy0}/s_u^A=3.11$ or K_0 = 0.6 and $-\sigma'_{yy0}/s_u^A=3.5$).

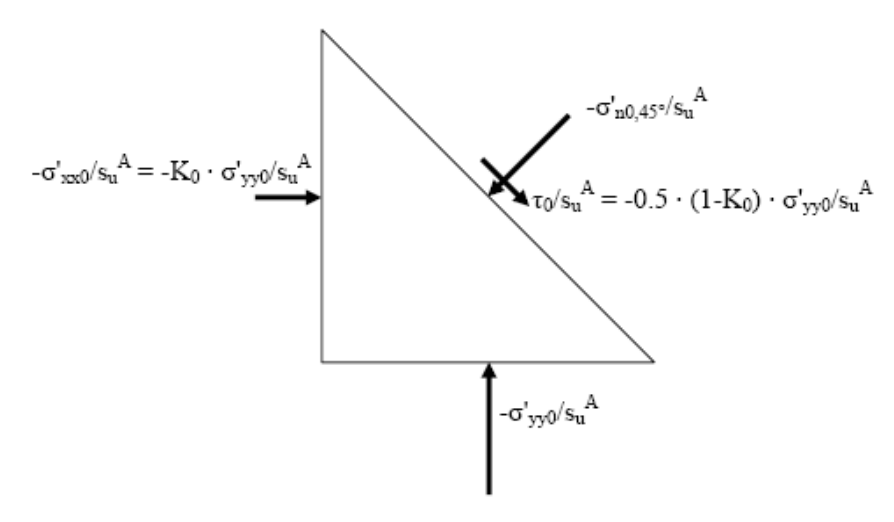


Figure 9–4: Definition of initial mobilised maximum shear stress τ_0 = $1/2 |\sigma'_{vv0} - \sigma'_{xx0}|$ for a soil element in a horizontal deposited layer.

A more detailed evaluation of the initial (in situ) mobilization can be done by assessing the in situ K_0 value and use the relationship: $\tau_0/s_u^A=-0.5(1-K_0)\sigma'_{vv0}/s_u^A$. Changing the default value for the initial mobilization should be considered in particular for overconsolidated materials where K_0 generally is higher than 0.6, however the NGI-ADP model is not intended used for heavily overconsolidated clays and should be used with care for $K_0 > 1.0$ (i.e. negative τ_0/s_u^A).

For non-horizontal layering (e.g. sloping ground) a KO procedure is normally not recommended. In such cases it is recommended to establish the initial stress condition by gravity loading using a material model suited for such a purpose (e.g. drained behavior with the Mohr-Coulomb model or the Hardening Soil model). After the equilibrium initial stresses are established for gravity loading in the first phase, one should switch to the NGI-ADP model in the relevant clusters for the next phase and run a NIL step (i.e. without changing the external loads). The hardening parameter of the NGI-ADP model will then be adjusted such that equilibrium is obtained (f=0). Then in the third phase the external loading can be applied.

9.2.12 Poisson's ratio (v')

The Undrained (C) drainage option is used. A pure total stress analysis is carried out where no distinction between effective stresses and pore pressures is made and all stress changes should be considered as changes in total stress. A Poisson's ratio close to 0.5 should be entered. v = 0.495 is given as default.

9.3 State parameters in the NGI-ADP model

In addition to the output of standard stress and strain quantities, the NGI-ADP model provides output (when being used) on state variables such as plastic shear strain γ_p and the hardening function r_{κ} . These parameters can be visualised by selecting the State parameters option from the Stresses menu. An overview of available state parameters is given below:

γ^p	Plastic shear strain : $\gamma^p = \sum d\gamma^p$	[-]
$d\gamma^p$	Described in <u>Eqn. 9–18 (p. 101)</u> .	[-]

r_{κ}	Hardening function: $r_{\kappa}=2rac{\sqrt{\gamma^p/\gamma_f^p}}{1+\gamma^p/\gamma_f^p}$	[-]
--------------	---	-----

The Soft soil model [ADV]

As soft soils, we consider near-normally consolidated clays, clayey silts and peat. A special feature of such materials is their high degree of compressibility. This is best demonstrated by oedometer test data as reported for instance by Janbu in his Rankine lecture (1985). Considering tangent stiffness moduli at a reference oedometer pressure of 100 kPa, he reports $E_{oed} = 1$ to 4 MPa for normally consolidated (NC) clays, depending on the particular type of clay considered. The differences between these values and stiffnesses for NC-sands are considerable as here we have values in the range of 10 to 50 MPa, at least for non-cemented laboratory samples. Hence, in oedometer testing, normally consolidated clays behave ten times softer than normally consolidated sands. This illustrates the extreme compressibility of soft soils.

A feature of soft soils is the linear stress-dependency of soil stiffness. According to the Hardening Soil model we have:

$$E_{oed} = E_{oed}^{ref} igg(rac{-\sigma_1'}{p^{ref}}igg)^m$$
 (10–1)

at least for c=0 and $\sigma'_3=K_0^{nc}\sigma_1'$. A linear relationship is obtained for m=1. Indeed, on using an exponent equal to unity, the above stiffness law reduces to:

$$E_{oed} = rac{-\sigma_1'}{\lambda^*}$$
 (10–2)

where

$$\lambda^* = rac{p^{ref}}{E_{oed}^{ref}}$$
 (10–3)

For the special case of m = 1, the Hardening Soil model yields $\dot{\epsilon} = \sigma^* \dot{\sigma}_1' / \sigma_1'$, which can be integrated to obtain the well-known logarithmic compression law $\epsilon = -\lambda^* \ln \left(-\sigma_1' \right)$ for primary oedometer loading.

For many practical soft-soil studies, the modified compression index λ^* is known and the PLAXIS 2D user can compute the oedometer modulus from the relationship:

$$E_{oed}^{ref}=rac{p^{ref}}{\lambda^*}$$
 (10–4)

From the above considerations it would seem that the Hardening Soil model is quite suitable for soft soils. Indeed, most soft soil problems can be analysed using this model, but the Hardening Soil model is not suitable when considering very soft soils with a high compressibility, i.e $E_{oed}^{ref}/E_{50}^{ref} < 0.5$. For such soils, the Soft Soil model may be used.

Some features of the Soft Soil model are:

- Stress dependent stiffness (logarithmic compression behaviour).
- Distinction between primary loading and unloading-reloading.
- Memory for pre-consolidation stress.
- Failure behaviour according to the Mohr-Coulomb criterion.

10.1 Isotropic states of stress and strain ($\sigma'_1 = \sigma'_2 = \sigma'_3$)

In the Soft Soil model, it is assumed that there is a logarithmic relation between changes in volumetric strain, ε_v , and changes in mean effective stress, p', which can be formulated as:

$$\varepsilon_v - \varepsilon_v^0 = -\lambda^* \ln \left(\frac{p' + c \cot(\varphi)}{p^0 + c \cot(\varphi)} \right)$$
(10-5)

In order to maintain the validity of Eqn. 10–5 (p. 109) a minimum value of p' is set equal to a unit stress. The parameter λ^* is the modified compression index, which determines the compressibility of the material in primary loading. Note that λ^* differs from the index λ as used by Burland (1965). The difference is that Eqn. 10–5 (p. 109) is a function of volumetric strain instead of void ratio. Plotting Eqn. 10–5 (p. 109) gives a straight line as shown in Figure 12–1 (p. 133).

During isotropic unloading and reloading a different path (line) is followed, which can be formulated as:

$$\varepsilon_{v}^{e} - \varepsilon_{v}^{e0} = -\kappa * \ln \left(\frac{p' + c \cot(\varphi)}{p^{0} + c \cot(\varphi)} \right)$$
(10-6)

Again, a minimum value of p' is set equal to a unit stress. The parameter κ^* is the modified swelling index, which determines the compressibility of the material in unloading and subsequent reloading. Note that κ^* differs from the index κ as used by Burland. The ratio λ^* / κ^* is, however, equal to Burland's ratio λ/κ . The soil response during unloading and reloading is assumed to be elastic as denoted by the superscript e in Eqn. 10–6 (p. 109). The elastic behaviour is described by Hooke's law. Eqn. 10–6 (p. 109) implies linear stress dependency on the tangent bulk modulus such that:

$$K_{ur} = rac{E_{ur}}{3(1 - 2v_{ur})} = rac{p' + c\cot(\varphi)}{k^*}$$
 (10–7)

in which the subscript ur denotes unloading / reloading. Note that effective parameters are considered rather than undrained soil properties, as might be suggested by the subscripts ur. Neither the elastic bulk modulus, K_{ur} , nor the elastic Young's modulus, E_{ur} , is used as an input parameter. Instead, v_{iir} (Poisson's ratio) and κ^* are used as input constants for the part of the model that computes the elastic strains.

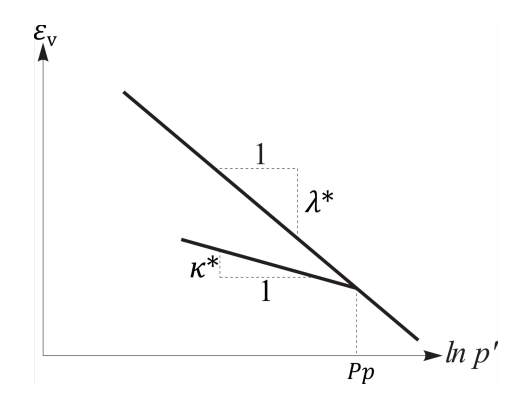


Figure 10-1: Logarithmic relation between volumetric strain and mean stress

An infinite number of unloading / reloading lines may exist in Figure 10-1 (p. 110), each corresponding to a particular value of the isotropic pre-consolidation stress p_p . The preconsolidation stress represents the largest stress level experienced by the soil. During unloading and reloading, this pre-consolidation stress remains constant. In primary loading, however, the pre-consolidation stress increases with the stress level, causing irreversible (plastic) volumetric strains.

10.2 | Yield function

The yield function of the Soft Soil model is defined as:

$$f=ar{f}-p_p$$
 (10–8)

where

= Function of the stress state (p', \tilde{q})

The pre-consolidation stress which is a function of plastic strain.

$$ar{f}=rac{ ilde{q}^2}{M^2\left(p'+c\cot\left(arphi
ight)
ight)}\,+p'$$
 (10–9)

$$p_p = p_p^0 \exp igg(rac{-arepsilon_v^p}{\lambda^* - \kappa^*} igg)$$
 (10–10)

where

similar deviatoric stress quantity as defined for the cap yield surface in the 6 The Hardening Soil model (Isotropic hardening) (p. 65):

$$ilde{q}={\sigma_1}'+(lpha-1){\sigma_1}' \quad lpha=rac{(3+\sin(arphi))}{(3-\sin(arphi))}$$
 (10–11)

The yield function (f = 0) describes an ellipse in the $p' - \tilde{q}$ -plane, as illustrated in Figure 10-2 (p. 111). The parameter M in Eqn. 10–9 (p. 110) determines the height of the ellipse. And it is responsible for the ratio of horizontal to vertical stresses in primary one-dimensional compression.

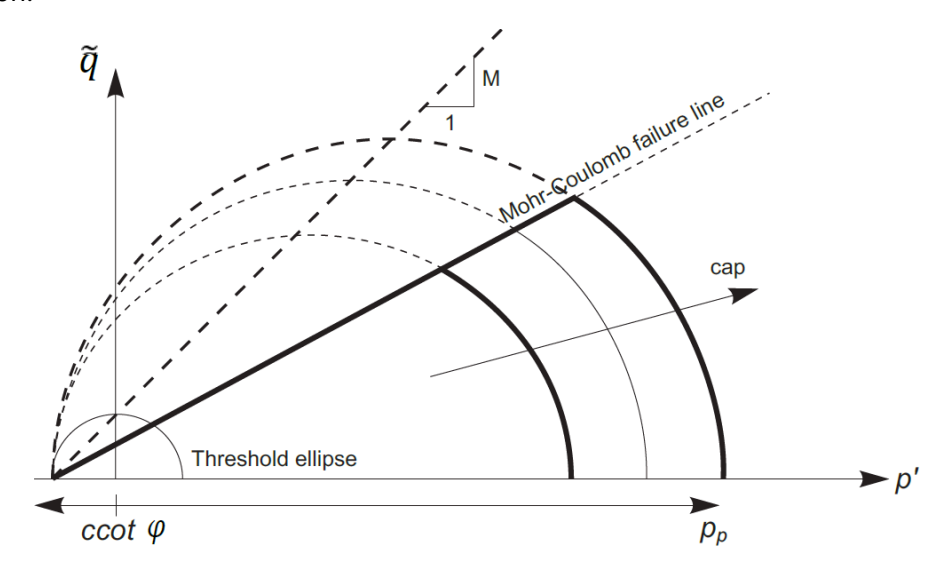


Figure 10-2: Yield surface of the Soft Soil model in p'- q-plane

As a result, the parameter M determines largely the coefficient of lateral earth pressure K_0^{nc} . In view of this, the value of M can be chosen such that a known value of K_0^{nc} is matched in primary one-dimensional compression. Such an interpretation and use of M differs from the original critical state line idea, but it ensures a proper matching of K_0^{nc} .

The tops of all ellipses are located on a line with slope M in the p' - \tilde{q} -plane. In <u>Burland (1965)</u> and Burland (1967) the M-line is referred to as the critical state line and represents stress states at post peak failure. The parameter M is then based on the critical state friction angle. In the Soft Soil model, however, failure is not necessarily related to critical state. The Mohr-Coulomb failure criterion is a function of the strength parameters φ and c, which might not correspond to the Mline.

The isotropic pre-consolidation stress p_p determines the extent of the ellipse along p' axis. During loading, an infinite number of ellipses may exist (see Figure 10-2 (p. 111)) each corresponding to a particular value of p_p . In tension (p' < 0), the ellipse extends to $ccot \varphi$ (Eqn. 10-9 (p. 110) and Figure 10-2 (p. 111)). In order to make sure that the right hand side of the ellipse (i.e. the 'cap') will remain in the 'compression' zone (p'>0) a minimum value of $ccot \varphi$ is adopted for p_p . For c = 0, a minimum value of p_p equal to a stress unit is adopted. Hence, there is a 'threshold' ellipse as illustrated in Figure 10-2 (p. 111).

The value of p_p is determined by volumetric plastic strain following the hardening relation, Eqn. 10-10 (p. 110). This equation reflects the principle that the pre-consolidation stress increases exponentially with decreasing volumetric plastic strain (compaction). p_p^0 can be regarded as the initial value of the pre-consolidation stress. The determination of p_p^0 is treated in 2.8 The initial pre-consolidation stress in advanced models (p. 27). According to Eqn. 10-10 (p. 110) the initial volumetric plastic strain is assumed to be zero.

In the Soft Soil model, the yield function, Egn. 10-8 (p. 110), describes the irreversible volumetric strain in primary compression, and forms the cap of the yield contour. To model the failure state, a perfectly-plastic Mohr-Coulomb type yield function is used. This yield function represents a straight line in p' - \tilde{q} -plane as shown in Figure 10-2 (p. 111). The slope of the failure line is smaller than the slope of the M-line.

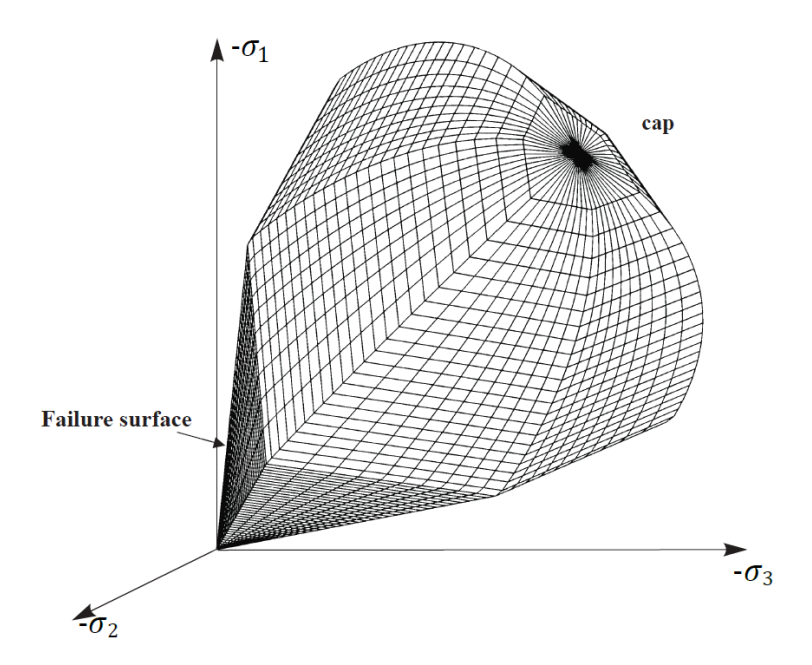


Figure 10-3: Representation of total yield contour of Soft Soil model in principal stress space

The total yield contour, as shown by the bold lines in Figure 10-3 (p. 112), is the boundary of the elastic stress area. The failure line is fixed, but the cap may increase in primary compression. Stress paths within this boundary give only elastic strain increments, whereas stress paths that tend to cross the boundary generally give both elastic and plastic strain increments.

For general states of stress (p', \tilde{q}) , the plastic behaviour of the Soft Soil model is defined by the combination of the cap yield function and the Mohr-Coloumb yield functions. The total yield contour in principal stress space is indicated in Figure 10-3 (p. 112).

10.3 Parameters of the Soft Soil model

The parameters of the Soft Soil model include compression and swelling indices, which are typical for soft soils, as well as the Mohr-Coulomb model failure parameters. In total, the Soft Soil model requires the following parameters to be determined:

Basic parameters:

λ*	Modified compression index	[-]
К*	Modified swelling index	[-]
V _{ur}	Poisson's ratio for unloading / reloading	[-]
С	Effective cohesion	[kN/m ²]
φ	Friction angle	[°]
Ψ	Dilatancy angle	[°]
σ_{t}	Tensile strength	[kN/m ²]

Miscellaneous parameters (use default settings):

K_0^{nc} C	Coefficient of lateral stress in normal consolidation	[-]
--------------	---	-----

M K_0^{nc} -parameter [-]

Instead of defining the stiffness by the basic stiffness parameters, alternative stiffness parameters can be used. These material constants are given by:

C_c	Compression index	[-]
Cs	Swelling index	[-]
e _{init}	Initial void ratio	[-]

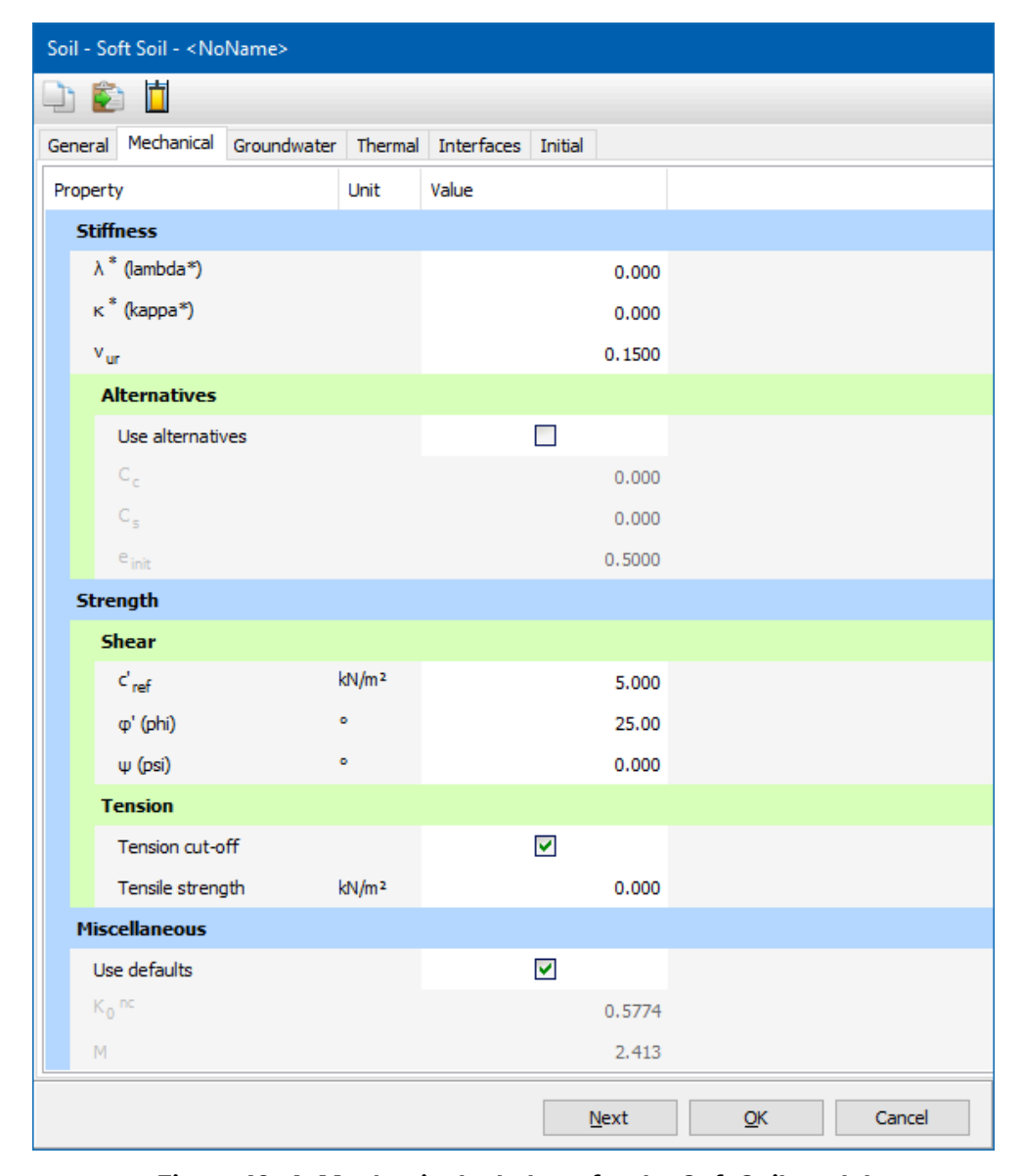


Figure 10-4: Mechanical tabsheet for the Soft Soil model

Figure 10-4 (p. 113) shows the PLAXIS 2D window for inputting the values of the model parameters. M is calculated automatically from the coefficient of the lateral earth pressure, K_0^{nc} , by means of Eqn. 10–13 (p. 115). Note that, physically, in the current model M differs from the similar parameter in the Modified Cam-Clay model where it is related to the material friction.

10.3.1 Modified swelling index and modified compression index

These parameters can be obtained from an isotropic compression test including isotropic unloading. When plotting the logarithm of the mean stress as a function of the volumetric strain for clay-type materials, the plot can be approximated by two straight lines (see Figure 10-1 (p. 110)). The slope of the primary loading line gives the modified compression index, and the slope of the unloading (or swelling) line gives the modified swelling index. Note that there is a difference between the modified indices κ^* and λ^* and the original Cam-Clay parameters κ and λ . The latter parameters are defined in terms of the void ratio e instead of the volumetric strain ε_{v} .

Apart from the isotropic compression test, the parameters κ^* and λ^* can be obtained from a one-dimensional compression test. Here a relationship exists with the internationally recognised parameters for one-dimensional compression and swelling indices, C_c and C_s . These relationships are summarised in Table 10-1 (p. 114) and Table 10-2 (p. 114).

Table 10-1: Relationship to Cam-Clay parameters

$$1. \;\; \lambda^* = rac{\lambda}{1+e}$$
 $2. \;\; \kappa^* = rac{\kappa}{1+e}$

Table 10-2: Relationship to internationally normalised parameters

$$\lambda^* = rac{C_c}{2.3(1+e)} \qquad \qquad 4. \quad \kappa^* pprox rac{2C_s}{2.3(1+e)}$$

Note: Remarks on Table 10−1 (p. 114) and Table 10−2 (p. 114)

- In relations 1 and 2, the void ratio, e, is assumed to be constant. In fact, e will change during a compression test, but this will give a relatively small difference in void ratio. For e one can use the average void ratio that occurs during the test or just the initial
- As further explained in 11.6 Formulation of elastic 3D-strains (p. 125) in relation 4 there is no exact relation between κ^* and the one-dimensional swelling index C_{s_i} because the ratio of horizontal and vertical stresses changes during one-dimensional unloading. For this approximation it is assumed that the average stress state during unloading is an isotropic stress state, hence $K_0=1$. This assumption is reasonable for moderately overconsolidated clays with friction angles in the range of 20° - 30°.
- In practice, swelling is often assumed to be equivalent to recompression behaviour, which, may not be right. Hence κ^* should be based on C_s rather than the recompression index C_r .
- The factor 2.3 in relation 3 is obtained from the ratio between the logarithm of base 10 and the natural logarithm.
- The ratio λ^* / κ^* (= λ / κ) ranges, in general, between 2.5 and 7.

10.3.2 Cohesion

The cohesion has the dimension of stresses. A small effective cohesion may be used, including a cohesion of zero. Entering a cohesion will result in an elastic region that is partly located in the 'tension' zone, as illustrated in Figure 10-2 (p. 111). The left hand side of the ellipse crosses the p'-axis at a value of $ccot \varphi$. In order to maintain the right hand side of the ellipse (i.e. the cap) in the 'pressure' zone of the stress space, the isotropic pre-consolidation stress p_p has a

minimum value of ccot φ . This means that entering a cohesion larger than zero may result in a state of 'overconsolidation', depending on the magnitude of the cohesion and the initial stress state. As a result, a stiffer behaviour is obtained during the onset of loading. It is not possible to specify undrained shear strength by means of high cohesion and a friction angle of zero. Input of model parameters should always be based on effective values. The PLAXIS option to model undrained behaviour using effective parameters may be used (Undrained (A). Please note that the resulting effective stress path may not be accurate, which may lead to an unrealistic undrained shear strength. Hence, when using *Undrained (A)* as drainage type, the resulting stress state must be checked against a known undrained shear strength profile.

10.3.3 Friction angle

The effective angle of internal friction represents the increase of shear strength with effective stress level. It is specified in degrees. Zero friction angle is not allowed. On the other hand, care should be taken with the use of high friction angles. It is often recommended to use φ_{cv} , i.e. the critical state friction angle, rather than a higher value based on small strains. Moreover, using a high friction angle will substantially increase the computational requirements.

10.3.4 Dilatancy angle

For the type of materials, which can be described by the Soft Soil model, the dilatancy can generally be neglected. A dilatancy angle of zero degrees is considered in the standard settings of the Soft Soil model.

10.3.5 Poisson's ratio

In the Soft Soil model, the Poisson's ratio v is the well known pure elastic constant rather than the pseudo-elasticity constant as used in the linear elastic perfectly-plastic model. Its value is usually be in the range between 0.1 and 0.2, with a default of 0.15. For loading of normally consolidated materials, the Poisson's ratio plays a minor role, but it becomes important in unloading problems. For example, for unloading in a one-dimensional compression test (oedometer), the relatively small Poisson's ratio will result in a small decrease of the lateral stress compared with the decrease in vertical stress. As a result, the ratio of horizontal and vertical stress increases, which is a well-known phenomenon in overconsolidated materials. Hence, the Poisson's ratio should not be based on the normally consolidated K_0^{nc} -value, but on the ratio of the horizontal stress increment to the vertical stress increment in oedometer unloading and reloading test such that:

$$\frac{\nu_{ur}}{1 - \nu_{ur}} = \frac{\Delta \sigma_{xx}}{\Delta \sigma_{yy}}$$
 (unloading and reloading)

10.3.6 $|K_0^{\text{nc}}$ -parameter

The parameter M is automatically determined based on the coefficient of lateral earth pressure in normally consolidated condition, K_0^{nc} , as entered by the user. The exact relation between Mand K_0^{nc} gives (Brinkgreve, 1994):

$$M=3\sqrt{rac{\left(1-K_{0}^{nc}
ight)^{2}}{\left(1+2K_{0}^{nc}
ight)^{2}}+rac{\left(1-K_{0}^{nc}
ight)\left(1-2
u_{ur}
ight)\left(\lambda^{*}/\kappa^{*}-1
ight)}{\left(1+2K_{0}^{nc}
ight)\left(1-2
u_{ur}
ight)rac{\lambda^{*}}{\kappa^{*}}-\left(1-K_{0}^{nc}
ight)\left(1+
u_{ur}
ight)}}}$$
 (10–13)

The value of M is indicated in the input window. As can be seen from Eqn. 10–14 (p. 116), M is also influenced by the Poisson's ratio v_{ur} and by the ratio λ^*/κ^* . However, the influence of K_0^{nc} is dominant. Eqn. 10-14 (p. 116) can be approximated by:

 $M \approx 3.0 - 2.8 K_0^{nc}$ (10-14)

10.4 State parameters in the Soft Soil model

In addition to the output of standard stress and strain, the Soft Soil model provides output (when being used) on state variables such as the hardening parameter y^p and the isotropic preconsolidation stress p_p . These parameters can be visualised by selecting the *State parameters* option from the Stresses menu. An overview of available state parameters is given below:

p _{eq}	Equivalent isotropic stress	[kN/m ²]
pp	sotropic preconsolidation stress $p_{eq} = p' + rac{q^2}{M^2(p' - c\cot(arphi))}$	[kN/m ²]
OCR	Isotropic overconsolidation ratio $OCR = p_p/p^{eq}$	[-]
γ ^p	Hardening parameter (equivalent mobilised plastic shear strain)	[-]
E _{ur}	Current stress-dependent elastic Young's modulus	[kN/m ²]
С	Current depth-dependent cohesion	[kN/m ²]

10.5 On the use of the Soft Soil model in dynamics calculations

When using the Soft Soil model in dynamics calculations, the modified swelling index κ^* needs to be selected such that the model correctly predicts wave velocities in the soil. This generally requires a smaller value than just an unloading-reloading index.

When subjected to dynamic or cyclic loading, the Soft Soil model will generate plastic strains when the preconsolidation stress is increased. However, it should be noted that stress cycles within the current hardening contour will only generate elastic strains and no (hysteretic) damping, nor accumulation of strains or pore pressure, nor liquefaction. In order to account for the soil damping in cyclic loading, Rayleigh damping may be defined.

Soft Soil Creep model (time dependent behaviour) [ADV]

11.1 Introduction

Both the Hardening Soil model and the Soft Soil model can be used to model the behaviour of compressible soft soils, but none of these models are suitable when considering creep, i.e. secondary compression. All soils exhibit some creep, and primary compression is thus always followed by a certain amount of secondary compression. Assuming the secondary compression (for instance during a period of 10 or 30 years) to be a certain percentage of the primary compression, it is clear that creep is important for problems involving large primary compression. This is for instance the case when constructing embankments on soft soils. Indeed, large primary settlements of footings and embankments are usually followed by substantial creep settlements in later years. In such cases it is desirable to estimate the creep from FEM-computations.

Foundations may also be founded on initially overconsolidated soil layers that yield relatively small primary settlements. Then, as a consequence of the loading, a state of normal consolidation may be reached and significant creep may follow. This is a treacherous situation as considerable secondary compression is not preceded by the warning sign of large primary compression. Again, computations with a creep model are desirable.

<u>Buisman (1936)</u> was probably the first to propose a creep law for clay after observing that soft-soil settlements could not be fully explained by classical consolidation theory. This work on 1D-secondary compression was continued by other researchers including, for example, <u>Bjerrum (1967)</u>, <u>Garlanger (1972)</u>, <u>Mesri & Godlewski (1977)</u> and <u>Leroueil (1977)</u>. More mathematical lines

of research on creep were followed by, for example, Sekiguchi (1977), Adachi & Oka (1982) and Borja & Kavaznjian (1985). This mathematical 3D-creep modelling was influenced by the more experimental line of 1D-creep modelling, but conflicts exist.

3D-creep should be a straight forward extension of 1D-creep, but this is hampered by the fact that present 1D-models have not been formulated as differential equations. For the presentation of the Soft Soil Creep model we will first complete the line of 1D-modelling by conversion to a differential form. From this 1D differential equation an extension was made to a 3D-model. This chapter gives a full description of the formulation of the Soft Soil Creep model. In addition, attention is focused on the model parameters. Finally, a validation of the 3D model is presented by considering both model predictions and data from triaxial tests. Here, attention is focused on constant strain rate triaxial tests and undrained triaxial creep tests. For more applications of the model the reader is referred to Vermeer, Stolle & Bonnier (1998), Vermeer & Neher (1999) and Brinkgreve (2004).

Some basic characteristics of the Soft Soil Creep model are:

- Stress-dependent stiffness (logarithmic compression behaviour)
- Distinction between primary loading and unloading-reloading
- Secondary (time-dependent) compression
- Ageing of pre-consolidation stress
- Failure behaviour according to the Mohr-Coulomb criterion

11.2 Basics of one-dimensional creep

When reviewing previous literature on secondary compression in oedometer tests, one is struck by the fact that it concentrates on behaviour related to step loading, even though natural loading processes tend to be continuous or transient in nature. Buisman (1936) was probably the first to consider such a classical creep test. He proposed the following equation to describe creep behaviour under constant effective stress:

$$arepsilon = arepsilon_c - C_B \log \left(rac{t}{t_c}
ight) \qquad for \qquad t > t_c$$
 (11–1)

where

The strain up to the end of consolidation.

Time measured from the beginning of loading.

Time to the end of primary consolidation.

 C_{B} Material constant

Please note that we do not follow the soil mechanics convention that compression is considered positive. Instead, compressive stresses and strains are taken to be negative. For further consideration, it is convenient to rewrite this equation as:

$$arepsilon = arepsilon_c - C_B \log \left(rac{t_c + t'}{t_c}
ight) \qquad for \qquad t' > 0$$
 (11–2)

with $t' = t - t_c$ being the effective creep time.

Based on the work by Bjerrum on creep, as published for instance in 1967, Garlanger (1972) proposed a creep equation of the form:

$$e=e_{c}-C_{lpha}\log\left(rac{ au_{c}+ au'}{ au_{c}}
ight) ~~with~~C_{lpha}=C_{B}\left(1+e_{0}
ight) ~~for:~~t'>0$$
 (11–3)

Differences between Garlanger's and Buisman's forms are modest. The engineering strain ε is replaced by void ratio e and the consolidation time t_c is replaced by the parameter τ_c . Eqn. 11–2 (p. 118) and Eqn. 11–3 (p. 119) are identical when choosing $\tau_c = t_c$. For the case that $\tau_c = t_{cr}$ differences between both formulations will vanish when the effective creep time t' increases.

For practical consulting, oedometer tests are usually interpreted by assuming $t_c = 24h$. Indeed, the standard oedometer test is a Multiple Stage Loading Test with loading periods of precisely one day. Due to the special assumption that this loading period coincides to the consolidation time t_c , it follows that such tests have no effective creep time.

Hence one obtains t'=0 and the log-term drops out of Eqn. 11-3 (p. 119). It would thus seem that there is no creep in this standard oedometer test, but this suggestion is false. Even highly impermeable oedometer samples need less than one hour for primary consolidation. Then all excess pore pressures are zero and one observes pure creep for the other 23 hours of the day. Therefore we will not make any assumptions about the precise values of τ_c and t_c .

Another slightly different possibility to describe secondary compression is the form adopted by Butterfield (1979):

$$arepsilon^H = arepsilon_c^H - c \ln \left(rac{ au_c + t'}{ au_c}
ight) \qquad for \qquad t' > 0$$
 (11–4)

where ε^H is the logarithmic strain defined as:

$$arepsilon^H = \ln\left(rac{V}{V_0}
ight) \, = \ln\left(rac{1+e}{1+e_0}
ight)$$
 (11–5)

with the subscript '0' denoting the initial values. The superscript 'H' is used to denote logarithmic strain, as the logarithmic strain measure was originally used by Hencky. For small strains it is possible to show that:

$$c = rac{C_{lpha}}{(1+e_0) \cdot \ln \, 10} = rac{C_B}{\ln \, 10}$$
 (11–6)

because then logarithmic strain is approximately equal to the engineering strain. Both Butterfield (1979) and den Haan (1994) showed that for cases involving large strain, the logarithmic small strain supersedes the traditional engineering strain.

11.3 On the variables τ_c and ε_c

In this section attention will first be focused on the variable τ_c . Here a procedure is to be described for an experimental determination of this variable. In order to do so we depart from Egn. 11-4 (p. 119). By differentiating this equation with respect to time and dropping the superscript 'H' to simplify the notation, one finds:

$$-\dot{arepsilon}=rac{c}{ au_c+t'}$$
 or $inversely: rac{-1}{\dot{arepsilon}}=rac{ au_c+t'}{c}$ (11–7)

which allows one to make use of the construction developed by Janbu (1969) for evaluating the parameters c and τ_c from experimental data. Both the traditional way, being indicated in Figure 11-1 (p. 120) a), as well as the Janbu method of Figure 11-1 (p. 120) b) can be used to determine the parameter c from an oedometer test with constant load.

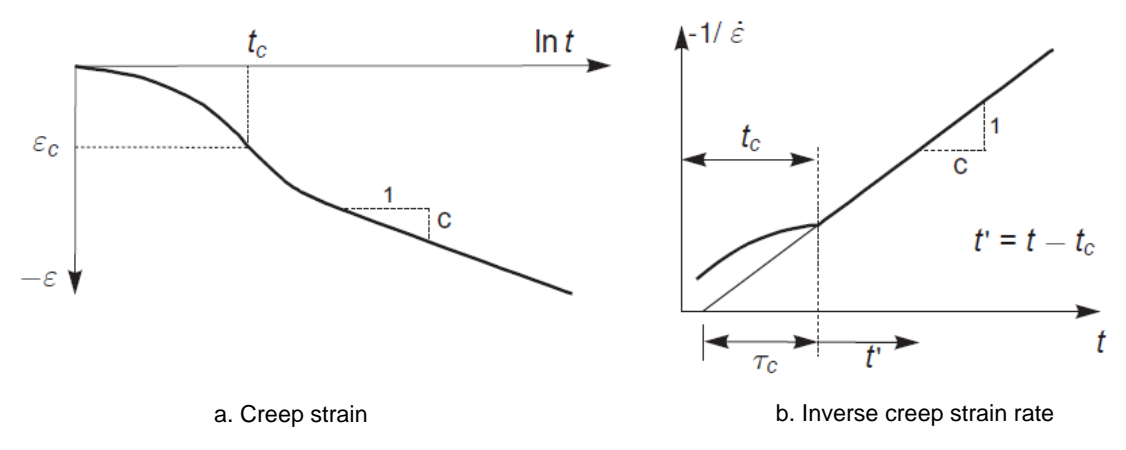


Figure 11–1: Standard oedometer test

The use of the Janbu method is attractive, because both τ_c and c follow directly when fitting a straight line through the data. In Janbu's representation of Figure 11–1 (p. 120) b), τ_c is the intercept with the (non-logarithmic) time axis of the straight creep line. The deviation from a linear relation for $t < t_c$ is due to consolidation.

Considering the classical literature it is possible to describe the end-of-consolidation strain ε_{cr} by an equation of the form:

$$arepsilon_c = arepsilon_c^e + arepsilon_c^c = -a \ln \left(rac{\sigma'}{\sigma'_0}
ight) - (b-a) \ln \left(rac{\sigma_{pc}}{\sigma_{p0}}
ight)$$
 (11–8)

Note that ε is a logarithmic strain, rather than a classical small strain although we conveniently omit the subscript 'H'. In the above equation σ'_0 represents the initial effective pressure before loading and σ' is the final effective loading pressure. The values σ_{p0} and σ_{pc} represent the pre-consolidation pressure corresponding to before-loading and end-of-consolidation states, respectively. In most literature on oedometer testing, one adopts the void ratio e instead of ε , and log instead of ln, the swelling (recompression) index C_s instead of a, and the compression index C_c instead of b. The above constants a and b relate to C_s and C_c as:

$$a=rac{C_s}{(1+e_0)\cdot \ln\,10} \ b=rac{C_c}{(1+e_0)\cdot \ln\,10}$$
 (11–9)

Combining Eqn. 11-4 (p. 119) and Eqn. 11-8 (p. 120) it follows that:

$$arepsilon = arepsilon^e + arepsilon^c = -a \, \ln \left(rac{\sigma'}{\sigma'_0}
ight) - (b-a) \, \ln \left(rac{\sigma_{pc}}{\sigma_{p0}}
ight) - c \ln \left(rac{ au_c + t'}{ au_c}
ight)$$
 (11–10)

where ε is the total logarithmic strain due to an increase in effective stress from σ'_0 to σ' , and a time period of $t_c + t'$.

In Figure 11–2 (p. 121) the terms of Eqn. 11–10 (p. 120) are depicted in an ε - In σ diagram. Notice that this figure has a division of strain increments into an elastic and a creep component. Also, for t' + tc = 1 day, one arrives precisely on the NC-line.

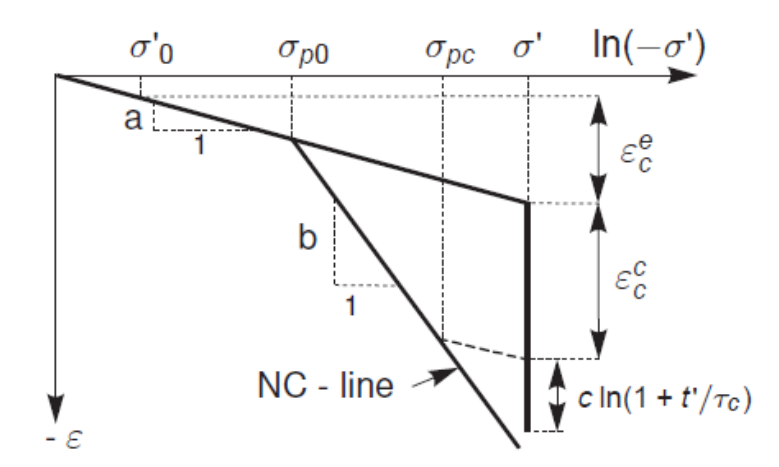


Figure 11-2: Idealised stress-strain curve from oedometer test with division of strain increments into an elastic and a creep component.

Up to this point, the more general problem of creep under transient loading conditions has not yet been addressed, as it should be recalled that restrictions have been made to creep under constant load. For generalising the model, a differential form of the creep model is needed. No doubt, such a general equation may not contain t' and neither τ_c as the consolidation time is not clearly defined for transient loading conditions.

11.4 Differential law for 1D-creep

The previous equations emphasize the relation between accumulated creep and time, for a given constant effective stress. For solving transient or continuous loading problems, it is necessary to formulate a constitutive law in differential form, as will be described in this section. In a first step we will derive an equation for τ_c . Indeed, despite the use of logarithmic strain and In instead of log, equation (Eqn. 11-10 (p. 120)) is classical without adding new knowledge. Moreover, the question on the physical meaning of τ_c is still open. In fact, we have not been able to find precise information on τ_c in the literature, apart from Janbu's method of experimental determination.

In order to find an analytical expression for the quantity τ_c , we adopt the basic idea that all inelastic strains are time dependent. Hence total strain is the sum of an elastic part $arepsilon^e$ and a time-dependent creep part ε^c . For non-failure situations as met in oedometer loading conditions, we do not assume an instantaneous plastic strain component, as used in traditional elastoplastic modelling. In addition to this basic concept, we adopt Bjerrum's idea that the preconsolidation stress depends entirely on the amount of creep strain being accumulated in the course of time. In addition to Eqn. 11-10 (p. 120) we therefore introduce the expression:

$$arepsilon=arepsilon^e+arepsilon^c=-a\ \ln\left(rac{\sigma'}{\sigma'_0}
ight)-(b-a)\ \ln\left(rac{\sigma_{pc}}{\sigma_{p0}}
ight)$$
 (11–11)

where

$$\sigma_p = \sigma_{p0} \exp\left(rac{-arepsilon^c}{b-a}
ight)$$
 (11–12)

Please note that ε^c is negative, so that σ_p exceeds σ_{p0} . The longer a soil sample is left to creep the larger σ_p grows. The time-dependency of the pre-consolidation pressure σ_p is now found by combining Eqn. 11-10 (p. 120) and Eqn. 11-11 (p. 121) to obtain:

$$arepsilon^c - arepsilon_c^c = -\left(b-a
ight) \ln\left(rac{\sigma_p}{\sigma_{pc}}
ight) = -c\left(rac{ au_c + t'}{ au_c}
ight)$$
 (11–13)

This equation can now be used for a better understanding of τ_c , at least when adding knowledge from standard oedometer loading. In conventional oedometer testing the load is stepwise increased and each load step is maintained for a constant period of $t_c + t' = \tau$, where τ is precisely one day.

In this way of stepwise loading the so-called normal consolidation line (NC-line) with $\sigma_p = \sigma'$ is obtained. On entering $\sigma_p = \sigma'$ and $t' = \tau - t_c$ into Eqn. 11–13 (p. 122) it is found that:

$$(b-a)\,\ln\left(rac{\sigma'}{\sigma_{pc}}
ight) = c\left(rac{ au_c + au - t_c}{ au_c}
ight) \;\; for: \;\; OCR = 1$$

It is now assumed that $(\tau_c - t_c) < \tau$. This quantity can thus be disregarded with respect to τ and it follows that:

$$rac{ au}{ au_c} = \left(rac{\sigma'}{\sigma_{pc}}
ight)^{rac{b-a}{c}} \quad or: \quad au_c = au \left(rac{\sigma_{pc}}{\sigma'}
ight)^{rac{b-a}{c}}$$
 (11–15)

Hence τ_c depends both on the effective stress σ' and the end-of-consolidation pre-consolidation stress σ_{pc} . In order to verify the assumption $(\tau_c - t_c) << \tau$, it should be realised that usual oedometer samples consolidate for relatively short periods of less than one hour. Considering load steps on the normal consolidation line, we have OCR=1 both in the beginning and at the end of the load step. During such a load step σ_p increases from σ_{p0} up to σ_{pc} during the short period of (primary) consolidation. Hereafter σ_p increases further from σ_{pc} up to σ' during a relatively long creep period. Hence, at the end of the day the sample is again in a state of normal consolidation, but directly after the short consolidation period the sample is under-consolidated with $\sigma_p < \sigma'$. For the usually very high ratios of $(b - a)/c \ge 15$, we thus find very small τ_c -values from Eqn. 11–15 (p. 122). Hence not only t_c but also τ_c tends to be small with respect to τ . It thus follows that the assumption $(\tau_c - t_c) << \tau$ is certainly correct.

Having derived the simple expression Eqn. 11–15 (p. 122) for τ_{cr} it is now possible to formulate the differential creep equation. To this end Eqn. 11-10 (p. 120) is differentiated to obtain:

$$\dot{arepsilon}=\dot{arepsilon}^e+\dot{arepsilon}^c=-arac{\dot{\sigma}'}{\sigma'}-rac{c}{ au_c}igg(rac{\sigma_{pc}}{\sigma_p}igg)^{rac{b-a}{c}}$$
 (11–16)

where $\tau_c + t'$ can be eliminated by means of Eqn. 11–13 (p. 122) to obtain:

$$\dot{arepsilon}=\dot{arepsilon}^e+\dot{arepsilon}^c=-arac{\dot{\sigma}'}{\sigma'}-rac{c}{ au_c}\left(rac{\sigma_{pc}}{\sigma_p}
ight)^{rac{\sigma-a}{c}}$$
 (11–17)

with:

$$\sigma_p = \sigma_{p0} \exp\left(rac{-arepsilon^c}{b-a}
ight)$$
 (11–18)

Again it is recalled that ε^c is a compressive strain, being considered negative in this manual. Eqn. 11–15 (p. 122) can now be introduced to eliminate τ_c and σ_{pc} and to obtain:

$$\dot{arepsilon}=\dot{arepsilon}^e+\dot{arepsilon}^c=-arac{\dot{\sigma}'}{\sigma'}-rac{c}{ au_c}igg(rac{\sigma'}{\sigma_p}igg)^{rac{b-a}{c}}$$
 (11–19)

11.5 Three-dimensional-model

On extending the 1D-model to general states of stress and strain, the well-known stress invariants for isotropic stress p and deviatoric stress q are adopted. These invariants are used to define a new stress measure named p^{eq} :

$$p^{eq}=p'+rac{ ilde{q}^2}{M^2\left(p'+c\,\cot\left(arphi
ight)
ight)}$$
 (11–20)

and \tilde{q} is a similar deviatoric stress quantity as defined in the Hardening Soil model and Soft Soil model. In Figure 11–3 (p. 123) it is shown that the stress measure p^{eq} is constant on ellipses in $p - \tilde{q}$ -plane. In fact we have the ellipses from the Modified Cam-Clay model as introduced by Roscoe & Burland (1968).

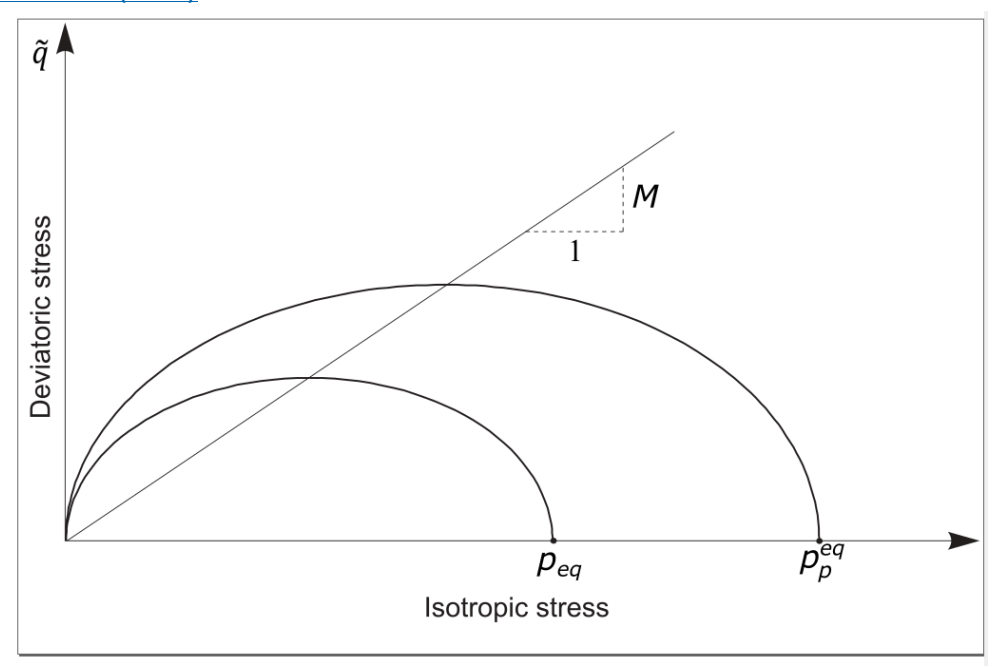


Figure 11–3: Diagram of p^{eq} -ellipse in a p- \tilde{q} -plane

The soil parameter M represents the slope of the so-called 'critical state line' as also indicated in Figure 11-3 (p. 123). We use:

$$M=rac{6\sin{\left(arphi_{cv}
ight)}}{3-\sin{\left(arphi_{cv}
ight)}}$$
 (11–21)

where

 φ_{cv} Critical-void friction angle, also referred to as critical-state friction angle.

The equivalent pressure p^{eq} is constant along ellipsoids in principal stress space.

To extend the 1D-theory to a general 3D-theory, attention is now focused on normally consolidated states of stress and strain as met in oedometer testing. In such situations it yields $\sigma'_{2} = \sigma'_{3} = K_{0}^{nc} \sigma'_{1}$, and it follows from Eqn. 11–20 (p. 123) that:

$$p_p^{eq} = \sigma_p \left[rac{1 + 2K_0^{nc}}{3} + rac{3\left(1 - K_0^{nc}
ight)^2}{M^2\left(1 + 2K_0^{nc}
ight)}
ight]$$
 (11–22)

where

Generalised pre-consolidation pressure, proportional to the one-dimensional one σ_n .

For a known stress state in p'-q stress space, p^{eq} can thus be computed from σ'_{1} , and with known values of K_0^{nc} , p_p^{eq} can thus be computed from σ_p . Omitting the elastic strain in the 1Dequation (Eqn. 11–19 (p. 122)), introducing the above expressions for p^{eq} and p_p^{eq} and writing ε_V instead of ε it is found that:

$$-\dot{arepsilon}_v^c=rac{\mu^*}{ au}\Big(rac{p^{eq}}{p_p^{eq}}\Big)^{rac{\lambda^*-\kappa^*}{\mu^*}} \quad where \quad p_p^{eq}=p_{p0}^{eq}\exp\left(rac{-arepsilon_v^c}{\lambda^*-\kappa^*}
ight)$$
 (11–23)

where

modified compression index

 κ^* = modified swelling index

modified creep index

For one-dimensional oedometer conditions, this equation reduces to Eqn. 11-19 (p. 122), so that one has a true extension of the 1D-creep model. It should be noted that the subscript '0' is once again used in the equations to denote initial conditions and that $\varepsilon_v^c = 0$ for time t = 0.

Instead of the parameters a, b and c of the 1D-model, the 3D-model uses the material parameters κ^* , λ^* and μ^* , who fit into the framework of critical state soil mechanics. Conversion between constants follows the rules:

$$\kappa^*pprox rac{2}{3}ig(1+2K_0ig)a\quad \lambda^*=b\quad \mu^*=c$$
 (11–24)

The expression for κ^* is an approximation under the assumption that the Poisson's ratio for unloading-reloading, $v_{ur} \approx 0.2$. There is no constant relation between κ^* and α , since during unloading and reloading under oedometer conditions the ratio of normal stress components changes and therefore the ratio between changes of p' and σ_1' deviates.

As yet the 3D-creep model is incomplete, as we have only considered a volumetric creep strain ε_{v}^{c} , whilst soft soils also exhibit deviatoric creep strains.

To introduce general creep strains, we adopt the view that creep strain is simply a timedependent plastic strain. It is thus logic to assume a flow rule for the rate of creep strain, as usually done in plasticity theory. For formulating such a flow rule, it is convenient to adopt the vector notation and considering principal directions:

$$\underline{\sigma} = (\sigma_1 \ \sigma_2 \ \sigma_3)^T \ and \ \underline{\varepsilon} = (\varepsilon_1 \ \varepsilon_2 \ \varepsilon_3)^T$$
 (11–25)

where T is used to denote a transpose. Similar to the 1D-model we have both elastic and creep strains in the 3D-model. Using Hooke's law for the elastic part, and a flow rule for the creep part, one obtains:

$$\underline{\dot{\varepsilon}} = \underline{\dot{\varepsilon}}^e + \underline{\dot{\varepsilon}}^c = \mathbf{D}^{-1}\underline{\dot{\sigma}} + \lambda \frac{\partial g^c}{\partial \underline{\sigma}'}$$
(11–26)

where the elasticity matrix and the plastic potential function are defined as:

where E_{ur} relates to the modified swelling index (Eqn. 11–32 (p. 125)). Hence we use the

equivalent pressure p^{eq} as a plastic potential function for deriving the individual creep strainrate components. The subscripts 'ur' are introduced to emphasize that both the elasticity modulus and Poisson's ratio will determine unloading-reloading behaviour. Now it follows from the above equations that:

$$\dot{arepsilon}_{v}^{c}=\dot{arepsilon}_{1}^{c}+\dot{arepsilon}_{2}^{c}+\dot{arepsilon}_{3}^{c}=\lambda\cdot\left(rac{\partial p^{eq}}{\partial\sigma_{1}^{\prime}}+rac{\partial p^{eq}}{\partial\sigma_{2}^{\prime}}+rac{\partial p^{eq}}{\partial\sigma_{3}^{\prime}}
ight)=rac{\partial p^{eq}}{\partial p^{\prime}}=\lambda\cdotlpha$$
 (11–28)

Hence we define $\alpha=\partial p^{eq}/\partial p'$. Together with Eqn. 11–25 (p. 124) and Eqn. 11–26 (p. 124) this leads to:

$$\underline{\dot{\varepsilon}} = \boldsymbol{D}^{-1}\underline{\dot{\sigma}}' + \frac{\dot{\varepsilon}_v^c}{\alpha}\frac{\partial p^{eq}}{\partial \underline{\sigma}'} = \boldsymbol{D}^{-1}\underline{\dot{\sigma}}' + \frac{1}{\alpha}\frac{\mu^*}{\tau} \left(\frac{p^{eq}}{p_p^{eq}}\right)^{\frac{\lambda^* - \kappa^*}{\mu^*}}\frac{\partial p^{eq}}{\partial \underline{\sigma}'} \tag{11-29}$$

where:

$$p_p^{eq} = p_{p0}^{eq} \exp\left(rac{-arepsilon_v^c}{\lambda^* - \kappa^*}
ight)$$
 (11–30)

or inversely:

$$-arepsilon_v^c = \left(\lambda^* - \kappa^*
ight) \ln\!\left(rac{p_p^{eq}}{p_{p0}^{eq}}
ight)$$
 (11–31)

11.6 Formulation of elastic 3D-strains

Considering creep strains, it has been shown that the 1D-model can be extended to obtain the 3D-model, but as yet this has not been done for the elastic strains.

To get a proper 3D-model for the elastic strains as well, the elastic modulus E_{ijr} has to been defined as a stress-dependent tangent stiffness according to:

$$E_{ur}=3igg(1-2v_{ur}igg)K_{ur}=-3igg(1-2v_{ur}igg)igg(rac{p'+c\cot{(arphi)}}{\kappa^*}igg)$$
 (11–32)

Hence, E_{ur} is not a new input parameter, but simply a variable quantity that relates to the input parameter κ^* . On the other hand v_{ur} is an additional true material constant.

Hence similar to E_{ur} , the bulk modulus K_{ur} is stress dependent according to the rule $\kappa_{ur}=-(p'+c\ cotarphi)^*/\kappa^*$ where in this context c is again the effective cohesion rather than the creep parameter. Now it can be derived for the volumetric elastic strain that:

$$\dot{\varepsilon}_{v}^{e} = \frac{\dot{p}'}{K_{wr}} = -\kappa^{*} \frac{\dot{p}'}{p' + c \cot(\varphi)}$$
or by integration:
$$-\varepsilon_{v}^{e} = \kappa^{*} \ln \left(\frac{p' + c \cot(\varphi)}{p'_{0} + c \cot(\varphi)} \right)$$
(11–33)

Hence in the 3D-model the elastic strain is controlled by the mean effective stress p', rather than by principal effective stress σ' as in the 1D-model. However the mean effective stress can be converted into principal stresses. For one-dimensional compression on the normal consolidation line, we have both $3~p'=\left(1+2K_0^{nc}
ight)\sigma'$ and $3~p_0'=\left(1+2K_0^{nc}
ight)\sigma_0'$ and it follows that $p'/p'_0 = \sigma'/\sigma'_0$. As a consequence, for c=0, we derive the simple rule $-\varepsilon^c_v = \kappa^* \ln \sigma'/\sigma'_0$, whereas the 1D-model involves $-\varepsilon_v^c=a\,\ln\,\sigma'/\sigma_0'$. It would thus seem that κ^* coincides with a. Unfortunately this line of thinking cannot be extended toward overconsolidated states of stress and strain. For such situations, it can be derived that:

$$rac{\dot{p}'}{p'} = rac{1 + v_{ur}}{1 - v_{ur}} rac{1}{1 + 2K_0} rac{\dot{\sigma}'}{\sigma'}$$
 (11–34)

and it follows that:

$$-\dot{arepsilon}_{v}^{e}=\kappa^{*}rac{\dot{p}'}{p'}=rac{1+v_{ur}}{1-v_{ur}}rac{\kappa^{*}}{1+2K_{0}}rac{\dot{\sigma}'}{\sigma'}$$
 (11–35)

where K_0 depends to a great extent on the degree of over-consolidation. Assuming that for soft clay the friction angle φ is in the order of 20-30° and OCR is in the order of 2-3, it is reasonable to assume $K_0 \approx 1$ and together with $v_{ur} \approx 0.2$ one obtains $-2\varepsilon_v^c \approx \kappa^* ln(\sigma'/\sigma'_0)$. Good agreement with the 1D-model is then found by taking $\kappa^* \approx 2a$. Note that for clays with significantly different friction angles and/or degrees of consolidation good agreement with practical results may be found for values of both $\kappa^* < 2a$ or $\kappa^* > 2a$.

11.7 Formulation of failure condition

The creep formulation does not include failure. Therefore, a Mohr-Coulomb type failure criterion. formulated in a perfect-plasticity framework, is added to the Soft Soil Creep model, generating plastic strains as soon as the failure condition is met. As soon as the Mohr-Coulomb failure yield criterion $f(\sigma', c, \varphi) = 0$ is met, instantaneous plastic strain rates develop according to the flow rule $\dot{\varepsilon}^p = \lambda \partial g/\partial \sigma'$ with g = g (σ' , ψ). For details see 3 Linear Elastic Perfectly Plastic Model (Mohr-Coulomb Model) (p. 31).

In each stress point, the stresses are calculated according to the creep formulation before considering the failure criterion. Subsequently, the new stress state is checked against the failure criterion and corrected, if applicable.

11.8 | Parameters of the Soft Soil Creep model

In addition to the parameters of the Soft Soil model, the Soft Soil Creep model involves a creep parameter in the form of the modified creep index μ^* . Figure 11.4 shows the PLAXIS window for inputting the values of the model parameters.

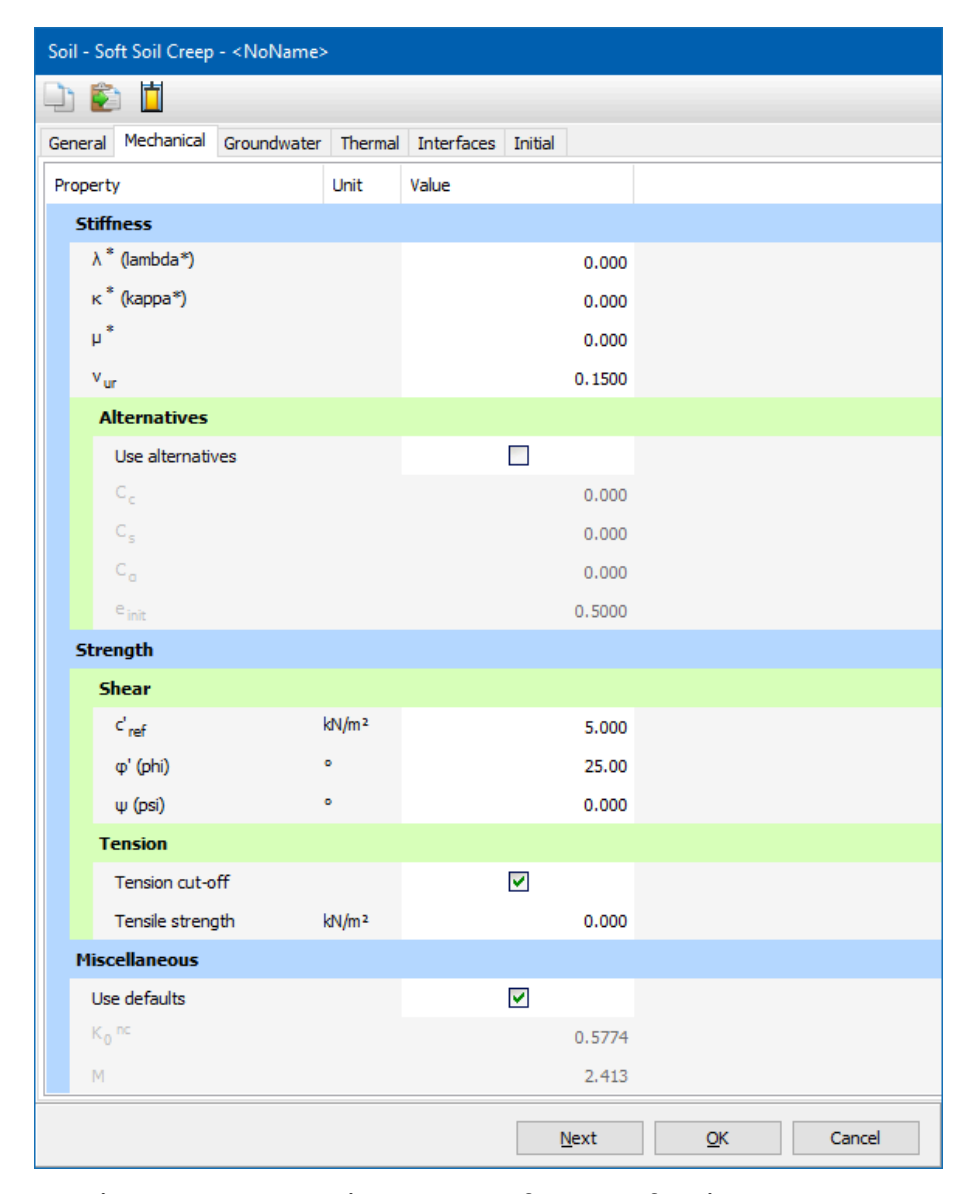


Figure 11-4: Mechanical tabsheet for the Soft Soil Creep model

In conclusion, the Soft Soil Creep model requires the following basic parameters and material constants:

Material constants:

λ^*	Modified compression index	[-]
К*	Modified swelling index	[-]
μ^*	Modified creep index	[-]
V _{ur}	Poisson's ratio for unloading - reloading (default 0.15)	[-]

Basic strength parameters:

C' _{ref}	Effective cohesion	[kN/m ²]
arphi'	Friction angle	[°]

Ψ	Dilatancy angle	[°]
σ_t	Tensile strength	[kN/m ²]

Miscellaneous parameters (use default settings):

K_0^{nc}	$\sigma'_{xx}/\sigma'_{yy}$ stress ratio in a state of normal consolidation	[-]
М	K_0^{nc} -related parameter (see below)	[-]

Instead of defining the stiffness by the basic stiffness parameters, alternative stiffness parameters can be used. These material constants are given by:

C_c	Compression index	[-]
Cs	Swelling index	[-]
C_{lpha}	Creep index for secondary compression	[-]
e _{init}	Initial void ratio	[-]

11.8.1 Modified swelling index, modified compression index and modified creep index

These parameters can be obtained from an isotropic compression test including isotropic unloading. When plotting the logarithm of the mean stress as a function of the volumetric strain for clay-type materials, the plot can be approximated by two straight lines (see Figure 10-1 (p. 110)). The slope of the primary loading line gives the modified compression index, and the slope of the unloading (or swelling) line gives the modified swelling index. Note that there is a difference between the modified indices κ^* and λ^* and the original Cam-Clay parameters κ and λ . The latter parameters are defined in terms of the void ratio e instead of the volumetric strain ε_{ν} . These relationships are summarised in Table 4. The parameter μ^* (Table 11–2 (p. 129)) can be obtained by measuring the volumetric strain on the long term and plotting it against the logarithm of time (see Figure 11-1 (p. 120)).

Apart from the isotropic compression test, the parameters λ^* , κ^* and μ^* can be obtained from a one-dimensional compression test. Here a relationship exists with the internationally recognised parameters for one-dimensional compression, swelling and creep indices, C_c , C_s and C_α . These relationships are summarised in Table 6. The factor 2.3 in Table 11-3 (p. 129), is obtained from the ratio between the logarithm of base 10 and the natural logarithm. The alternative stiffness parameters can also be calculated from this table. Since the void ratio e is not a constant, in the conversion from the alternative parameters to the original model parameters in PLAXIS the void ratio e is defined as the initial void ratio e_{init} . Entering a particular value for one of the alternatives C_c , C_s or C_α results in a change of λ^* , κ^* or μ^* , respectively.

For a rough estimate of the model parameters, one might use the correlation $\lambda^* \approx I_n(\%)/500$, the fact that λ^*/μ^* is in the range between 15 to 25 and the general observation λ^*/κ^* is between 2.5 and 7.

Table 11–1: Relationship to Cam-Clay parameters

$\lambda^* = rac{\lambda}{1+e}$ $\kappa^* = rac{\kappa}{1+e}$

Table 11-2: Relationship to a,b,c parameters

λ^* = b μ^* = c μ^* = c

Table 11-3: Relationship to internationally normalised parameters

$\lambda^* = rac{C_c}{2.3(1+e)}$	$\kappa^* pprox rac{2}{2.3} rac{C_s}{(1+e)}$	$\mu^* pprox rac{1}{2.3} rac{C_lpha}{(1+e)}$
	(· · /	` ' '

Note:

As already indicated in 11.6 Formulation of elastic 3D-strains (p. 125), there is no exact relation between the isotropic compression index κ^* and the one-dimensional swelling indices α and C_s , because the ratio of horizontal and vertical stress changes during one-dimensional unloading. For the approximation it is assumed that the average stress state during unloading is an isotropic stress state, hence K_0 =1. This is a reasonable assumption for moderately overconsolidated clays with a friction angle in the range of $20^{\circ}-30^{\circ}$.

For characterising a particular layer of soft soil, it is also necessary to know the initial preconsolidation pressure σ_{p0} . This pressure may, for example, be computed from a given value of the overconsolidation ratio (OCR). Subsequently, σ_{p0} can be used to compute the initial value of the generalised pre-consolidation pressure p_p^{eq} (see 2.8 The initial pre-consolidation stress in advanced models (p. 27)).

11.8.2 Poisson's ratio

In the case of the Soft Soil Creep model, the Poisson's ratio is purely an elasticity constant rather than a pseudo-elasticity constant as used in the Mohr-Coulomb model. Its value is usually in the range between 0.1 and 0.2. If the standard setting for the Soft Soil Creep model parameters is selected, then the value v_{ur} with a default of 0.15 is automatically adopted. For loading of normally consolidated materials, the Poisson's ratio plays a minor role, but it becomes important in unloading problems. For example, for unloading in a one-dimensional compression test (oedometer), the relatively small Poisson's ratio will result in a small decrease of the lateral stress compared with the decrease in vertical stress. As a result, the ratio of horizontal and vertical stress increases, which is a well-known phenomenon for overconsolidated materials. Hence, the Poisson's ratio should not be based on the normally consolidated K_0^{nc} -value, but on the ratio of difference in horizontal stress to difference in vertical stress in oedometer unloading and reloading:

$$\frac{\nu_{ur}}{1-\nu_{ur}} = \frac{\Delta \sigma_{xx}}{\Delta \sigma_{yy}}$$
 (Unloading and reloading)

11.8.3 K_0^{nc} - parameter

By default, M is automatically determined based on the coefficient of lateral earth pressure in normally consolidated condition, K_0^{nc} , as entered by the user. The exact relationship between Mand K_0^{nc} can be formulated as Brinkgreve (1994):

$$M = \sqrt{rac{\left(1 - K_0^{nc}
ight)^2}{\left(1 + 2K_0^{nc}
ight)^2} + rac{\left(1 - K_0^{nc}
ight)\left(1 - 2
u_{ur}
ight)\left(\lambda^*/\kappa^* - 1
ight)}{\left(1 - 2K_0^{nc}
ight)\left(1 - 2
u_{ur}
ight)\lambda^*/\kappa^* - \left(1 - K_0^{nc}
ight)\left(1 +
u_{ur}
ight)}}$$
 (11–37)

Hence the user cannot enter directly a particular value of M. Instead he can choose values for K_0^{nc} . Note that the particular selection of M has an influence on lateral deformation of pseudovertical loading problems. For details, see Brinkgreve (2004).

$$M pprox 3.0 - 2.8 K_0^{nc}$$
 (11–38)

11.9 State parameters in the Soft Soil Creep model

In addition to the output of standard stress and strain quantities, the Soft Soil Creep model model provides output (when being used) on state variables such as the isotropic pre-consolidation stress p_p . These parameters can be viewed by selecting the *State parameters* option from the Stresses menu. An overview of available state parameters is given below:

	Equivalent isotropic stress	
p _{eq}	$igg p_{eq}=p'+q^2/M^2ig(p'+c\cot{(arphi)}ig)$	[-]
pp	Isotropic pre-consolidation stress	[-]
OCR	Isotropic overconsolidation $OCR = p_p/p_{eq}$	[-]

11.10 On the use of the Soft Soil Creep model in dynamics calculations

When using the Soft Soil Creep model in dynamics calculations, the modified swelling index κ^* needs to be selected such that the model correctly predicts wave velocities in the soil. This generally requires a smaller value than just an unloading-reloading index.

When subjected to dynamic or cyclic loading, the Soft Soil Creep model will generate plastic strains when the preconsolidation stress is increased. However, it should be noted that stress cycles within the current creep contour will only generate elastic strains and no (hysteretic) damping, nor accumulation of strains or pore pressure, nor liquefaction. In order to account for the soil damping in cyclic loading, Rayleigh damping may be defined.

11.11 On the use of the Soft Soil Creep model in practical applications

In the Soft Soil Creep model, creep strains are generated as long as there is effective stress. In oedometer tests and other lab tests, self-weight stresses of the soil sample are negligible and the effective stress in the sample is dominated by external loading conditions. However, when it comes to practical applications, the effective stress in the soil is generally dominated by the initial self-weight stresses. As a consequence, creep will occur without additional loading.

Following the formulation of the model, the rate at which creep strains occur highly depends on the overconsolidation ratio as well as the ratio of the (modified) compression index over

the (modified) creep index. Regarding the latter, it should be considered that natural clays may involve structure (bonding) whilst the Soft Soil Creep model does not include such effects. This requires the effective stress range in the application to be taken into account when determining the compression and creep indices from one-dimensional compression tests. This may also have an effect on the pre-consolidation stress to be used in the application. Moreover, considering 'normally-consolidated' soft soil deposits in practice, it would seem logical to set the initial OCR-value equal to 1.0. However, this would lead to unrealistic large creep strain rates due to the initial stresses, without even considering additional loading.

In order to avoid these unrealistic creep strain rates, it is recommended to set the initial OCRvalue larger than 1.0. A value in the order of 1.2-1.4 will generally work, but in some cases even higher values might be needed. Please keep in mind that this changes the pre-consolidation pressure, such that the material becomes lightly overconsolidated and the pre-consolidation stress may not correspond anymore to what is observed in compression tests.

The above may be validated from a practical viewpoint by considering that the layer has aged since its deposition in geological history. Moreover, in particular the top few metres of an existing soft soil layer have been subjected to various possible external influences (traffic, weather, temperature changes, changes in saturation, etc.). Accurate measurements of the preconsolidation pressure on soil samples that are assumed to be 'normally-consolidated' would typically show a pre-consolidation pressure that is noticeably larger than the initial effective stress. However, lab tests are often performed on soil samples that have been disturbed to a certain extent, and therefore the measurement of the pre-consolidation stress in practice is often inaccurate.

In conclusion, the determination of model parameters for the Soft Soil Creep model requires a cautious interpretation of test data, in view of the envisioned practical application. It is recommended, before commencing any 2D or 3D analysis, to perform a careful calibration of model parameters. This can be done by performing simulations using the PLAXIS Soil Test facility in combination with an analysis of a one-dimensional soil column (based on the in-situ soil layering), in which a realistic time interval is considered.

The Sekiguchi-Ohta model [ADV]

The Sekiguchi-Ohta model has been developed to formulate a constitutive law for normally consolidated clay. Particular emphasis is placed on taking the effect of time and stress-induced anisotropy into consideration. A complete description of the model has been presented in Sekiguchi & Ohta (1977) and lizuka & Ohta (1987).

12.1 Formulation of the Sekiguchi-Ohta model

The Sekiguchi-Ohta model combines the concepts lying behind the well known Cam Clay model (Roscoe, Schofield & Thurairajah (1963)) and the rheological model developed by Murayama & Shibata (1966). The Cam Clay model was further developed by Ohta & Hata (1973) counting for the stress induced anisotropy for anisotropically consolidated clays. However due to the fact that this model deals with the stress-strain behaviour of the soil in equilibrium, the time effect is not considered. The rheological model is further developed by Sekiguchi (1977) to describe the time-dependent and elastoplastic behaviour for normally consolidated clays.

12.1.1 Isotropic states of stress and strain ($\sigma'_1 = \sigma'_2 = \sigma'_3$)

In the Sekiguchi-Ohta model, it is assumed that there is a logarithmic relation between changes in volumetric strain, ε_v , and changes in mean effective stress, p', which can be formulated as:

$$arepsilon_v - arepsilon_v^0 = -\lambda^* \ln \left(rac{p'}{p^0}
ight) \hspace{1.5cm} \left(virgin\ compression
ight)$$

The parameter λ^* is the modified compression index, which determines the compressibility of the material in primary loading. Note that λ^* differs from the index λ as used by Burland (1965). The difference is that Eqn. 12–1 (p. 133) is a function of volumetric strain instead of void ratio. Plotting Eqn. 12–1 (p. 133) gives a straight line as shown in Figure 12–1 (p. 133).

During isotropic unloading and reloading a different path (line) is followed, which can be formulated as:

$$arepsilon_v^e - arepsilon_v^{e0} = -\kappa^* \ln \left(rac{p'}{p^0}
ight) \hspace{1.5cm} \left(unloading \ and \ reloading
ight)$$

The parameter κ^* is the modified swelling index, which determines the compressibility of the material in unloading and subsequent reloading. Note that κ^* differs from the index κ as used in the Cam-Clay models. The ratio λ^*/κ^* is, however, equal to the ratio λ/κ . The soil response during unloading and reloading is assumed to be elastic as denoted by the superscript e in Eqn. 12-2 (p. 133). Eqn. 12-2 (p. 133) implies linear stress dependency on the tangent bulk modulus such that:

$$K_{ur}\equiv rac{E_{ur}}{3(1-2
u_{ur})}=rac{p'}{\kappa^*}$$
 (12–3)

in which the subscript ur denotes unloading/reloading. Neither the elastic bulk modulus, K_{ur} , nor the elastic Young's modulus, E_{ur} , is used as an input parameter. Instead, v_{ur} and κ^* are used as input constants for the part of the model that computes the elastic strains.

An infinite number of unloading/reloading lines may exist in Figure 12-1 (p. 133), each corresponding to a particular value of the isotropic pre-consolidation stress p_p . The preconsolidation stress represents the largest stress level experienced by the soil. During unloading and reloading, this pre-consolidation stress remains constant. In primary loading, however, the pre-consolidation stress increases with the stress level, causing irreversible (plastic) volumetric strains.

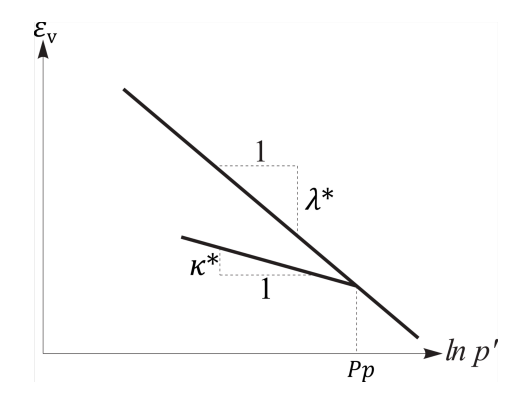


Figure 12–1: Logarithmic relation between volumetric strain and mean stress

12.1.2 Inviscid (time-independent) formulation

The yield function of the inviscid model in triaxial space is expressed by the following equation:

$$f = MD \ln\left(rac{p'}{p_n}
ight) + Drac{ar{q}}{p'}$$
 (12-4)

$$\overline{q} = \sqrt{3} \ \overline{J}_2 \quad and \ \overline{J}_2 = \frac{1}{2} \left(\overline{s}_{xx}^2 + \overline{s}_{yy}^2 + \overline{s}_{zz}^2 \right) + \overline{s}_{xy}^2 + \overline{s}_{yz}^2 + \overline{s}_{zx}^2$$
 (12–5)

where

MCritical state frictional parameter.

DCoefficient of dilatancy.

p'Mean effective stress.

 p_p = Isotropic hardening stress parameter.

 \overline{q} Relative deviatoric stress

 \overline{s} $s-p~\eta_c~$ where g and η_c are defined as follows:

$$s = egin{bmatrix} \sigma_{xx} - p \ \sigma_{yy} - p \ \sigma_{zz} - p \ \sigma_{xy} \ \sigma_{yz} \ \sigma_{zx} \end{pmatrix} \ and \ \eta_c = rac{s_c}{p_p} \ (12 ext{-}6)$$

$$\overline{s} = egin{bmatrix} \sigma_{xx} - p - p \eta_{xx} \ \sigma_{yy} - p - p \eta_{yy} \ \sigma_{zz} - p - p \eta_{zz} \ \sigma_{xy} - p \eta_{xy} \ \sigma_{yz} - p \eta_{yz} \ \sigma_{zx} - p \eta_{zx} \end{bmatrix}$$
 (12–7)

The isotropic stress $p=rac{\sigma_{xx}+\sigma_{yy}+\sigma_{zz}}{3}$

 η_c can be calculated by assuming initially normally consolidated:

$$\eta_c^T = \left(-\frac{1 - K_0^{nc}}{2 + 2K_0^{nc}} \quad 2\frac{1 - K_0^{nc}}{2 + 2K_0^{nc}} \quad -\frac{1 - K_0^{nc}}{2 + 2K_0^{nc}} \quad 0 \quad 0 \quad 0 \right) \tag{12-8}$$

It is assumed that the model follows the associted flow rule: q=f

The isotropic hardening stress parameter of the model is defined as:

$$p_p=p_{p0}e^{rac{\left(arepsilon_v^p-arepsilon_{v0}^p
ight)}{MD}}$$
 (12–9)

where

$$MD = \lambda^* - \kappa^*$$

 ε^p_{v0} = Initial plastic volumetric strain

The relative deviatoric stress is defined as:

Hence, the parameter D is an auxiliary parameter implicitly defined as $D = (\lambda^* - \kappa^*)/M$.

12.1.3 Viscid (time-dependent) formulation

The flow function of the visco-plastic (viscid) model is written as:

$$F=lpha^*\ln\!\left(1+rac{\dot{v}_0t}{lpha^*}\!\exp\!\left(rac{f(\sigma)}{lpha^*}
ight)
ight)-arepsilon_v^{vp}=0$$
 (12–10)

where

$$f(\sigma)=MD\lnrac{p'}{p'_0}\,+Drac{\overline{q}}{p'}$$
 (12–11)

The flow function F can be transformed to a function of stress and hardening parameter q as follows:

$$g(\sigma',h)=f(\sigma')-h(arepsilon_v^{vp},t)=0$$
 (12–12)

where the hardening parameter h is defined as:

$$h(arepsilon_v^{vp},t) = lpha^* \ln iggl\{ rac{lpha^*}{\dot{v}_0 t} iggl[\exp iggl(rac{arepsilon_v^{vp}}{lpha^*} iggr) - 1 iggr] iggr\}$$
 (12–13)

The initial time to calculate the hardening parameter h should not be zero, because it is not determined due to 1/t in Eqn. 12-13 (p. 135). To be able to calculate the initial volumetric visco-plastic strain, it is assumed that the hardening parameter h is equal to zero. Hence, the initial visco-plastic volumetric strain can be calculated as follows:

$$h(arepsilon_v^{vp},t) = lpha^* \ln iggl\{ rac{lpha^*}{\dot{v}_0 t} iggl[\exp iggl(rac{arepsilon_v^{vp}}{lpha^*} iggr) - 1 \, iggr] iggr\} = 0$$
 (12–14)

$$arepsilon_{v0}^{vp}=lpha^*\ln\!\left(rac{\dot{v}_0t}{lpha^*}+1
ight)$$
 (12–15)

 $arepsilon_{v0}^{vp}$ is used as the initial visco-plastic volumetric strain to calculate the current visco-plastic volumetric strain.

12.2 Parameters of the Sekiguchi-Ohta model

12.2.1 Model parameters of the inviscid model

Basic parameters for soil stiffness:

λ*	Modified compression index	[-]
К*	Modified swelling index	[-]

Alternative parameters can be used to define soil stiffness:

C_C	Compression index	[-]
C _s	Swelling index or reloading index	[-]
e _{init}	Initial void ratio	[-]

Advanced parameters for soil stiffness:

V _{ur}	Poisson's ratio for unloading-reloading	[-]
K_0^{nc}	Coefficient of lateral stress in normal consolidation	[-]

Parameters for soil strength:

		1
М	Tangent of the critical state line	[-]

12.2.1.1 Modified compression index and modified swelling index (λ^* and κ^*)

These parameters can be obtained from an isotropic compression test including isotropic unloading. When plotting the logarithm of the mean effective stress as a function of the volumetric strain for clay type materials, the plot can be approximated by two straight lines, see Figure 12-2 (p. 136). The slope of the primary loading line gives the modified compression index λ^* , and the slope of the unloading (or swelling) line gives the modified swelling index κ^* .

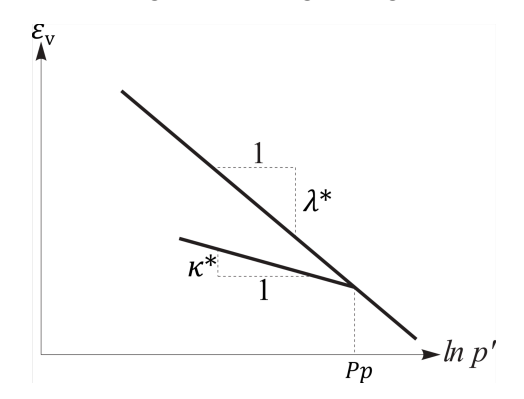


Figure 12-2: Logarithmic relation between volumetric strain and mean stress

12.2.1.2 Poisson's ratio (v_{ur})

The poisson's ratio v_{ur} is a real elastic parameter and not a pseudo-elasticity constant as used in the Mohr-Coulomb model. Its value will usually be in the range between 0.1 and 0.2.

12.2.1.3 Earth pressure coefficient at rest (K_0^{nc})

The K_0^{nc} parameter is defined as the stress ratio in one-dimensional compression in a state of normal consolidation:

$$K_0^{nc} = rac{\sigma'_{xx}}{\sigma'_{yy}}$$

The K_0^{nc} -parameter determines the singular point in the Sekiguchi-Ohta model yield contour. Hence, $K_0^{\dot{n}c}$ relates to the inclination of the stress path in one-dimensional compression where α , as described in the Eqn. 12–16 (p. 136) is the slope of the K_0 in the p - q plane.

$$lpha = rac{3ig(1-K_0^{nc}ig)}{1+2K_0^{nc}}$$
 (12–16)

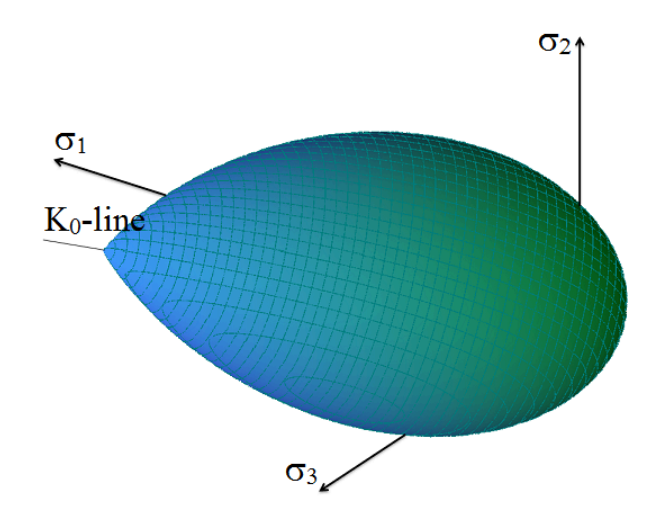


Figure 12-3: The Sekiguchi-Ohta model yield surface in principal stress space

12.2.1.4 Slope of the critical state line (M)

In order to obtain the correct shear strength, the parameter M should be based on the friction angle φ . The critical state line is comparable with the Drucker-Prager failure criteria, and represents a (circular) cone in the principal stress space. Hence, the value of M can be obtained from φ in a similar way as the Drucker-Prager friction constant α is obtained from φ . For details see also the 8 Modified Cam-Clay model (p. 93).

12.2.1.5 Initial overconsolidation ratio (OCR₀)

The initial overconsolidation ratio OCR₀ is defined as the highest vertical effective stress experienced in the past, σ'_{p} , divided by the current stress σ'_{vv} . A soil which is currently experiencing its highest stress is said to be normally consolidated and to have an OCR of 1.

12.2.1.6 Initial pre-overburden pressure (POP_0)

The initial pre-overburden pressure POP_{O_t} expressed in the unit of stress, is defined as:

$$POP_0 = \sigma_p' - \sigma_{yy}'$$

 σ'_p vertical pre-consolidation stress (the greatest vertical stress reached previously)

In-situ effective vertical stress.

12.2.2 Model parameters of the viscid model

Compared to the inviscid Sekiguchi-Ohta model, the viscid Sekiguchi-Ohta model requires the coefficient of secondary compression α^* and the initial volumetric strain rate \dot{v}_0 as two additional parameters of input. All other parameters remain the same as in the inviscid Sekiguchi-Ohta model.

• Basic parameters for soil stiffness:

λ*	Modified compression index	[-]
----	----------------------------	-----

κ*	Modified swelling index	[-]
α*	Coefficient of secondary compression	[-]
\dot{v}_0	Initial volumetric strain rate	[day ⁻¹]

Alternative parameters can be used to define soil stiffness:

C _C	Compression index	[-]
C_{s}	Swelling index or reloading index	[-]
C_{lpha^*}	Secondary compression index	[-]
e _{init}	Initial void ratio	[-]

Parameters for soil strength:

М	Tangent of the critical state line	[-]
---	------------------------------------	-----

Advanced parameters for soil stiffness:

V _{ur}	Poisson's ratio for unloading-reloading	[-]
K_0^{nc}	Coefficient of lateral stress in normal consolidation	[-]

12.2.2.1 Coefficient of secondary compression (α^*)

The coefficient of secondary compression α^* is defined as:

$$lpha^* = rac{darepsilon_v}{d(\ln t)}$$
 (12–17)

at time t_c (the end of primary consolidation).

12.2.2.2 Initial volumetric strain rate (\dot{v}_0)

The initial volumetric strain rate \dot{v}_0 at reference state is expressed as:

$$\dot{v}_0 = \frac{\alpha^*}{t_c} \tag{12-18}$$

12.3 | State parameters in the Sekiguchi-Ohta model

In addition to the output of standard stress and strain, the Sekiguchi-Ohta model provides output (when being used) on state variables such as the isotropic pre-consolidation stress p_p and the isotropic overconsolidation ration OCR. These parameters can be visualised by selecting from the Stresses menu in the State parameters option. An overview of available state parameters is given below:

Peq	Equivalent isotropic stress $P_{eq} = rac{p'}{\exp\left(-rac{ ilde{q}}{Mp'} ight)}$	[kN/m ²]
pp	Isotropic preconsolidation stress	[kN/m ²]
OCR	Isotropic over-consolidation ratio $(OCR = p^p/p^{eq})$	[-]

The UDCAM-S model [ADV]

For the design of offshore structures under a design storm (i.e. a combination of wave, wind and current loading), the stiffness and the bearing capacity of the foundation have to be calculated accounting for the effect of cyclic loading. The response of saturated soils under cyclic loading is different from the case of the static loading. It may be increased due to strain rate effects and reduced due to the degradation process, pore pressure build-up and destructuration.

The soil strength in static undrained conditions can be described by the undrained shear strength of the soil s_u , which is dependent on the effective stress level, stress path and the material. However, by cyclic loading of the soil, the soil strength depends in addition on the value of the combination of the average and cyclic stresses in the soil. The shear strength is therefore written as $\tau_{f,cy}$ instead of the static undrained shear strength s_u . The undrained cyclic shear strength is described by Andersen, Kleven & Heien (1988), as:

$$au_{f,cy} = (au_a + au_{cy})_f$$
 (13–1)

where

 τ_a = Average shear stress at failure.

 $\tau_{f,cy}$ = The cyclic undrained shear strength.

The two aforementioned stress components are shown in Figure 13–1 (p. 141) (Andersen & Jostad, 2009), where the process of excess pore pressure build-up in cyclic loading is depicted. The shear stress, the pore pressure and the shear strain are divided into two components: the average component and the cyclic component. In a cyclic triaxial test the stress is varying with the cyclic shear stress τ_{cy} with respect to the average shear stress τ_a . The effective stress decreases due to the increase in pore pressure and the stress paths move to the left, generally defined as either 15% average shear strain or 15% cyclic shear strain. After a certain number of

cycles N the soil reaches a failure strength. The same soil can thus fail at a lower shear stress in cyclic loading than in monotonic loading.

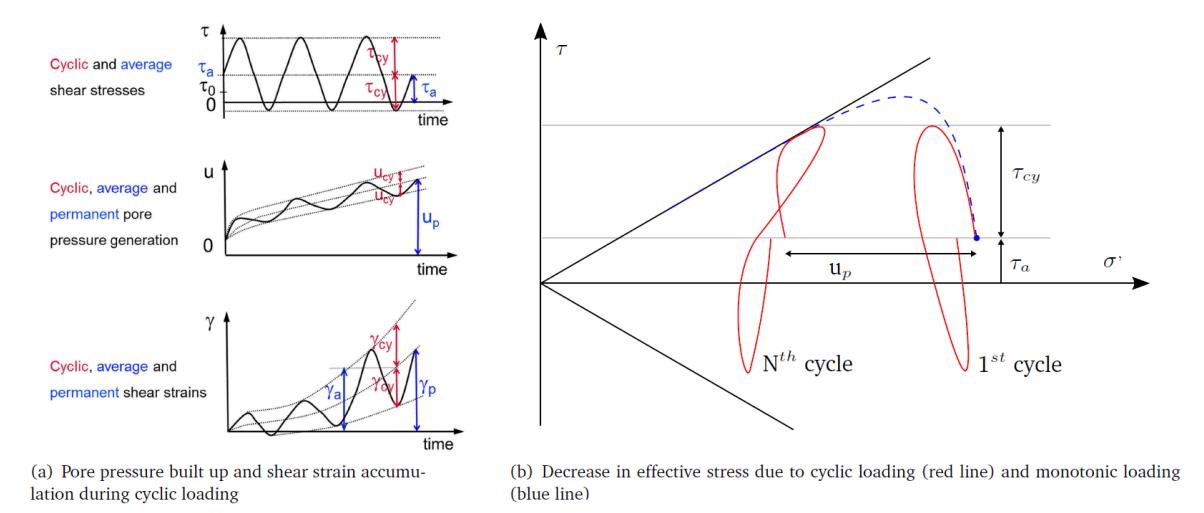


Figure 13-1: Generation of pore pressures and strains in a cyclic triaxial test

Stress anisotropy (or stress path dependent behaviour) is an important aspect regarding the stability of a system. This means that the stress state is varying in the soil, and thus have to be accounted for. As shown in Figure 13-2 (p. 141) (Andersen, 2015), the soil behaviour along a potential failure surface, indicated by the dashed line, can be interpolated between by three undrained cyclic laboratory tests:

- Direct Simple Shear test (DSS).
 - Symmetric loading ($\tau_a = 0$).
 - ° Asymmetric loading ($\tau_a \neq 0$).
- Anisotropically consolidated Triaxial Compression test (TXC).
- Anisotropically consolidated Triaxial Extension test (TXE).

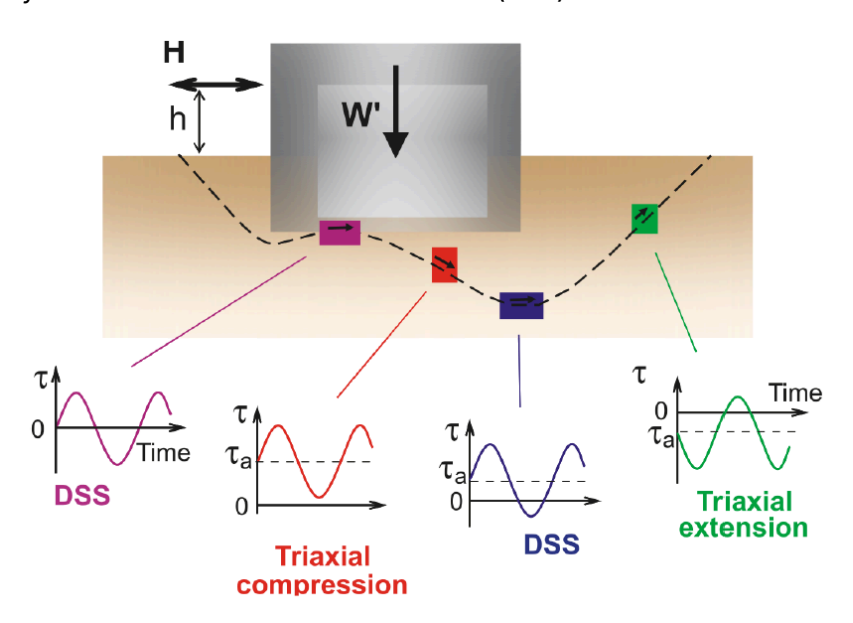


Figure 13-2: Ideal stress conditions along a potential failure surface in the soil beneath a gravity base structure under cyclic loading

The Simplified UnDrained Cyclic Accumulation Model (UDCAM-S) is an advanced model to deal with undrained soil behaviour and degradation of the strength and stiffness in cyclic loading of clay or low permeable silty soils. The UDCAM-S model is derived from the UDCAM model by NGI (Andresen & Jostad, 2009) with simplifications in order to be more suitable for engineering practice. The material model is based on the NGI-ADP model (Andresen & Jostad, 1999) for the undrained behavior of clays, implementing a pre-processing procedure called cyclic accumulation tool (Reference Manual - Chapter 6 - Cyclic accumulation and optimisation tool) to obtain the adjusted parameter set based on the type of analysis the user has to perform:

- Cyclic: to calculate cyclic displacements or stiffness to be used in dynamics analysis of the structure.
- Average: to calculate accumulated (permanent) displacements of the foundation.
- Total: to calculate total (average + cyclic) displacements, capacity or stiffnesses to be used in pseudo-static analysis of the structure.

Except from the calculation of the degraded parameter set with the cyclic accumulation tool, the UDCAM-S model inherits the same formulation and implementation of the NGI-ADP model. For more information about the formulation of the NGI-ADP model, reference is made to Chapter 9.

13.1 Parameters of the UDCAM-S model

The UDCAM-S model requires a total of ten parameters.

The actual components can be cyclic, average or total (average + cyclic):

• Parameters for stiffness:

G_{max}/ au^C	Ratio unloading/reloading shear modulus over (plane strain) active shear strength	[-]
Υ _f ^C	Shear strain in triaxial compression	[%]
Y _f ^E	Shear strain at failure in triaxial extension	[%]
V_f DSS	Shear strain at failure in direct simple shear	[%]

Parameters for strength:

$ au_{ref}^{C}$	Degraded reference shear strength in triaxial compression	[kN/m ²]
y_{ref}	Reference level	[m]
$ au_{inc}^{C}$	Increase of degraded triaxial compression shear strength with depth	[kN/m²/m]
τ ^E /τ ^C	Ratio of degraded triaxial compression shear strength triaxial extension over degraded triaxial compression shear strength	[-]
τ ₀ /τ ^C	Initial mobilisation	[-]
τ ^{DSS} /τ ^C	Ratio of degraded direct simple shear strength over degraded triaxial compression shear strength	[-]

Advanced parameters:

13.1.1 Ratio of the initial shear modulus to the degraded TXC shear strength (G_{max}/ au^C)

Ratio of the initial shear modulus to the degraded shear strength at failure in the triaxial compression test. If the shear strength is increasing with depth the constant ratio for G_{max}/ au^C gives a shear stiffness increasing linearly with depth.

13.1.2 Shear strain at failure in triaxial compression (γ_f^C)

This parameter γ_f^C (%) defines the shear strain at which failure is obtained in undrained triaxial compression mode of loading.

13.1.3 Shear strain at failure in triaxial extension (γ_f^E)

This parameter γ_f^E (%) defines the shear strain at which failure is obtained in undrained triaxial extension mode of loading.

13.1.4 Shear strain at failure in direct simple shear (γ_f^{DSS})

This parameter γ_f^{DSS} (%) defines the shear strain at which failure is obtained in undrained simple shear mode of loading.

13.1.5 Reference degraded TXC shear strength (au_{ref}^C)

The reference degraded TxC shear strength at failure in the triaxial compression test is the shear strength obtained in triaxial compression stress paths at the reference depth y_{ref} , expressed in the unit of stress.

13.1.6 Reference depth (Yref)

This is the reference depth y_{ref} at which the reference TXC shear strength τ^C is defined. Below this depth the shear strength and stiffness may increase linearly with increasing depth. Above the reference depth the shear strength is equal to au_{ref}^C .

13.1.7 Increase of degraded TXC shear strength with depth (τ_{inc}^{C})

The parameter au^C_{inc} defines the increase (positive) or decrease (negative) of the undrained TXC shear strength with depth, expressed in the unit of stress per unit of depth. Above the reference depth the shear strength is equal to au_{ref}^C , below the reference depth the shear strength is defined as:

$$au^C(y) = au^C_{ref} + \left(y_{ref} - y\right) au^C_{inc}$$
 (13–2)

13.1.8 Ratio of the degraded TXE shear strength to the undrained TXC shear strength (au^E/ au^C)

The ratio τ^E/τ^C defines the degraded undrained shear strength for triaxial extension mode of loading in relation to the degraded undrained shear strength in triaxial compression mode of

loading. Please note that active / passive strength input is defined for plane strain conditions. However, it is generally acceptable and only slightly conservative to use the strength obtained from a triaxial compression test as input for the active plane strain condition (i.e. $\tau_C^A = \tau^C$) and the strength obtained from a triaxial extension test as input for the passive plane strain condition (i.e. $\tau^P = \tau^E$).

13.1.9 Ratio of the degraded DSS shear strength to the undrained TXC shear strength (au^{DSS}/ au^c)

The ratio au^{DSS}/ au^c defines the degraded undrained shear strength in direct simple shear mode of loading in relation to the degraded undrained shear strength in triaxial compression mode of loading.

13.1.10 | Initial mobilization (τ_0/τ^C)

The initial mobilization au_0/ au^C is clearly defined for nearly horizontally deposited normally consolidated or lightly overconsolidated clay layers where the vertical stress is the major principle stress σ'_1 . As defined in Figure 13–3 (p. 144), the initial mobilization can be calculated from the earth pressure coefficient at rest K_0 by the following equation:

$$au_0/ au^C = -0.5(1 - K_0)\sigma_{w0}^{'}/ au^C$$
 (13–3)

where

 σ'_{yyo} = initial (in situ) vertical effective stress (compression negative).

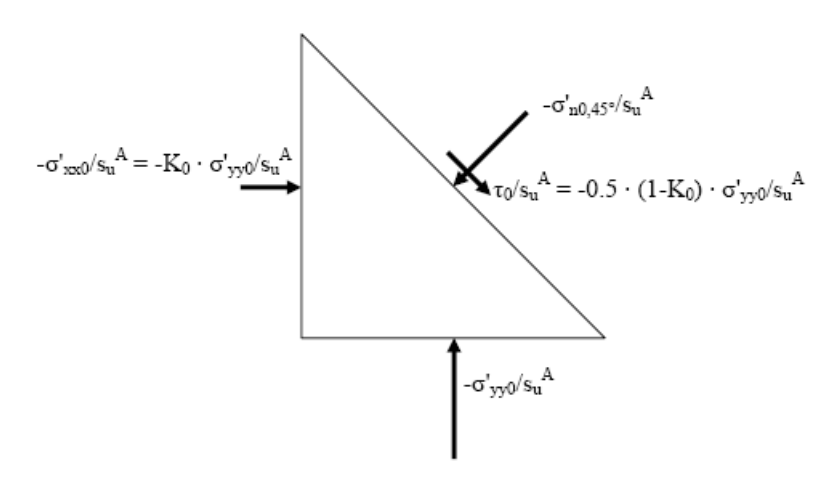


Figure 13–3: Definition of initial mobilised maximum shear stress τ_0 = $1/2 |\sigma'_{yy0} - \sigma'_{xx0}|$ for a soil element in a horizontal deposited layer.

Changing the default value for the initial mobilization should be considered in particular for overconsolidated materials where K_0 generally is higher than 0.6, however the UDCAM-S model (like NGI-ADP model) is not intended used for heavily overconsolidated clays and should be used with care for $K_0 > 1.0$ (i.e. negative τ_0/τ^C).

13.1.11 Poisson's ratio (ν')

Only Undrained (C) drainage option as a pure total stress analysis is carried out where no distinction between effective stresses and pore pressures is made and all stress changes should be considered as changes in total stress. A Poisson's ratio of v = 0.495 should be used for the calculation.

13.2 | State parameters in the UDCAM-S model

Υp	Plastic shear strain	[-]
r_{κ}	Hardening function	[-]

$$r_{\kappa}=2rac{\sqrt{\gamma^{p}/\gamma_{f}^{p}}}{1+\gamma^{p}/\gamma_{f}^{p}}$$
 (13–4)

13.3 On the use of the UDCAM-S model in dynamics calculations

The model should not be used in dynamics calculations.

The Concrete model [ADV]

Generally, for concrete structure elements, a linear elastic material model is adopted due to their strength compared to the one of the soil. However, in some kind of geotechnical problems, the complex non-linear behaviour of the concrete structures must be inspected for a reliable redistribution of stress-strain in the continuum and a correct design. Distinction can be made between the main features of the complex concrete behaviour: limited strength in compression and tension, time-dependent strength and stiffness, strain hardening/softening, creep and shrinkage.

The Concrete model was originally developed to model the behaviour of shotcrete, but it is also useful for soil reinforcement (e.g. concrete columns), soil improvements (e.g. jet grouting columns) and concrete structures (e.g. beams). The current engineering approach to model shotcrete linings in numerical simulations assumes a linear elastic material with a stepwise increase of the (artificially low) Young's modulus in subsequent excavation stages. While realistic lining deformations may be obtained with this method, lining stresses are usually too high, in particular if the lining is subjected to significant bending. With the Concrete model more realistic stress distributions can be obtained, as the non-linearity of the material behaviour is taken into account. Furthermore, the stability of the tunnel can be checked at all intermediate stages without the need for additional capacity checks of the lining cross section.

The Concrete model is an elastoplastic model for simulating the time-dependent strength and stiffness of concrete, strain hardening-softening in compression and tension as well as creep and shrinkage (Schadlich & Schweiger, 2014). Hence, differently from what is seen in Eqn. 3–1 (p. 32) , the total strain ε is not only decomposed into elastic strain ε^e and plastic strain ε^p but also considers creep strain ε^{cr} and shrinkage strain ε^{shr} :

$$\underline{\varepsilon} = \underline{\varepsilon}^e + \underline{\varepsilon}^p + \underline{\varepsilon}^{cr} + \underline{\varepsilon}^{shr} \tag{14-1}$$

When subjected to deviatoric loading, concrete shows different behaviours: in compression, the strength increases non-linearly up to a peak value and then softens to a residual one; in

tension, it's considered linear elastic until reaching the tensile strength and then softens to the residual value. The Concrete model employs a Mohr-Coulomb yield surface for deviatoric loading, combined with a Rankine yield surface in the tensile regime.

Most of the input parameters for the Concrete model can be derived from standard uniaxial tension and compression tests. Some basic characteristics of the Concrete model and their relevant input parameters are:

Limited strength in compression and tension.	f _{c,28} , f _{t,28}
Time-dependent strength and stiffness.	$f_{c,1}/f_{c,28}$, E_1/E_{28} , ε^p_{cp} , t_{hydr}
Strain hardening in compression	f_{cOn}
Strain softening in compression and tension	f_{cfn} , f_{cun} , $G_{c,28}$, f_{tun} , $G_{t,28}$
Stress- and stiffness-dependent creep strains	$oldsymbol{arphi}^{ extsf{cr}}$, t_{50}^{cr}
Stress-independent shrinkage strains	$arepsilon_{50}^{shr}$, t_{50}^{shr}

The stress-strain approach for hardening and softening is proposed by Schütz, Potts & Zdravkovi'c (2011), involving mobilised compression and tensile strength through the uniaxial plastic peak strain ε_p^{cp} at 1h, 8h, 24h and the fracture energy of the material both in compression, G_c , and in tension, G_t . Furthermore, thanks to the time-dependent internal laws of the Concrete model for f_c , f_t , G_c and G_t , the hardening-softening of the yield surfaces completely follows the evolution of the material in time. The time-dependency of elastic stiffness, compressive and tensile strength is taken into account following an approach similar to the recommendation of CEB-FIP model code (1990) as well as EN 14487-1. The ability of young concrete to withstand large deformations at early age, thanks to its initial high plastic ductility, is represented by a time-dependent plastic peak strain ε_{cp}^p (Meschke, Kropik & Mang, 1996).

14.1 Formulation of the Concrete model

The Concrete model employs a composite yield surface; Mohr-Coulomb surface for deviatoric loading and Rankine surface in the tensile regime with isotropic compression softening (Figure 14-1 (p. 148)). In the Concrete model formulation, the yield function is named with capital F in order to distinguish it from the yield stress f. The sign convention is strictly tension-positive and σ_1 is the major (tensile) principle stress and σ_3 is the minor (compressive) principle stress.

The yield functions can be formulated in terms of principal stresses in relation to the uniaxial compressive and tensile yield stresses, f_{cv} and f_{tr} as:

$$F_c = rac{\sigma_1 - \sigma_3}{2} + rac{\sigma_1 + \sigma_3 - 2\,\sigma_{rot}}{2}\,rac{f_{cy}}{2\,\sigma_{rot} + f_{cy}}$$
 (14–2)

$$F_t = \sigma_1 - f_t \tag{14-3}$$

where

Intersection of the Mohr-Coulomb failure envelope and the isotropic axis.

For a given maximum inclination of the Mohr-Coulomb envelope, σ_{rot} can be written as:

$$\sigma_{rot} = rac{f_c}{2} \left(rac{1}{sin(arphi_{max})} - 1
ight)$$
 (14–4)

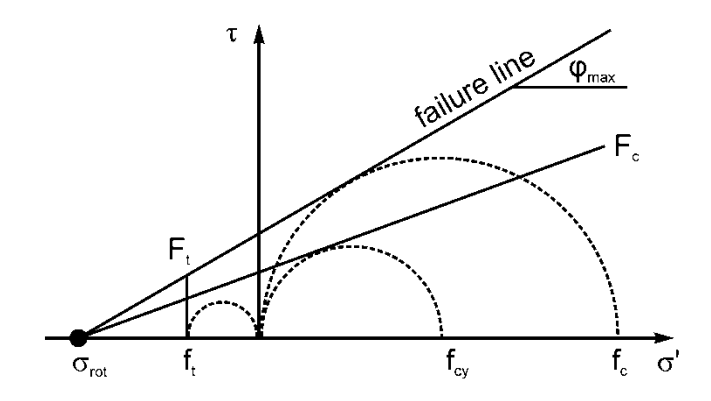


Figure 14-1: Yield surfaces and failure envelope for Concrete model

14.2 Strain hardening and softening

14.2.1 | Compression

In compression, the Concrete model follows the approach proposed by Schütz, Potts & Zdraykovi'c (2011). The stress-strain curve is divided in four parts (Figure 14-2 (p. 148)):

- Part I quadratic strain hardening
- Part II linear strain softening
- Part III linear strain softening
- Part IV constant residual strength

Due to the time-dependency of the involved material parameters, a normalised hardening/ softening parameter $H_c=\varepsilon_3^p/\varepsilon_{cp}^p$ is used, with ε_3^p = minor plastic strain (calculated from F_c) and ε_{cp}^{p} = plastic peak strain in uniaxial compression.

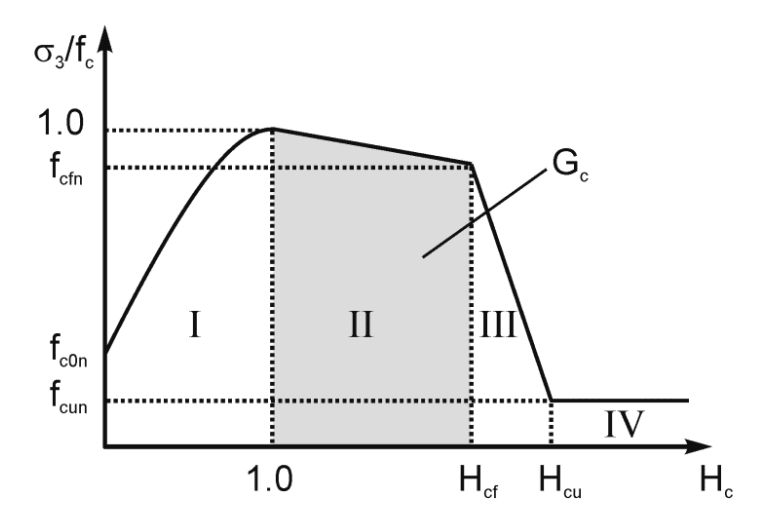


Figure 14-2: Normalised stress-strain curve in compression

In part I, the uniaxial yield stress f_{cy} is mobilised with H_c according to a quadratic function:

$$f_{cy,I} = f_c \left(f_{c0n} + (1 - f_{c0n}) \left(2H_c - H_c^2 \right) \right)$$
 (14–5)

where f_{c0n} is the initial ratio f_{cv}/f_c . During mobilisation the yield surface F_c rotates around the anchor point σ_{rot} on the isotropic axis, activating the shear isotropic hardening.

Full mobilisation of f_c coincides with H_c = 1, after which (i.e. part II) linear softening takes place, until the failure strength f_{cf} = $f_{cfn}f_c$ is reached at $H_{cf}=arepsilon_{cf}^p/arepsilon_{cp}^p$. Strength reduction is assumed to be caused by the destruction of inter-particle bonds, and consequently a parallel shift of the fully mobilised Mohr-Coulomb failure envelope:

$$f_{cy,II} = f_c \left(1 + (f_{cfn} - 1) \left(\frac{H_c - 1}{H_{cf} - 1} \right) \right)$$
 (14-6)

where $arepsilon_{cf}^p$ is derived from the fracture energy in compression, G_{c} , and the characteristic length of the finite element, L_{eq} , which provides the necessary regularisation to avoid mesh dependent numerical results:

$$arepsilon_{cf}^p = arepsilon_{cp}^p - rac{2G_c}{(1+f_{cfn})f_c\,L_{eq}}$$
 (14–7)

 L_{eq} is calculated by PLAXIS from the size of the finite element, A_{el} , and the number of stress points per element n_{GP} , (Polling, 2000):

$$L_{eq} \, = \, 2 \sqrt{rac{A_{el}}{\sqrt{3} \, n_{GP}}}$$
 (14–8)

Note: When using the **SoilTest** with the Concrete Model, since there is no mesh, $L_{eq} = 1$.

In part III the linear strain softening is governed by the condition that the energy in elastic unloading must not be greater than the plastic strain energy absorbed by the crack (no spanback of stress-strain curve on stress point level). That delivers the plastic ultimate strain ε_{cu}^p as:

$$arepsilon_{cu}^p = arepsilon_{cf}^p - rac{2f_c \left(f_{cfn} - f_{cun}
ight)}{E}$$
 (14-9)

with f_{cun} = residual strength level = f_{cu} / f_c and E = elastic Young's modulus. The yield stress F_{cv} follows as:

$$f_{cy,III} = f_c \left(f_{cfn} + (f_{cun} - f_{cfn}) \left(rac{H_c - H_{cf}}{H_{cu} - H_{cf}}
ight)
ight)$$
 (14–10)

where $H_{cu}=arepsilon_{cu}^p/arepsilon_{cp}^p$. In part IV, there is no further softening of the stress-strain curve, which vields:

$$f_{cu,IV} = f_c f_{cun} \tag{14-11}$$

To account for the increasing ductility with increasing confining pressure, the total peak strain $arepsilon_{cp}=arepsilon_{cp}^p+arepsilon_{cp}^e$ increases with the confining pressure, σ_{1} , as in a triaxial compression test, governed by the input parameter a:

$$arepsilon_{cp} = arepsilon_{cp,UC} igg(1 + a \, rac{\sigma_1}{-f_c} igg)$$
 (14–12)

For instance, a = 1 and σ_1 = - f_c yield a 100% increase of total peak strain ε_{cp} compared to the uniaxial compression test. Internally, the increase of ε_{cp} is translated into an increase of ε_{cp}^p which is assumed to be governed by the mean stress $p = (\sigma_1 + \sigma_2 + \sigma_3)/3$ according to:

$$arepsilon_{cp}^p = arepsilon_{cp,UC}^p igg(1 + b \, rac{p + f_c/3}{-f_c}igg)$$
 (14–13)

$$b=rac{2sin(arphi_{max})rac{f_c}{E}+a(1-sin(arphi_{max}))\left(arepsilon_{cp}^p-rac{f_c}{E}
ight)}{arepsilon_{cp}^p\left(1-sin(arphi_{max})/3
ight)}$$
 (14–14)

14.2.2 | Tension

The Concrete model behaviour in tension is linear elastic until the tensile strength f_t is reached, then softens with a linear strain softening (Figure 14-3 (p. 150)). The strain softening is governed by the normalised tension softening parameter $H_t=arepsilon_1^p/arepsilon_{tu}^p$ with $arepsilon_1^p$ = major principal plastic strain (calculated from F_t) and ε_{tu}^p = Plastic ultimate strain in uniaxial tension as:

$$f_{ty} = f_t \left(1 + \left(f_{tun} - 1 \right) H_t \right)$$
 (14–15)

Similar to softening in compression, ε_{tu}^p is derived from the fracture energy in tension, G_t :

$$arepsilon_{tu}^p = rac{2G_t}{(1+f_{tun})f_t L_{eq}}$$
 (14–16)

Once the residual strength $f_{tu} = f_{tun} f_t$ is reached, no further softening takes place.

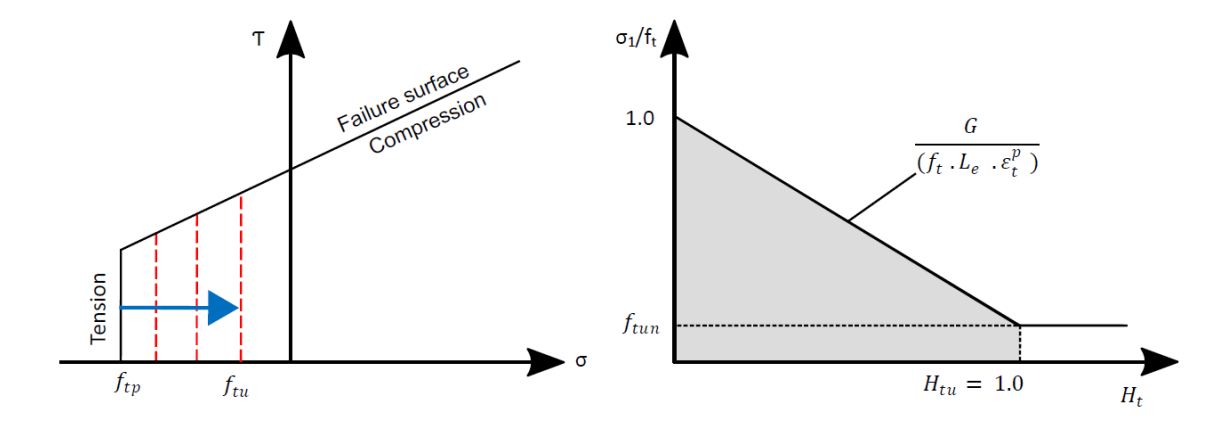


Figure 14-3: Tension softening

14.3 Time-dependency of the Concrete model

14.3.1 Strength and Stiffness

The Concrete model takes into account the time-dependent behaviour of material parameters. The stiffness and strength of concrete increase rapidly with time due to the hydration of the cement paste. The increase of Young's modulus E in the model follows an approach similar to the recommendation of CEB-FIP model code (1990):

$$E(t) = E_{28} \, e^{s_{stiff} \left(1 - \sqrt{t_{hydr}/t}
ight)}$$
 (14–17)

where

 E_{28} Young's modulus of cured concrete.

 t_{hydr} Time until full curing (e.g. usually taken as 28 days).

time (days).

 s_{stiff} Parameter governing stiffness evolution with time.

 s_{stiff} is related to the stiffness ratio at 1 day, E_1/E_{28} , and t_{hydr} , as:

$$s_{stiff} = -rac{ln(E_1/E_{28})}{\sqrt{t_{hudr}/t_{1d}}-1}$$
 (14–18)

where t_{1d} is the duration of one day in the unit time. The Young's modulus is constant for t<1hand for $t>t_{hvdr}$.

For the uniaxial compressive strength f_c , the Concrete model implements two different approaches. The first, as for E, is similar to the recommendation of CEB-FIP model code (1990) for concrete. The relations are the same as before but exchanging s_{stiff} with $s_{strength}$, which depends now on the strength ratio at 1 day, $f_{c,1}/f_{c,28}$, and t_{hvdr} (equations Eqn. 14–19 (p. 151) and Eqn. 14–20 (p. 151)). A lower limit of $f_c = 0.005 f_{c,28}$ is used at very early age. The CEB-FIP type approach yields very low concrete strength at ages <2h.

$$f_c(t) = f_{c,28} \, e^{s_{strength} \left(1 - \sqrt{t_{hydr}/t}
ight)}$$
 (14–19)

$$s_{strength} = -rac{ln(f_{c,1}/f_{c,28})}{\sqrt{t_{hydr}/t_{1d}-1}}$$
 (14–20)

Alternatively, the strength evolution can be modelled in accordance to the shotcrete strength classes J1, J2 and J3 of EN 14497-1, which define ranges of shotcrete strength at different shotcrete ages up to 24h. Mean values of these ranges have been assumed for class J1 and J2 in the Concrete model with class J3 lying 50% above the boundary between classes J2 and J3 (Table 14-1 (p. 151)). Between 24h and t_{hvd}, an approach proposed by Oluokun, Burdette & Deatherage (1991) is adopted:

$$f_c = \alpha_c e^{-b_c/t} \tag{14-21}$$

$$f_c = lpha_c e^{-b_c/t}$$
 (14–21) $lpha_c = rac{f_{c,28}}{e^{ln(\kappa)/(t_{hydr}-t_1d)}} b_c = (-t_{hydr}/(t_{hydr}-t_{1d})) ln(\kappa) \kappa = f_{c,24h}/f_{c,28}$ (14–22)

where f_c is the time-dependent compressive strength and $f_{c,24h}$ is the compressive strength at 24h (Table 14–1 (p. 151)).

Table 14-1: Mean uniaxial compressive strength of J1, J2 and J3 strength classes

Time[hr]	J1[MPa]	J2[MPa]	J3[MPa]
<0.1	0.15	0.35	0.75
0.5	0.23	0.715	1.65
12	2.0	5.5	12.0
24	3.5	12.0	28.5

The ratio of f_t/f_c and the values of f_{cfn} , f_{cun} and f_{tun} are assumed to be constant in curing for both approaches.

14.3.2 Plastic Deformability

The ability of young concrete to withstand large deformations is not only a result of its low elastic modulus at this age, but also due to its high plastic ductility. With concrete aging this ductile behaviour decreases.

In the Concrete model this behaviour is represented by a time-dependent plastic peak strain ε_{cp}^p . Similar to the approach proposed by Meschke, Kropik & Mang (1996), a tri-linear function in time is adopted. Input values are the plastic peak strains at t = 1h, 8h and 24h. Beyond 24h, ε_{cp}^{p} is assumed to be constant (Figure 14-4 (p. 152)).

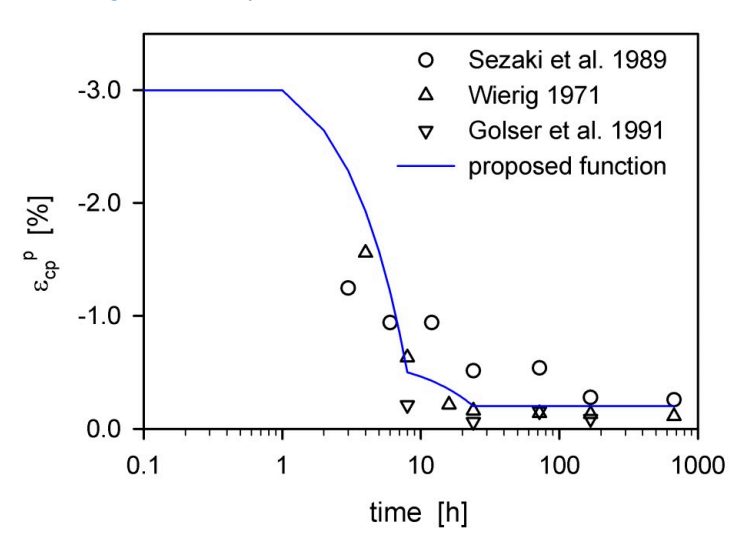


Figure 14–4: Reduction of $arepsilon_{cp}^p$ with aging in the Concrete model compared to experimental data from uniaxial compression tests. The chosen ε_{cv}^p values are -3%, -0.5% and -0.2%.

14.3.3 Fracture energy

The plastic time-dependency during softening is taken into account with the change of fracture energies with time, which is automatically computed by PLAXIS. In tension, the tensile failure strain $arepsilon_{tu}^p$ is derived from the tensile fracture energy and tensile strength of the cured concrete, regardless of the current concrete age. Since the tensile strength f_t increases with time, but ε_{tu}^p remains constant, the current fracture G_t increases proportionally with the increase of f_t .

The plastic failure strain in compression, ε_{cf}^p , is coupled to the plastic peak strain ε_{cp}^p such that the ratio $\varepsilon_{cf}^p/\varepsilon_{cp}^p$ remains constant. As ε_{cp}^p decreases with time (Figure 14–4 (p. 152)), ε_{cf}^p and hence G_c reduce. On the other hand, the compressive strength f_c increases with time, which results in higher values of G_c . The influence of these counteracting trends brings high values of the fracture energy at early age, a sharp drop at \approx 12h and a linear increase of G_c with f_c afterward (Figure 14-5 (p. 153)). The high fracture energy at very early age is a consequence of the desired ductile behaviour at this stage. As very young concrete effectively does not fail at all in compression, the fracture energy theoretically should be infinite.

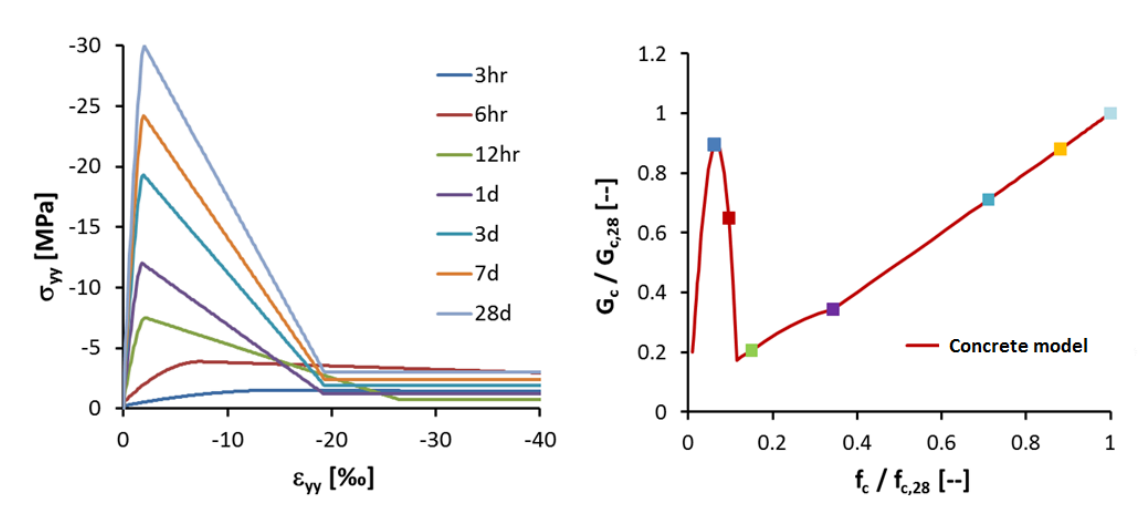


Figure 14-5: Stress-strain curves in uniaxial compression at different ages and development of compressive fracture energy with compressive strength

14.3.4 Viscoelastic Creep

The Concrete model employs a viscoelastic approach for creep. Creep strains, $arepsilon^{cr}$, increase linearly with stress σ and are related to elastic strains via the creep factor φ^{cr} :

$$arepsilon^{cr}(t) = rac{arphi^{cr}\,\sigma}{oldsymbol{D}^e}\,rac{t-t_0}{t+t_{50}^{cr}}$$
 (14–23)

The evolution of creep with time t is governed by the start of loading at time t_0 and the parameter t_{50}^{cr} . For instantaneous loading (t_0 = 0), t_{50}^{cr} equals the time until 50% of the creep strains have evolved. For concrete utilization higher than 45% of f_c , non-linear creep effects are accounted for by replacing φ^{cr} with the following equation from Eurocode 2:

$$\varphi_k^{cr} = \varphi^{cr} e^{1.5(k_\sigma - 0.45)}$$
 (14–24)

with $k_{\sigma} = \sigma_c / f_{cm}$ being the degree of concrete utilisation in compression. Due to the timedependency of the linear elastic stiffness matrix D^e , the creep history is stored as normalised values of $\varepsilon^{cr}(t) \cdot E(t)$.

Note:

The creep history is adjusted for the stress state at first activation of the concrete cluster, such that no creep strains are produced by initial stresses. The state variables are taken over if the previous material was also defined with the Concrete model, in which case creep will also continue. If a reset of state variables is desired, a nil step with a different material (e.g. linear elastic) is required.

14.3.5 | Shrinkage

The Concrete model refers to shrinkage as the isotropic loss of volume with time, which is independent of the stress state. Shrinkage strains ε^{shr} are calculated according to the recommendation of ACI (1992) as:

$$arepsilon^{shr}(t) = arepsilon_{\infty}^{shr} rac{t}{t + t_{50}^{shr}}$$
 (14–25)

with $arepsilon_{\infty}^{shr}$ being the final axial shrinkage strain and t_{50}^{shr} the time when 50% of shrinkage has occurred.

14.4 Parameters of the Concrete model

The Concrete model involves a number of parameters which are generally familiar to structural engineers. These parameters with their standard units are listed below.

• Parameters for stiffness:

E ₂₈	Young's modulus of cured concrete at t _{hydr}	[kN/m ²]
ν	Poisson's ratio	[-]

• Parameters for strength:

Compression parameters				
f _{c,28}	Uniaxial compressive strength of cured concrete at t_{hydr}	[kN/m ²]		
f _{cOn}	Normalised failure strength	[-]		
f_{cfn}	Normalised initially mobilised strength	[-]		
f_{cun}	Normalised residual strength	[-]		
G _{c,28}	Compressive fracture energy of cured concrete at $t_{\it hydr}$	[kN/m]		
$arphi_{max}$	Maximum friction angle	[°]		
Ψ	Dilatancy angle	[°]		
Y _{fc}	Safety factor for compressive strength	[-]		

Tension parameters				
f _{t,28}	Uniaxial tensile strength of cured concrete at t_{hydr}	[kN/m ²]		
$f_{ m tun}$	Ratio of residual vs. peak tensile strength	[-]		
G _{t,28}	Tensile fracture energy of cured concrete at t_{hydr}	[kN/m]		
V _{ft}	Safety factor for tensile strength	[-]		

• Parameters for ductility:

$arepsilon_{cp}^p$	Uniaxial plastic failure strain	
а	Increase $arepsilon_{cp}$ with increase of p	[-]

Time-dependent parameters:

t _{hydr}	Time for full hydration	[day]	
Stiffness paramete	ers		

E ₁ / E ₂₈	Time-dependency ratio of elastic stiffness	[-]			
Strength paramete	Strength parameters				
$f_{c,1}/f_{c,28}$	Time-dependency of compressive strength	[-]			
Ductility					
$arepsilon_{cp,1h}^p$	Uniaxial plastic failure strain at 1h (negative value)	[-]			
$arepsilon_{cp,8h}^p$	Uniaxial plastic failure strain at 8h (negative value)	[-]			
$arepsilon_{cp,24h}^p$					
Shrinkage	Shrinkage				
$arepsilon_{\infty}^{shr}$	Final shrinkage strain (negative value)	[-]			
t_{50}^{shr}	Time for 50% of shrinkage strains	[day]			
Creep					
ϕ^{cr}	Ratio between creep and elastic strains	[-]			
t^{cr}_{50}	Time for 50% of creep strains	[day]			

The Concrete model allows two drainage types: non-porous, which is the general approach for concrete structural elements, and drained, in case of semi-permeable walls or tunnel linings.

14.4.1 Recommended values for the parameters of the Concrete model

14.4.1.1 Elastic parameters

Differently from the Mohr-Coulomb model, the Concrete model employs time-dependent stiffness. If Time dependent strength and stiffness is turned off then the editing of E_1/E_{28} is disabled and it's set to 1. If Time dependent strength and stiffness is turned on, a E_1/E_{28} is defined, generally a range of 0.5 - 0.7 is recommended with E_{28} between 25 GPa and 30 GPa.

14.4.1.2 Strength in compression

The uniaxial compressive strength of cured concrete $f_{c,28}$ can be derived from uniaxial compressive test results. The time-dependency of compressive strength expressed as $f_{c,1}/f_{c,28}$ is recommended in the range of 0.2-0.3 for cast concrete, whilst it depends on the strength class (i.e. J1, J2 and J3) for shotcrete. The stress-strain curve in compression (Figure 14-2 (p. 148)) is defined through the normalised strength values. The normalised mobilised strength f_{c0n} contributes to the part I hardening, a value in the range of 0.1 - 0.25 is recommended. The normalised failure strength f_{cfn} rules the part II softening, a value of 0.1 is recommended. The normalised residual strength f_{cun} rules the part III softening and the residual strength, a value of 0.1 is recommended. f_{cfn} must be greater or almost equal to f_{cun} in order to avoid input error. f_{cfn} or f_{cun} = 1 implies no softening in the respective regions.

14.4.1.3 Time-dependency of compressive strength

The uniaxial compressive strength is defined at the time t_{hvdr} , time for full hydration (usually 28 days). If Time dependent strength and stiffness is turned off then $f_{c,1}/f_{c,28}$ is set automatically equal to 1 and the editing is disabled. If Time dependent behaviour is turned on, then the user can choose in the combo box Strength functions among:

- CEB-FIP model code (1990): the user can define $f_{c,1}/f_{c,28}$. The default value = 1 corresponds to no time-dependency. For cast concrete a value of [0.2, 0.3] is recommended.
- Shotcrete strength class J1: $f_{c,1}/f_{c,28}$ is automatically computed in accordance with the selected strength class (Table 14-1 (p. 151)).
- Shotcrete strength class J3: $f_{c,1}/f_{c,28}$ is automatically computed in accordance with the selected strength class (Table 14-1 (p. 151)).

14.4.1.4 Strength in tension

The tensile strength $f_{t,28}$ can in principle be derived from uniaxial tensile test results. Due to the experimental difficulties involved in these tests, however, indirect tests or direct correlations with the compressive strength are more common. Both for concrete and shotcrete, a value of $f_{t,28}$ = $0.1f_c$ is recommended. The ratio of residual vs. peak tensile strength f_{tun} is recommended to be 0.



Note:

In shotcrete linings the tensile strength is essential for tunnel stability. Neglecting or considering low values of it could result in unrealistic failure.

14.4.1.5 Parameters ϕ_{max} , ψ and a

Determination of φ_{max} , ψ and a requires triaxial tests on cured concrete. The impact of these parameters in typical tunnelling calculations, however, is small, as at least one of the major principal stresses in the lining is close to 0. Furthermore, not all of these will be typically available, so values in the range of 35°- 43°, 0°- 10° and 16 - 20 are respectively suggested for φ_{max} , ψ and a.

14.4.1.6 Fracture energy

The compressive fracture energy of cured concrete $G_{c,28}$ can be estimated from the stressstrain curve of uniaxial compression tests. However a value in the range of 30kN/m - 70kN/m is recommended. The tensile fracture energy of cured concrete $G_{t,28}$ can be estimated from the stress-strain curve of uniaxial tensile tests. Due to the experimental difficulties involved in these tests, the fracture energy can be estimated as following. For plain shotcrete, a value in the range of 0.05kN/m - 0.15kN/m is recommended. However, the shotcrete can be reinforced using steel fibres, in this case $G_{t,28}$ can be estimated with the correlation proposed by Barros & Figueiras (1999):

$$G_{t,28} = \left(1 + 13.159W_f^{1.827}\right)G_{t0}$$
 (14–26)

where

 G_{to} = The fracture energy of plain shotcrete W_t fibre percentage in weight [kg/m³]

For plain concrete, the value is strictly dependent on the strength class and the maximum aggregate size d_{max} (Table 14–2 (p. 157), CEB-FIP model code (1990)).

Table 14-2: Fracture energy G_{t.28} for plain concrete

d _{max} (mm)	G _{t,28} (N/m)							
-max(·····)	C12	C20	C30	C40	C50	C60	C70	C80
8	26.91	34.06	42.18	49.67	56.71	63.39	69.78	75.93
16	32.30	40.87	50.61	59.61	68.05	76.07	83.73	91.11
32	62.44	79.02	97.86	115.24	131.56	147.06	161.88	176.15

14.4.1.7 **Ductility**

If Time dependent behaviour is turned off then a single peak parameter ε_{cp}^p is available instead of $arepsilon_{cp,1h}^p$, $\overset{\cdot}{arepsilon_{cp,8h}^p}$ and $arepsilon_{cp,24h}^p$ and no-dependency of ductility in time is considered. If *Time* dependent behaviour is turned on, then the user can define $\varepsilon^p_{cp,1h}$, $\varepsilon^p_{cp,8h}$ and $\varepsilon^p_{cp,24h}$. Values in the range of -0.03 to -0.01, -0.0015 to -0.001 and -0.0012 to -0.0007 are respectively suggested for $\varepsilon_{cp,1h}^p$, $\varepsilon_{cp,8h}^p$ and $\varepsilon_{cp,24h}^p$.

14.4.1.8 Creep

Creep properties of concrete can be derived from uniaxial multistage creep tests. Deriving creep properties from such a test requires additional information about strength, stiffness and ductility development with time. The user can follow the recommendation of Eurocode 2 for cast concrete, instead values in the range of 2 - 3 for φ_{cr} are suggested for shotcrete tunnel linings. t_{50}^{cr} is recommended in a range of 1d - 5d. If *Creep behaviour* is inactive, φ_{cr} and t_{50}^{cr} are disabled for editing and both set to 0. If *Creep behaviour* is active, the parameters can be defined.

14.4.1.9 | Shrinkage

Concrete shrinkage is strongly influenced by environmental conditions and water-cement-ratio, such that low air humidity and high water-cement ratios amplify it. Due to less aggregate content and higher water-cement ratio, shrinkage of shotcrete is more pronounced than for conventional cast concrete (Austin & Robins, 1995). If Shrinkage behaviour is inactive, $\varepsilon_{\infty}^{shr}$ and t_{50}^{shr} are disabled. If Shrinkage behaviour is active, the user can set the parameters.

Eurocode 2 recommends final shrinkage strains, $\varepsilon_{\infty}^{shr}$, for cast concrete of -0.0002 to -0.0006 depending on air humidity, concrete class and the effective size of the structural element. For tunnel linings values in the range of -0.0015 to -0.0005 for $arepsilon_{\infty}^{shr}$ and of 28d - 100d for t_{50}^{shr} are suggested.

14.4.1.10 Safety factors

To facilitate calculations based on design values of concrete strength, the Concrete model implements the possibility to use separate safety factors γ_{fc} and γ_{ft} for compressive and tensile strength. In fact PLAXIS design approach is not advisable for these two parameters, because:

- In case the user defines the time-dependency of strength through the classes J1, J2 and J3, the shotcrete strength values at 0.5h, 12h and 24h are not related to $f_{c,28}$. Using a lower value of $f_{c,28}$ therefore does not affect the shotcrete strength at early age, if the early strength
- If lower concrete strength is used due to safety considerations, also the fracture energy should be reduced to obtain similar stress-strain curves.
- The creep factor increases for concrete utilisation $>0.45 f_c$. Using design values for f_c would therefore overestimate creep effects.

For these reasons input safety factors γ_{fc} and γ_{ft} have been introduced. The characteristic, timedependent compressive and tensile strengths f_c and f_t as well as the corresponding fracture energies G_c and G_t , are divided by γ_{fc} and γ_{ft} in each calculation step, but concrete utilization always refers to the characteristic values of f_c and f_t .

14.4.2 | Summary of recommended parameters for **Concrete model**

Table 14-3 (p. 158) groups the Concrete model parameters as a function of the material properties and the time dependency.

Table 14-3: Recommended parameters and values for the Concrete model

Parameter	Recommended values	Unit				
1. Stiffness parameters (non-time dependent)						
E ₂₈	[25, 30]	[GPa]				
ν	[0.15, 0.25]	[-]				
2. Strength parameters						
Strength in compression						
f _{c,28}	Depending on strength class	[kN/m ²]				
f _{cOn}	[0.10, 0.25]	[-]				
f_{cfn}	[0.1]	[-]				
f_{cun}	[0.1]	[-]				
G _{c,28}	[30, 70]	[kN/m]				
ϕ_{max}	[35, 43]	[°]				
Ψ	[0, 10]	[°]				
V _f c	Safety factor depending on design standard	[-]				
Strength in tension						
f _{t,28}	Depending on strength class	[kN/m ²]				
f _{tun}	[0]	-				

Parameter	Recommended values	Unit
G _{t,28}	[0.05, 0.15] plain shotcrete, [Table 14–2 (p. 157)] cast concrete	[kN/m]
Y _{ft}	Safety factor depending on design standard	[-]
Ductility		
$arepsilon_{cp}^p$		[-]
а	[16, 20]	[-]
3. Time dependent parameter	rs	
t _{hydr}	[28]	[day]
Stiffness		
E ₁ /E ₂₈	[0.5, 0.7]	[-]
Strength		
f _{c,1} /f _{c,28}	[J1, J2, J3] shotcrete, [0.2, 0.3] cast concrete	[-]
Ductility		
$arepsilon_{cp,1h}^p$	[-0.01, -0.03]	[-]
$arepsilon_{cp,8h}^p$	[-0.001, -0.0015]	[-]
$arepsilon_{cp,24h}^p$	[-0.0007, -0.0012]	[-]
а	[16, 20]	[-]
Shrinkage		
$arepsilon_{\infty}^{shr}$	[-0.0005, -0.0015] shotcrete tunnel lining, [-0.0002, -0.0006] cast concrete	[-]
t_{50}^{shr}	[28, 100]	[day]
Creep	'	
$arphi^{cr}$	[2, 3] shotcrete tunnel lining, [Eurocode 2] cast concrete	[°]
t^{cr}_{50}	[1, 5]	[day]

14.5 | State parameters in the Concrete model

In addition to the output of standard stress and strain, the Concrete model provides an output on state variables such as the current elastic modulus E(t) and the current compressive yield stress f_{cv} . These parameters can be visualised by selecting the **State parameters** option from the Stresses menu. An overview of available state parameters is given below:

Δt	Age of concrete	day
Е	Average Young's modulus in current step	[kN/m ²]
f _c	Uniaxial compressive strength at the end of the current step	[kN/m ²]
f_{cy}	Current compressive yield stress	[kN/m ²]
H _c	Normalised compressive strain hardening parameter	[-]
H _t	Normalised tensile strain hardening parameter	[-]
UtilFC	Concrete utilisation factor in compression	[-]
UtilFT	Concrete utilisation factor in tension	[-]
$arepsilon_{xx}^{cr}.E(t)$	Normalised creep history strain in xx direction	[-]
$arepsilon_{yy}^{cr}.E(t)$	Normalised creep history strain in yy direction	[-]
$arepsilon_{zz}^{cr}$. $E(t)$	Normalised creep history strain in zz direction	[-]
$arepsilon_{xy}^{cr}$. $E(t)$	Normalised creep history strain in xy direction	[-]
$arepsilon_{yz}^{cr}.E(t)$	Normalised creep history strain in yz direction	[-]
$arepsilon_{xz}^{cr}.E(t)$	Normalised creep history strain in xz direction	[-]

Some parameters are further explained in the following two sections:

14.5.1 Concrete utilisation factor in compression UtilFC

The concrete utilisation factor in compression *UtilFC* is defined as:

$$UtilFC = \sigma_{rot} \left(\frac{\sigma_3 - \sigma_1}{\sigma_1 - \sigma_{rot}} \right) / (\gamma_{fc} f_c) \quad \left(Hardening \right)$$

$$UtilFC = \sigma_{rot} \left(\frac{\sigma_3 - \sigma_1}{\sigma_1 - \sigma_{rot}} \right) / (\gamma_{fc} f_{cy}) \quad \left(Softening \right)$$
(14-28)

$$UtilFC = \sigma_{rot} \left(\frac{\sigma_3 - \sigma_1}{\sigma_1 - \sigma_{rot}} \right) / (\gamma_{fc} f_{cy}) \quad \left(Softening \right)$$
 (14–28)

The utilisation factor is constant in hardening and is related to the maximum uniaxial compressive strength at the end of the current step f_c . After the peak value is reached and the softening is taking place, the utilisation factor is related to the current compressive yield stress f_{cy} and follows the stress-strain curve in softening (Figure 14–2 (p. 148)).

14.5.2 Concrete utilisation factor in tension *UtilFT*

The concrete utilisation factor in tension *UtilFT* is defined as:

$$UtilFT = \frac{\sigma_1}{f_t \gamma_{ft}} \ (Softening)$$
 (14–29)

The utilisation factor is constant during the linear softening in tension and is related to the maximum uniaxial tensile strength at the end of the current step f_t . When the residual value is reached, then $f_t = f_{tun}$.

14.6 On the use of the Concrete model in dynamics calculations

Generally the time steps and the time interval for the usual dynamics calculations are in the range of seconds. However, the time scale in concrete hardening is in the range of hours to days. For this reason, in dynamics analysis, the use of the Concrete model with timedependency of the parameters is not recommended unless the concrete elements are not totally cured in the previous construction stages. Otherwise, in dynamics analysis the *Time* dependent strength and stiffness, the Creep behaviour and the Shrinkage behaviour should be disabled, nevertheless the Concrete model continues to take into account the stressstrain hardening and softening.

14.7 | Warning

The problems involving tension softening with low fracture energy could affect the convergence of the FE-calculation, even though the model itself can never fail physically. The crack initiation massively increases the global error, even though the step size is gradually reduced by the global iteration procedure.

A structure made of strain softening material behaves in a brittle or ductile manner, not only depending on the material behaviour formulated at stress point level, but also on the size of the structure, with the response becoming ever more brittle the larger the structure is. This is due to the increase of energy released by the unloading part of the structure compared to the fracture energy dissipated in the crack. If the energy in unloading is larger than the fracture energy of the crack, both forces and displacements need to decrease in order to reach equilibrium.

However, in tunnelling the shotcrete never involves failure with low fracture energy. The problem could occur in other applications regarding rigid inclusions in the ground.

The UBC3D-PLM model [ULT]

During an earthquake, the seismic waves propagate from the source till the ground surface, causing ground shaking. The soil deposit acts as a filter causing the variation of the seismic waves in terms of amplitude, duration and frequency content at any depth of the soil deposit. The effects of an earthquake can be different, such as structural damages, landslides and soil liquefaction.

The term liquefaction is used to describe a variety of phenomena that occurs in saturated cohesionless soils under undrained conditions. Under static and cyclic loading, dry cohesionless soils tend to densify. If these soils are saturated and the applied load acts in a short time, as in the case of an earthquake, the tendency to densify causes an increase in excess pore pressures that cannot rapidly be dissipated and consequently a decrease in the effective stresses occurs. When this happens, the soil behaves as a fluid.

This phenomenon can be explained considering that the shear resistance τ for cohesionless soils is given by Coulomb's formula:

$$au = \sigma'_{vo} an(arphi)$$
 (15–1)

where

 σ'_{vo} = The initial effective stress

 φ = The friction angle.

According to Terzaghi's formula, the effective stress is given by:

$$\sigma'_{vo}=\sigma_{vo}-p_w$$
 (15–2)

where

 σ_{vo} The total vertical stress.

 p_w The pore pressure.

When the excess pore pressures Δp_w develop during an earthquake, the equation can be written as:

$$\sigma'_{vo} = \sigma_{vo} - (p_w + \Delta p_w) \tag{15-3}$$

which means that the effective stress state tends to decrease and, when it reaches zero, also the shear resistance is null.

In order to evaluate the potential liquefaction hazard of a site, it is necessary to identify the predisposing and triggering factors for liquefaction. The predisposing factors are the characteristics of the soil deposit such as particle size and shape, gradation and plasticity characteristics. The triggering factors depend on the earthquake magnitude, duration and peak ground acceleration. To establish if liquefaction can occur in a specific site subjected to a selected earthquake semi-empirical procedures or nonlinear dynamic analyses can be used.

The UBC3D-PLM model ² is an effective stress elasto-plastic model which is capable of simulating the liquefaction behaviour of sands and silty sands under seismic loading (Tsegave (2010), Petalas & Galavi (2012)). The UBC3D-PLM model formulation is based on the original UBCSAND (University of British Columbia Sand) model introduced by Puebla, Byrne & Phillips (1997) and Beaty & Byrne (1988). The original UBCSAND is a 2D model formulated in the classical plasticity theory with a hyperbolic strain hardening rule, based on the original Duncan-Chang model. The hardening rule relates the mobilised friction angle to the plastic shear strain at a given stress. The UBCSAND model contains a 2D Mohr-Coulomb yield surface and a corresponding non-associated plastic potential function. The flow rule in the model is based on the stress-dilatancy theory developed by (Rowe (1962)), linearised and simplified according to energy considerations.

The main difference between the UBCSAND model and the UBC3D-PLM model is the generalized 3D formulation of the latter. The UBC3D-PLM model uses the Mohr-Coulomb yield condition in a 3D principal stress space for primary loading, and a yield surface with a simplified kinematic hardening rule for secondary loading. Moreover, a modified non-associated plastic potential function based on Drucker-Prager's criterion is used for the primary yield surface, in order to maintain the assumption of stress-strain coaxiality in the deviatoric plane for a stress path beginning from the isotropic line Tsegave (2010).

The assessment of the liquefaction potential of a soil deposit can be done by performing a dynamic site response analysis. Generally the following steps are needed to perform such an analysis (Laera & Brinkgreve, 2015):

- Definition of the geotechnical model of the soil deposit, in terms of soil layer distribution, water table depth, appropriate dynamic boundary conditions and soil mechanical properties to describe its behaviour under static and cyclic loading.
- Definition of the seismic input motion, according to the specific site and the probabilistic study as reported in the current regulations (i.e. Eurocode 8, NTC 2008, etc.).
- Definition of the numerical model to perform the analysis including the appropriate dynamic boundary conditions.

A site response analysis requires a deep and extended investigation of the soil deposit to identify the soil layer distribution and hydraulic conditions as well as the mechanical properties of the soil. When possible, the investigation should be extended until the depth of a rock or rocklike formation. In situ and laboratory tests should be performed to evaluate index properties, stiffness and strength of the soil layers with regard to their behaviour under cyclic loading (Cross-hole and Down-hole in situ tests, among others, and cyclic triaxial, cyclic direct simple

² PLM = PLAXIS Liquefaction Model

shear and resonant column laboratory tests). However, in many cases only data from drained triaxial tests (CD TxC) or in situ tests like SPT or CPT are available. For this reason the UBC3D-PLM model implements a specific formulation with input parameters based on these tests.

Main characteristics of the UBC3D-PLM model and the corresponding input parameters are given below:

- Stress dependent stiffness according to a power law k_B^{*e} , k_G^{*e} , m_e , n_e , n_p .
- Plastic straining due to primary deviatoric loading k_C^{*p} .
- Densification due to the number of cycles during secondary loading f_{dens} .
- Post-liquefaction stiffness degradation f_{Epost}
- Failure according to the Mohr-Coulomb failure criterion φ_{cv} , φ_p and c.

15.1 Elasto-plastic behaviour and hardening rule

The UBC3D-PLM model incorporates a non-linear, isotropic law for the elastic behaviour that is defined in terms of the elastic bulk modulus K and the elastic shear modulus G, which are defined by the following equations:

$$K=k_B^{*e}p_{ref}igg(rac{p'}{p_{ref}}igg)^{m_e}$$
 (15–4)

$$G=k_G^{*e}p_{ref}igg(rac{p'}{p_{ref}}igg)^{n_e}$$
 (15–5)

where

Bulk modulus factor.

Shear modulus factor.

 p_{ref} = Reference pressure

power for stress dependency of the bulk modulus K

power for stress dependency of the shear modulus G

Pure elastic behaviour with G_{max} is predicted by the model during the unloading process. Once the stress state reaches the yield surface, plastic behaviour is taken into account as long as the stress point is not going immediately back into the elastic zone.

Note: The implicit Poisson's ratio calculated from elastic bulk and shear modulus from Eqn. 15-4 (p. 164) and Eqn. 15-5 (p. 164) is suitable for dynamics calculation, but using it for gravity loading may give improper initial stress state. Therefore, the user is advised to use another material for the stress initialization.

The first yield surface is defined from a set of Mohr-Coulomb functions. The position and size of the yield surface is defined based on the hardening law. More specifically, plastic hardening based on the principle of strain hardening is used in the model (similar to the Hardening Soil model). The hardening rule governs the amount of plastic strain as a result of mobilisation of

the shear strength ($\sin \varphi_{mob}$). The mobilised friction angle derived from the Mohr-Coulomb yield criterion, is given as:

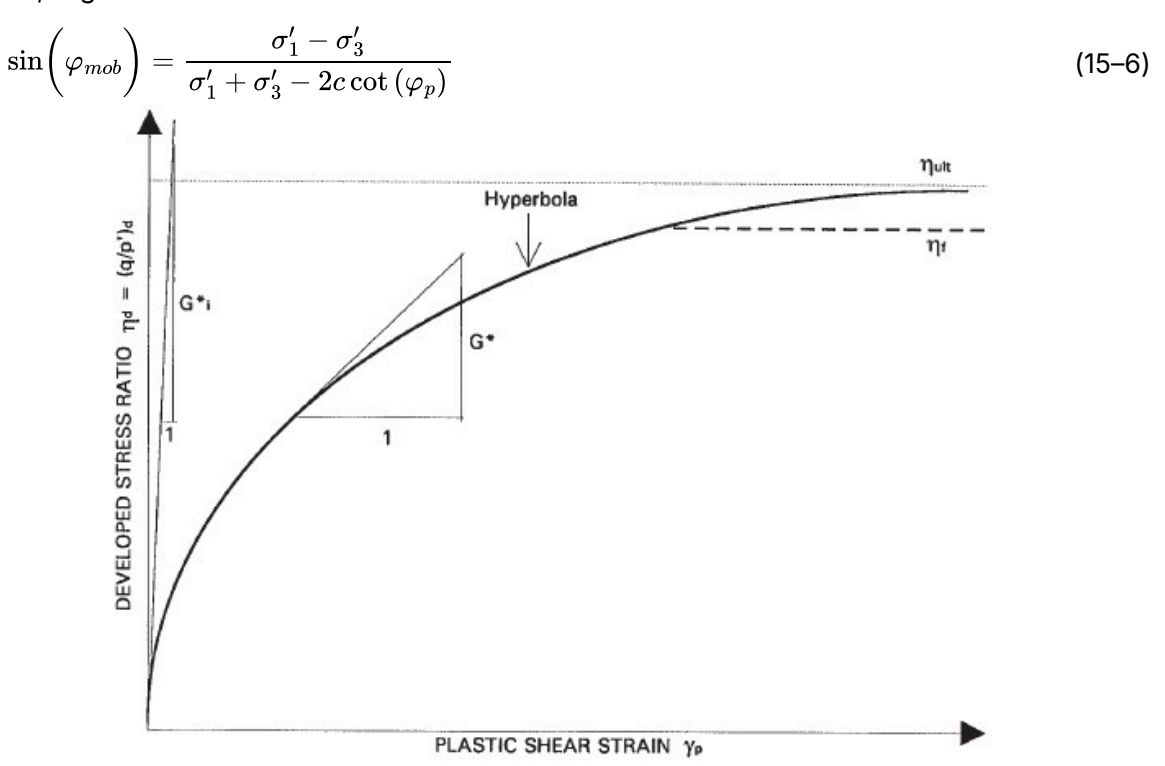


Figure 15-1: The original UBCSAND hardening rule

The hyperbolic hardening rule (Beaty & Byrne, 1988) is presented schematically in Figure 15-1 (p. 165). It relates the increment of the sine of the mobilised friction angle (calculated according to Eqn. 15-6 (p. 165)) to the plastic shear strain increment as follows (Puebla, Byrne & Phillips, 1997):

$$d\gamma_p = \left(\frac{1}{G^*}\right) d\sin\left(\varphi_{mob}\right) \tag{15-7}$$

$$G^* = k_G^{*p} igg(rac{p'}{p_{ref}}igg)^{n_p} igg(1 - igg(rac{\sin\left(arphi_{mob}
ight)}{\sin\left(arphi_p
ight)}igg)^2$$
 (15–8)

where k_G^{*p} is the plastic shear modulus factor; n_p is the plastic shear modulus exponent; $arphi_{mob}$ is the mobilised friction angle, which is defined by the stress ratio; φ_p is the peak friction angle; and R_f is the failure ratio η_f / η_{ult} , ranging from 0.5 to 1.0, where η_f is the stress ratio at failure and η_{ult} is the asymptotic stress ratio from the best fit hyperbola. The hardening rule as reformulated by Tsegaye (2010) in UBC3D-PLM model is given as:

$$d\sin\left(arphi_{mob}
ight) = 1.5k_G^{*p} \left(rac{p'}{p_{ref}}
ight)^{n_p} rac{p_{ref}}{p'} \left(1 - \left(rac{\sin\left(arphi_{mob}
ight)}{\sin\left(arphi_p
ight)}
ight) R_f
ight)^2 d\lambda$$
 (15–9)

where $d\lambda$ is the plastic strain increment multiplier.

15.2 Flow rule

The plastic potential function specifies the direction of the plastic strain. A non-associated flow rule based on the Drucker-Prager plastic potential function is used in the UBC3D-PLM model (Tsegaye, 2010). The plastic potential function g is formulated as:

$$g=q-Mig(p'+c\cot{(arphi_p)}ig)$$
 (15–10)

$$g=q-Mig(p'+c\cot{(arphi_p)}ig)$$
 (15–10) $M=rac{6\sin{(\psi_M)}}{3-\sin{(\psi_M)}}$

where the Drucker-Prager surface is fixed in the compression point.

In the UBC3D-PLM model the flow rule of the original UBCSAND model is used, which is derived from energy considerations by Puebla, Byrne & Phillips (1997). Similar to the Hardening Soil model it is based on three observations (Figure 15-2 (p. 166)):

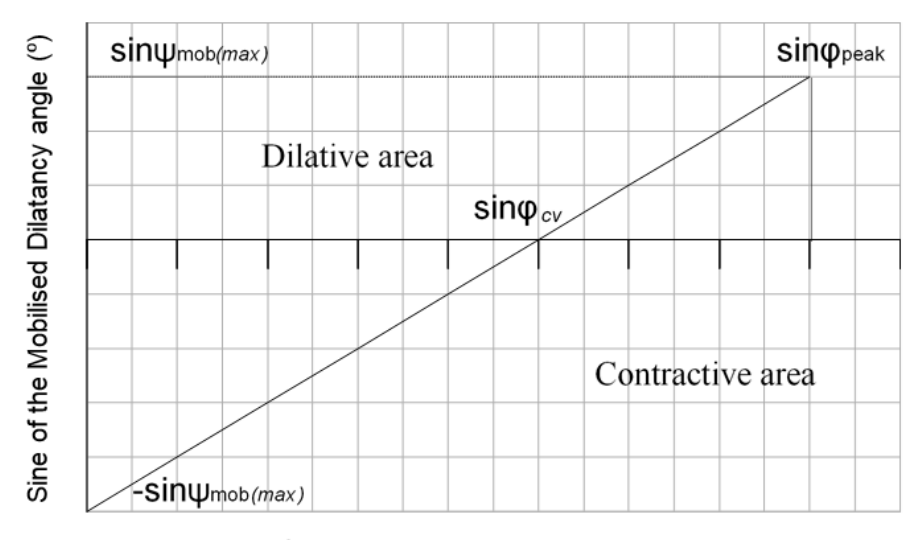
- There is a unique stress ratio, defined by the constant volume friction angle φ_{cv} , for which plastic shear strains do not cause plastic volumetric strains.
- Stress ratios which lie below $\sin \varphi_{cv}$ exhibit contractive behaviour, while stress ratios above $\sin\,\phi_{cv}$ lead to a dilative response. This means that the constant volume friction angle works as the phase transformation angle.
- The amount of contraction or dilatancy depends on the difference between the current stress ratio and the stress ratio at $\sin \varphi_{cv}$.

The increment of plastic volumetric strain $d\varepsilon_v^p$ is calculated as follows:

$$darepsilon_v^p = \sin(\psi_m) d\gamma^p$$
 (15–12)

$$\sin(\psi_m) = \sin(\varphi_m) - \sin(\varphi_{cv}) \tag{15-13}$$

where, φ_{cv} is the constant volume friction angle.



Sine of the Mobilised Friction angle (°)

Figure 15-2: Graphical representation of the modified Rowe's flow rule as used in UBC3D-PLM model

Based on the mobilised friction angle an unloading-reloading criterion is defined in the model as follows:

$$\sin\left(\varphi_{mob}^{e}\right) < \sin\left(\varphi_{mob}^{0}\right) \ \left(unloading; \ elastic \ behaviour\right)$$

$$\sin\left(\varphi_{mob}^{e}\right) > \sin\left(\varphi_{mob}^{0}\right) \ \left(Loading \ or \ reloading; \ plastic \ behaviour\right)$$

$$(15-14)$$

$$\sin\left(\varphi_{mob}^{e}\right) > \sin\left(\varphi_{mob}^{0}\right) \ \left(Loading \ or \ reloading; \ plastic \ behaviour\right)$$
 (15–15)

The previous mobilised friction angle $\sin(\varphi^0_{mob})$ is memorised from the previous calculation step, while the current one $\sin(arphi_{mob}^e)$ is calculated based on the current stresses. During loading, the friction angle is mobilised, and hardening plasticity occurs. During unloading, pure elastic behaviour is predicted until the stress point reaches the p' axis.

15.3 Load state during liquefaction

The UBC3D-PLM model employs two yield surfaces to guarantee a smooth transition into the liquefied state of the soil and to enable the distinction between primary and secondary loading (Figure 15-3 (p. 167)). The UBC3D-PLM model incorporates a densification law through a secondary yield surface with a kinematic hardening rule that improves the precision of the evolution of the excess pore pressure. This surface generates lower plastic deformations compared to the primary yield surface.

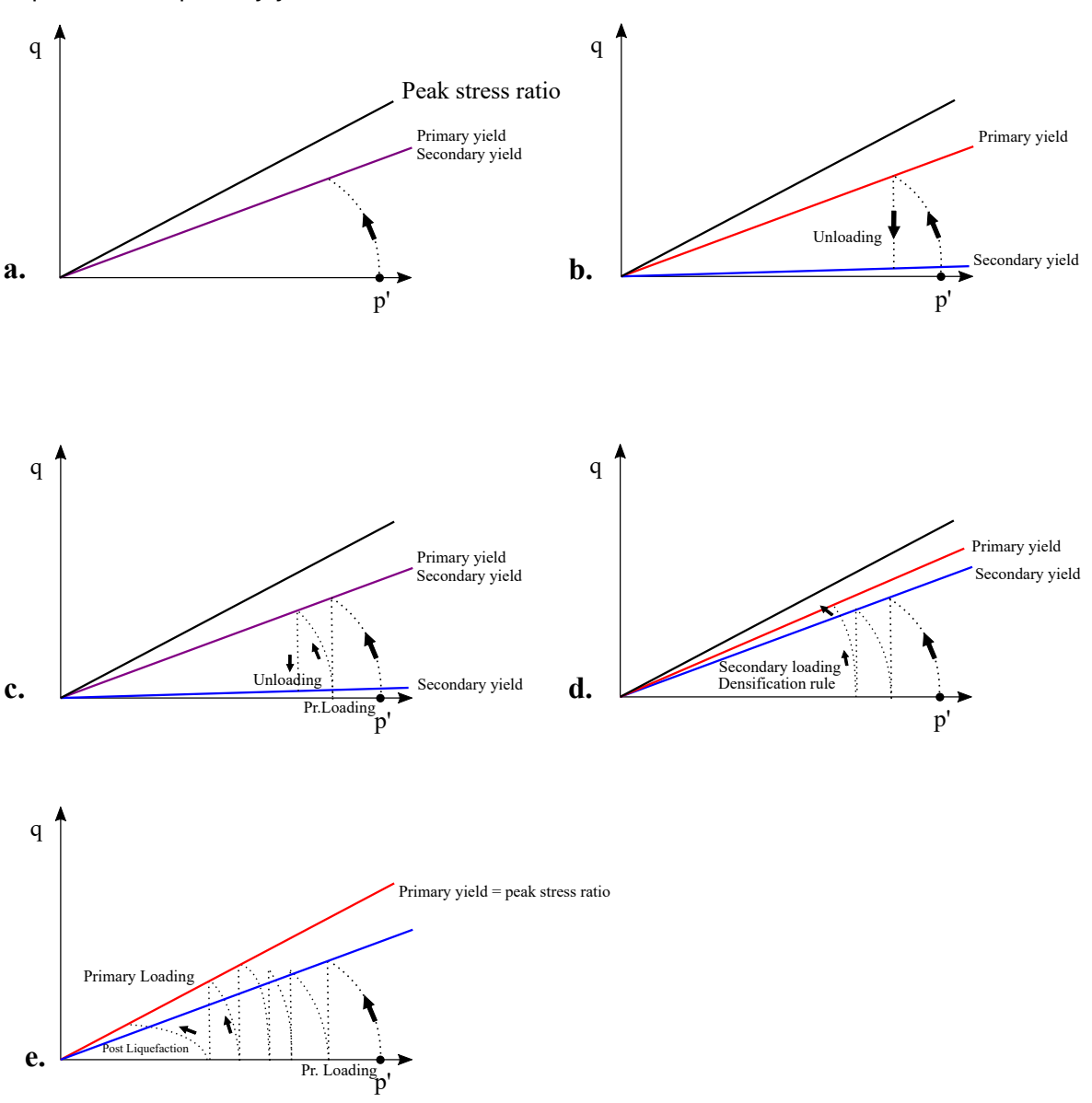


Figure 15-3: Introduction of two yield surfaces in order to include soil densification, smooth transition in liquefaction and post-liquefaction behaviour

The plastic shear modulus factor $k_G^{st p}$ during primary loading is identical with the one entered as input parameter by the user and is used in the hardening rule governing the hardening of the primary yield surface. The plastic shear modulus factor $k_G^{st_p}$ during the secondary loading is a function of the number of cycles followed during the loading process. A simple rule based on stress reversals of loading to unloading and vice versa is used to define the counting of cycles.

This leads to an increase of the excess pore pressure during undrained cyclic loading with a decreasing rate until the liquefied state is approached. The modification of the plastic shear modulus factor during the secondary loading is calculated as follows:

$$k_{G, ext{ secondary}}^{*p} = k_{G}^{*p} \Big(4 + rac{n_{rev}}{2} \Big) hardf_{dense}$$
 (15–16)

where

 k_C^{*p} = Input plastic shear modulus factor.

Secondary plastic shear modulus factor.

 n_{rev} Number of shear stress reversals from loading to unloading or vice versa.

hard = Factor which is correcting the densification rule for loose soils.

 f_{dens} Multiplier which is a user input parameter to adjust the densification rule.

For loose sands, characterised by a value of $(N_1)_{60}$ (i.e. normalised penetration resistance for SPT procedures) between 5 and 9, the densification rule is modified Beaty & Byrne (2011), Naesgaard (2011). The correction rule is as follows:

$$hard = \min(1; \max(0.5; 0.1(N_1)_{60}))$$
 (15–17)

Note: The normalised penetration resistance $(N_1)_{60}$ from SPT tests is an input parameter used to define only the hard factor. However, the user can correlate the other input parameters of the UBC3D-PLM model using $(N_1)_{60}$ (15.5 Parameters of the UBC3D-PLM model (p. 169)).

The plastic shear modulus is limited according to the maximum normalised SPT value $(max(N_1)_{60})$ corresponding to dense soils.

$$k_{G,\max}^{*p} \leq k_G^{*e} \Big((N_1)_{60,max} \Big)^2 \cdot 0.003 + 100$$
 (15–18)

This rule is the result of calibrating a number of direct simple shear tests. Thus, the calibration factor plays a key role when the user wants to model different stress paths (i.e. cyclic triaxial tests, etc.) and the final value is a matter of judgement according to the most critical stress path for a specific problem. It finally leads to an increase of the excess pore pressure during undrained cyclic loading until the liquefied state is approached. The rate of generation of excess pore pressure decreases by increasing number of cycles.

15.4 Post-liquefaction rule and cyclic mobility

An important issue during the modelling of cyclic liquefaction in sands is the volumetric locking. The evolution of the plastic volumetric strains, after the stress path reaches the yield surface defined by the peak friction angle, becomes constant due to the formulation of the flow rule (in Eqn. 15–12 (p. 166)). In the case $\sin \varphi_{mob}$ becomes $\sin \varphi_p$ and remains constant meaning that $\sin \psi_m$ is also constant.

Consequently the stiffness degradation of loose non-cohesive soils due to the post liquefaction behaviour as well as dense non-cohesive soils due to the cyclic mobility cannot be modelled. This limitation is overcome in the formulation of the UBC3D-PLM model with the equation which gradually decreases the plastic shear modulus as a function of the generated plastic deviatoric strain during dilation, due to the deconstruction of the soil skeleton which occurs during dilative behaviour. This leads to the decreased soil stiffness during the contraction phase which follows after the unloading phase. This behaviour is presented in Figure 15-4 (p. 169) picturing the process of cyclic mobility of a dense sand. The aforementioned stiffness degradation is computed as follows:

$$k_{G,\,post-liquefaction}^{*p}=k_{G}^{*p}E_{
m dil}$$
 (15–19)
 $E_{
m dil}=\maxig(e^{-110arepsilon_{dil}};f_{Epost}ig)$ (15–20)

where k^{*p}_{G} is the input plastic shear modulus factor, $k^{*p}_{G,post-liquefaction}$ is the plastic shear modulus factor during liquefaction, ε_{dil} is the accumulation of the plastic deviatoric strain which is generated during dilation of the soil element. The minimum value of E_{dil} term in the above mentioned equation is limited by the input parameter f_{Epost} .

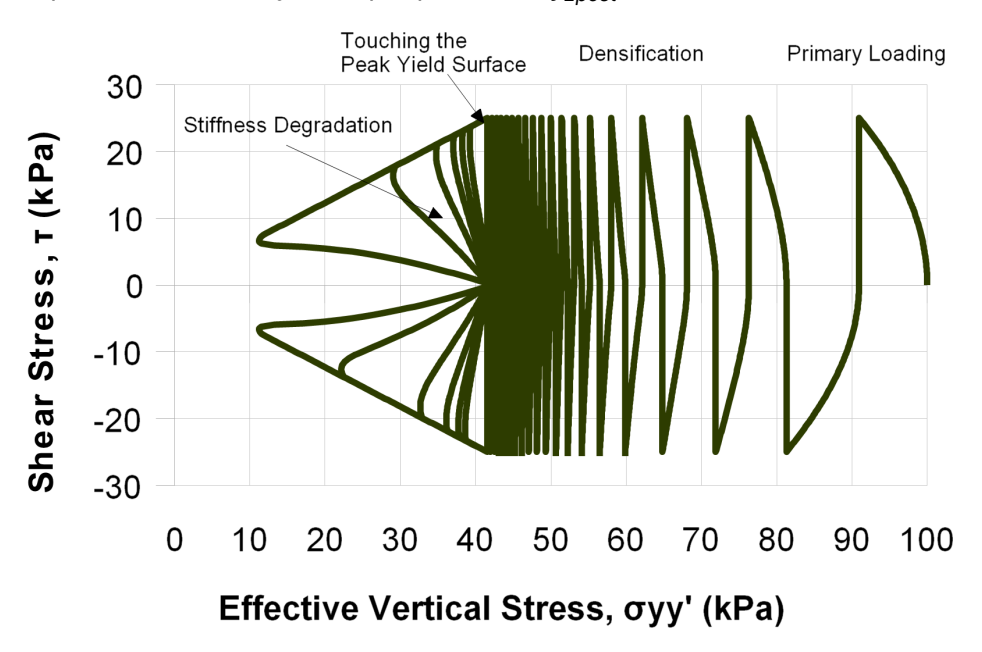


Figure 15-4: Undrained cyclic shear stress path reproduced with **UBC3D-PLM** model for a dense sand. Cyclic mobility, stiffness degradation and soil densification are indicated on the graph

15.5 Parameters of the UBC3D-PLM model

Usually, in earthquake engineering, when the onset of liquefaction is the modelling target, a cyclic triaxial or a cyclic direct simple shear test is the proper way to extract all the parameters for the UBC3D-PLM model. However, in many cases only data from drained triaxial tests (CD TxC) or in situ tests (SPT) are available. For this reason the UBC3D-PLM model implements a specific formulation with input parameters based on these tests. However, some of the equations based on SPT values proposed by Beaty & Byrne (2011) for the generic calibration of the UBCSAND model should be used with careful consideration for the calibration of the UBC3D-PLM model.

The parameters with their standard units are listed below.

Stiffness parame	eters:	
$k_B^{*_e}$	Elastic bulk modulus factor	[-]
k_G^{*e}	Elastic shear modulus factor	[-]
k_G^{*p}	Plastic shear modulus factor	[-]
m_e	Rate of stress-dependency of elastic bulk modulus	[-]
n_e	Rate of stress-dependency of elastic bulk modulus	[-]
n_p	Rate of stress-dependency of plastic shear modulus	[-]
p _{ref}	Reference pressure	[kN/m ²]
Strength parame	eters:	
$arphi_{cv}$	Constant volume friction angle	[°]
$arphi_{ m p}$	Peak friction angle	[°]
С	Cohesion	[kN/m ²]
σ_t	Tension cut-off and tensile strength	[kN/m ²]
Field data		
(N ₁) ₆₀	Normalised SPT value	[-]
Advanced parar	neters:	<u>.</u>
R_f	Failure ratio	[-]
f_{dens}	Densification factor	[-]
<i>f</i> _{Epost}	Post-liquefaction factor	[-]

The UBC3D-PLM model allows two drainage types: Drained and Undrained A. The other undrained calculations are not available due to the effective stress nature of the model.

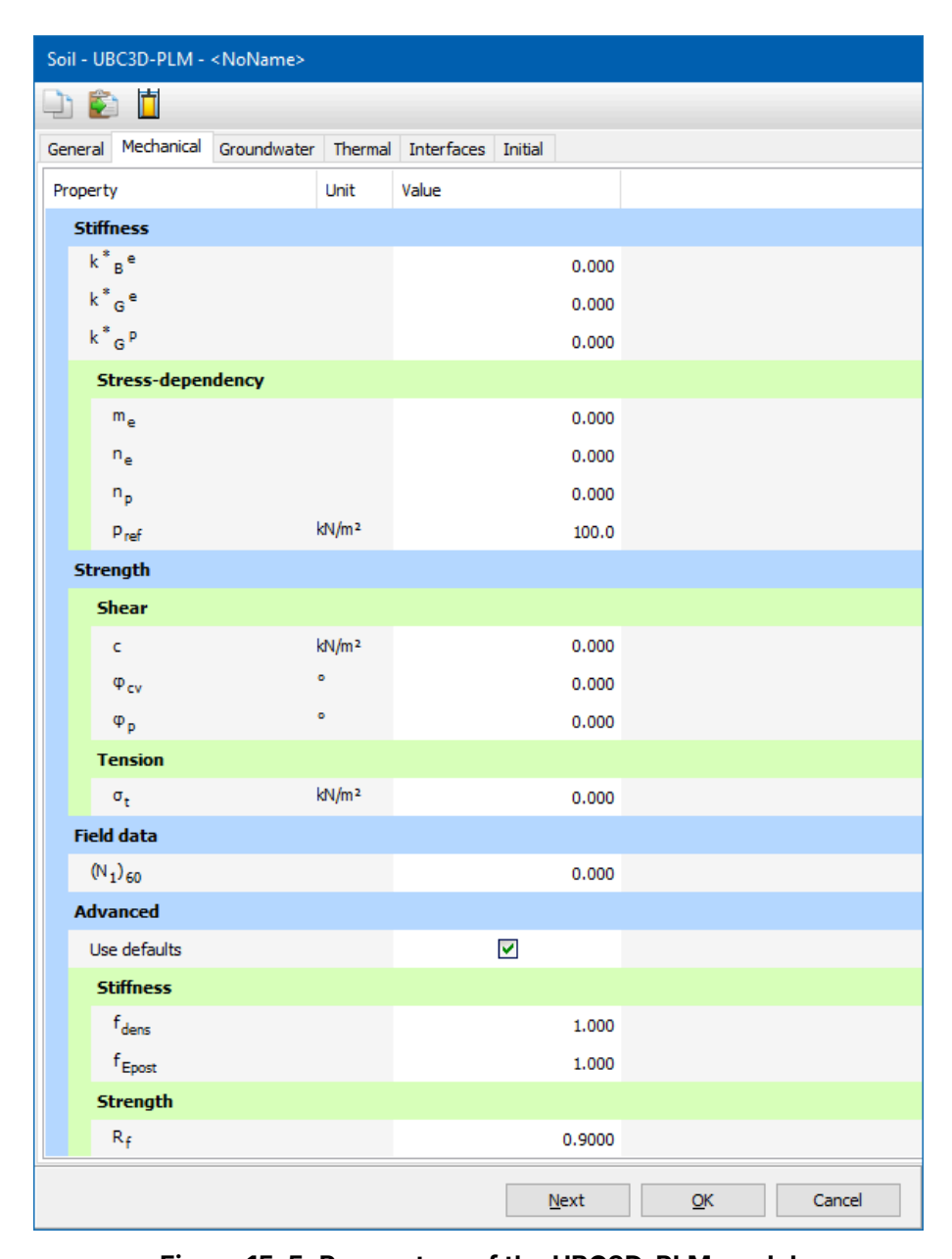


Figure 15-5: Parameters of the UBC3D-PLM model

15.5.1|Stiffness modulus factors k_B^{*e} , k_G^{*e} & k_G^{*p} and indexes m_e , n_e and n_p

Beaty & Byrne (2011) proposed a set of equations based on the normalised N_{SPT} value, $(N_1)_{60}$ for the initial generic calibration of the UBCSAND 904aR model. Makra (2013) revised the proposed equations and highlighted the differences between the original UBCSAND 2D formulation and the UBC3D-PLM model, as implemented in PLAXIS. The proposed equations for the generic initial calibration are the following:

$$k_G^{*e} = 21.7 \times 20 \times (N_1)_{60}^{0.3333}$$
 (15–21)

$$k_G^{*e} = 21.7 \times 20 \times (N_1)_{60}^{0.3333}$$
 (15–21)
$$k_B^{*e} = 0.7 \times k_G^{*e}$$
 (15–22)

$$k_B^{*p} = k_G^{*e} \times (N_1)_{60}^2 \times 0.003 + 100$$
 (15–23)

The index parameters m_{e_I} n_e and n_p should be calibrated by curve fitting. The range of these values is 0-1. The suggested default values are $m_{e=}n_{e}=0.5$ and $n_{p}=0.4$. Alternatively the

relative density correlations can be used to calibrate the above mentioned parameters as suggested by Souliotis & Gerolymos (2016).

f 0 Note: The implicit Poisson's ratio that is defined based on k_B^{*e} and k_G^{*e} is suitable for dynamics calculation, but it does not generate a proper initial stress state if the initial stress condition is established by gravity loading procedure. In such a case the user should define another material set for the stress initialization step with proper characteristics.

15.5.2 Strength parameters φ_{cv} , φ_{p} and c

The strength parameters of the primary yield surface φ_{cv} , φ_p and c can be derived directly from CD TxC or DSS tests. The default value for the cohesion c is 0, as in most cases for granular soils without relevant fine component. The peak friction angle φ_p can be calculated from SPT

$$arphi_p = arphi_{cv} + rac{(N_1)_{60}}{10} + ext{max}igg(0; rac{(N_1)_{60} - 15}{5}igg)$$
 (15–24)

The constant volume friction angle φ_{cv} can be derived directly from SPT test using one of the correlations available in literature (Bolton, 1986; Mayne, 2001).

1 Note: In the UBC3D-PLM model, the constant volume friction angle φ_{cv} plays the role of the phase transformation angle φ_{pt} .

15.5.3 Advanced parameters R_f , f_{dens} and f_{Epost}

The densification factor f_{dens} is a multiplier that controls the scaling of the plastic shear modulus factor during secondary loading. The acceptable range is 0 - 1, when a value below 1 means that k_G^{*p} becomes lower and the behaviour is softer. It is recommended to use f_{dens} = 1.0 (Petalas & Galavi, 2012) because the variation of the densification does not significantly affect liquefaction triagering.

 f_{Epost} is the parameter to adjust post-liquefaction behaviour. The acceptable range of f_{Epost} is 0.1 - 1 and a value of 0.2 - 1 is recommended. Resistance is underestimated for very dense sands, which can be counterbalanced by an increase of the f_{Epost} parameter.

The failure ratio R_f has a default value of 0.9, but it can be also estimated from the SPT test based on the original UBCSAND (Beaty & Byrne, 2011):

$$R_f \approx 1.1((N_1)_{60})^{-0.15} < 0.99$$
 (15–25)

15.5.4 Normalised SPT value (N₁)60

The SPT blow count N_{SPT} is affected by a number of procedural details such as rod lengths, hammer energy, sampler details and borehole size which are accounted using correction factors. In addition, if the N_{SPT} is corrected by the overburden stress effects one obtains the normlised penetration resistance $(N_1)_{60}$, expressed as:

$$(N_1)_{60} = C_N C_E C_R C_B C_S N_{SPT} (15-26)$$

where

 C_N overburden correction factor.

 C_E $ER_m/60$.

 ER_m = Measured value of the delivered energy as a percentage (%) of the theoretical

free-fall hammer energy.

 C_R Correction factor to account for different rod lengths.

 C_{R} Correction factor for nonstandard borehole diameters.

 C_S Correction factor that depends on the sampler.

 N_{SPT} Calculated as $N_2 + N_3$ considering that N_1 , N_2 and N_3 are the number of blows

needed for the tube to penetrate each 15 cm.

The suggested values for C_B , C_R and C_S are given in Table 15–1 (p. 173).

Table 15-1: List of values of the different coefficient for the correction of the SPT test

Coefficient	Condition	Value
General		
	65÷115 mm (standard)	1.00
Borehole diameter, C_B	150 mm	1.05
	200 mm	1.15
	3÷4 m	0.75
	4÷6 m	0.85
Rod length, C_R	6÷10 m	0.95
	10÷30 m	1.00
	>30 m	1.00
Type of sampler, C_S	Standard	1.00
Type of sampler, og	Non standard	1.1÷1.3

If $(N_1)_{60}$ is not known, the following approximation (adapted from Beaty & Byrne (2011)) with relative density RD (expressed in %) can be used:

$$\left(N_{1}
ight)_{60}pproxrac{RD^{2}}{15^{2}}$$
 (15–27)

15.6 State parameters in the UBC3D-PLM model

In addition to the output of standard stress and strain, the UBC3D-PLM model provides output of state variables, such as the excess pore pressure ratio in terms of vertical effective stresses $r_{u,\sigma'v}$ and the mobilised peak friction angle $\varphi_{p,reached}$. These parameters can be visualised by selecting the State parameters option from the Stresses menu. An overview of available state parameters is given below:

sin φ _{mob}	Sine of the mobilised friction angle (<u>Eqn. 15–6 (p. 165)</u>)	[-]
sin φ _{mob,max}	Sine of the maximum mobilised friction angle	[-]
Φ p,reached	Flag indicating whether peak friction angle has been reached (0/1)	[-]
n _{rev}	Number of half cycles	[-]
$r_{u,\sigma'v}$	Excess pore pressure ratio in terms of vertical effective stress (Eqn. 15–28 (p. 174))	[-]
r _{u,σ'v,max}	Maximum excess pore pressure ratio in terms of vertical effective stress	[-]
$r_{u,p'}$	Excess pore pressure ratio in terms of mean effective stress (Eqn. 15–29 (p. 174))	[-]
$r_{u,p',max}$	Maximum excess pore pressure ratio in terms of mean effective stresses	[-]
$arepsilon_{dil,total}$	Accumulated dilative plastic deviatoric strain	[-]

 $r_{u,\sigma'v}$, $r_{u,p'}$, $\varphi_{p,reached}$ are further explained in the following subsections:

15.6.1 Excess pore pressure ratio in terms of vertical effective stresses $r_{u,\sigma'v}$

The liquefaction potential in terms of vertical effective stress can be expressed by means of the excess pore pressure ratio $r_{u,\sigma'v}$ given by:

$$r_{u,\sigma'v} = rac{\sigma'_{v0} - \sigma'_{v}}{\sigma'_{v0}} = 1 - rac{\sigma'_{v}}{\sigma'_{v0}}$$
 (15–28)

where σ'_{V} is the current vertical effective stress during the dynamics calculation and σ'_{VO} is the initial effective vertical stress prior to the seismic motion. When $r_{u,\sigma'v}$ is equal to 1, the corresponding layer is in a complete liquefied state. Consider zones with a maximum $r_{u,\sigma'v}$ greater than 0.7 to be liquefied.

15.6.2 Excess pore pressure ratio in terms of mean effective stress $r_{u,p'}$

The state variable $r_{u,\sigma'_{v}}$ gives similar information as $r_{u,p'}$ but instead of the vertical effective stress the mean effective stress is used:

$$r_{u,p'} = rac{p_0' - p'}{p_0'} = 1 - rac{p'}{p_0'}$$
 (15–29)

where p' is the current mean effective stress during the dynamics calculation and p'_0 is the initial mean effective stress prior to the seismic motion. When $r_{u,p'}$ equals 1, the soil is in a liquified state.

15.6.3 Reached peak friction angle $\varphi_{p,reached}$

The reached peak friction angle $\varphi_{p,reached}$ is a flag indicating if φ_p has been reached (0 = no, 1 = ves).

15.7 On the use of the UBC3D-PLM model in dynamics calculations

When subjected to dynamic or cyclic loading, the UBC3D-PLM model generates plastic strains when mobilising the soil's material strength (shear hardening). A Rayleigh damping can be defined to simulate the initial soil's damping characteristics.

The UBC3D-PLM model has been developed for simulating the dynamic behaviour of noncohesive soils and it is particularly suitable for analysing the problems involving generation of pore pressure in undrained behaviour and liquefaction. For the same reason, it is less suitable for use in static analysis. This limitation can be overcome by using Hardening Soil model (6 The Hardening Soil model (Isotropic hardening) (p. 65)) or Hardening Soil model with small-strain stiffness(7 The Hardening Soil model with small-strain stiffness (HSsmall) (p. 80)) instead.

The UBC3D-PLM model develops overdamping due to use of G_{max} in elastic unloading. In the problems not involving generation of pore pressure in undrained behaviour, liquefaction or softening due to dilatancy, this limitation can be overcome by using the Hardening Soil model with small-strain stiffness (7 The Hardening Soil model with small-strain stiffness (HSsmall) (p. 80)) instead.

User-defined soil models [ADV]/[ULT] + [GSE]

16.1 Introduction

PLAXIS has a facility for User-defined Soil Models (UDSM). This facility allows users to implement a wide range of constitutive soil models (stress-strain-time relationship) in PLAXIS. Such models must be programmed in FORTRAN (or another programming language), then compiled as a Dynamic Link Library (DLL) and then added to the UDSM sub-folder of the PLAXIS program directory.

In principle the user provides information about the current stresses and state variables and PLAXIS provides information about the previous ones and also the strain and time increments. In the material data base of the PLAXIS input program, the required model parameters can be entered in the material data sets.

Setting	Description
$\sigma_{ij}^{t} + \Delta t, \kappa^{t+\Delta t}$	Current stresses and state variables.
σ_{ij}^{t} , κ^{t}	Previous stresses and state variables.
Δε _{ij} , Δ t	Strain and time increments.

Note:

- Please note that the PLAXIS organization cannot be held responsible for any malfunctioning or wrong results due to the implementation and/or use of userdefined soil models.
- For a detailed view of the UDSMs offered in PLAXIS please check Bentley Communities website.

16.2 Implementation of User Defined (UD) soil Models in calculations program

16.2.1 Main Functionalities UD Models

The PLAXIS calculations program has been designed to allow for UDSM. There are mainly six tasks (functionalities) to be performed in the calculations program:

- Initialization of state variables
- Calculation of constitutive stresses (stresses computed from the material model at certain step)
- Return of the state variables
- Return of attributes matrix
- Creation of effective material stiffness matrix
- Creation of elastic material stiffness matrix

These main tasks (and other tasks) have to be defined by the user in a subroutine called 'User_Mod'. In this subroutine more than one user-defined soil model can be defined. If a UD soil model is used in an application, the calculation program calls the corresponding task from the subroutine User_Mod. To create a UD soil model, the User_Mod subroutine must have the following structure:

Subroutine Name	List of arguments
User_mod	<pre>(IDTask, iMod, IsUndr, iStep, iTer, Iel,Int, X, Y, Z, Time0, dTime, Props, Sig0, Swp0, StVar0, dEps, D, Bulk_W, Sig, Swp, StVar, ipl, nStat, NonSym, iStrsDep, iTimeDep, iTang, iPrjDir, iPrjLen, iAbort)</pre>

IDTask =	=	Identification of the task (1 = Initialise state variables; 2 = Calculate constitutive stresses; 3 = Create effective material stiffness matrix; 4 = Return the number of state variables; 5 = Return matrix attributes (NonSym, iStrsDep, iTimeDep, iTang); 6 = Create elastic material stiffness matrix).
iMod =	=	User-defined soil model number (This option allows for more than one UD model, up to 10).
IsUndr =	=	Drained condition (IsUndr = 0) or undrained condition (IsUndr = 1). In the latter case, PLAXIS will add a large bulk stiffness for water.

iStep Current calculation step number

iter Current iteration number

Iel Current element number

Int Current local stress point number (1..3 for 6-noded elements, or 1..12 for 15-

noded elements)

X,Y,ZGlobal coordinates of current stress point

Timeo Time at the start of the current step

dTime =Time increment of current step

Props Array(1..50) with User-defined model parameters for the current stress point

Sigo Array(1..20) with previous (= at the start of the current step) effective stress components of the current stress point and some other variables (σ^{i0}_{xx} , σ^{i0}_{yy} ,

 σ^{0}_{zz} , σ^{0}_{xy} , σ^{0}_{yz} , σ^{0}_{zx} , ρ_{steady} , $\Sigma Mstage^{0}$, $\Sigma Mstage$, Sat^{0} , Suc^{0} , ΣMsf^0 , ΣMsf , SatEff, SatRes, Temp, Temp0). Where: SatEff is the effective saturation. Temp0 is the temperature at the beginning of the current step and

Temp is the updated temperature during the step calculation. In 2D calculations

 σ_{vz} and σ_{zx} should be zero.

Swpo Previous excess pore pressure of the current stress point}

StVaro = Array(1..nStat) with previous values of state variables of the current stress

point

dEps Array(1..12) with strain increments of the current stress point in the current step

 $(\Delta\varepsilon_{xx}, \Delta\varepsilon_{yy}, \Delta\varepsilon_{zz}, \Delta\gamma_{xy}, \Delta\gamma_{yz}, \Delta\gamma_{zx}, \varepsilon_{xx}^{0}, \varepsilon_{yy}^{0}, \varepsilon_{zz}^{0}, \gamma_{xy}^{0}, \gamma_{yz}^{0}, \gamma_{zx}^{0})$. In 2D calculations $\Delta\gamma_{yz}$, $\Delta\gamma_{zx}$, γ_{yz}^{0} and γ_{zx}^{0} should be zero. In PLAXIS 2D this array

may also contain non-local strains. Contact PLAXIS for more details.

DEffective material stiffness matrix of the current stress point (1..6, 1..6)

 $Bulk_W =$ Bulk modulus of water for the current stress point (for undrained calculations

and consolidation)

Sig Array (1..6) with resulting constitutive stresses of the current stress point (σ'_{xx})

 σ'_{VV} , σ'_{ZZ} , σ'_{XV} , σ'_{VZ} , σ'_{ZX})

Swp Resulting excess pore pressure of the current stress point

StVar Array(1..nStat) with resulting values of state variables for the current stress

point

ipl Plasticity indicator: 0 = no plasticity, 1 = Mohr-Coulomb (failure) point; 2 =

Tension cut-off point, 3 = Cap hardening point, 4 = Cap friction point, 5 =

Friction hardening point, 6 = Plotting liquefaction indicators.

nStat Number of state variables (unlimited) NonSym= Parameter indicating whether the material stiffness matrix is non-symmetric (NonSym = 1) or not (NonSym = 0) (required for matrix storage and solution). iStrsDep= Parameter indicating whether the material stiffness matrix is stress-dependent (iStrsDep = 1) or not (iStrsDep = 0). iTimeDe₽ Parameter indicating whether the material stiffness matrix is time-dependent (iTimeDep = 1) or not (iTimeDep = 0). iTang =Parameter indicating whether the material stiffness matrix is a tangent stiffness matrix, to be used in a full Newton-Raphson iteration process (iTang = 1) or not (iTanq = 0).iPrjDir =Project directory (for debugging purposes) iPrjLen =Length of project directory name (for debugging purposes) *iAbort* = Parameter forcing the calculation to stop (iAbort = 1).

In the above, 'increment' means 'the total contribution within the current step' and not per iteration. 'Previous' means 'at the start of the current step', which is equal to the value at the end of the previous step.

In the terminology of the above parameters it is assumed that the standard type of parameters is used, i.e. parameters beginning with the characters A-H and O-Z are double (8-byte) floating point values and the remaining parameters are 4-byte integer values.

The parameters IDTask to dEps and iPrjDir and iPrjLen are input parameters; The values of these parameters are provided by PLAXIS and can be used within the subroutine. These input parameters should not be modified (except for StVar0 in case IDTask= 1). The parameters D to iTang and iAbort are output parameters. The values of these parameters are to be determined by the user. In case IDTask = 1. StVar0 becomes output parameter.

The user subroutine should contain program code for listing the tasks and output parameters IDTask= 1 to 6). After the declaration of variables, the *User_Mod* subroutine must have the following structure (here specified in pseudo code):

```
Case IDTask of
   1 Begin
        { Initialise state Variable StVar }
   2 Begin
        { Calculate constitutive stresses Sig (and Swp) }
   3 Begin
        { Create effective material stiffness matrix D }
     End
   4 Begin
        { Return the number of state variables nStat }
   5 Begin
        { Return matrix attributes NonSym, iStrsDep, iTimeDep }
     End
   6 Begin
        { Create elastic material stiffness matrix De }
     End
End Case
```

If more than one UD model is considered, distinction should be made between different models, indicated by the UD model number iMod.

16.2.1.1 *Initialise state variables (IDTask = 1)*

State variables (also called the hardening parameters) are, for example, used in hardening models to indicate the current position of the yield loci. The update of state variables is considered in the calculation of constitutive stresses based on the previous value of the state variables and the new stress state. Hence, it is necessary to know about the initial value of the state variables, i.e. the value at the beginning of the calculation step. Within a continuous calculation phase, state variables are automatically transferred from one calculation step to another. The resulting value of the state variable in the previous step, StVar, is stored in the output files and automatically used as the initial value in the current step, StVar0. When starting a new calculation phase, the initial value of the state variables is read from the output file of the previous calculation step and put in the StVarO array. In this case it is not necessary to modify the StVar0 array.

However, if the previous calculation step does not contain information on the state variables (for example in the very first calculation step), the StVarO array would contain zeros. For this case the initial value has to be calculated based on the actual conditions (actual stress state) at the beginning of the step. Consider, for example, the situation where the first state variable is the minimum mean effective stress, p' (considering that compression is negative). If the initial stresses have been generated using the K_0 -procedure, then the initial effective stresses are non-zero, but the initial value of the state variable is zero, because the initialization of this userdefined variable is not considered in the K_0 -procedure. In this case, part 1 of the user subroutine may look like:

```
1 Begin
 { Initialise stage variables StVar()}
 p = (SIg0[1] + Sig0[2] + Sig0[3]) /3.0
StVar0[1] = Min(StVar0[1], p)
End
```

16.2.1.2 | Calculate constitutive stresses (IDTask = 2)

This task constitutes the main part of the user subroutine in which the stress integration and correction are performed according to the user-defined soil model formulation. Let us consider a simple example using a linear elastic D-matrix as created under IDTask = 3.

In this case the stress components, Sig, can directly be calculated from the initial stresses, Sig0, the material stiffness matrix, D, and the strain increments, dEps: Sig[i] = Sig0[i] + Σ (D[i, i]*dEps[i]). In this case, part 2 of the user subroutine may look like:

```
2 Begin
       { Calculate constitutive stresses Sig (and Swp) }
  For i=1 to 6 do
   Sig[i] = Sig0[i]
For j=1 to 6 do
Sig[i] = Sig[i] + D[i,j]*dEps[j]
   End for{j}
  End for {i}
 End
```

16.2.1.3 Create effective material stiffness matrix (IDTask = 3

The material stiffness matrix, D, may be a matrix containing only the elastic components of the stress-strain relationship (as it is the case for the existing soil models in PLAXIS), or the full elastoplastic material stiffness matrix (tangent stiffness matrix). Let us consider the very simple example of Hooke's law of isotropic linear elasticity. There are only two model parameters involved: Young's modulus, E, and Poisson's ratio, v. These parameters are stored, respectively, in position 1 and 2 of the model parameters array, Props(1..50). In this case, part 3 of the user subroutine may look like:

```
3 Begin
   { Calculate effective material stiffness matrix D }
   E = Props[1]
   v = Props[2]
   G = 0.5 \times E/(1.0+v)
   Fac = 2*G/(1.0-2*v){ make sure that v<0.5!!}
   Term1 = Fac*(1-v)
   Term2 = Fac*v
   D[1,1] = Term1
   D[1,2] = Term2
   D[1,3] = Term2
   D[2,1] = Term2
   D[2,2] = Term1
   D[2,3] = Term2
   D[3,1] = Term2
   D[3,2] = Term2
   D[3,3] = Term1
   D[4,4] = G
   D[5,5] = G
   D[6,6] = G
 End
```

(By default, D will be initialised to zero, so the remaining terms are still zero; however, it is a good habit to explicitly define zero terms as well.)

If undrained behaviour is considered (IsUndr = 1), then a bulk stiffness for water (Bulk_W) must be specified at the end of part 3. After calling the user subroutine with IDTask = 3 and IsUndr = 1, PLAXIS will automatically add the stiffness of the water to the material stiffness matrix D such that: D[i=1..3, j=1..3] = D[i, j]+ Bulk_W. If Bulk_W is not specified, PLAXIS will give it a default value of 100*Avg(D[i=1..3, j=1..3]).

16.2.1.4 Return the number of state variables (IDTask = 4)

This part of the user subroutine returns the parameter nStat, i.e. the number of state variables. In the case of just a single state parameter, the user subroutine should look like:

```
{ Return the number of state variables nStat }
nStat = 1
End
```

16.2.1.5 Return matrix attributes (IDTask = 5)

The material stiffness matrix may be stress-dependent (such as in the Hardening Soil model) or time-dependent (such as in the Soft Soil Creep model). When using a tangent stiffness matrix, the matrix may even be non-symmetric, for example in the case of non-associated plasticity. The last part of the user subroutine is used to initialize the matrix attributes in order to update and store the global stiffness matrix properly during the calculation process. For the simple example of Hooke's law, as described earlier, the matrix is symmetric and neither stress- nor time-dependent. In this case the user subroutine may be written as:

```
5 Begin
  { Keturn the matrix attributes NonSym, IStrsDep, }
  { iTimeDep, iTang }
  NonSym = 0
  iStrsDep = 0
  iTimeDep = 0
  iTanq = 0
 End
```

For NonSym = 0 only half of the global stiffness matrix is stored using a profile structure, whereas for Nonsym = 1 the full matrix profile is stored.

For iStrsDep = 1 the global stiffness matrix is created and decomposed at the beginning of each calculation step based on the actual stress state (modified Newton-Raphson procedure).

For iTimeDep = 1 the global stiffness matrix is created and decomposed every time when the time step changes.

For iTang = 1 the global stiffness matrix is created and decomposed at the beginning of each iteration based on the actual stress state (full Newton-Raphson procedure; to be used in combination with iStrsDep=1).

16.2.1.6 | Create elastic material stiffness matrix (IDTask = 6)

The elastic material stiffness matrix, D^e , is the elastic part of the effective material stiffness matrix as described earlier.

In the case that the effective material stiffness matrix was taken to be the elastic stiffness matrix. this matrix may just be adopted here. However in the case that an elastoplastic or tangent matrix was used for the effective stiffness matrix, then the matrix to be created here should only contain the elastic components.

The reason that an elastic material stiffness matrix is required is because PLAXIS calculates the current relative global stiffness of the finite element model as a whole (CSP = Current Stiffness Parameter). The CSP parameter is defined as:

$$CSP = rac{Total\ work}{Total\ elastic\ work}$$
 (16–1)

The elastic material stiffness matrix is required to calculate the total elastic work in the definition of the CSP. The CSP equals unity if all the material is elastic whereas it gradually reduces to zero when failure is approached.

The CSP parameter is used in the calculation of the global error. The global error is defined as:

$$Global\ error = \frac{|unbalance\ force|}{|currently\ activated\ load| + CSP.\ |previously\ activated\ load|} \tag{16-2}$$

The unbalance force is the difference between the external forces and the internal reactions. The currently activated load is the load that is being activated in the current calculation phase, whereas the previously activated load is the load that has been activated in previous calculation phases and that is still active in the current phase.

Using the above definition for the global error in combination with a fixed tolerated error results in an improved equilibrium situation when plasticity increases or failure is approached. The idea is that a small out-of-balance is not a problem when a situation is mostly elastic, but in order to accurately calculate failure state, safety factor or bearing capacity, a stricter equilibrium condition must be adopted.

Part 6 of the user subroutine looks very similar to part 3, except that only elastic components are considered here. It should be noted that the same variable D is used to store the elastic material stiffness matrix, whereas in Part 3 this variable is used to store the effective material stiffness matrix.

```
6 Begin
   { Create elastic material stiffness matrix D }
   D[1,1]
   D[1,2]
   D[1,3]
  D[6,6]
  End
```

16.2.2 Using predefined subroutines from the source code

In order to simplify the creation of user subroutines, a number of FORTRAN subroutines and functions for vector and matrix operations are available in the source code (to be included in the file with the user subroutine). The available subroutines may be called by User Mod subroutine to shorten the code. An overview of the available subroutines is given in C Modelling of embedded structures (p. 251).

16.2.3 Definition of user-interface functions

In addition to the user-defined model itself it is possible to define functions that will facilitate its use within the PLAXIS user-interface. If available, PLAXIS Input will retrieve information about the model and its parameters using the procedures described hereafter.

```
procedure GetModelCount(var C:longint) ;
C
              number of models (return parameter)
```

This procedure retrieves the number of models that have been defined in the DLL. PLAXIS assumes that model IDs are successive starting at model ID = 1.

```
procedure GetModelName(var iModel : longint;
               var Name : shortstring) ;
iModel =
              User-defined soil model number to retrieve the name for (input parameter)}
Name =
              Model name (return parameter)
```

This procedure retrieves the names of the models defined in the DLL.

```
procedure GetParamCount(var iModel : longint; var C: longint) ;
```

iModel = User-defined soil model number (input parameter)

Cnumber of parameters for the specified model (return parameter)

This procedure retrieves the parameter name of a specific model.

```
Procedure GetParamName(var iModel,iParam : longint;
              var Name : shortstring);
```

iModel = User-defined soil model number (input parameter)

iParam =Parameter number (input parameter)

Name = parameter name (return parameter)

This procedure retrieves the parameter name of a specific parameter.

```
Procedure GetParamUnit(var iModel,iParam : longint;
              var Units : shortstring)
```

iModel = User-defined soil model number (input parameter)

iParam =Parameter number (input parameter)

Units Parameter units (return parameter)

This procedure retrieves the parameter units of a specific parameter. Since the chosen units are dependent on the units of length, force and time chosen by the user the following characters should be used for defining parameter units:

'L' or 'l' for units of length 'F' or 'f' for units of force 'T' or 't' for units of time.

For model names, model parameter names and model parameter units special characters can be used for indicating subscript, superscript or symbol font (for instance for Greek characters).

Symbol	Description
^	From here characters will be superscript
_	From here characters will be subscript
@	From here characters will be in symbol font
#	Ends the current superscript or subscript.

Pairs of '^..#','_...#' and '@...#' can be nested.

For example:

A UD model parameter uses the oedometer stiffness as parameter. The parameter name can be defined as 'E_oed#' and its units as 'F/L^2#'.

When defining a unit containing one of the letters 'I', 'f' or 't', like ' cal/mol', these letters will be replaced by the unit of length, the unit of force or the unit of time respectively. To avoid this,

these letters should be preceded by a backslash. For example 'cal/mol' should be defined as ' ca\I/mo\I' to avoid getting 'cam/mom'.

The state variables to be displayed in the Output program can be defined.

```
procedure GetStateVarCount(var iModel : longint; var C :longint) ;
```

iModel = User-defined soil model number (input parameter)

Cnumber of state variables for the specified model (return parameter)

This procedure retrieves the number of state variables of a specific model.

```
procedure GetStateVarName(var iModel,iParam : longint;
                       var Name : shortstring);
```

iModel = Used-defined soil model number (input parameter)

iParam =Parameter number (input parameter)

Name = Parameter name (return parameter)

This procedure retrieves the state parameter name of a specific parameter.

```
Procedure GetStateVArUnit(var iModel,iParam : longint;
                       var Units : shortstring) ;
```

iModel = User-defined soil model number (input parameter)

iParam = Parameter number (input parameter)

Units Parameter units (return parameter)

This procedure retrieves the state parameter units of a specific parameter.

All procedures are defined in Pascal but equivalent procedures can be created, for instance in a Fortran programming language. Please make sure that the data format of the parameters in the subroutine headers is identical to those formulated before. For instance, the procedures mentioned above use a "shorstring" type; a" shortstring" is an array of 256 characters where the first character contains the actual length of the shortstring contents. Some programming languages only have null-terminated strings; in this case it may be necessary to use an array of 256 bytes representing the ASCII values of the characters to return names and units. An example of Fortran subroutines is included in the software package.

16.2.4 UDSM additional information

To allow the use of some specific options as required and passed by the PLAXIS calculation program, the following subroutine can optionally be defined within the UDSM implementation:

```
Subroutine setDLLExtraInfo( iInfo, rInfo )
```

iinfo array of integers containing the following data:

- iinfo(1): "Special option" specified value (see Special option for User Defined Soil Models [ADV] of the Reference manual).
- iInfo(2): temperature measure unit, being 1: K, 2: °C, 3: °F.

- ilnfo(3): length measure unit, being 1: mm, 2: cm, 3: m, 4: km, 5: in, 6: ft, 7: vd.
- iInfo(4): force measure unit, being 1: N, 2: KN, 3: MN, 4: lbf, 5: kip.
- iInfo(5): time measure unit, being 1: sec, 2: min, 3: hour, 4: day.

rInfo array of floating points, currently not used.

The main purpose of this subroutine is to offer to users implementing a UDSM a way to retrieve and store (e.g. in a module) the measure units adopted at the same time by the PLAXIS calculation kernel and therefore comply with these or transform to and from these within the UDSM implementation.

16.2.5 Compiling the user subroutine

The user subroutine User_Mod has to be compiled into a DLL file using an appropriate compiler. Note that the compiler must have the option for compiling DLL files. Below are examples for two different FORTRAN compilers. It is supposed that the user subroutine User Mod is contained in the file USRMOD.FOR.

After creating the user subroutine User_Mod, a command must be included to export data to the DLL. 64-bit compiler must be used.

The following statement has to be inserted in the subroutine just after the declaration of variables:

Using GNU Fortran:

```
!DEC$ATTRIBUTES DLLExport :: User Mod
```

Using Intel Visual Fortran:

```
!DEC$ ATTRIBUTES DLLExport, StdCall, Reference :: User Mod
```

In order to compile the USRMOD.FOR into a DLL file, the following command must be executed:

Using GNU Fortran:

```
gfortran USRMOD.FOR -o usermod64.dll -shared -fno-underscoring -static
```

• Using Intel Visual Fortran:

```
ifort /winapp USRMOD.FOR DFUsrLib.lib /dll
```

In all cases USRMOD64.DLL file will be created. It can be renamed to 'any64' .dll. This file should be placed in the usdm folder under the PLAXIS program directory, thereafter it can be used together with the existing PLAXIS calculations program (PLASW.EXE in PLAXIS 2D or PLASW3DF.EXE in PLAXIS 3D). Once the User-defined Soil Model is used, PLAXIS will execute the commands as listed in the USRMOD64.DLL file.

16.2.6 Debugging possibilities

When making computer programs, usually some time is spent to 'debug' earlier written source code. In order to be able to effectively debug the user subroutine, there should be a possibility for the user to write any kind of data to a file. Such a 'debug-file' is not automatically available and has to be created in the user subroutine.

After the debug-file is created, data can be written to this file from within the user subroutine. This can be done by using, for example, the availably written subroutines (D Fortran subroutines for User-defined soil models (p. 253)).

16.3 Input of UD model parameters via userinterface

Input of the model parameters for user-defined soil models can be done using the PLAXIS material data base. In fact, the procedure is very similar to the input of parameters for the existing PLAXIS models.

When creating a new material data set for soil and interfaces in the material data base, a window appears with six tabsheets: General, Mechanical, Groundwater, Thermal, Interfaces, Initial Figure 16–1 (p. 187). A user-defined model can be selected from the Material model combo box in the General tabsheet.

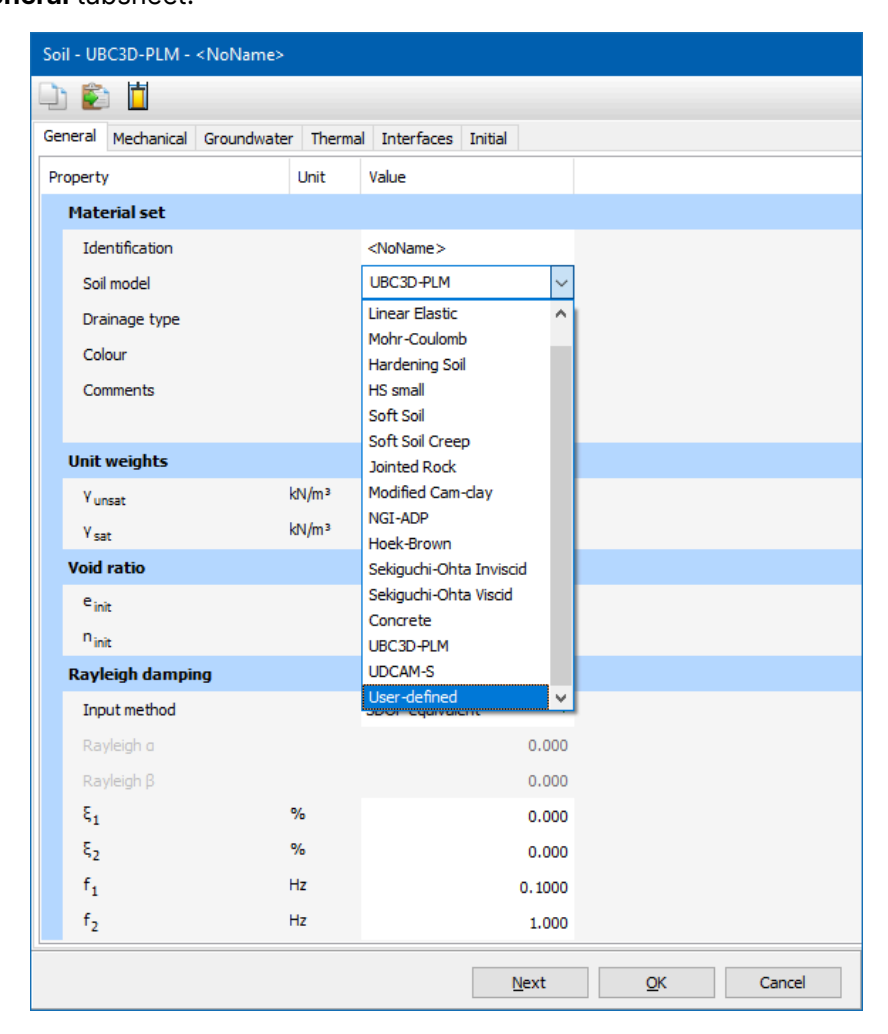


Figure 16–1: Selection Window. Selection of user-defined soil models

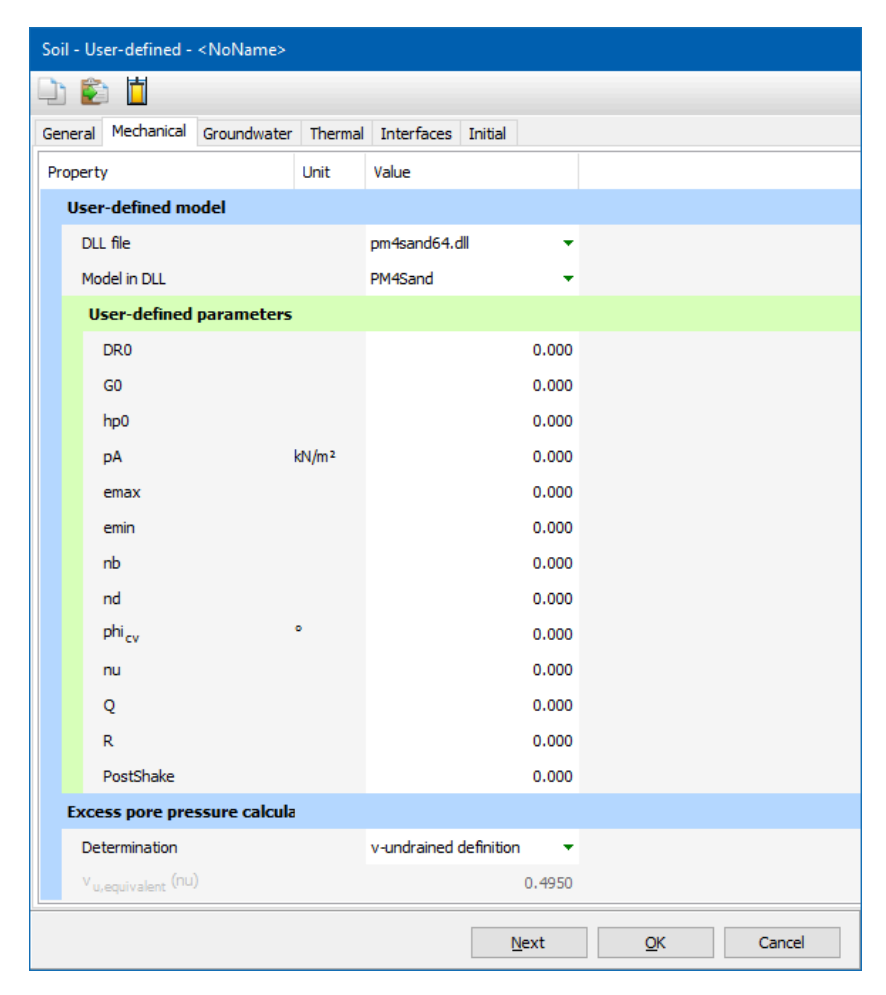


Figure 16-2: Selection window. Input of parameters

After inputting general properties, the appropriate UD model can be chosen from the available models that have been found by PLAXIS Input.

The Mechanical tabsheet shows two combo boxes; the top combo box lists all the DLLs that contain valid UD models and the next combo box shows the models defined in the selected DLL. Each UD model has its own set of model parameters, defined in the same DLL that contains the model definition.

When an available model is chosen PLAXIS will automatically read its parameter names and units from the DLL and fill the parameter table below.

16.3.1 Interfaces

The Interfaces tabsheet, Figure 16–3 (p. 189), contains the material data for interfaces.

Normally, this tabsheet contains the R_{inter} parameter. For user-defined soil models the interface tabsheet is slightly different as for a user-defined soil model the interface properties cannot be taken from the material set, but should be explicitly defined. The stiffness can be specified in 2 ways through the Stiffness determination parameter: either a Direct specification of the interface stiffness parameters k_n and k_s , or by specification of the interface stiffness from the oedometer stiffness modulus, E_{oed}^{ref} . Additionally, the interface strength parameters c_{inter} , ϕ_{inter} and ψ_{inter}

must be specified. Hence, the interface shear strength is directly given in strength parameters instead of using a factor relating the interface shear strength to the soil shear strength, as it is the case in PLAXIS models.

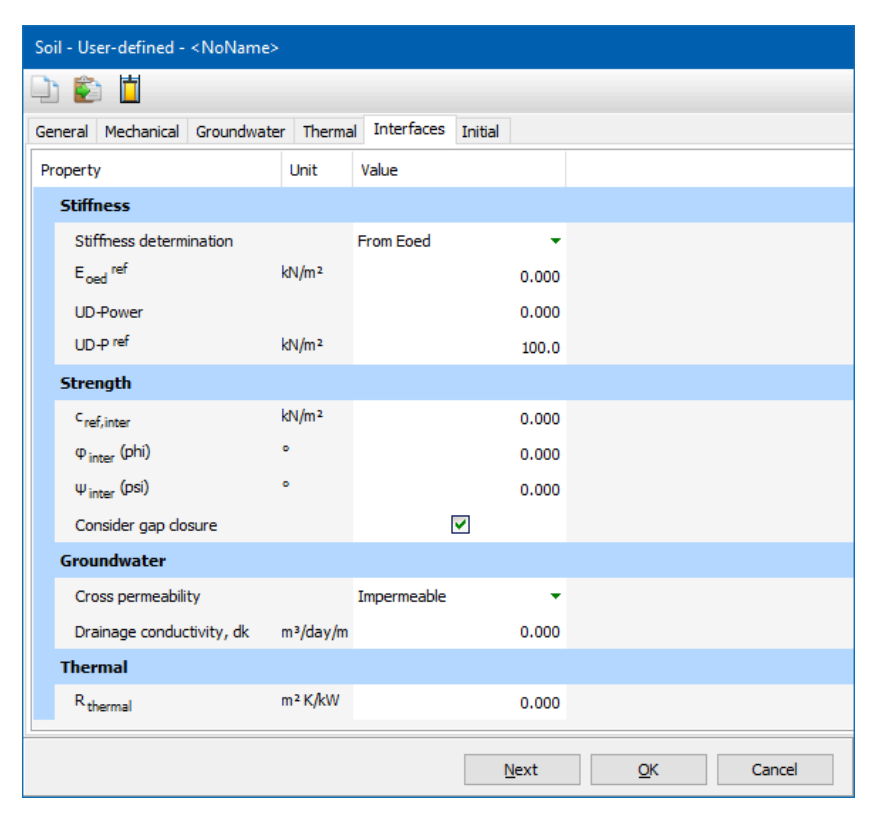


Figure 16-3: Interface tabsheet

In addition, two parameters are included to enable stress-dependency of the interface stiffness according to a power law formulation:

$$E_{oed}\left(\sigma_{n}^{'}\right)=E_{oed}^{ref}\left(rac{\sigma_{n}^{'}}{UD-P^{ref}}
ight)^{UD-Power}$$
 (16–3)

where

 $UD ext{-}Pow$ er Rate of stress dependency of the interface stiffness

UD- p^{ref} = Reference stress level (usually 100 kN/m²)

 σ'_n Effective normal stress in the interface stress point.

After having entered values for all parameters, the data sets can be assigned to the corresponding soil clusters, in a similar way as for the existing material models in PLAXIS. The user-defined parameters are transmitted to the calculation program and appear for the appropriate stress points as Props(1..50) in the User Mod subroutine.

Application of advanced soil models

In this chapter, advanced soil models will be utilised in various applications in order to illustrate the particular features of these models.

17.1 Hardening Soil model: Response in drained and undrained triaxial tests

In this section, the Hardening Soil model is utilised for the simulations of drained and undrained triaxial tests. Arbitrary sets of model parameters, <u>Table 17–1 (p. 190)</u>, representing sands of different properties, are considered.

Table 17-1: Arbitrary Hardening Soil parameters for sands of different densities

Parameter	Loose	Medium	Dense	Unit
E_{50}^{ref} (for p_{ref} = 100 kPa)	20000	30000	40000	[kN/m ²]
E _{ur} ^{ref} (for p _{ref} = 100 kPa)	60000	90000	120000	[kN/m ²]
E_{oed}^{ref} (for p_{ref} = 100 kPa)	20000	30000	40000	[kN/m ²]
Cohesion c	0.0	0.0	0.0	[kN/m ²]

Parameter	Loose	Medium	Dense	Unit
Friction angle ϕ	30	35	40	0
Dilatancy angle ψ	0	5	10	0
Poisson's ratio v _{ur}	0.2	0.2	0.2	-
Power m	0.5	0.5	0.5	-
K_0^{nc} (using Cap)	0.5	0.43	0.36	-
Tensile strength	0.0	0.0	0.0	[kN/m ²]
Failure ratio	0.9	0.9	0.9	-

A triaxial test can simply be modelled by means of an axisymmetric geometry of unit dimensions (1m x 1m), that represent a quarter of the soil specimen, Figure 17-1 (p. 191). These dimensions are not realistic, but they are selected for simplicity. The dimension of the model does not influence the results, provided that the soil weight is not taken into account. In this configuration the stresses and strains are uniformly distributed over the geometry. The deformation magnitudes in x- and y-direction of the top right hand corner correspond to the horizontal and vertical strains respectively.

The left hand side and the bottom of the geometry are axes of symmetry. At these boundaries the displacements normal to the boundary are fixed and the tangential displacements are kept free to allow for 'smooth' movements. The remaining boundaries are fully free to move.

The value of the applied loads can be controlled by the load multipliers such as $\Sigma MloadA$ and SMIoadB. However, in PLAXIS 2DPLAXIS 3D, and as described in the Reference Manual , the load configurations and magnitudes can be specified in the Input program. Then in the calculation program these loads can be activated or deactivated by means of the Staged construction option. For this case, and to simulate the confining pressure p', distributed loads of -100 kN/m² representing the principal stresses σ'_1 (load A) and σ'_3 (load B) are applied in the Input, as shown in Figure 17-1 (p. 191).

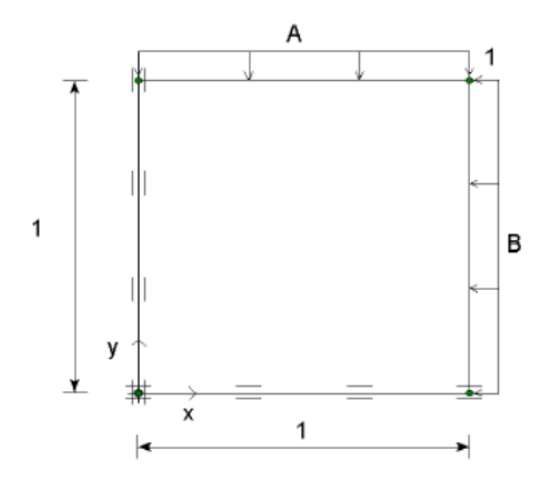


Figure 17-1: Simplified configuration of a triaxial test

A very course mesh is sufficient for this simple analysis. Initial stresses and steady pore pressures are not taken into account.

In the calculation program, the calculation of all phases can be done by means of the Staged **construction** process. In the first phase, the confinement pressure p' is applied by activating

load A and B. In the second phase the displacements are reset to zero and the sample is vertically loaded up to failure while the horizontal load is kept constant. This implies modification of load A by double clicking the load in the geometry model. As a result a load window appears in which the input values of the load can be changed. (Details of the procedure can be found in the Reference and Tutorial manuals). The latter phase is carried out for drained as well as undrained conditions.

These calculations are performed for the three different sets of material parameters, Table 17-1 (p. 190). The computational results are presented in the figures on the following pages.

Figure 17-2 (p. 192) shows the principal stress difference versus the axial strain for the drained condition. This shows a hyperbolic relationship between the stress and the strain, which is typical for the Hardening Soil model. Obviously, the failure level is higher when the sand is denser. The Hardening Soil model does not include softening behaviour, so after reaching failure the stress level does not reduce, at least in the drained tests.

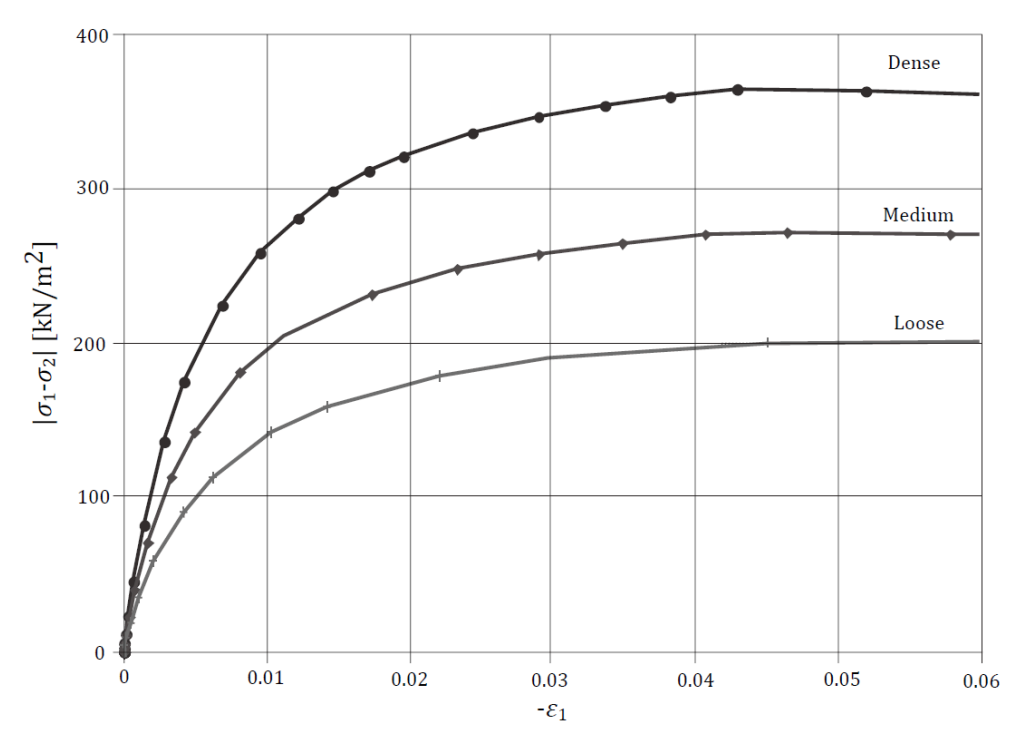


Figure 17-2: Results of drained triaxial tests using the Hardening Soil model, Principal stress difference versus axial strain.

Figure 17-3 (p. 193) shows the axial strain versus the volumetric strain for the drained test. This graph clearly shows the influence of dilatancy in the denser sands. In contrast to the Mohr-Coulomb model, the transition from elastic behaviour to failure is much more gradual when using the Hardening Soil model. In fact, in the Hardening Soil model, plastic strain occurs immediately after load application.

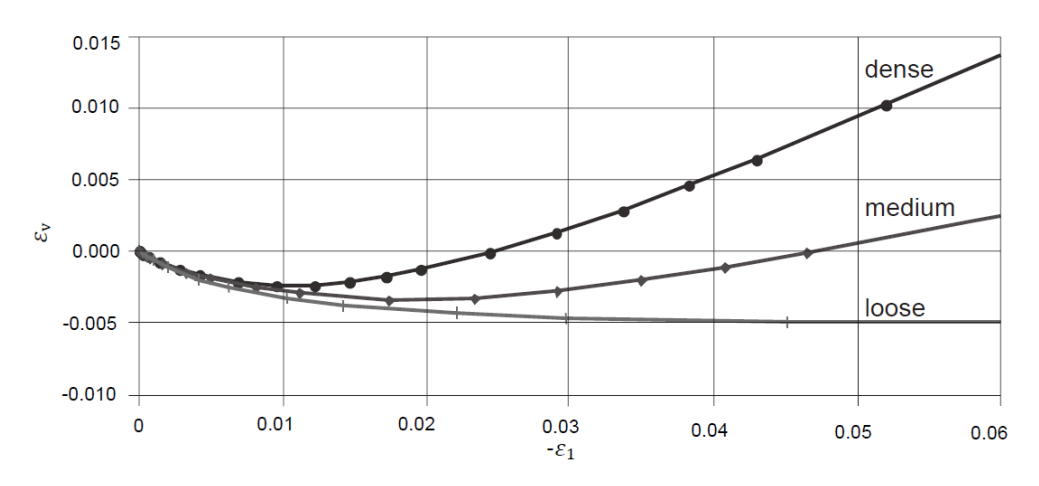


Figure 17-3: Results of drained triaxial tests using the Hardening Soil model, Volumetric strain versus axial strain

In the undrained tests, Figure 17-4 (p. 193), the failure level is, in principle, lower than that of the drained tests. However, for the medium and dense sands the stress level continues to increase after reaching the failure level due to the fact that dilatancy occurs which causes reduction of excess pore pressures and thus increase of the effective stresses. This can be seen in Figure 17-5 (p. 194).

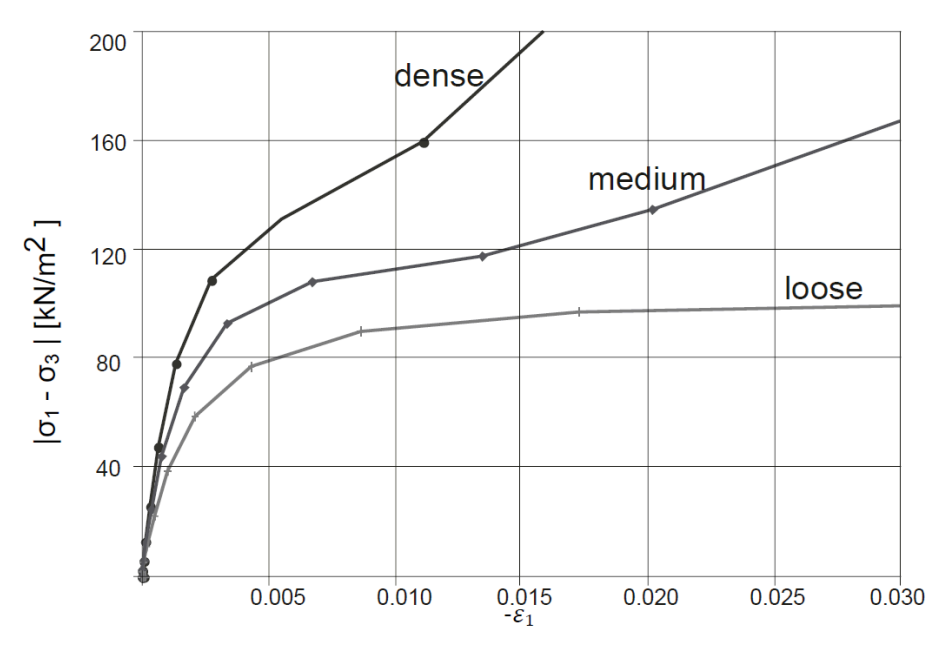


Figure 17-4: Results of undrained triaxial tests using the Hardening Soil model, Principal stress difference versus axial strain

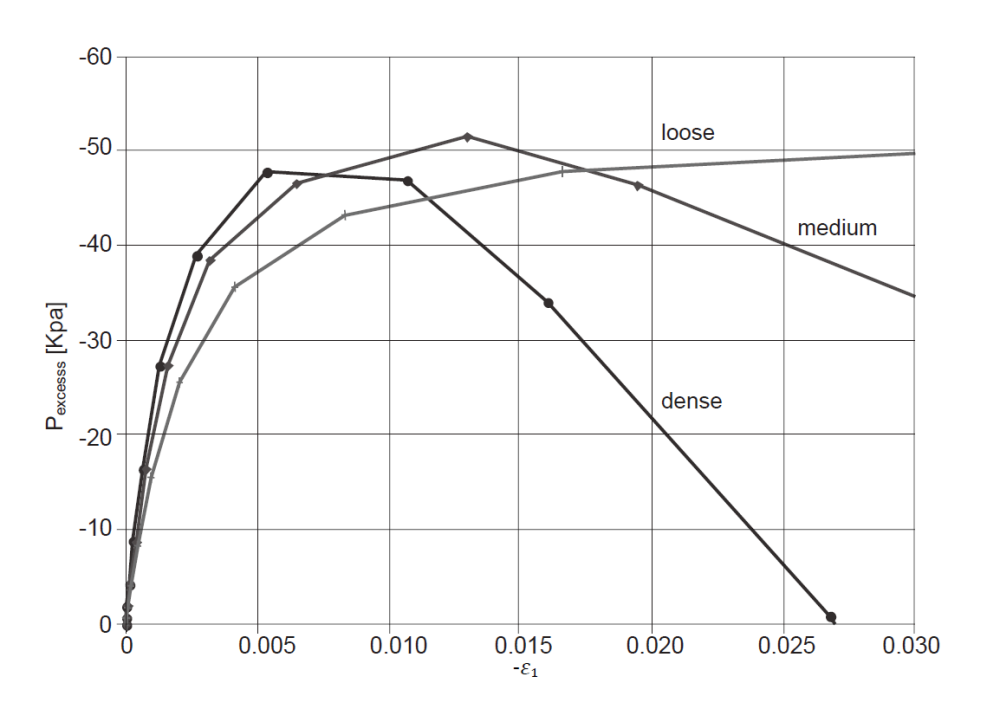


Figure 17-5: Results of undrained triaxial tests using the Hardening Soil model, Excess pore pressure vs axial strain

Figure 17-6 (p. 195) shows the effective stress paths, for the medium sand, during both the drained and undrained tests. During first phase (isotropic loading), both tests were drained. In the second phase there is a clear distinction between the two tests. In the undrained test the effective horizontal stress reduces while the vertical stress increases due to the development of excess pore pressures. The decrease in horizontal effective stress is more than when if the Mohr-Coulomb model would have been used. This is attributed to the plastic compaction (Cap hardening) that occurs in the Hardening Soil model.

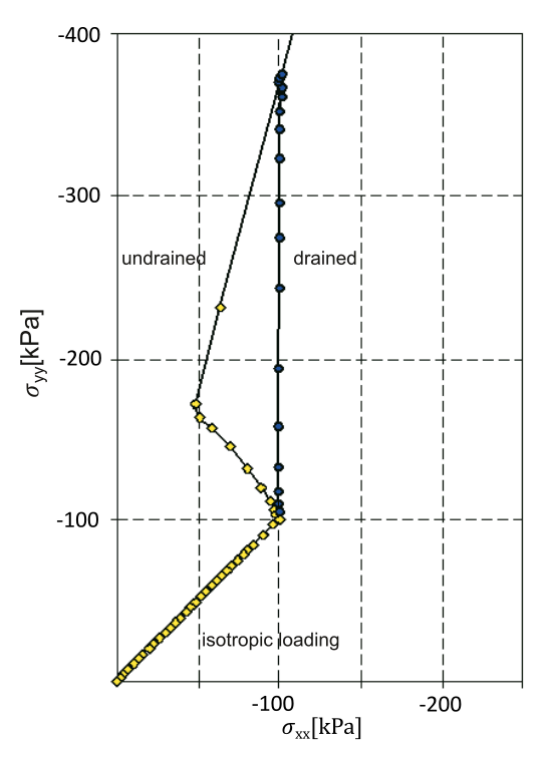


Figure 17-6: Stress paths for drained and undrained triaxial tests using the Hardening Soil model for medium sand

17.2 Application of the Hardening Soil model on real soil tests

In this section the ability of the Hardening Soil model to simulate laboratory tests on sand is examined by comparing PLAXIS calculation results with those obtained from laboratory tests provided by Prof. J. Desrues (University Joseph Fourier, Grenoble, France). Extensive laboratory tests were conducted on loose and dense Hostun sand. On the basis of these tests the model parameters for the Hardening Soil model were determined and they are presented in Table 17-2 (p. 195).

Table 17-2: Hardening Soil parameters for loose and dense Hostun sand

Parameter	Loose sand	Dense sand	Unit
Unit weight γ	17	17.5	kN/m ³
E_{50}^{ref} (p _{ref} = 100 kPa)	20000	37000	kN/m ²
E_{ur}^{ref} (p _{ref} = 100 kPa)	60000	90000	kN/m ²
E _{oed} ^{ref} (p _{ref} = 100 kPa)	16000	29600	kN/m ²
Cohesion c'	0.0	0.0	kN/m ²
Friction angle ϕ'	34.0	41.0	0

Parameter	Loose sand	Dense sand	Unit
Dilatancy angle ψ	0.0	14.0	0
Poisson's ratio v _{ur}	0.2	0.2	-
Power m	0.65	0.5	-
K ₀ ^{nc}	0.44	0.34	-
Tensile strength	0.00	0.00	kN/m ²
Failure ratio	0.9	0.9	-

17.2.1 Triaxial Test

Standard drained triaxial tests were performed on loose and dense sand specimens. The procedure for the simulation of the triaxial tests in PLAXIS has been described in 17.1 Hardening Soil model: Response in drained and undrained triaxial tests (p. 190). In the first phase the sample is isotropically compressed up to a confining pressure of $p' = -300 \text{ kN/m}^2$. In the second phase the sample is vertically loaded up to failure while the horizontal stress (confining pressure) is kept constant. The computational results and the measured data are presented in Figure 17-7 (p. 196) to Figure 17-10 (p. 197).

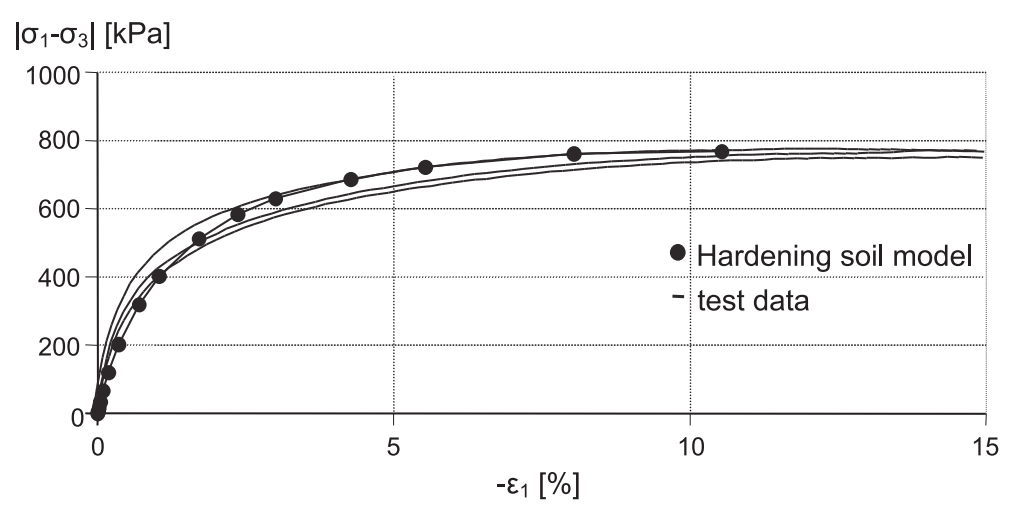


Figure 17-7: Results of drained triaxial tests on loose Hostun sand, deviatoric stress versus axial strain

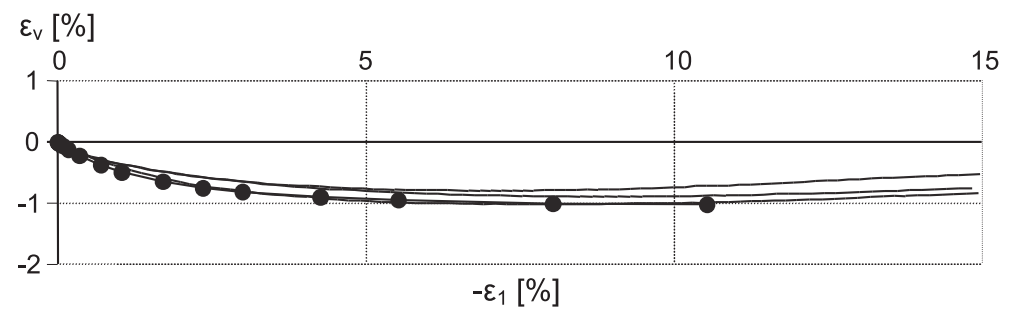


Figure 17-8: Results of drained triaxial tests on loose Hostun sand, volumetric strain versus axial strain

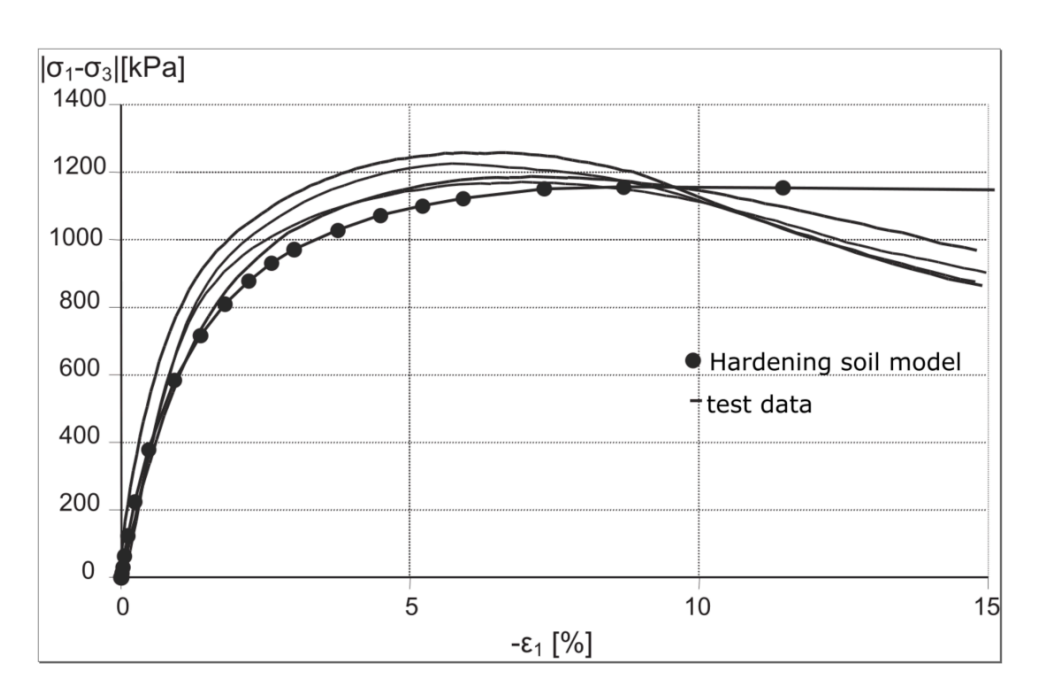


Figure 17-9: Results of drained triaxial tests on dense Hostun sand, deviatoric stress versus axial strain

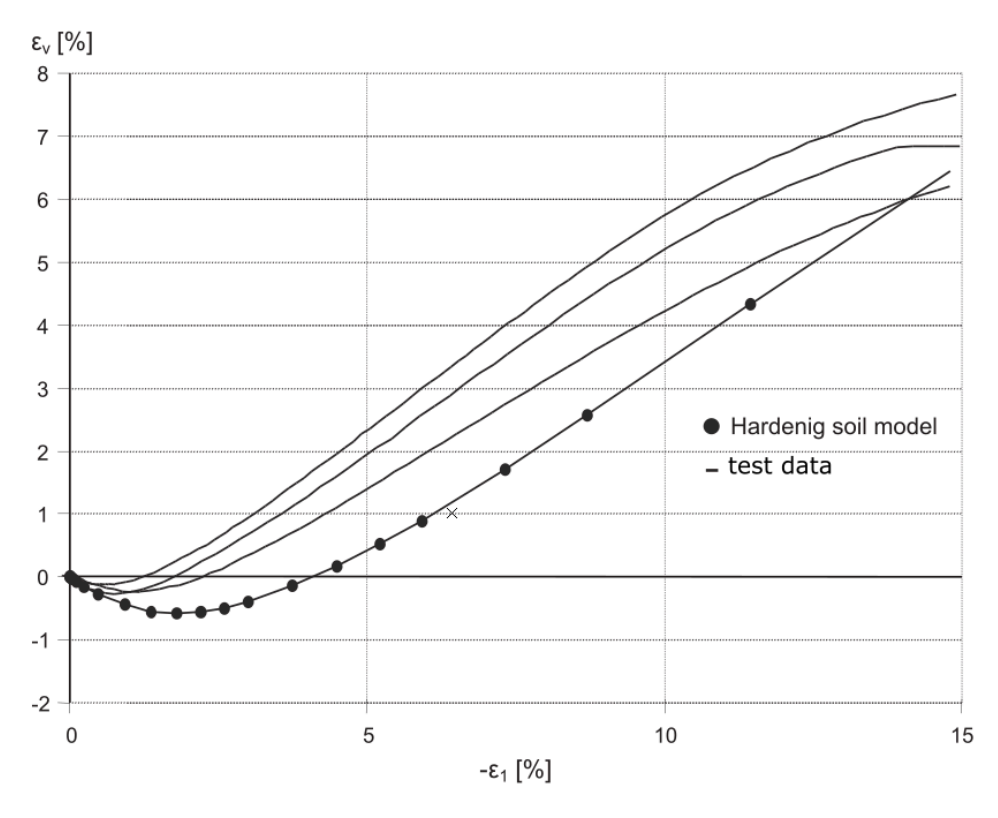


Figure 17-10: Results of drained triaxial tests on dense Hostun sand, volumetric strain versus axial strain

The figures show that the computational results match reasonably with the test data. It can be seen that the material response (measured and computed) show gradual transition from elastic to plastic behaviour. As such the relation between the deviatoric stress and the axial strain can be approximated by a hyperbola.

The failure level is fully controlled by the friction angle (the cohesion is zero). The test results on dense sand show softening behaviour after the peak load has been reached. Modelling of the softening behaviour, however, is not incorporated in the Hardening Soil model, and thus, the deviatoric stress remains constant. It can also be seen from the test data that the dilatancy reduces during softening. However, in the Hardening Soil model the dilatancy continues to infinity, unless the dilatancy cut-off option has been used.

17.2.2 Oedometer test

As for the triaxial tests, a set of oedometer tests on both loose and dense sands (Table 17–2 (p. 195)) was conducted. In PLAXIS 2D the oedometer test is simulated as an axisymmetric geometry with unit dimensions (Figure 17-11 (p. 198)). A coarse mesh is sufficient for this case.

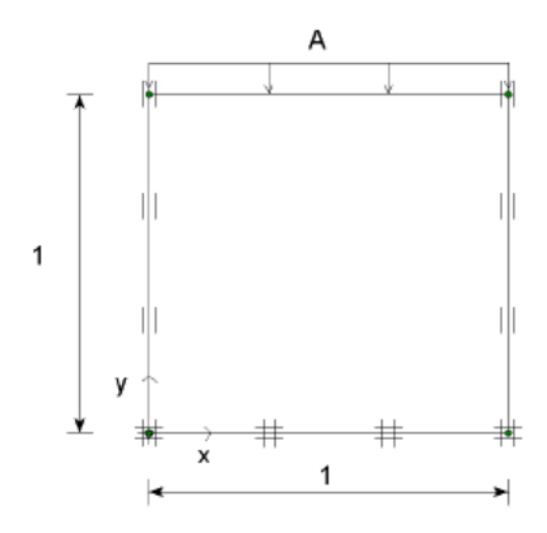


Figure 17–11: Simplified configuration of an oedometer test

The computational results as compared with those obtained from the laboratory tests are shown in Figure 17-12 (p. 199) and Figure 17-13 (p. 199).

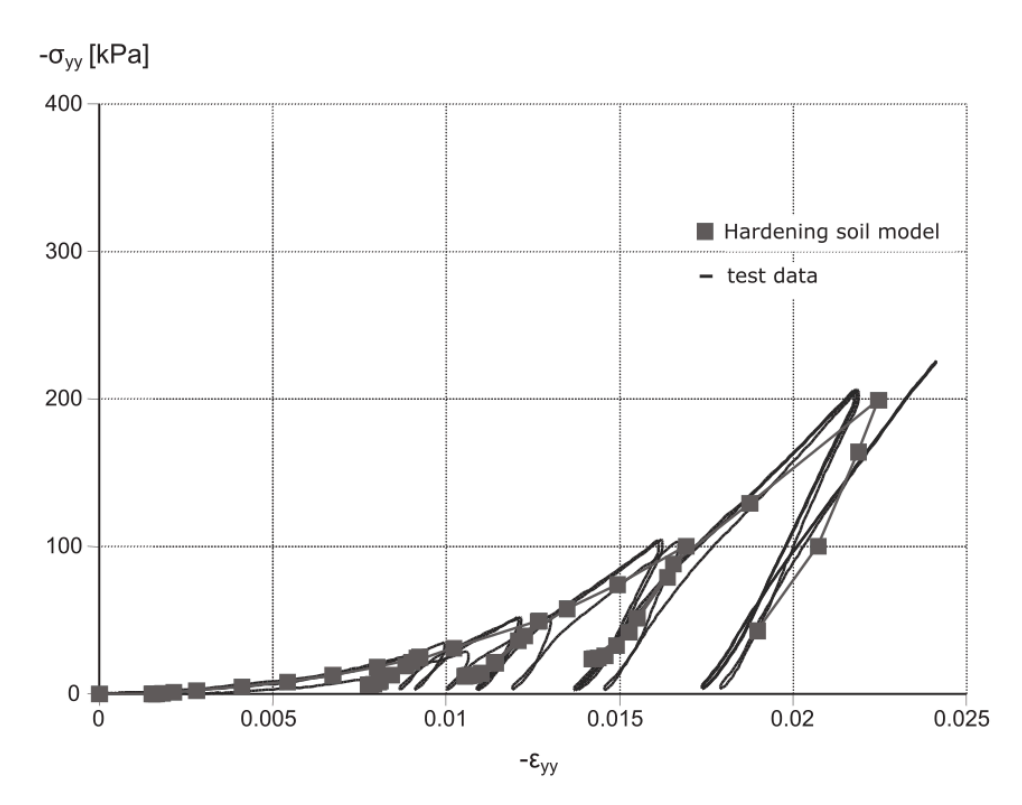


Figure 17-12: Results of oedometer test on loose Hostun sand, axial stress versus axial strain

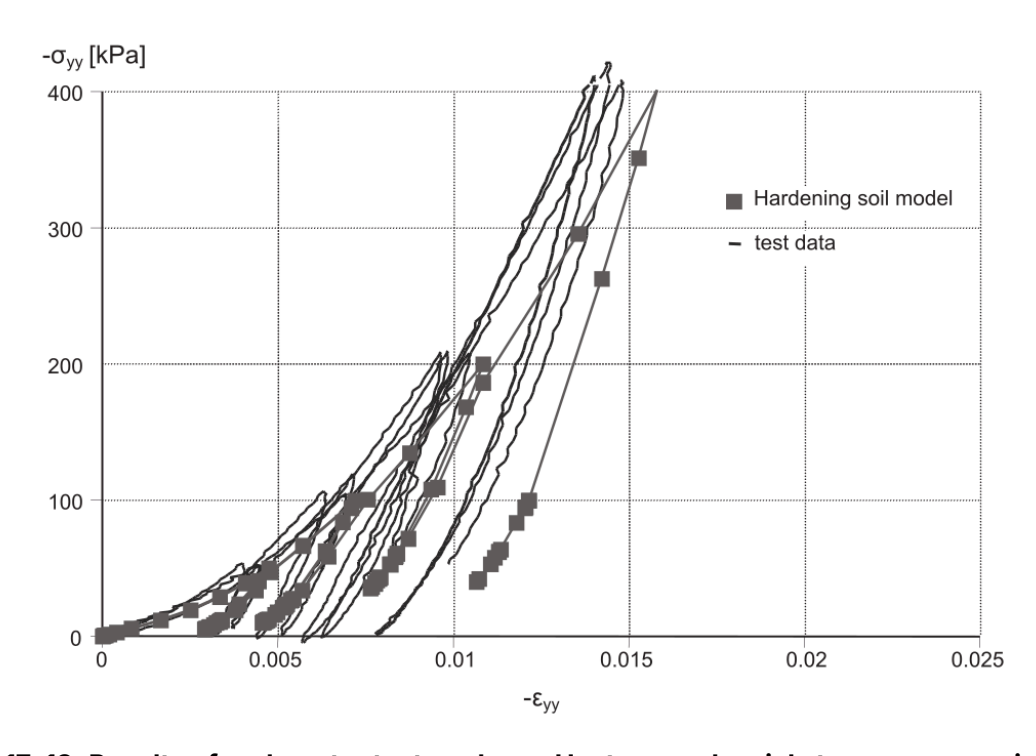


Figure 17-13: Results of oedometer test on dense Hostun sand, axial stress versus axial strain

From a stress free state the loose sand sample is loaded consecutively to 25 kPa, 50 kPa, 100 kPa and 200 kPa with intermediate unloading. The dense sand sample is loaded to 50 kPa, 100 kPa, 200 kPa and 400 kPa with intermediate unloading.

As it can be seen, the computational results show a reasonable agreement with the test data. No doubt, distinction should be made between loose and dense soil, but it seems that for a soil with

a certain density the stiffness behaviour under different stress paths can be well captured with a single set of model parameters. (A small offset of 0.15% has been applied to the computational results of the loose sample in order to account for the relative soft response at the beginning of the test.)

17.2.3 Pressiometer test

In this section the Pressiometer test is simulated and results from PLAXIS 2DPLAXIS 3D and laboratory tests (Branque, 1997) are compared. Laboratory testing results on dense sand with material parameters listed in Table 17–2 (p. 195) are used.

In the field, the pressiometer of 0.044 m diameter covered with a membrane of 0.16 m height is attached to the Cone penetration shaft. In the laboratory, the pressiometer is attached to a 0.044 m pipe ($r_0 = 0.022$ m) and placed in a circular calibration chamber with a diameter of 1.2 m and a height of 1.50 m. A high overburden pressure of 500 kPa is applied to the surface to simulate the stress state at larger depths.

In PLAXIS 2D a quarter of the geometry is simulated by an axisymmetric model (Figure 17-14 (p. 200)). The left boundary is placed 0.022 m away from the vertical axis of symmetry. A line displacement is generated at the left model boundary, set to be free in vertical direction and fixed in horizontal direction. The overburden pressure is simulated by the load A, and the volumetric expansion of the pressiometer is simulated by imposing a horizontally distributed load, load B (Figure 17-14 (p. 200)). Therefore the initial boundary conditions have to be changed at the level of the pressiometer in order to allow for horizontal displacements.

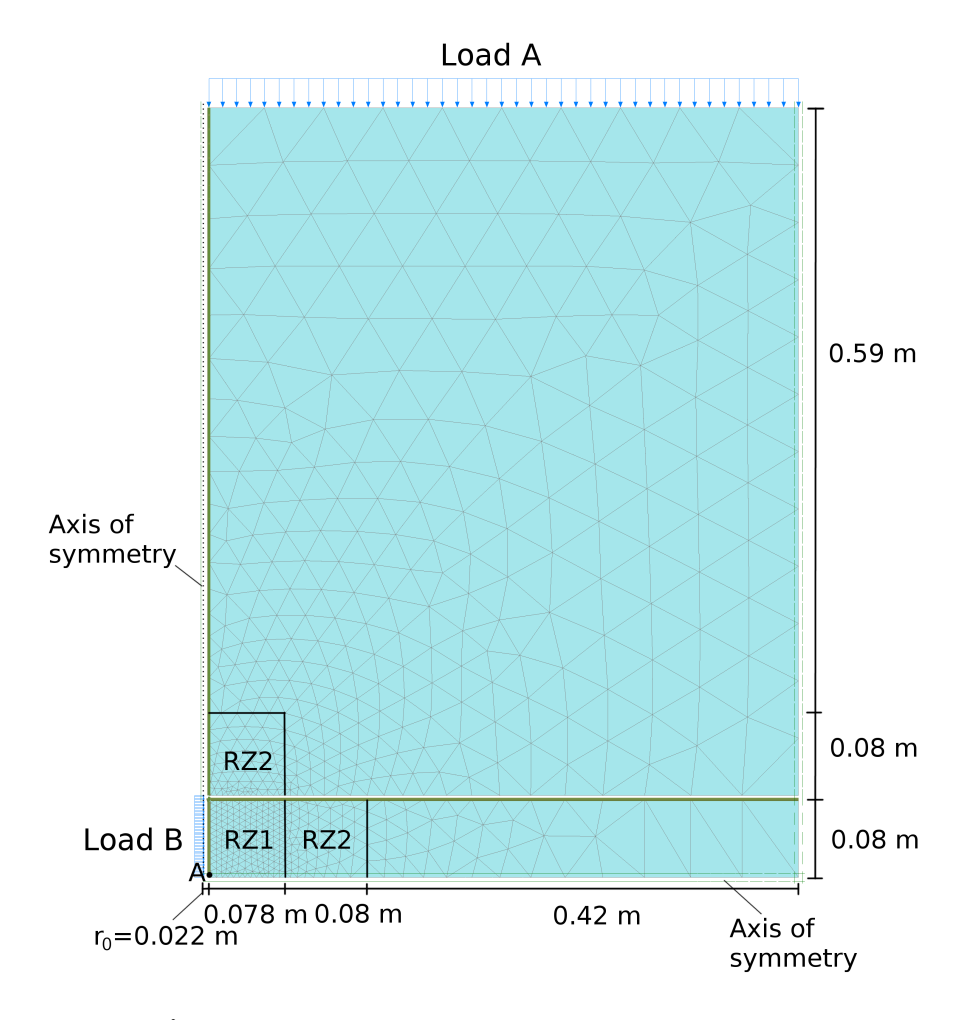


Figure 17-14: Model geometry and generated mesh

To allow for a discontinuity in horizontal displacements, a vertical interface along the shaft of the pressiometer borehole and a horizontal interface just above the pressiometer are introduced. Both interfaces are set rigid ($R_{inter} = 1.0$). Extra geometry lines are created around the pressiometer to locally generate a finer mesh (Figure 17–14 (p. 200)). A Coarseness factor equal to 0.1 is used for the refinement zone 1 (RZ1) and a Coarseness factor of 0.3 is used for the refinement zone 2 (RZ2). For the *Element distribution* the *Medium* option is selected .

After the generation of initial stresses in the Initial Phase, the vertical overburden load (load A) is applied in *Phase 1*. The left model boundary is horizontally fixed via the line displacement as discussed above, while the bottom and right model boundaries are set to Normally fixed via the in the Model explorer window. A plastic calculation is performed. For the subsequent calculation phases, the left model boundary should be set to Free via the Deformations option in the **Model explorer** window.

In **Phase 2**, the line displacement which is placed at the level of the pressiometer, at the left boundary, is deactivated. The Load B is activated in order to maintain equilibrium, i.e. zero deformation. The magnitude of this load increases linearly with depth and it is calculated based on the vertical stress and Jaky's formula (for normally consolidated soils). Thus the horizontal load acting on the node located at the top of the pressiometer equals 176.0 kPa and the horizontal load acting on the node located at the bottom model boundary equals 176.5 kPa. A plastic calculation is performed in Phase 2 as well.

In both Phases 1 and 2, the *Tolerated error* is set equal to 0.0001 and the *Max load fraction* per step is set to 0.01 to increase the accuracy of the numerical calculation. This is important in order to meticulously replace the horizontal fixity with the horizontal load at the level of the pressiometer in Phase 2.



Note:

Note that the values at the edges of the horizontal load mentioned above are calculated analytically and may slightly differ from the numerical results at the corresponding nodes, at the end of Phase 1. This is because the numerically obtained values depend on the selected number of mesh elements (mesh discretization) and on the used numerical settings for the plastic calculation in Phase 1. The user may check this discrepancy and if necessary use the numerical values to maintain equilibrium.

In the following calculation **Phase 3**, the pressure (load B) is further increased by use of Staged construction. Thus the load B is set equal to 2500 kPa. An Updated mesh analysis is used. The Tolerated error is 0.01 (default value) and the **Max load fraction per step** is set to 0.1. The results of this calculation are presented in Figure 17–15 (p. 202) and Figure 17–16 (p. 203).

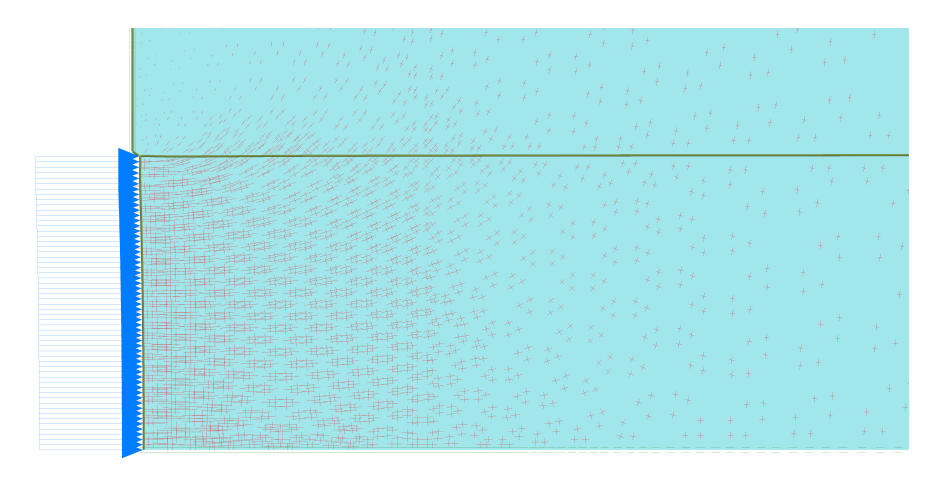


Figure 17-15: Effective principal stress distribution at the vicinity of the pressiometer, for a pressure of 2427 kPa (scaled up 4x10-6 times)⁻⁶ times)

Figure 17-15 (p. 202) shows details of effective principal stress distribution when the pressure in the pressiometer is 2427 kPa. The high passive stresses appear very locally near the pressiometer. Just above the pressiometer the vertical stress is very low due to arching effects. Away from the pressiometer, a K_0 -like stress state exists.

Figure 17–16 (p. 203) depicts a comparison of the numerical results with those obtained from the laboratory test. A Node A at the interface, at the bottom left corner of the model, is selected to illustrate the results (Figure 17-14 (p. 200)). In Figure 17-16 (p. 203) the pressiometer pressure P is plot against volumetric deformation $\Delta V/V_0$. Because the calculation in Phase 3 was run by accounting for large deformations (updated mesh analysis), the pressure P in the pressiometer is calculated by \eqnref{PressiometerPressureP}, based on the output quantity $\Sigma Mstage$ of Phase 3, the value of the applied Load B in Phase 2 ($LoadB_2 = 176.5$ kPa), the value of the applied Load B in Phase 3 ($LoadB_3 = 2500 \text{ kPa}$) and a correction factor to account for large deformations:

$$P=\left(LoadB_{2}+\sum Mstage(LoadB_{3}-LoadB_{2})
ight)rac{r_{0}}{r_{0}+u_{rr}}$$
 (17-1)

where

Initial radius (0.022 m)

 u_{rr} Radial deformation of the Node A

Note:

By considering updated mesh analysis, the area E upon which pressure P acts, should be adjusted to the increasing radius, from r_0 to $r_0 + u_{rr}$. Assuming an angle θ of 1 rad, the length of the corresponding arc is $s = r \theta$. The area E is equal to the length s times the height of the membrane H (0.08 m). Force equilibrium between the initial state (r_0) and every next step of the calculation (r_0 + u_{rr}) results in the correction factor $\frac{r_0}{r_0+u_{rr}}$. The latter is taken into account in Eqn. 17-1 (p. 202).

The volumetric deformation $\Delta V/V_0$ cannot be directly obtained from PLAXIS and it is calculated by Eqn. 17–2 (p. 203), based on the initial radius r_0 and the lateral expansion u_{rr} of the pressiometer at the Node A:

$$rac{\Delta V}{V_0} = rac{\left(r_0 + u_{rr}\right)^2 - r_0^2}{r_0^2}$$
 (17–2)

Based on Figure 17-16 (p. 203) it is concluded that the agreement between the numerical results and the experimental data is very good, both for the initial part of the loading curve and for larger volumetric deformations up to 30%. The original set of parameters for the dense sand that were derived from triaxial testing seem to match the pressiometer data guite well.

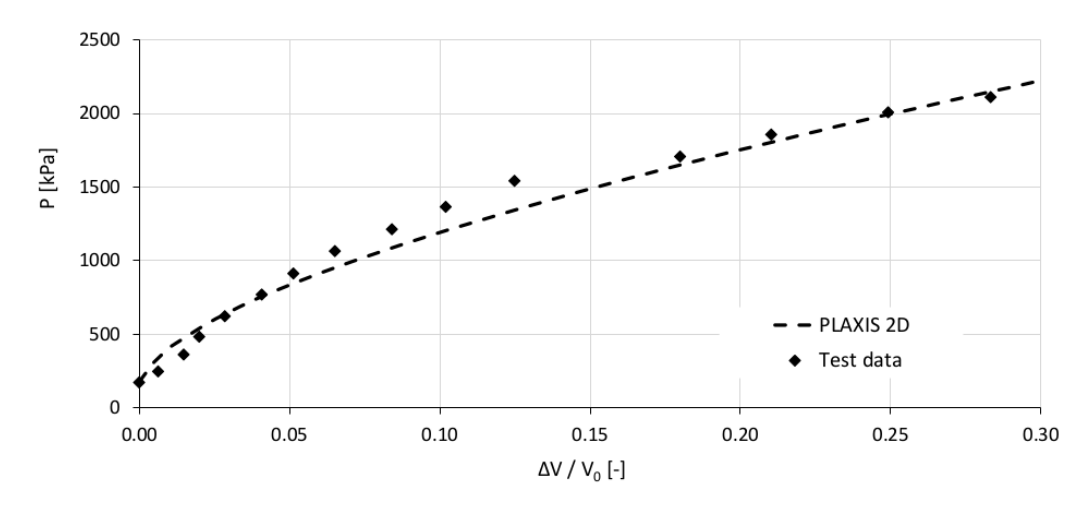


Figure 17-16: Comparison of numerical results and pressiometer test data

17.2.4 Conclusions of the Application of the Hardening Soil model on real soil tests

The test results indicate that by using the Hardening Soil model it is possible to simulate different laboratory tests with different stress paths. This cannot be obtained with simple models such as the Mohr-Coulomb model without changing input parameters. Hence, the parameters in the Hardening Soil model are consistent and more or less independent from the particular stress path. This makes the Hardening Soil model a powerful and an accurate model, which can be used in many applications.

17.3 Application of the Hardening Soil model with small-strain stiffness on real soil tests

In this section, the ability of the Hardening Soil model with small-strain stiffness (HS small model) to simulate laboratory tests is examined. Both, the laboratory test data and the basic HS parameters are identical to those presented in the previous section. The two additional small strain parameters used in the Hardening Soil model are quantified in Table 17-3 (p. 204).

Table 17-3: Additional HSsmall model parameter for loose and dense Hostun sand

Parameter	Loose sand	Dense sand	Unit
G_0^{ref} (p _{ref} = 100 kPa)	70000	112500	[kN/m ²]
Y0.7	0.0001	0.0002	[-]

Triaxial tests on loose and dense Hostun sand are presented in Figure 17-17 (p. 204) and Figure 17-18 (p. 205) respectively. As a reference, the previously obtained results from the Hardening Soil model are plotted as well.

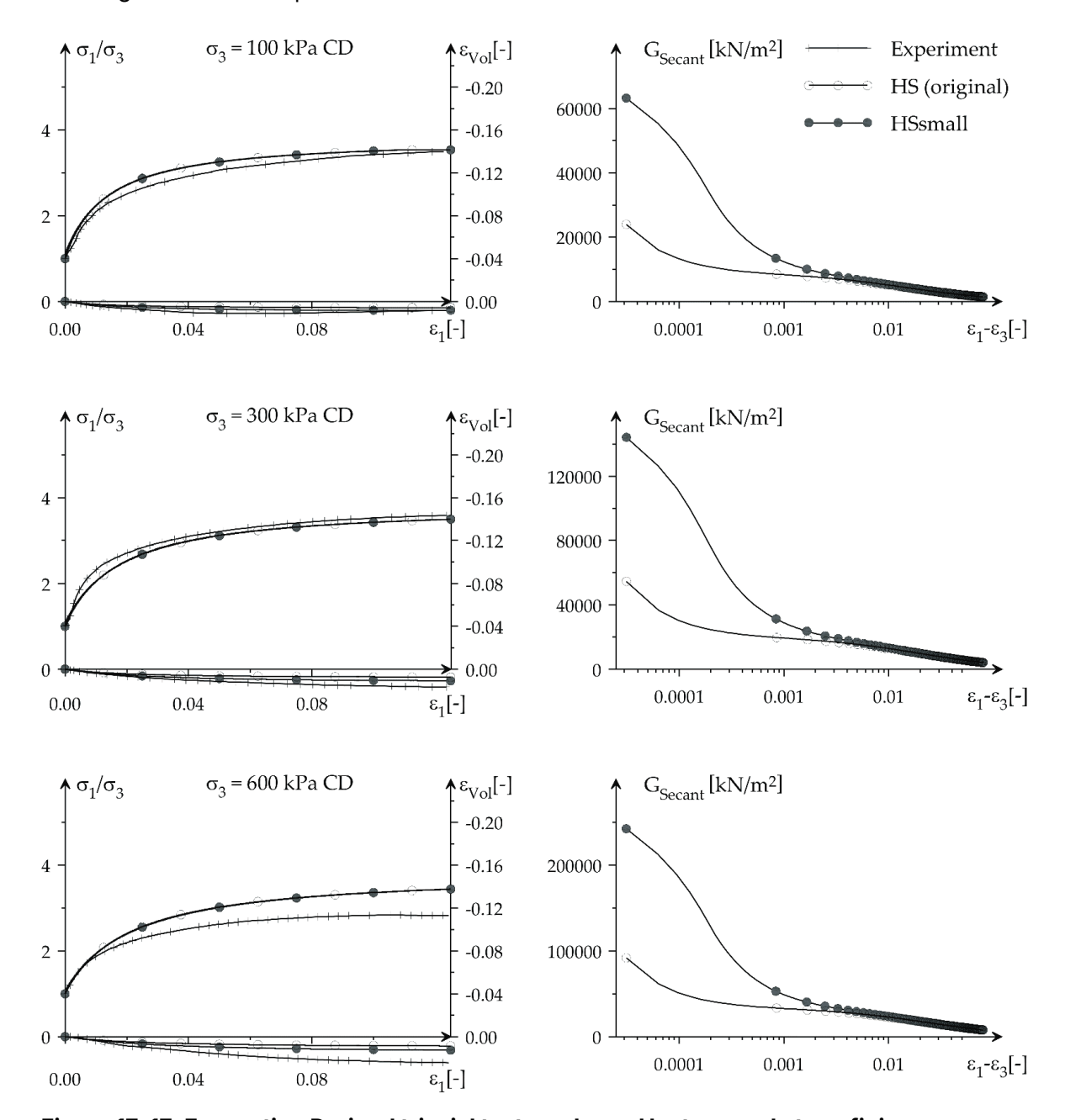


Figure 17-17: Excavation Drained triaxial tests on loose Hostun sand at confining pressures of 100, 300, and 600 kPa. Left: Stress-strain data. Right: Shear modulus reduction

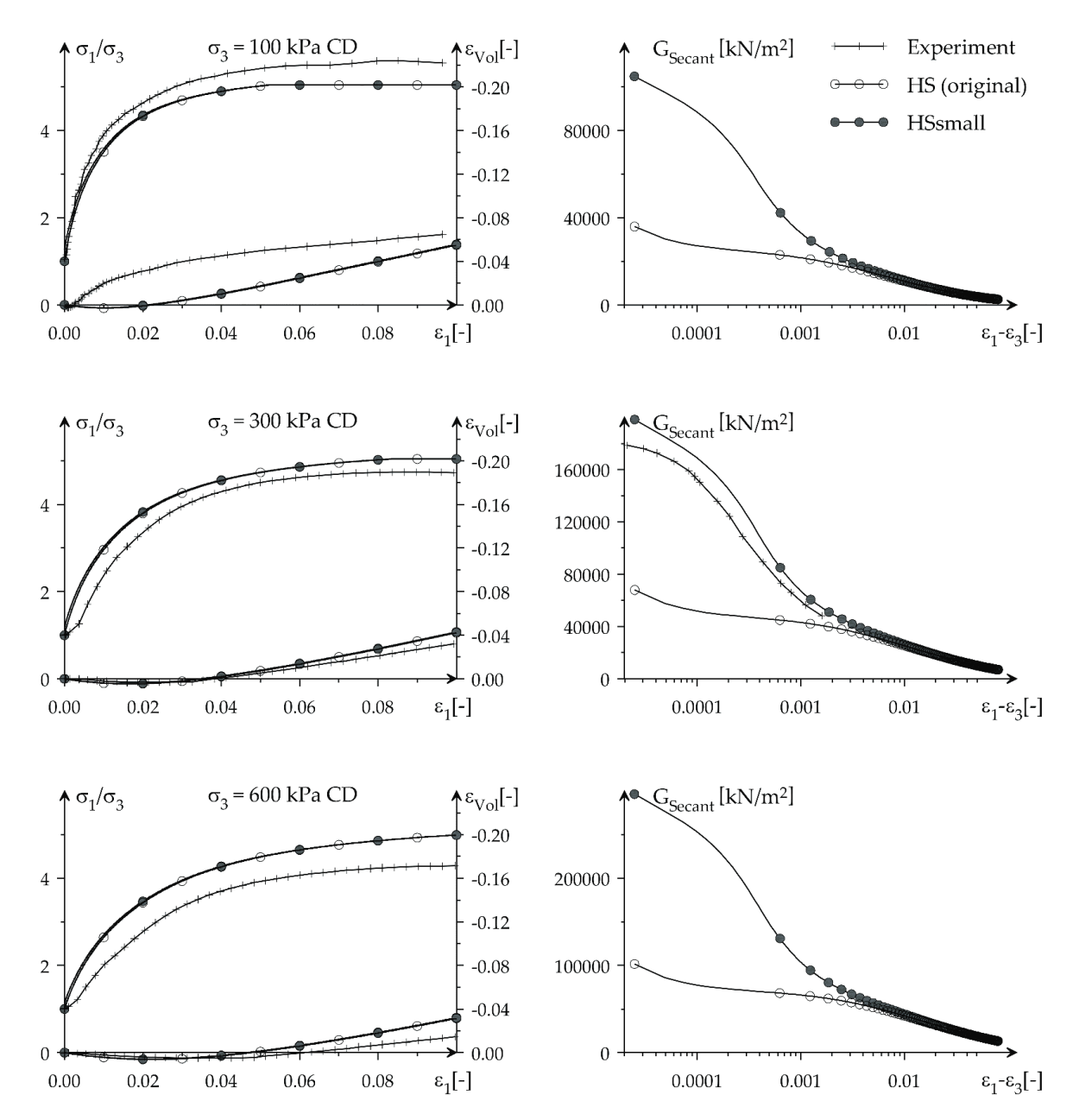


Figure 17-18: Drained triaxial tests on dense Hostun sand at confining pressures of 100, 300, and 600 kPa. Left: Stress-strain data. Right: Shear modulus reduction

The overall stress-strain data obtained from both models seems almost identical. Only a closer look at the small-strain domain shows a clear difference: The Hardening Soil model with smallstrain stiffness follows a S-shaped stiffness reduction curve with much higher initial stiffness than the one of the Hardening Soil model. Generally, both models match the test data at different confining pressures reasonably well.

Figure 17-19 (p. 206) presents results from a cyclic triaxial test by Rivera & Bard on dense sand. The Hardening Soil model with small-strain stiffnesssmall simulation of the test shows material damping which could not be obtained when simulating the test with the Hardening Soil model. As virgin loading is conducted in triaxial compression, the unloading sequence in triaxial extension gives some plasticity. Therefore the first unloading / reloading loop is not closed.

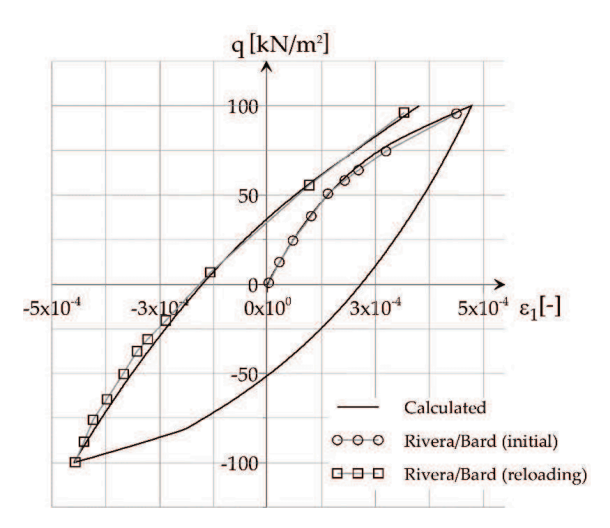


Figure 17-19: Hysteresis loop in a drained triaxial test on dense Hostun sand. Test data published in Biarez & Hicher (1994).

17.4 | Soft Soil Creep model : Undrained triaxial tests at different loading rates

In this section the Soft Soil Creep model (see 11 Soft Soil Creep model (time dependent behaviour) [ADV] (p. 117)) is utilised for the simulation of clay in an undrained triaxial test, at various strain rates. The model parameters are obtained from test results on Haney Clay and are listed in Table 17-4 (p. 206).

The initial isotropic preconsolidation pressure $P_p = 373 \text{ kN/m}^2$, as reported in the literature, is obtained by specifying a POP of 433 kN/m² in the initial conditions.

Table 17-4: Soft Soil Creep model parameters for Haney clay

Parameter	Symbol	Value	Unit
Modified compression index	λ^*	0.105	-
Modified swelling index	к *	0.016	-
Secondary compression index	μ^*	0.004	-
Poisson's ratio	v_{ur}	0.15	-
Cohesion	С	0.0	[kN/m ²]
Friction angle	φ	32	[°]
Dilatancy angle	Ψ	0.0	[°]
Coefficient of lateral stress	K_0^{nc}	0.61	[-]
Permeability	k_x , k_y	0.0001	[m/day]

Parameter	Symbol	Value	Unit
Pre overburden pressure	POP	433	[kN/m ²]

Modelling of the triaxial test is as described in 17.1 Hardening Soil model: Response in drained and undrained triaxial tests (p. 190). However, here, a guarter of the real dimension of the test set-up is simulated (17.5 x 17.5 mm²). Figure 17-20 (p. 207) illustrates the model geometry. The specimen surfaces (top and right hand side in Figure 17-20 (p. 207)) are assumed drained whereas the other boundaries are assumed closed.

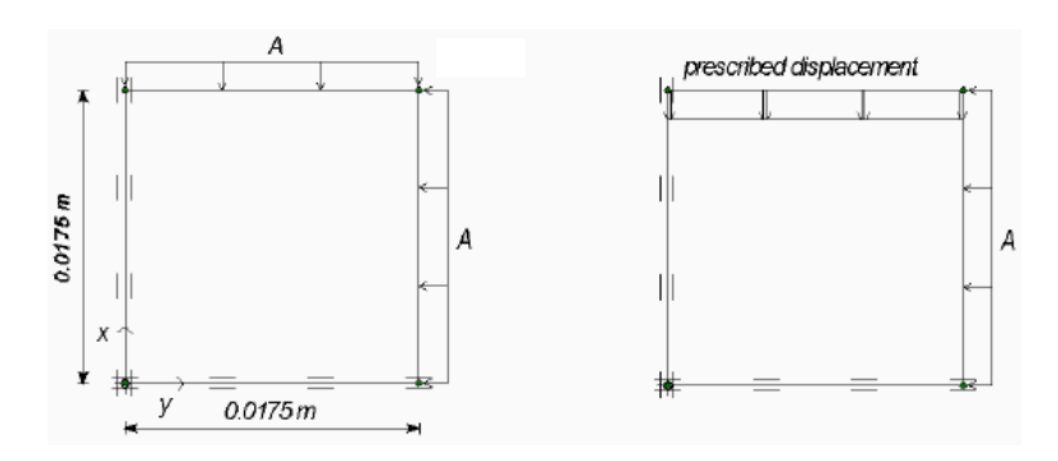


Figure 17-20: Modelling of triaxial test on Haney clay. Left, Initial configuration. Right, configuration for phases 9 to 11

The Very coarse option is selected for the Element distribution. To generate the graphs presented further below, mesh points need to be selected. More specifically, a node located at the top model boundary (e.g. with coordinates (0.0175, 0.0175)) is needed to generate Figure 17-21 (p. 207), while a stress point with coordinates (0.0110, 0.0050) is needed for Figure 17-22 (p. 208).

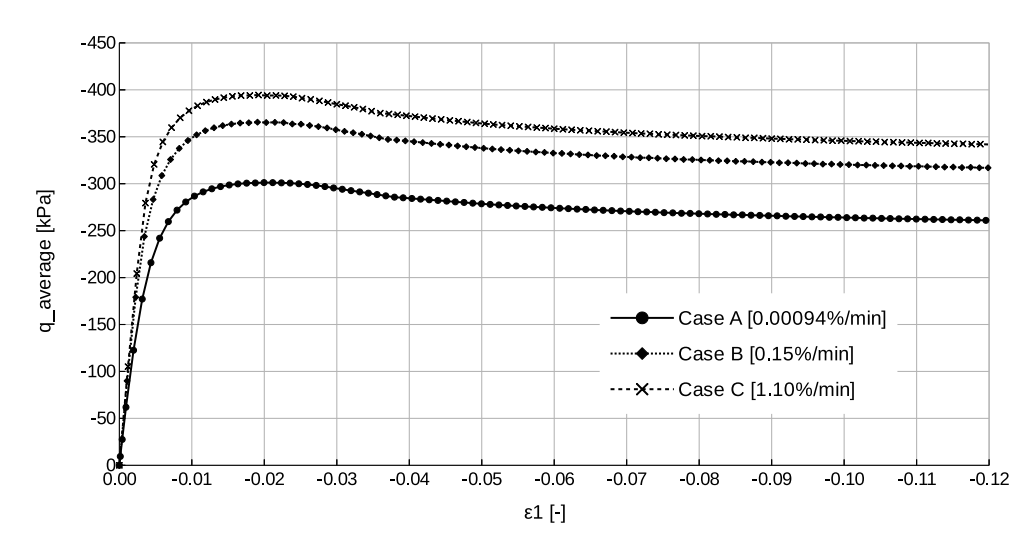


Figure 17-21: Average deviatoric stress versus axial strain for different strain rates

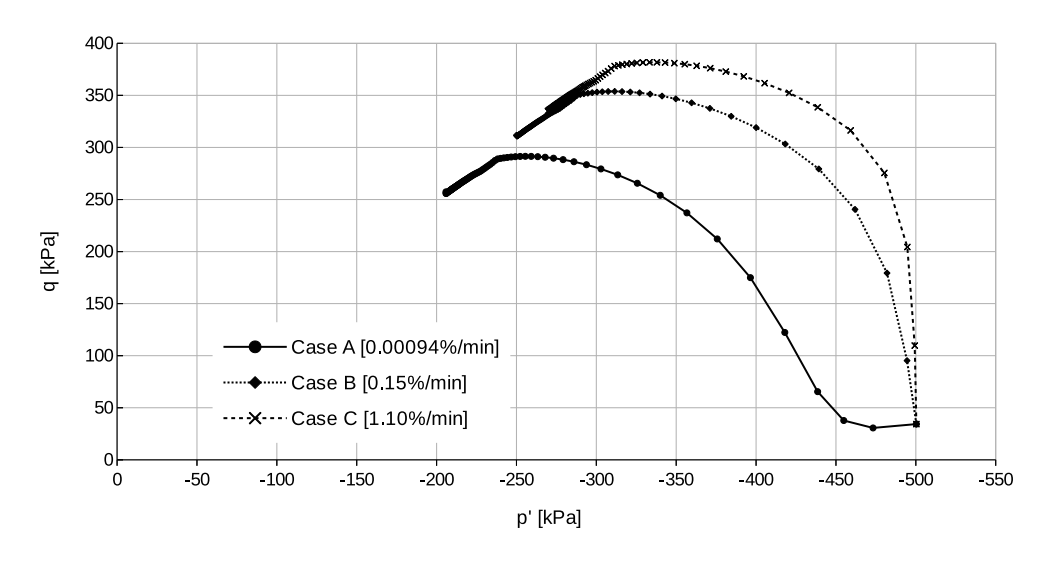


Figure 17-22: p'- q stress paths for different strain rates for a point at position (0.0110, 0.0050)

In addition to isotropic loading, prescribed displacements are also applied. Both types of loading are simulated using the Staged construction option. During isotropic loading, horizontal and vertical loads are applied. The calculation phases for isotropic loading consist of undrained plastic and consolidation analyses.

After the isotropic loading phases, the displacements are reset to zero. The vertical load is deactivated and the prescribed displacement is activated. Rate of loading is simulated by applying prescribed displacements at different velocities. As such, a total of 12% axial strain (2.1 mm, vertical displacement) is applied in 8.865 days (0.00094%/min), 0.0556 days (0.15%/min) and 0.00758 days (1.10%/min) respectively. Each of the prescribed displacement loading phases 9 to 11 starts from the end of the last consolidation phase 8. The calculation scheme is listed in Table 17-5 (p. 208).

Table 17-5: Loading scheme for triaxial tests at different loading rates

Phase	Starts from	Calculation	Top load	Side load	Displacement	Time interval
		type	[kPa]	[kPa]	[m]	
						[day]
1	0	Plastic	-65	-65	Inactive	0.00
2	1	Consolidation	-65	-65	Inactive	0.01
3	2	Plastic	-130	-130	Inactive	0.00
4	3	Consolidation	-130	-130	Inactive	0.01
5	4	Plastic	-260	-260	Inactive	0.00
6	5	Consolidation	-260	-260	Inactive	0.01
7	6	Plastic	-520	-520	Inactive	0.00
8	7	Consolidation	-520	-520	Inactive	0.01
9	8	Plastic	Inactive	-520	0.0021	8.865
10	8	Plastic	Inactive	-520	0.0021	0.0556
11	8	Plastic	Inactive	-520	0.0021	0.00758

The computational results are presented in Figure 17–21 (p. 207) and Figure 17–22 (p. 208). Figure 17–21 (p. 207) illustrates the average deviatoric strain $q_{average}$ versus the principal strain ε_1 for phases 9 to 11. The average deviatoric strain is obtained as:

$$q_{average} = rac{2F_Y}{R^2} - \sigma_3$$
 (17–3)

where:

R=0.0175 and σ_3 =-520 kN/m³

In Eqn. 17-3 (p. 209), Fy is the reaction force against the applied prescribed displacement (Force_y). The principal strain ε_1 is obtained by dividing the vertical displacement u_y of a node located at the top boundary by the height of the model (0.0175 m). The starting point in Figure 17–21 (p. 207) is deliberately selected to be zero.

Based on Figure 17-21 (p. 207), it can be seen that the shear strength highly depends on the strain rate; the higher strain rate the higher the shear strength.

Figure 17–22 (p. 208) shows the p' - q stress paths from the prescribed displacement loading phases. For higher strain rates there is a smaller reduction of the mean effective stress, which allows for larger ultimate deviatoric stress. It should be noted that the stress state is not homogeneous at all, because of the inhomogeneous (excess) pore pressure distribution. This is due to the fact that points close to draining boundaries consolidate faster than points at a larger distance.

In addition to the full tests as described before, the last part of the test can also be done in a simplified way using the Soil Test facility. Since the Soil Test facility operates on a single stress point, it is not possible to start the undrained triaxial tests from an inhomogeneous stress state, as considered in the full finite element based model. Instead, we start from an isotropic effective stress of 500 kN/m².

Table 17-6: Input parameters for the Soil Test facility

Input parameter	A(0.00094%/min)	B(0.15%/min)	C(1.10%/min)
Type of test	Triaxial, Undrained	Undrained & Triaxial	Undrained
Direction	Compression	Compression	Compression
Consolidation	Isotropic	Isotropic	Isotropic
Initial effect. stress $ \sigma_3' $	500 kN/m ²	500 kN/m ²	500 kN/m ²
Maximum strain $ arepsilon_1 $	12.0%	12.0%	12.0%
Time Δ t	8.865 days	0.0556 days	0.00758 days
Number of steps	200	200	200
Vert. precons. stress	433 kN/m ²	433 kN/m ²	433 kN/m ²

17.5 | Soft Soil Creep model: Response in onedimensional compression test

In this section the behaviour of the Soft Soil Creep model is illustrated on the basis of a onedimensional compression test on clay. Two types of analysis are performed. First, the test

is simulated assuming drained conditions in order to demonstrate the logarithmic stressstrain relationship and the logarithmic time-settlement behaviour on the long term (secondary compression). Second, the test is simulated more realistically by including undrained conditions and consolidation. Since the consolidation process depends on the drainage length, it is important to use actual dimensions of the test set-up. In this case an axisymmetric configuration with specimen height of 0.01 m, Figure 17-23 (p. 210), is used. The material parameters are shown in Table 17-7 (p. 210). The parameter values are selected arbitrarily, but they are realistic for normally consolidated clay. The vertical preconsolidation stress is fixed at 50 kPa (POP = 50 kPa).

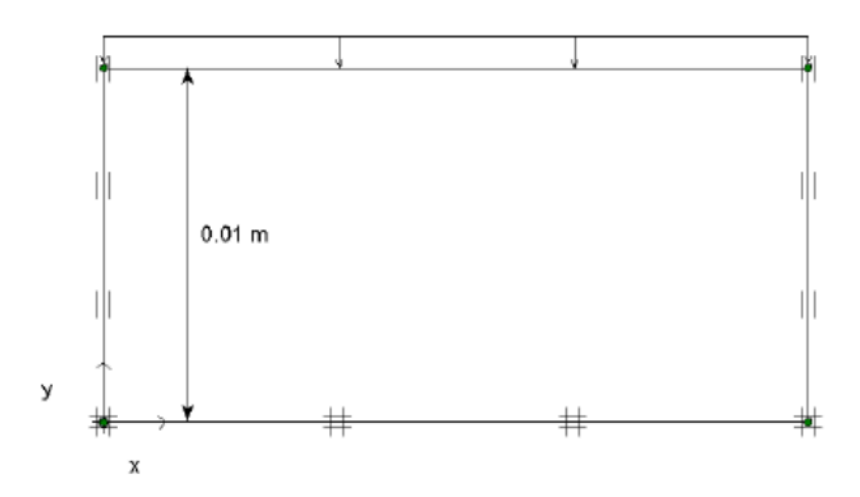


Figure 17-23: One-dimensional compression test

Table 17-7: Soft Soil Creep model parameters for one-dimensional compression test

Parameter	Symbol	Value	Unit
Unit Weight	γ	19	kN/m ³
Permeability	k_x , k_y	0.0001	m/day
Modified compression index	λ*	0.10	-
Modified swelling index	K*	0.02	-
Secondary compression index	μ^*	0.005	-
Poisson's ratio	v_{ur}	0.15	-
Cohesion	С	1.0	kN/m ²
Friction angle	φ	30	0
Dilatancy angle	Ψ	0.0	0
Coefficient of lateral stress	K ₀ ^{nc}	0.5	-

17.5.1 Drained analysis

In the first analysis successive plastic loading steps are applied using drained conditions. The load is doubled in every step using Staged construction with time increments of 1 day. After the last loading step an additional creep period of 100 days is applied. The calculation scheme is listed in Table 17-8 (p. 211). All calculations are performed with a tolerance of 1%.

Table 17-8: Calculation scheme for the drained case

Phase	Calculation type	Loading input	Load [kPa]	Time interval [day]	End time [day]
1	Plastic	Staged construction	10	1	1
2	Plastic	Staged construction	20	1	2
3	Plastic	Staged construction	40	1	3
4	Plastic	Staged construction	80	1	4
5	Plastic	Staged construction	160	1	5
6	Plastic	Staged construction	320	1	6
7	Plastic	Staged construction	640	1	7
8	Plastic	Staged construction	640	100	107

17.5.2 Undrained analysis

In the second analysis the loading steps are instantaneously applied using undrained conditions. After each loading step a consolidation of 1 day is applied to let the excess pore pressures fully dissipate. After the last loading step, an additional creep period of 100 days is again introduced. The calculation scheme for this analysis is listed in Table 17–9 (p. 211). All calculations are performed with a reduced tolerance of 1%.

Table 17-9: Calculation scheme for second analysis

Phase	Calculation type	Loading input	Load [kPa]	Time interval [day]	End time [day]
1	Plastic	Staged construction	10	0	0
2	Consolidation	Staged construction	10	1	1
3	Plastic	Staged construction	20	0	1
4	Consolidation	Staged construction	20	1	2

Phase	Calculation type	Loading input	Load [kPa]	Time interval [day]	End time [day]
5	Plastic	Staged construction	40	0	2
6	Consolidation	Staged construction	40	1	3
7	Plastic	Staged construction	80	0	3
8	Consolidation	Staged construction	80	1	4
9	Plastic	Staged construction	160	0	4
10	Consolidation	Staged construction	160	1	5
11	Plastic	Staged construction	320	0	5
12	Consolidation	Staged construction	320	1	6
13	Plastic	Staged construction	640	0	6
14	Consolidation	Staged construction	640	1	7
15	Consolidation	Staged construction	640	100	107

Figure 17–24 (p. 213) shows the load-settlement curves of both analyses. It can be seen that, after consolidation, the results of the undrained test match those of the drained test. The influence of the preconsolidation stress can clearly be seen, although the transition between reloading and primary loading is not as sharp as when using the Soft Soil model. In fact, the results presented here are more realistic. The transition is indeed around 50 kPa.

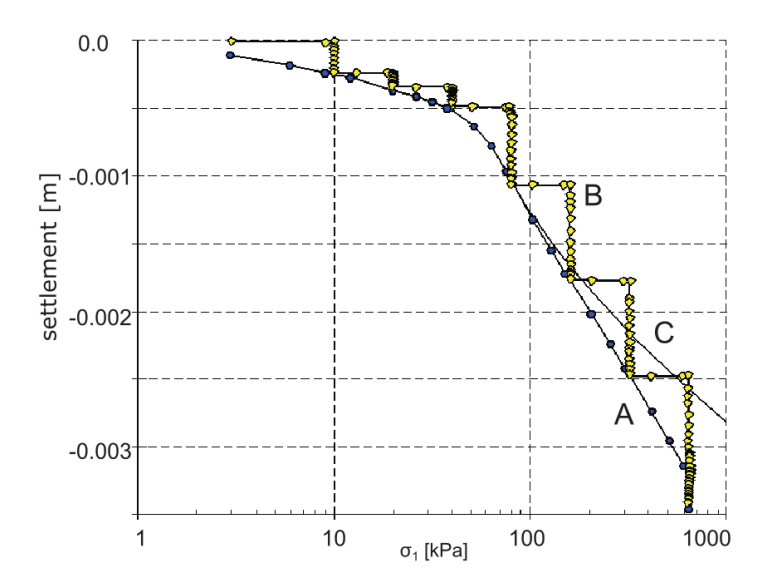


Figure 17-24: Load-settlement curve of oedometer test with Soft Soil Creep model. A) Transient loading with doubling of loading within one day. B) Instantaneous loading with doubling of load at the beginning of a new day. C) As 'A' using Updated Mesh calculation

From the slope of the primary loading line one can back-calculate the modified compression index $\lambda^*=\Delta \varepsilon_1/\ln\,\left(\frac{\sigma_1+\Delta\sigma_1}{\sigma_1}\right)\approx 0.\,10$. Note that 1 mm settlement corresponds to ε_1 = 10%. For an axial strain of 30% one would normally use an Updated mesh analysis, which has not been done in this simple analysis. If, however, the Soft Soil Creep model would have been used in an Updated mesh analysis with axial strains over 15% one would observe a stiffening effect as indicated by line C in Figure 17-24 (p. 213).

Figure 17-25 (p. 214) shows the time-settlement curves of the drained and the undrained analyses. From the last part of the curve one can back-calculate the secondary compression index $\mu^* = \Delta \varepsilon_1 / \ln (\Delta t / t_0) \approx 0.005$ (with t_0 = 1 day).

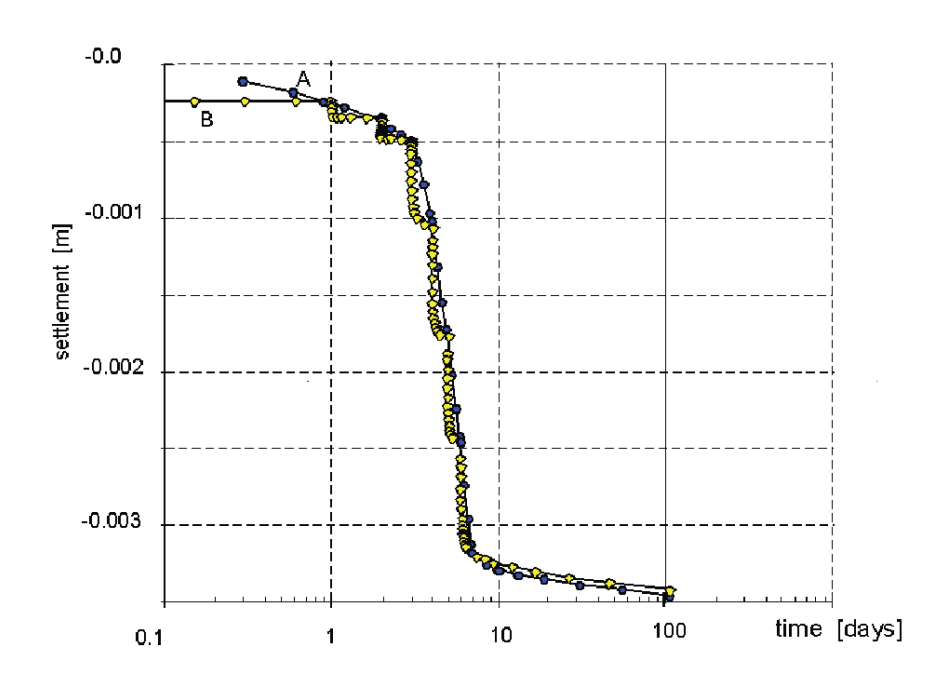


Figure 17-25: Time-settlement curve of oedometer test with Soft Soil Creep model. A) Transient loading with doubling of loading within one day. B) Instantaneous loading with doubling of load at the beginning of a new day

Another interesting phenomenon is the development of lateral stresses. During primary loading, the lateral stress is determined by $K_0^{\ \ nc}$, appropriate for normally consolidated soil. During unloading, the lateral stress decreases much less than the vertical stress, so that the ratio σ'_{xx} σ'_{vv} increases.

To show these effects the calculation is continued after with a new drained unloading phase that starts from phase 7 (see Table 17-8 (p. 211)) in which the vertical stress is reduced to -80 kPa.

Figure 17-26 (p. 214) shows the stress state for two different calculation phases, both at a vertical stress level of 80 kPa. The plot in the left hand side shows the stress state after primary loading. As expected the horizontal stress is found to be approximately -40 kPa (corresponding to $K_0^{nc} = 0.5$). The plot in the right hand side shows the final situation after unloading down to -80 kPa. In this case the horizontal stress is decreased from -320 kPa to approximately -220 kPa, ($\Delta \sigma'_{xx} = 100$ kPa), i.e, much less than the decrease of the vertical stress ($\Delta \sigma'_{vv} = 560$ kPa). Thus, a situation where σ'_{xx} is larger than σ'_{yy} is obtained.

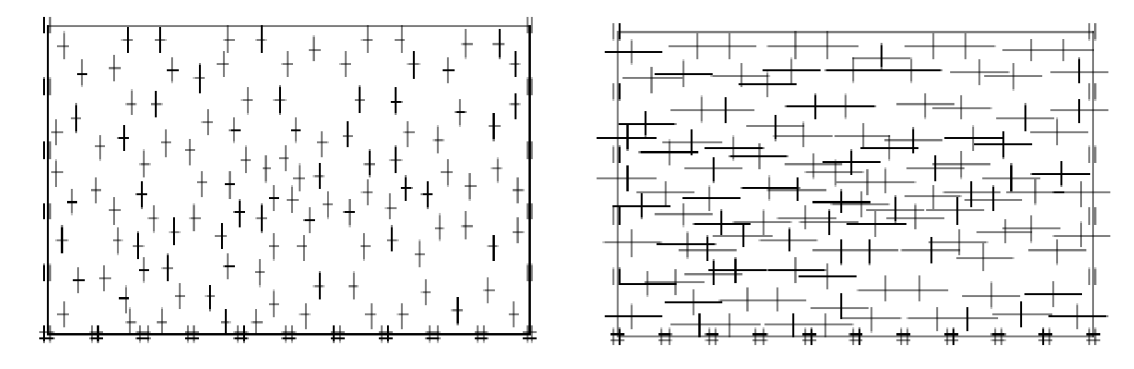


Figure 17-26: Stress states at vertical stress level of -80 kPa. Left, after primary loading σ 'xx≈ 40 kPa. Right, after unloading from -640 kPa σ 'xx≈ -220 kPaσ 'xx≈ 40 kPa. Right, after unloading from -640 kPa σ 'xx≈ -220 kPa

During sudden unloading in a one-dimensional compression test, the behaviour is purely elastic. Hence, the ratio of the horizontal and vertical stress increments can be determined as:

$$\frac{\Delta \sigma_{xx}^{'}}{\Delta \sigma_{yy}^{'}} = \frac{\nu_{ur}}{1 - \nu_{ur}} \tag{17-4}$$

It is easy to verify that the results correspond to Poisson's ratio $v_{ur} = 0.15$ as listed in Table 17–3 (p. 204).

17.6 Soft Soil model: Response in isotropic compression test

In this section it will be demonstrated that the Soft Soil model obeys a logarithmic relationship between the volumetric strain and the mean stress in isotropic compression. For this purpose the test set up is simulated as that presented in Figure 17-1 (p. 191). The vertical load (A) and the horizontal load (B) are simultaneously applied to the same level so that a fully isotropic stress state occurs. The parameters of the Soft Soil model are chosen arbitrarily, but the values are realistic for normally consolidated clay. The parameters are presented in Table 17–10 (p. 215).

Table 17-10: Soft Soil model parameters for isotropic compression test

Modified compression index	λ^*	0.1
Modified swelling index	* K*	0.02
Poisson's ratio	V _{ur}	0.15
Friction angle	φ	30°
Cohesion	С	1.0 kPa
Normally consolidated K ₀	K ₀ & K ₀ ^{nc}	0.5

From a stress-free state, the model is isotropically loaded to a mean stress of p' = 100 kPa, after which the displacements are reset to zero. As a result, the material becomes 'normally consolidated', i.e., the preconsolidation stress is equivalent to the current state-of-stress. After that, the isotropic pressure is increased to p' = 1000 kPa. This loading path is denoted as 'primary loading'. Then, the sample is isotropically 'unloaded' to p'=100 kPa. Finally, the sample is loaded up to p'=10000 kPa. In the last loading path, the maximum preload of 1000 kPa is exceeded, and hence, it consists of two parts: the part of the loading path for which p' <1000 kPa is referred to as 'reloading', and the part of the loading path for p' > 1000 kPa consists of further primary loading. The calculation phases are indicated in Table 17-11 (p. 215).

Table 17-11: Calculation phases for isotropic compression test on clay

Sta	ige	Initial stress	Final stress
0	Initial situation	-	$p^0 = 100 \text{ kPa}$
1	Primary loading	$p^0 = 100 \text{ kPa}$	p ¹ = 1000 kPa
2	Unloading	$p^1 = 1000 \text{ kPa}$	$p^2 = 100 \text{ kPa}$

Sta	nge	Initial stress	Final stress
3	Reloading	$p^2 = 100 \text{ kPa}$	p ³ = 1000 kPa
4	Primary loading	p ³ = 1000 kPa	$p^4 = 10000 \text{ kPa}$

The computational results are presented in Figure 17–27 (p. 216), which shows the relation between the vertical strain ε_{vv} and the vertical stress σ'_{vv} .

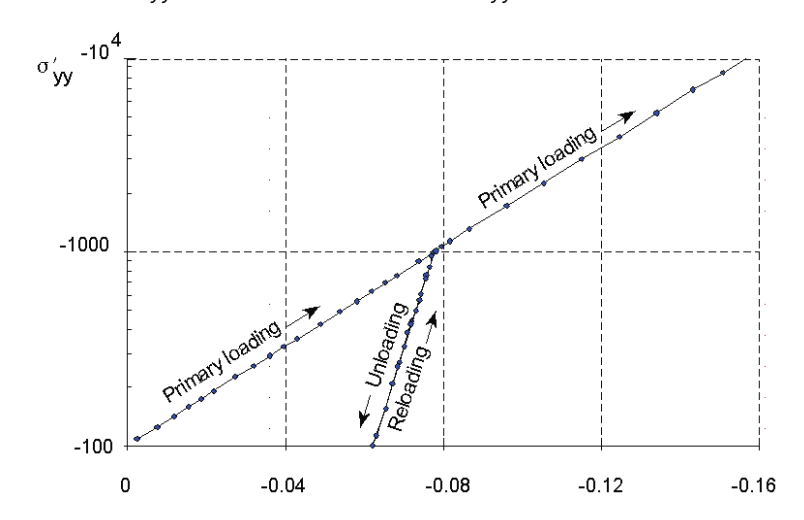


Figure 17-27: Results of isotropic compression test

The latter quantity is plotted on a logarithmic scale. The plot shows two straight lines, which indicates that there is indeed a logarithmic relation for loading and unloading. The vertical strain is 1/3 of the volumetric strain, ε_{v} , and the vertical stress is equal to the mean stress, p'. The volumetric strains obtained from the calculation are given in Table 17-12 (p. 216).

Table 17-12: Volumetric strains from various calculation phases

Phase	Initial strain	Final strain	
0	-	$\varepsilon_{V}^{0} = 0.000$	
1	$\varepsilon_{\rm V}^{\ 0} = 0.000$	$\varepsilon_{v}^{-1} = -0.235$	
2	$\varepsilon_{V}^{1} = -0.235$	ε_{V}^{2} = - 0.188	
3	$\varepsilon_{\rm V}^{\ 2}$ = - 0.188	$\varepsilon_{V}^{3} = -0.235$	
4	$\varepsilon_{V}^{3} = -0.235$	$\varepsilon_{V}^{4} = -0.471$	

From these strains and corresponding stresses, the parameters λ^* and κ^* can be backcalculated using Eqn. 11-1 (p. 118) and Eqn. 11-2 (p. 118).

$$\begin{array}{lll} Phase~1:~~\lambda^*=&-\frac{\varepsilon_v^1-\varepsilon_v^0}{ln(p^1/p^0)}=&\frac{0.235}{ln(1000/100)}=&0.102\\ Phase~2:~~\kappa^*=&-\frac{\varepsilon_v^2-\varepsilon_v^1}{ln(p^2/p^1)}=&\frac{0.188-0.235}{ln(100/1000)}=&0.020\\ Phase~3:~~\kappa^*=&-\frac{\varepsilon_v^3-\varepsilon_v^2}{ln(p^3/p^2)}=&\frac{0.235-0.188}{ln(1000/100)}=&0.020 \end{array}$$

$$Phase~4:~~\lambda^{~*}=~-rac{arepsilon_{v}^{4}-~arepsilon_{v}^{3}}{ln(p^{4}/p^{3})}=rac{0.471-0.235}{ln(10000/1000)}=~0.102$$

The back-calculated values correspond to the input values as given in Table 17–10 (p. 215).

Note that the Soft Soil model does not include time effects such as in the secondary compression. Such behaviour is included in the Soft Soil Creep model.

17.7 | Hardening Soil model and Hardening Soil model with small-strain stiffness: **Excavation in Berlin sand**

In the previous example, the advantage of the Hardening Soil model's distinct loading and unloading stiffness was highlighted. With those, the calculated excavation heave could be reduced to a more realistic, but in most cases still too high value. In the Berlin excavation example, now the further advantage of considering small-strain stiffness in the analysis is demonstrated.

The working group 1.6 Numerical methods in Geotechnics of the German Geotechnical Society (DGGT) has organised several comparative finite element studies (benchmarks). One of these benchmark examples is the installation of a triple anchored deep excavation wall in Berlin sand. The reference solution by Schweiger (2002) is used here as the starting point for the next validation example: Both, the mesh shown in Figure 17–28 (p. 217), and the soil parameters given in Table 17-13 (p. 217) are taken from this reference solution. However, the bottom soil layer 3 defined by <u>Schweiger (2002)</u> is assigned the parameters of layer 2 in the HSsmall analysis. In the reference solution this layer's only purpose is the simulation of small-strain stiffness due to a lack of small-strain stiffness constitutive models back then.

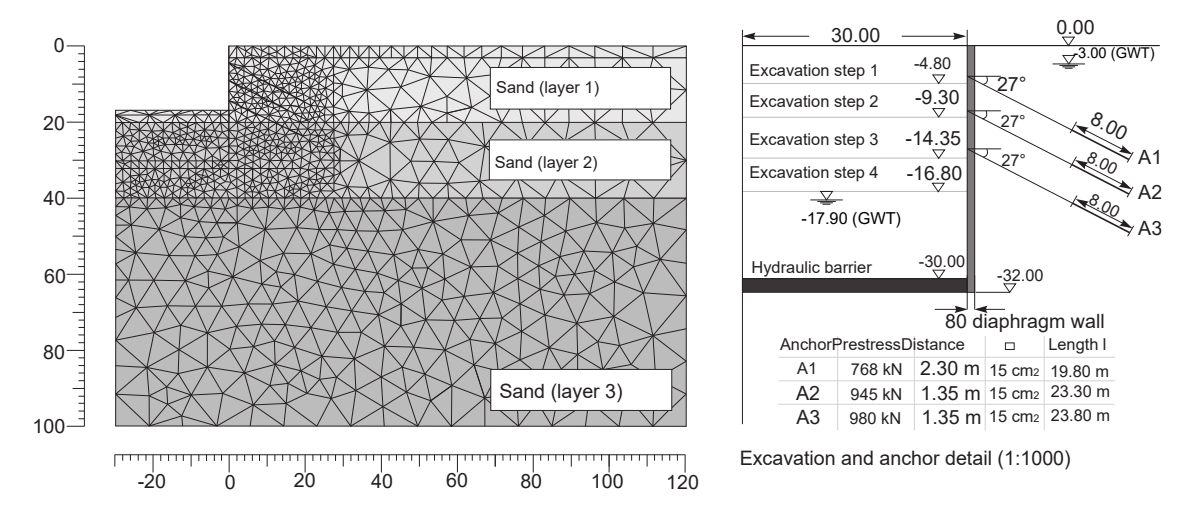


Figure 17-28: Excavation in Berlin sand: plane strain mesh (left) and geometry detail (right)

Table 17-13: Hardening Soil model and HS small model parameters for the three sand layers in the excavation project

Parameter	Layer 1	Layer 2	Layer 3	Unit
Unit weight above/below phreatic level	19 / 20	19 / 20	19 / 20	kN/m ³

Parameter	Layer 1	Layer 2	Layer 3	Unit
E_{50}^{ref} (p _{ref} = 100 kPa)	45000	75000	105000	kN/m²
E_{ur}^{ref} (p_{ref} = 100 kPa)	45000	75000	105000	kN/m²
E_{oed}^{ref} (p _{ref} = 100 kPa)	180000	300000	315000	kN/m²
G_0^{ref} (p _{ref} = 100 kPa)	168750	281250	NA	kN/m²
Shear strain $\mbox{\mbox{$\backslash$}}$ $\mbox{\mbox{\mbox{$\backslash$}}}$ $\mbox{\mbox{\mbox{$\backslash$}}}$ $\mbox{\mbox$	0.0002	0.0002	NA	-
Cohesion c	1	1	1	kN/m ²
Friction angle ϕ	35	38	38	0
Dilatancy angle ψ	5	6	6	o
Poisson's ratio v _{ur}	0.2	0.2	0.2	-
Power m	0.55	0.55	0.55	-
K ₀ nc	0.43	0.38	0.38	-
Tensile strength	0	0	0	kN/m ²
Failure ratio	0.9	0.9	0.9	

Figure 17–29 (p. 219) shows results from the finite element calculation using the original Hardening Soil model and the Hardening Soil model with small-strain stiffness. The small-strain stiffness formulation in the Hardening Soil model with small-strain stiffness accumulates more settlements right next to the wall, whereas the settlement trough is smaller. The triple anchored retaining wall is deflected less when using the HSsmall model, almost fitting the measured deflection. Calculated excavation heave at the end of excavation is shown in Figure 17-30 (p. 219) . Compared to the HS results, the heave which is due to elastic unloading, is roughly halved when using the Hardening Soil model with small-strain stiffness.

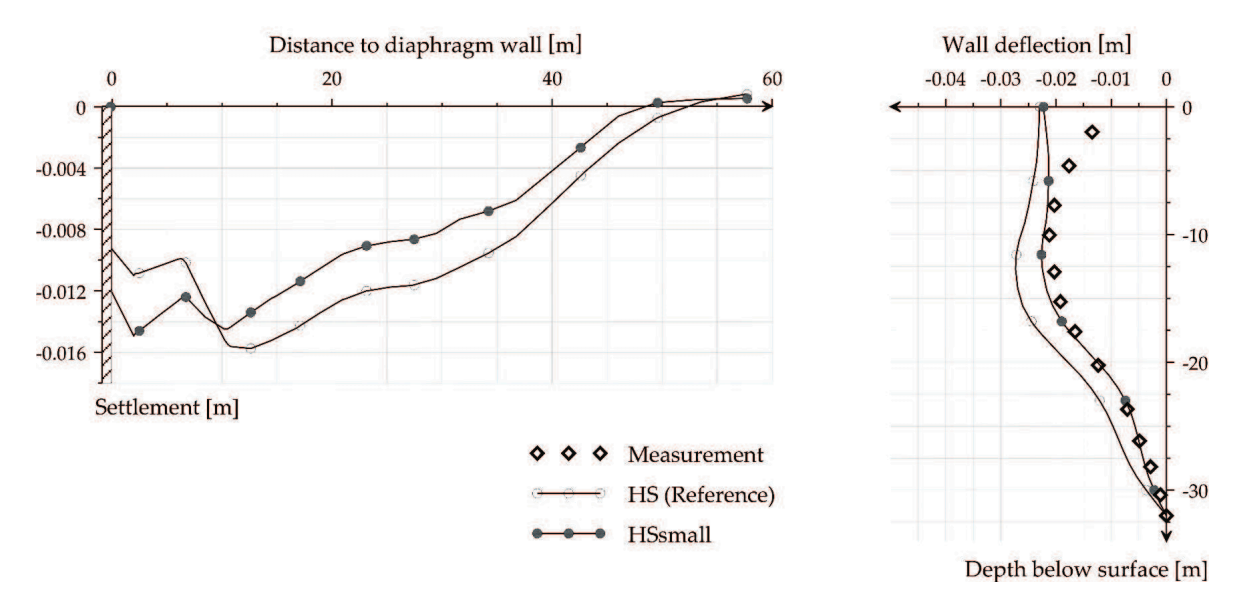


Figure 17-29: Hardening Soil model and Hardening Soil model with smallstrain stiffness predictions versus measured displacements after the final excavation step. Left: Surface settlement trough. Right: Lateral wall deflection.

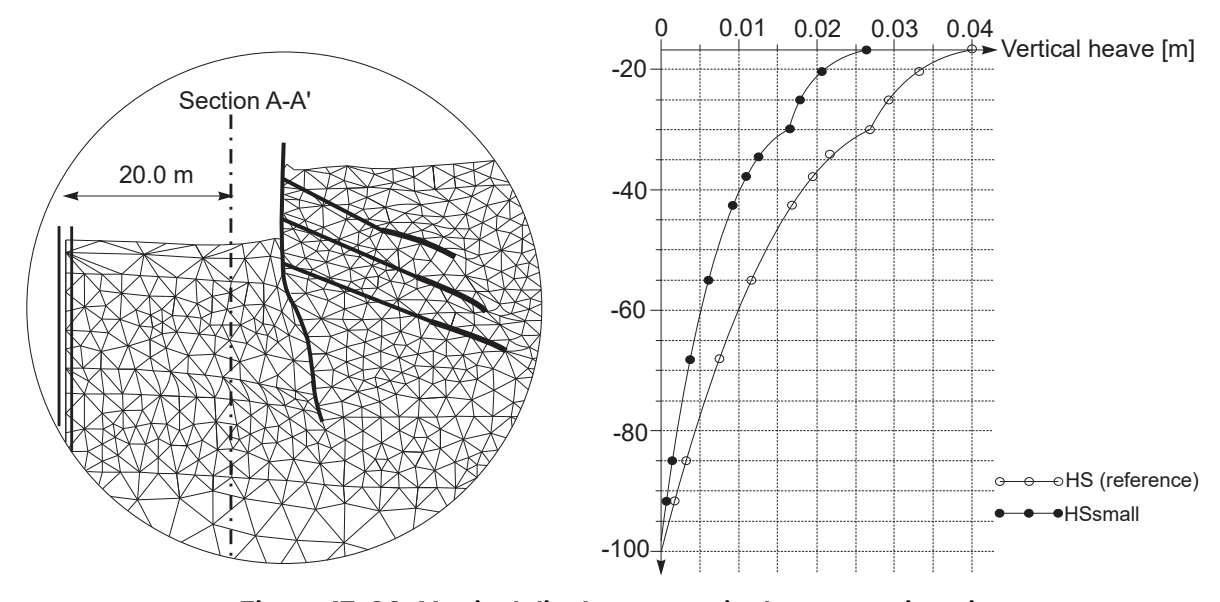


Figure 17-30: Vertical displacements in the excavation pit at a distance of 10 m from the retaining wall (Section A-A)

Structural Behaviour

18.1 Anchors

The elastic behaviour of an anchor involves only a relationship between axial force N and displacement (elongation) u of the form:

$$N = \frac{EA}{L}U \tag{18-1}$$

The anchor stiffness *EA* is defined by the user based on the material stiffness *E* and cross section *A*.

In case of elastoplastic behaviour of the anchor the maximum tension force is bound by $F_{max,tens}$ and the maximum compression force is bound by $F_{max,comp}$.

18.2 2D Geogrids

The PLAXIS program allows for orthotropic behaviour of geogrid elements, which is defined by the parameters EA_1 and EA_2 . The stiffnesses are defined by the user and are based on the material tension stiffnesses (E_1 , E_2) and the cross section areas (A_1 , A_2) corresponding to the local axes of the geogrid. Geogrid elements cannot sustain compression forces.

The relationship between the force and the strain in axisymmetric models is defined as:

$$\begin{bmatrix} N \\ H \end{bmatrix} = \begin{bmatrix} EA_1 & 0 \\ 0 & EA_2 \end{bmatrix} \begin{bmatrix} \varepsilon \\ \varepsilon_H \end{bmatrix} \tag{18-2}$$

where H is the hoop force and ε_H is the hoop strain. For plane strain model H = 0.

When plasticity is considered, the maximum tensile forces can be defined:

N _{p,1}	The maximum force in 1-direction (in-plane).	[kN/m]
N _{p,2}	The maximum force in 2-direction (out-of-plane, anisotropic behaviour).	[kN/m]

A non-linear N- ε diagram may be specified in case of elastoplasticity:

N ₁ - eps ₁	The N - ε diagram in 1-direction (in-plane).
N ₂ - eps ₂	The N - ε diagram in 2-direction (out-of-plane, anisotropic behaviour).

A Visco-elastic (time-dependent) behaviour may be specified based on a visco-elastic perfectly-plastic Kelvin-Voigt model in each direction. Parameters which are required for timedependent visco-elasticity are:

EA _{1,short}	Elastic stiffness during initial(instantaneous) strain increment in 1-direction (in-plane).	[kN/m]
EA _{2,short}	Elastic stiffness during initial(instantaneous) strain increment in 2-direction (out-of-plane, anisotropic behaviour).	[kN/m]
EA _{1,long}	Elastic stiffness during (infinitely) long strain increment in 1-direction (in-plane).	[kN/m]
EA _{2,long}	Elastic stiffness during (infinitely) long strain increment in 1-direction (out-of-plane, anisotropic behaviour).	[kN/m]
N _{p,1}	Maximum force in 1-direction (in-plane).	[kN/m]
N _{p,2}	The maximum force in 2-direction (out-of-plane, anisotropic behaviour).	[kN/m]
Retardation time	The time where a linear extrapolation of the initial creep rate intersects the long-term displacement line.	[day]

For more information about the determination of the parameters see the Reference Manual -Chapter 6 - Material data sets for geogrids.

18.3 | 2D plates

The PLAXIS 2D program allows for orthotropic elasto-plastic material behaviour in plate elements. The elastic behaviour is defined by the following parameters:

EA ₁	Axial stiffness.	[kN/m]
EA ₂	Stiffness in the out-of-plane direction.	[kN/m]
EI	Bending stiffness	[kNm²/m]
ν	Poisson's ratio	[-]

The material behaviour in plate elements is defined by the following relationship between strains and stresses.

$$\begin{bmatrix} \sigma_N \\ \sigma_2 \\ \tau \end{bmatrix} = \begin{bmatrix} \frac{2G}{1-\nu} & \frac{2G\nu}{1-\nu} & 0 \\ \frac{2G}{1-\nu} & \frac{2G}{1-\nu} & 0 \\ 0 & 0 & kG \end{bmatrix} \begin{bmatrix} \varepsilon_N \\ \varepsilon_2 \\ \gamma \end{bmatrix}$$
(18–3)

In which k is the shear correction factor, which is taken as 5/6. For isotropic material:

$$G = \frac{E_1}{2(1+\nu)} \tag{18-4}$$

For anisotropic plates, the following relationship between strains and stresses is used:

$$\begin{bmatrix} \sigma_N \\ \sigma_2 \\ \tau \end{bmatrix} = \begin{bmatrix} E_1 & 0 & 0 \\ 0 & E_2 & 0 \\ 0 & 0 & kG \end{bmatrix} \begin{bmatrix} \varepsilon_N \\ \varepsilon_2 \\ \gamma \end{bmatrix}$$
 (18–5)

where $E_1 = EA_1/d$ and $E_2 = EA_2/d$. Note that the Poisson's ratio (v) is assumed to be zero in anisotropic case.

The material behaviour in plate elements is defined by the following relationship between structural forces and strains:

$$N = EA_1\varepsilon$$
 (18–6)

$$H = EA_2\varepsilon_H$$
 (18–7)

$$Q = \frac{kEA}{2(1+\nu)}\gamma^* \tag{18-8}$$

$$M = EI\kappa$$
 (18–9)

The modified shear strain y^* takes into account the shear strain y and some additional terms in order to give a more accurate approximation of the problem. k is the shear correction factor, which is taken as 5/6. This implies that the shear stiffness is determined from the assumption that the plate has a rectangular cross section. In the case of modelling a solid wall, this will give the correct shear deformation. However, in the case of steel profile elements, like sheet-pile walls, the computed shear deformation may be too large. You can check this by judging the value of d_{eq} , which can be computed as $\sqrt{12EI/EA}$. For steel profile elements, d_{eq} should be at least of the order of a factor 10 times smaller than the length of the plate to ensure negligible shear deformations.

When plasticity is considered, the maximum bending moment and maximum normal force can be defined:

M_p	Maximum bending moment.	[kNm/m]
N _{p,1}	Maximum axial force (in-plane).	[kN/m]
N _{p,2}	Maximum axial force (out-of-plane).	[kN/m]

The maximum bending moment is given in units of force times length per unit width. The maximum axial force, N_p , is specified in units of force per unit of width. When the combination of a bending moment and an axial force occurs in a plate, then the actual bending moment or axial force at which plasticity occurs is lower than respectively M_p or N_p . The relationship between M_p and N_p is visualised in Figure 18–1 (p. 223). The diamond shape represents the ultimate combination of forces for which plasticity will occur. Force combinations inside the diamond will result in elastic deformations only.

By default the maximum moment is set to 1.10^{15} units if the material type is set to elastic (the default setting).

Bending moments and axial forces are calculated at the stress points of the beam elements. When yield function is violated, stresses are redistributed according to the theory of plasticity, so that the maxima are complied with. This will result in irreversible deformations. Output of bending moments and axial forces is given in the nodes, which requires extrapolation of the values at the stress points. Nodal forces are not checked against the maximum forces.

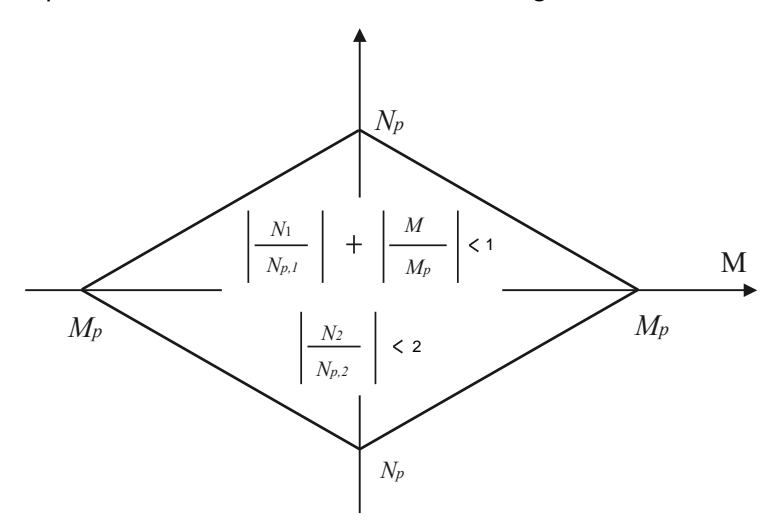


Figure 18-1: Combinations of maximum bending moment and axial force

When plasticity is defined employing an user-defined moment-curvature (M-κ) diagram, the bending behaviour of the plate is governed by the defined moment-curvature. The curvature, κ , is specified in the unit of length and the moment, M, in the unit of force times length per unit of width in the out-of-plane direction. The M- κ diagram is assumed to govern the plate's behaviour in both positive and negative loading directions.

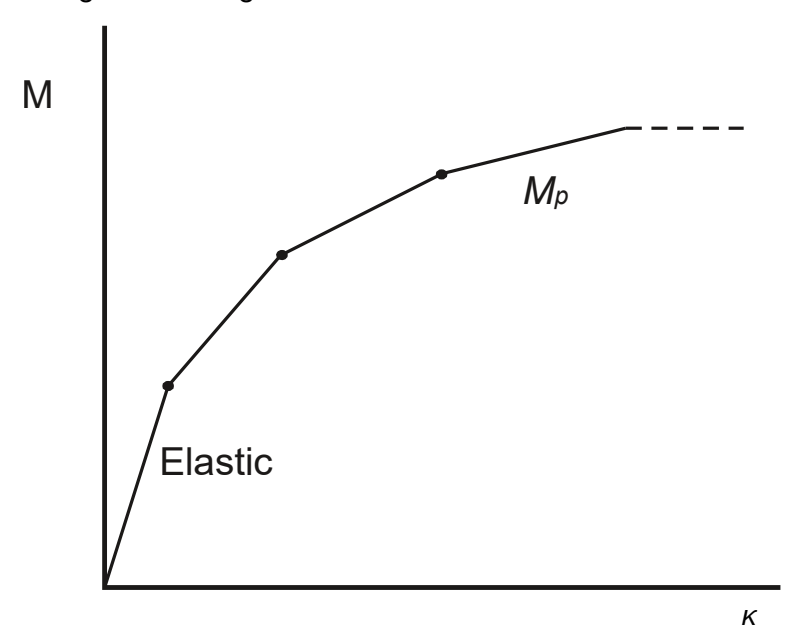


Figure 18-2: М-к diagram иdiagram

The first segment in the M-κ diagram determines the plate's elastic bending stiffness EI: $EI = M(1)/\kappa(1)$ (18-10) Additional segments in the M- κ diagram define the plate's non-linear elastoplastic behaviour. The last defined M-value is assumed to be the maximum bending moment, M_p , at which the plate fails. Elastic bending strains are calculated from the aforementioned El value, whereas additional bending (following the defined M- κ diagram) is assumed to be plastic, as long as the loading is in the same direction. Upon unloading from an elastoplastic state, the behaviour is initially elastic, but after significant unloading it may again generate plastic strains.

In the elastoplastic $(M-\kappa)$ plates, the axial force N is considered elastic and independent from the bending moment M. The axial force influences the stresses and displacements of the element but without affecting the bending moment. In the elastoplastic $(M-\kappa)$ plates, the $M-\kappa$ diagram is assumed to be the only one governing the plate's flexural behaviour.

18.4 2D Embedded beams

An embedded beam in PLAXIS 2D consists of plate elements with embedded interface elements to describe the interaction with the soil at the pile skin and at the pile foot (bearing capacity). The material parameters of the embedded beam distinguish between the parameters of the pile and the parameters of the skin resistance and foot resistance. The plate elements can have an elastic or an elastoplastic behaviour. In case plasticity can occur, the plate elements behave accordingly to a 2D plate (Figure 18-3 (p. 225)).

The elastic behaviour is defined by the following parameters:

E	Young's modulus in axial direction.	[kN/m ²]
Α	Beam cross section area.	[m ²]
I	Moment of inertia against bending around the beam axis.	[m ⁴]

The material behaviour in plate elements is defined by the following relationship between strains and stresses.

$$\begin{bmatrix} \sigma_N \\ \tau \end{bmatrix} = \begin{bmatrix} E & 0 \\ 0 & kG \end{bmatrix} \begin{bmatrix} \varepsilon_N \\ \gamma \end{bmatrix} \tag{18-11}$$

where

Normal stress

Shear stress

GShear modulus $G = \frac{E}{2(1+\nu)}$

κ Shear correction factor taken as 5/6

Normal strain

The material behaviour in plate elements is defined by the following relationship between structural forces and strains:

$$N=EA_{1}arepsilon_{N}$$
 (18–12)

$$Q = \frac{kEA}{2(1+\nu)}\gamma^* \tag{18-13}$$

$$M = EI\kappa$$
 (18–14)

The modified shear strain y^* takes into account the shear strain y and some additional terms in order to give a more accurate approximation of the problem.

The interaction of the pile with the soil at the skin of the pile is described by linear elastic behaviour with a finite strength and is defined by the following parameter:

T _{max}	Maximum traction allowed at the skin of the embedded beam (can vary along the pile)	[kN/m]
------------------	---	--------

The constitutive equation at the skin of the pile is defined by (see Figure 18–3 (p. 225)):

$$\begin{bmatrix} t_s \\ t_n \end{bmatrix} = \begin{bmatrix} K_s & 0 \\ 0 & K_n \end{bmatrix} \begin{bmatrix} u_s^p - u_s^s \\ u_s^p - u_n^s \end{bmatrix} \tag{18-15}$$

where

Displacement of the pile

Displacement of the soil

 K_{s} The elastic shear stiffness (against longitudinal (axial) displacement differences) of the embedded interface elements and K_n denotes the elastic axial stiffness (against transverse (lateral) displacement differences) of the embedded interface elements.

These values are calculated using the interface stiffness factors and the pile spacing defined by the user:

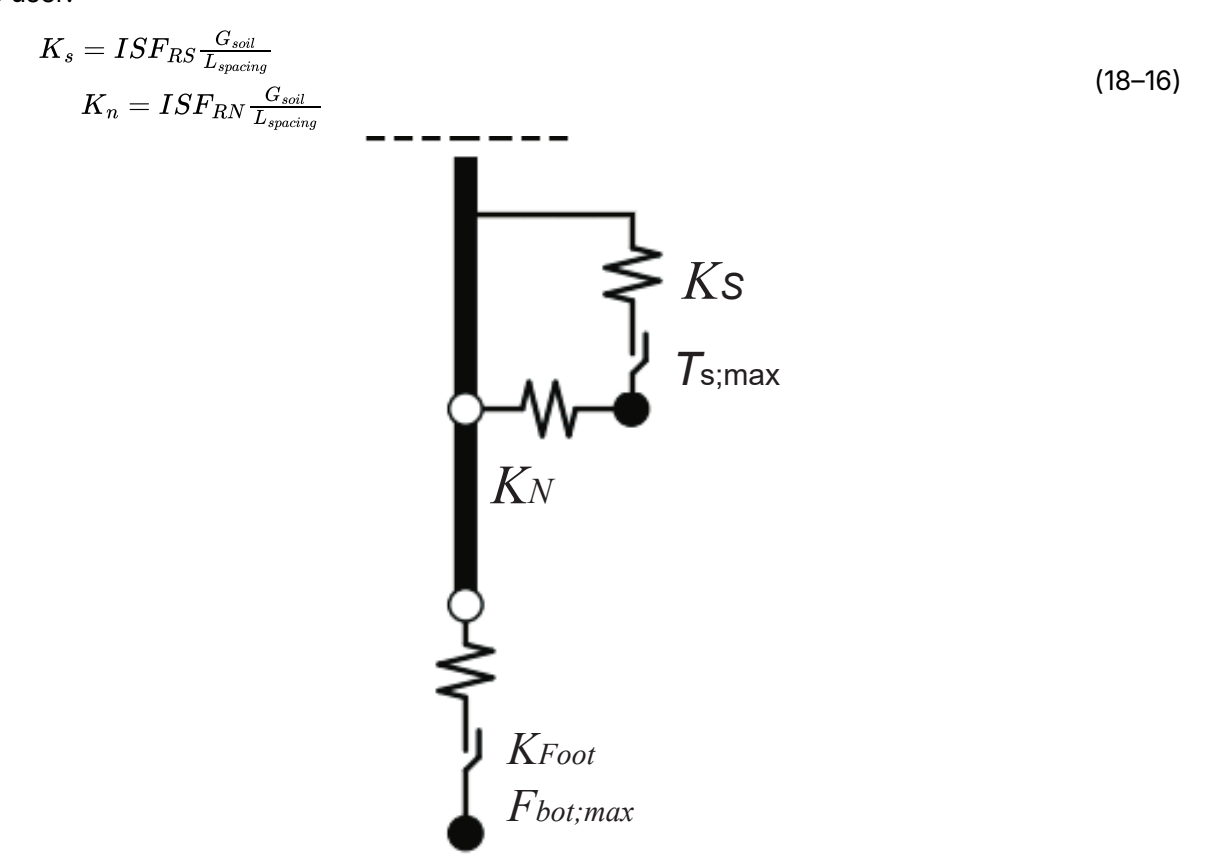


Figure 18-3: Stiffness of the embedded interface elements for piles

Default interface stiffness factors are calculated based on the pile spacing (Lspacing) in relation to the pile diameter (D_{eq}):

$$ISF_{RS} = 2.5 \left(\frac{L_{spacing}}{D_{eq}} \right)^{-0.75}$$
 (18–17)
$$ISF_{RN} = 2.5 \left(\frac{L_{spacing}}{D_{eq}} \right)^{-0.75}$$
 (18–18)
$$ISF_{KF} = 25 \left(\frac{L_{spacing}}{D_{eq}} \right)^{-0.75}$$
 (18–19)

$$ISF_{RN}=2.5igg(rac{L_{spacing}}{D_e q}igg)^{-0.75}$$
 (18–18)

$$ISF_{KF} = 25igg(rac{L_{spacing}}{D_{eq}}igg)^{-0.75}$$
 (18–19)

The normal stress t_n remains elastic if the Lateral resistance option is set to Unlimited. An elastoplastic behaviour is possible setting the Lateral resistance to Linear or Multi-linear.

For the shear stress in axial direction t_s to remain elastic it is given by:

$$(t_s) < T_{max} \tag{18-20}$$

For plastic behaviour the shear force t_s is given by:

$$(t_s) = T_{max} \tag{18-21}$$

The interaction of the pile with the soil at the foot of the pile is described by a linear elastic perfectly plastic interface element. The strength of the base is described by the following parameter:

F _{max}	Maximum force allowed at the foot of the embedded beam.	[kN]
------------------	---	------

In addition, no tension forces are allowed. In order to ensure that a realistic pile bearing capacity as specified can actually be reached, a zone in the soil surrounding the pile foot is identified where any kind of soil plasticity is excluded (elastic zone; Figure 18-4 (p. 227)). The size of this zone is determined by the embedded beam's equivalent radius R_{eq} (Reference Manual).

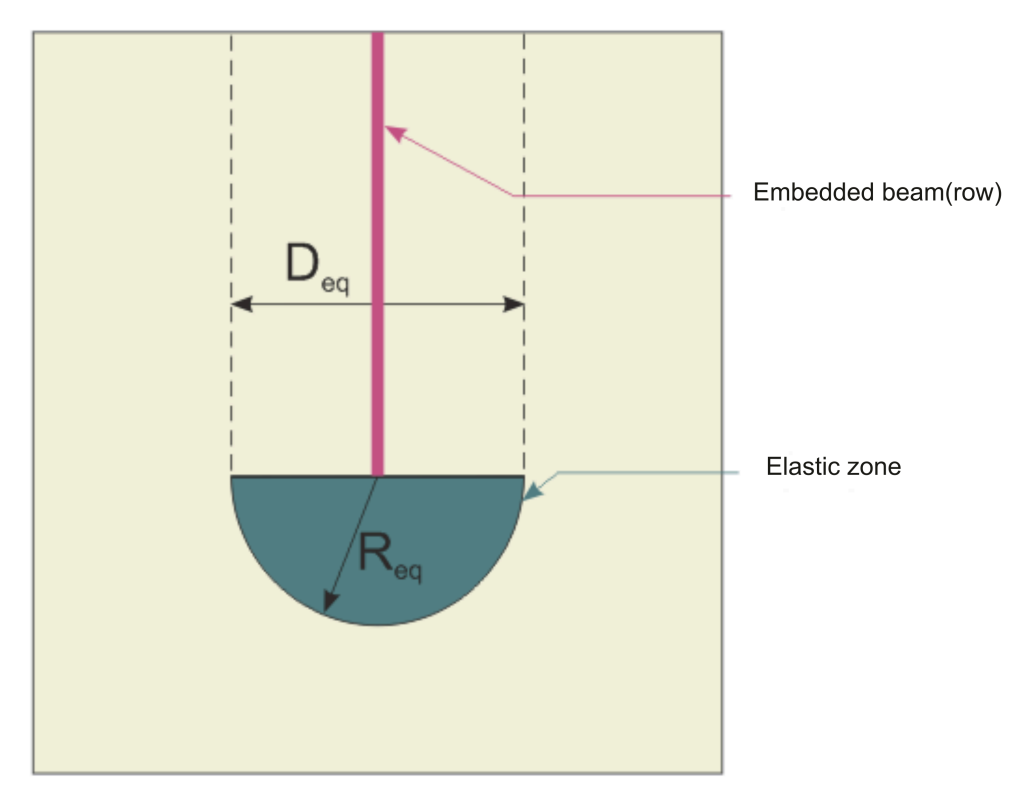


Figure 18-4: Elastic zone surrounding the bottom of the pile (after Sluis, 2012)

The constitutive relationship at the foot of the pile and its failure criterion are defined by:

$$F_{foot} = K_{foot} \left(u_{foot}^p - u_{foot}^s
ight) < F_{max}$$
 (18–22)

where

Stiffness of the spring which is defined in the same way as the stiffness of the embedded interface elements:

$$K_{foot} = ISF_{KF} rac{G_{soil}R_{eq}}{L_{s}}$$
 (18–23)

In case of plastic behaviour, the foot force F_{foot} is given by:

$$F_{foot} = F_{max} \tag{18-24}$$

Hydraulic Models

19.1 Van Genuchten model

A Soil Water Characteristic Curve (SWCC) is introduced to describe hydraulic parameters of the groundwater flow in unsaturated zones (usually above the phreatic surface). The SWCC describes the capacity of the soil to keep water at different stresses. There are many models which describe the hydraulic behaviour of unsaturated soils. The most common in the groundwater literature is the model proposed by $\underline{\text{van Genuchten (1980)}}$, which is used in PLAXIS. The Van Genuchten function is a three-parameter equation and relates the saturation to the pressure head ψ :

$$S(\psi) = S_{res} + (S_{sat} - S_{res})[1 + (g_a|\psi|)^{g_n}]^{g_c}$$
 (19–1)

where

 ψ = $-rac{p_w}{\gamma_w}$

 p_w = Suction pore stress.

 γ_w = Unit weight of the pore fluid.

 S_{res} = A residual saturation which describes a part of the fluid that remains in the pores even at high suction heads.

 S_{sat} In general at saturated conditions the pores will not be completely filled with water as air can get trapped and the saturation in this situation, S_{sat} , will be less than one. However, the default is $S_{sat} = 1.0$

 g_a A fitting parameter which is related to the air entry value of the soil and has to be measured for a specific material. It is in the unit of 1/L and is a positive value.

 g_n A fitting parameter which is a function of the rate of water extraction from the soil once the air entry value has been exceeded. This parameter has to be measured for a specific material.

 g_c A fitting parameter which is used in the general Van Genuchten equation. In PLAXIS the following assumption is made to convert the Van Genuchten to a two-parameter equation (Eqn. 19-2 (p. 229)).

$$g_c = \left(\frac{1 - g_n}{g_n}\right) \tag{19-2}$$

The Van Genuchten relationship provides reasonable results for low and intermediate suctions. For very high suction values, saturation remains at the residual saturation.

Figure 19–1 (p. 229) and Figure 19–2 (p. 230) show the effect of the parameters g_a and g_n on the shape of the SWCC.

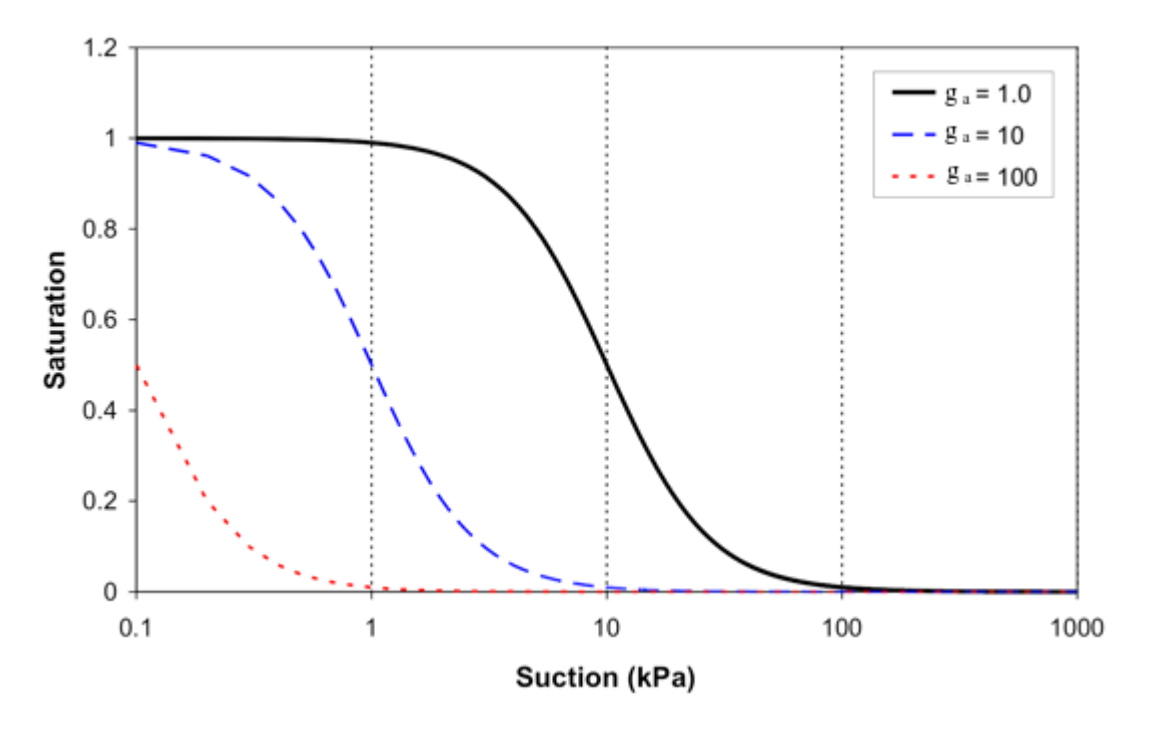


Figure 19–1: Effect of the parameter g_a on the SWCC

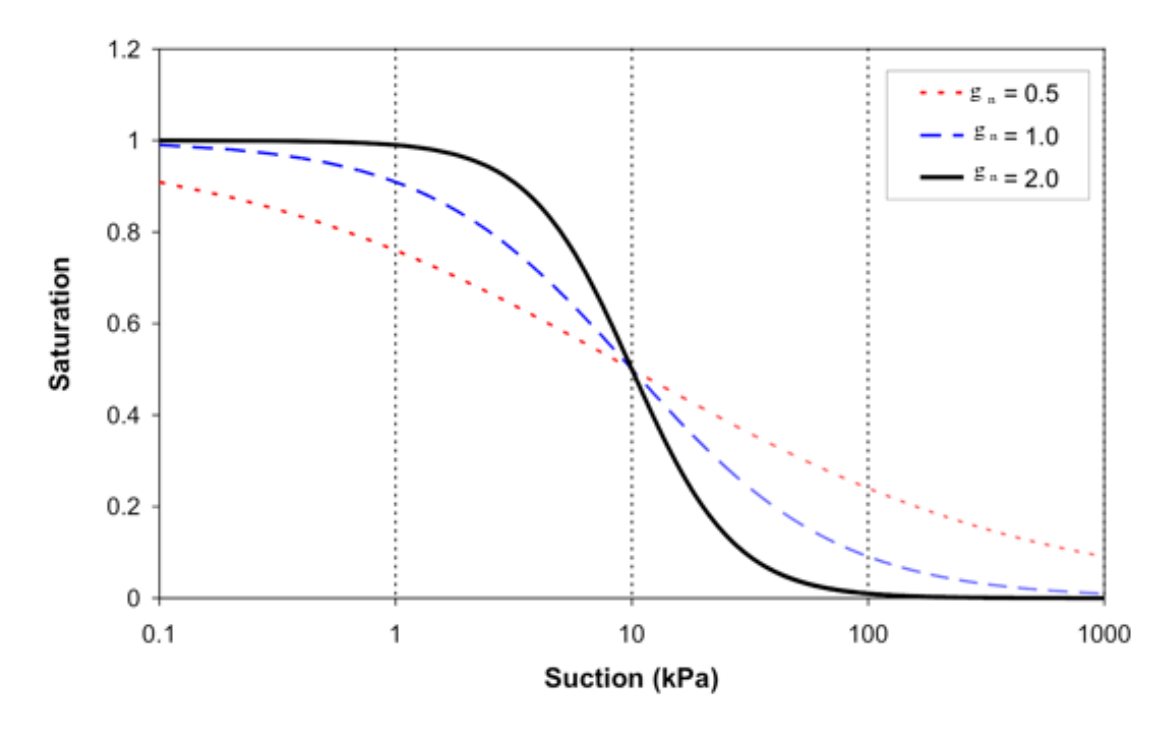


Figure 19–2: Effect of the parameter g_n on the SWCC

Relative permeability is related to the saturation via the effective saturation. The effective saturation S_{eff} is expressed as:

$$S_{eff} = \frac{S - S_{res}}{S_{sat} - S_{res}} \tag{19-3}$$

The relative permeability according to Van Genuchten now reads:

$$k_{rel}(S) = max \left[(S_{eff})^{g_l} \left(1 - \left[1 - S_{eff}^{\left(rac{g_n}{g_n-1}
ight)}
ight]^{\left(rac{g_n-1}{g_n}
ight)}
ight)^2, 10^{-4}
ight]$$
 (19–4)

 g_l is a fitting parameter and has to be measured for a specific material. Note that using the above expressions, the relative permeability can be related to the suction pore pressure directly.

The derivative of the degree of saturation with respect to the suction pore pressure reads:

$$rac{\partial S(p_w)}{\partial p_w} = (S_{sat} - S_{res}) igg[rac{1 - g_n}{g_n} igg] igg[g_n igg(rac{g_a}{\gamma_w} igg)^{g_n} \cdot p_w^{-(g_n - 1)} igg] igg[1 + igg(g_a \cdot rac{p_w}{\gamma_w} igg)^{g_n} igg]^{igg(rac{1 - 2g_n}{g_n} igg)}$$
 (19–5)

Figure 19-3 (p. 231) and Figure 19-4 (p. 231) present the Van Genuchten relations for a sandy material with parameters S_{sat} = 1.0, S_{res} = 0.027, g_a = 2.24 m⁻¹, g_l = 0.0 and g_n = 2.286 graphically.

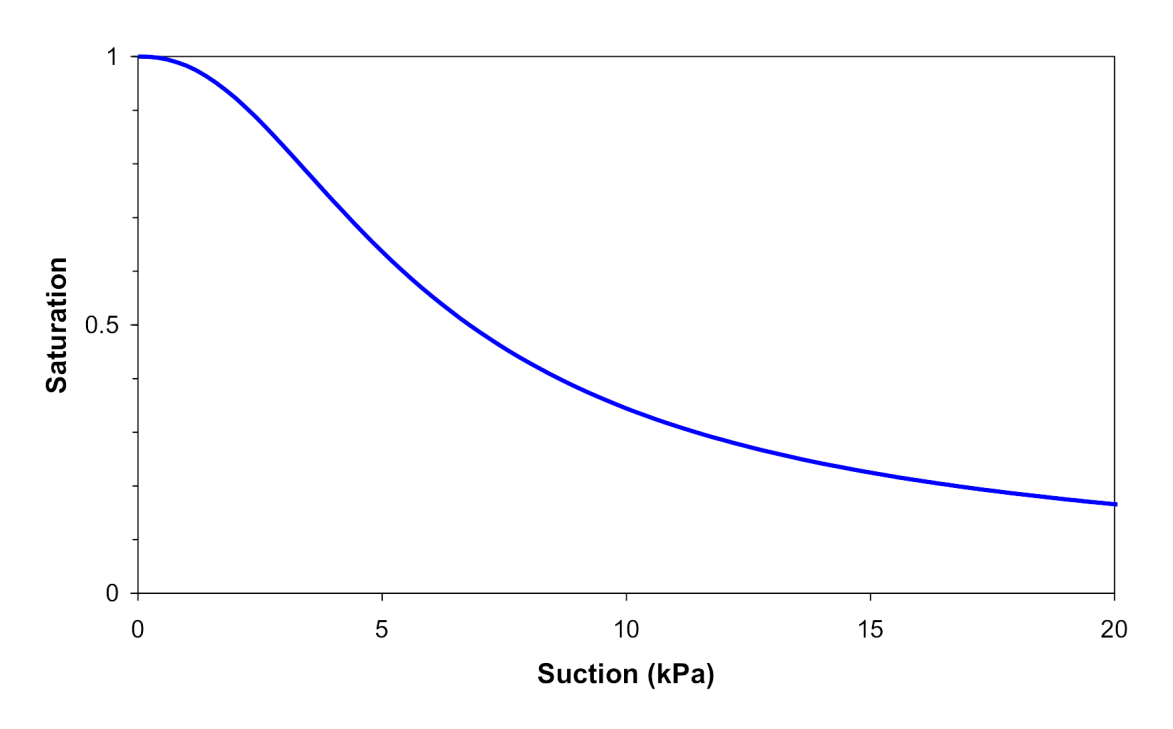


Figure 19-3: Van Genuchten suction-saturation permeability

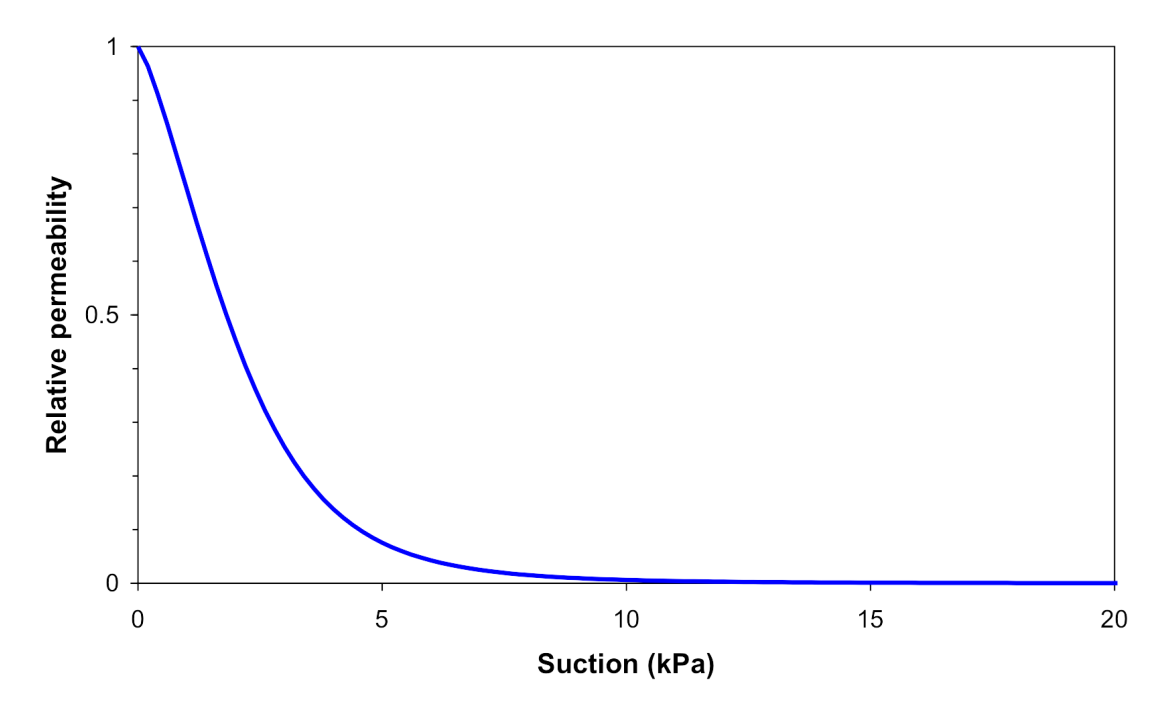


Figure 19-4: Van Genuchten suction-relative permeability

19.2 | Approximate Van Genuchten model

As an alternative, PLAXIS for flow analysis supports a linearised Van Genuchten model for which the approximate Van Genuchten parameters can be derived. According to this concept saturation relates to the pore pressure head as:

$$S(\psi)=\left\{egin{array}{ll} 1&if\ \psi\geq0\ 1+rac{\psi}{|\psi_s|}&if\ \psi_s<\psi<0\ 0&if\ \psi\leq\psi_s \end{array}
ight.$$
 (19–6)

The variable ψ_S is a material dependent pressure head which specifies the extent of the unsaturated zone under hydrostatic conditions. Below this threshold value the saturation is assumed to be zero. For saturated conditions the degree of saturation equals one.

The linearised Appoximate Van Genuchten relation between relative permeability and pressure head is written as:

$$k_{rel}\left(\psi
ight)=egin{cases} 1 & if\ \psi\geq0 \ 10^{rac{4\psi}{|\psi_k|}} & if\ \psi_k<\psi<0 \ 10^{-4} & if\ \psi<\psi_k \end{cases}$$
 (19–7)

According to this formulation the permeability in the transition zone is described as a log-linear relation of pressure head where ψ_k is the pressure head at which the relative permeability is reduced to 10^{-4} . In the Approximate Van Genuchten model the permeability remains constant for values of the pressure head higher than ψ_k . Under saturated conditions the relative permeability equals one and the effective permeability is equal to the saturated permeability which is assumed to be constant.

The input parameters of the "approximate Van Genuchten model" are derived from the classical Van Genuchten model. These parameters are translated into approximately equivalent process parameters for the numerically more robust linearised model. For ψ_S the translation is as follows:

$$\psi_S = \frac{1}{S_{\psi = -1.0 \,\mathrm{m}} - S_{sat}} \tag{19-8}$$

The parameter ψ_k is set equal to the pressure head at which the relative permeability according to Van Genuchten is 10^{-2} , with a lower limit of -0.5 m. Figure 19–5 (p. 233) presents the functional relation between pressure and saturation according to the approximate Van Genuchten model using ψ_k = 1.48 m. The corresponding pressure-relative saturation relation ψ_s = 1.15 m is given in Figure 19-6 (p. 233).

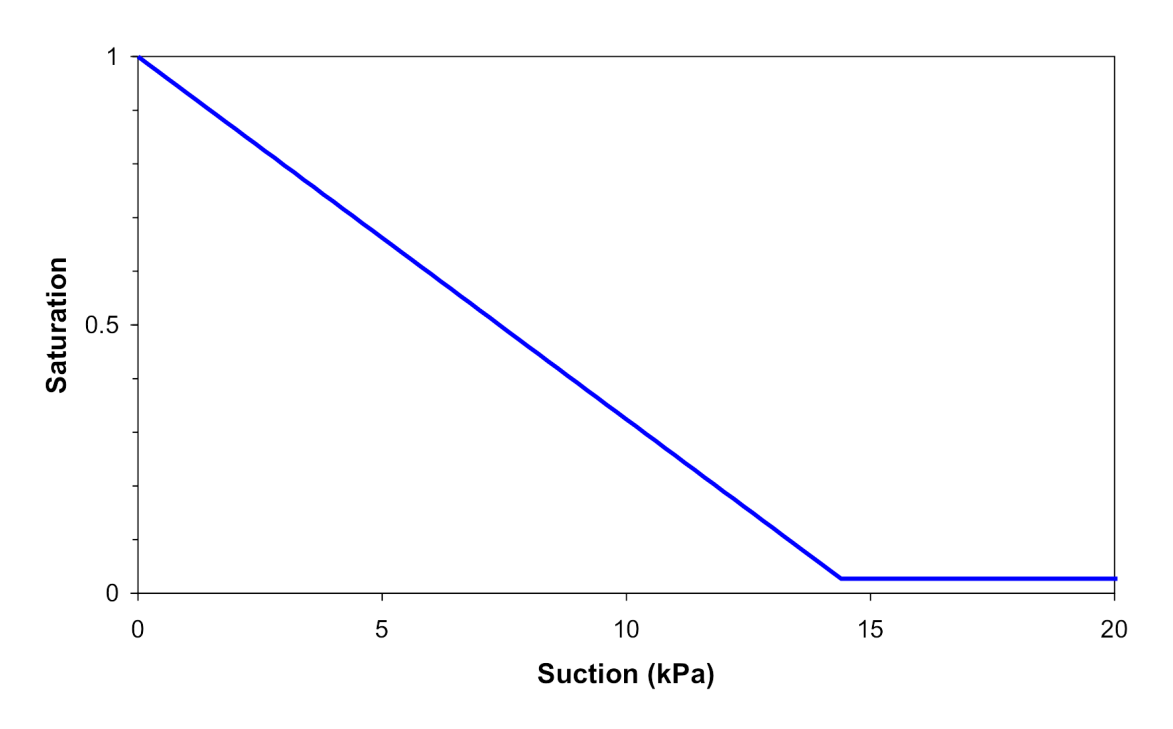


Figure 19–5: Approximate Van Genuchten pressure-saturation

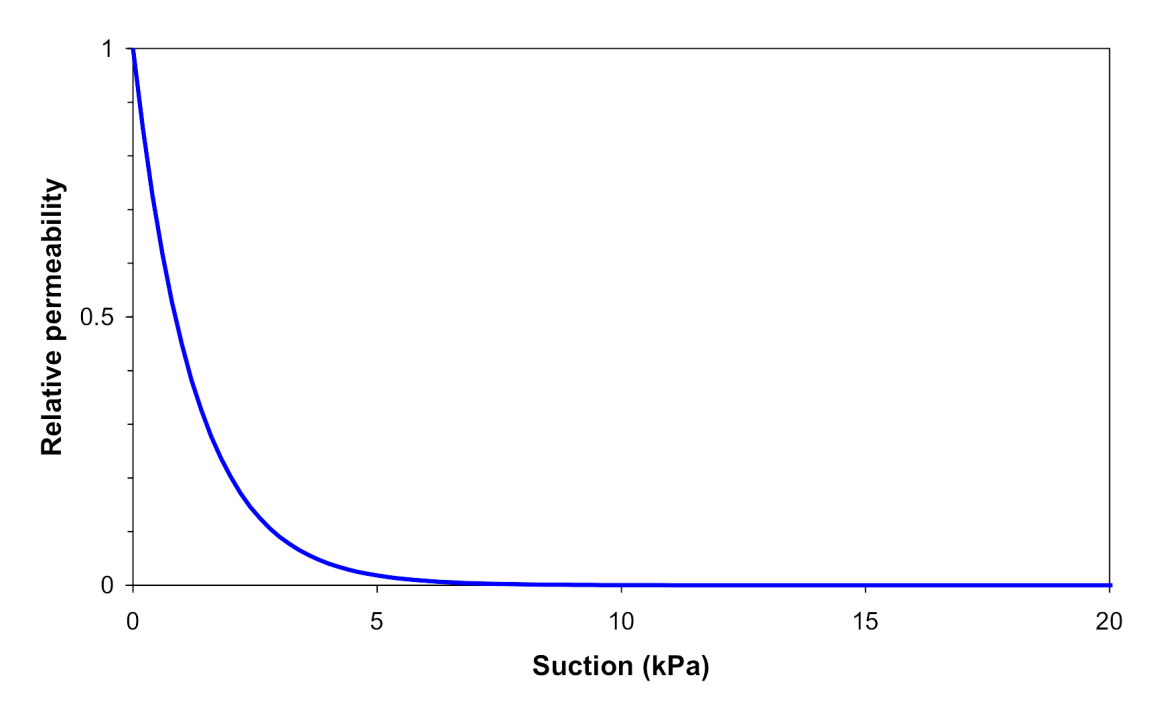


Figure 19–6: Approximate Van Genuchten pressure-relative permeability

References

- 1. (1990). CEB-FIP model code Fédération internationale du béton.
- 2. (1992). ACI 209R-92 American Concrete Institute.
- **3.** (2004). Eurocode 2: Design of concrete structures . European Committee for Standardization.
- **4.** Adachi, T., Oka, F. (1982). Constitutive equation for normally consolidated clays based on elasto-viscoplasticity. Soils and Foundations, 22, 57–70.
- **5.** Alpan, I. (1970). The geotechnical properties of soils. Earth-Science Reviews, 6, 5–49.
- **6.** Andersen, K., Kleven, A., Heien, D. (1988). Cyclic soil data for deisgn of gravity structures. Journal of Geotechnical engineering, 114, 517–539.
- **7.** Andersen, K.H. (2009). Bearing capacity under cyclic loading â Ă T offshore, along the coast, and on land. Canadian Geotechnical Journal, 46, 513–535.
- **8.** Andersen, K.H. (2015). Cyclic soil parameters for offshore foundation design. Frontiers in Offshore Geotechnics III, 5–82.
- **9.** Andresen, L. (2002). Capacity analysis of anisotropic and strain-softening clay. Ph.d. thesis, University of Oslo, Institute of Geology.
- **10.** Andresen, L., Jostad, H.P. (1999). Application of an anisotropic hardening model for undrained response of saturated clay. Proc. NUMOG VII, 581–585.
- **11.** Andresen, L., Jostad, H.P. (2009). A fe procedure for calculation of displacements and capacity of foundations subjected to cyclic loading. Proc. COMGEO I.
- 12. Atkinson, J.H., Bransby, P.L. (1978). The Mechanics of Soils. McGraw-Hill, London.
- **13.** Atkinson, J.H., Sallfors, G. (1991). Experimental determination of soil properties. In Proc. 10th ECSMFE, 3, 915–956.
- **14.** Austin, S.A., Robins, P.J. (1995). Sprayed Concrete: Properties, Design and Installation. Whittles Publishing, Dunbeath.
- **15.** Barros, J.A.O., Figueiras, J.A. (1999). Flexural behaviour of sfrc: testing and modelling. Journal of Materials in Civil Engineering, ASCE 11, 331–339.

- Beaty, M.H., Byrne, P.M. (1998). An effective stress model for predicting liquefaction 16. behaviour of sand. Geotechnical Earthquake Engineering and Soild Dynamics, ASCE Geotechnical Special Publication 75, 766–777.
- 17. Beaty, M.H., Byrne, P.M. (2011). Ubcsand constitutive model. Itasca UDM website 904aR.
- 18. Beaty, M.H., Perlea, V.G. (2011). Several observations on advanced analyses with liquefiable materials. Thirty first annual USSD conference on 21st century dam designadvances and adaptations, 1369-1397.
- 19. Belytschko, T., Lasry, D. (1989). Localization limiters and numerical strategies for strainsoftening materials. In Proc. France-US Workshop on Strain localization and size effect due to cracking and Damage editor= (Mazars & Bazant). 349-362.
- 20. Benz, T. (2006), Small-Strain Stiffness of Soils and its Numerical Consequences, Ph.d. thesis, Universität Stuttgart.
- 21. Benz, T., Schwab, R., Vermeer, P.A., Kauther, R.A. (2007). A hoek-brown criterion with intrinsic material strength factorization. Int.J. of Rock Mechanics and Mining Sci., 45(2), 210-222.
- Biarez, J., Hicher, P.Y. (1994). Elementary Mechanics of Soil Behaviour. A A Balkema, 22. Rotterdam, The Netherlands.
- Billington, E.W. (1988). Generalized isotropic yield criterion for incompressible materials. 23. Acta Mechanica, 72, 1-20.
- Bjerrum, L. (1967). Engineering geology of norwegian normally-consolidated marine clays 24. as related to settlements of buildings. Seventh Rankine Lecture, Geotechnique 17, 81-118.
- 25. Bolton, M.D. (1986). The strength and dilatancy of sands. Géotechnique, 36(1), 65-78.
- Borja, R.I., Kavaznjian, E. (1985). A constitutive model for the -"-t behaviour of wet clays. 26. Geotechnique, 35, 283-298.
- 27. Borja, R.I., Lee, S.R. (1990). Cam-clay plasticity, part 1: implicit integration of elasto-plastic constitutive relations. Computer Methods in Applied Mechanics and Engineering, 78, 48-72.
- Branque, D. (1997). Utilisation d'un modèle Élasto-plastique avec dilatance dans 28. l'interprétation de l'essai pressiométrique sur sable. Ph.d. thesis, Ecole Centrale Paris.
- Brinkgreve, R.B.J. (1994). Geomaterial Models and Numerical Analysis of Softening. 29. Dissertation. Delft University of Technology.
- Brinkgreve, R.B.J. (2004). Time-dependent behaviour of soft soils during embankment 30. construction - a numerical study. Proc. NUMOG IX, 631–637.
- 31. Brinkgreve, R.B.J., Engin, E., Engin, H. (2010). Validation of empirical formulas to derive model parameters for sands. In T. Benz, S. Nordal (eds.), 7th European Conference Numerical Methods in Geotechnical Engineering. Numge 2010, Trondheim, volume 1, 137-
- 32.
- 33. Brinkgreve, R.B.J., Vermeer, P.A. (1992). On the use of cam-clay models. In Proc. IV Int. Symposium on Numerical Models in Geomechanics (eds. G.N. Pande, S. Pietruszczak). Balkema, Rotterdam, volume 2, 557-565.
- Buisman, K. (1936). Results of long duration settlement tests. Proceedings 1st International 34. Conference on Soil Mechanics and Foundation Engineering, Mass. Vol. 1, 103–107.
- 35. Burland, J.B. (1965). The yielding and dilation of clay. Géotechnique, 15, 211–214. (Correspondence).
- 36. Burland, J.B. (1967). Deformation of Soft Clay. Dissertation. Cambridge University.
- Burns, N.H., Siess, C.P. (1962). Load-deformation characteristics of beam-column 37. connections in reinforced concrete. Civil Engineering Studies, SRS no. 234.Universty of Illinois, Urbana.
- Butterfield, R. (1979). A natural compression law for soils (an advance on e-log p'). 38. Geotechnique, 29, 469-480.

- Carranza-Torres, C. (2004). Elastoplastic solution of tunnel problems using the generalized for of the hoek-brown failure criterion. Int.J. of Rock Mechanics and Mining Sci., 41(3), 480-481.
- 40. Chen, W.F. (1975). Limit analysis and soil plasticity. Elsevier, Amsterdam.
- 41. Davis, E.H., Christian, J.T. (1971). Bearing capacity of anisotropic cohesive soil. Journal of Soil Mechanics and Foundation Division, 97, 753-769.
- 42. Deere, D.U. (1968). Rock mechanics in engineering practice. London: Wiley.
- den Haan, E.J. (1994). Vertical Compression of Soils. Thesis, Delft University. 43.
- 44. Drucker, D.C., Prager, W. (1952). Soil mechanics and plastic analysis or limit design. Quart. Appl. Math., 10(2), 157–165.
- Duncan, J.M., Chang, C.Y. (1970). Nonlinear analysis of stress and strain in soil. ASCE J. of 45. the Soil Mech. and Found. Div., 96, 1629-1653.
- 46. Fung, Y.C. (1965). Foundations of Solid Mechanics. Prentice-Hall, New Jersey, USA.
- 47. Garlanger, J.E. (1972). The consolidation of soils exhibiting creep under constant effective stress. Géotechnique, 22, 71-78.
- 48. Grimstad, G., Andresen, L., Jostad, H.P. (2010). Anisotropic shear strength model for clay. International Journal for Numerical and Analytical Methods in Geomechanics, (Accepted for publication).
- 49. Hardin, B.O., Black, W.L. (1969). Closure to vibration modulus of normally consolidated clays. Proc. ASCE: Journal of the Soil Mechanics and Foundations Division, 95(SM6), 1531–1537.
- Hardin, B.O., Drnevich, V.P. (1972). Shear modulus and damping in soils: Design equations 50. and curves. Proc. ASCE: Journal of the Soil Mechanics and Foundations Division, 98(SM7), 667-692.
- 51. Hill, R. (1950). The Mathematical Theory of Plasticity. Oxford University Press, London,
- Hoek, E. (1999). Putting numbers to geology-an engineers's viewpoint. Quarterly Journal **52**. of Engineering Geology, 32, 1–9.
- Hoek, E. (2006). Practical Rock Engineering. E-book. 53.
- 54. Hoek, E., Carranza-Torres, C., Corkum, B. (2002). Hoek-brown failure criterion - 2002 edition. volume 1, 267-273.
- 55. Hoek, E., Diederichs, M.S. (2006). Empirical estimation of rock mass modulus, volume 43, 203-215.
- 56. lizuka, A., Ohta, H. (1987). A determination procedure of input parameters in elastoviscoplastic finite element analysis. Soils and Foundations, 27, 71–87.
- **57.** Jaky, J. (1944). The coefficient of earth pressure at rest. J. Soc. Hung. Eng. Arch.,
- 58. Janbu, N. (1963). Soil compressibility as determined by oedometer and triaxial tests. Proc. ECSMFE Wiesbaden, 1, 19–25.
- 59. Janbu, N. (1969). The resistance concept applied to soils. Proceedings of the 7h ICSMFE, Mexico City, 1, 191–196.
- 60. Janbu, N. (1985). Soil models in offshore engineering (25th rankine lecture). Géotechnique, 35, 241-280.
- Jostad, H.P., Torgerstrud, Engin, H. (2015). A fe procedure for calculation of fixity of jack-61. up foundations with skirts using cyclic strain contour diagrams. In The 15th International Conference: The Jack-up Platform. London.
- 62. Koiter, W.T. (1953). Stress-strain relations, uniqueness and variational theorems for elastoplastic materials with a singular yield surface. Quart. Appl. Math., 11, 350-354.
- Koiter, W.T. (1960). General theorems for elastic-plastic solids. In I.N. Sneddon, R. Hill (eds.), Progress in Solid Mechanics. North-Holland, Amsterdam, volume 1, 165-221.
- Kondner, R.L. (1963). A hyperbolic stress strain formulation for sands. 2. Pan. Am. ICOSFE 64. Brazil, 1, 289-324.
- Kormeling, H.A., Reinhardt, H.W. (1969). Determination of the fracture energy of normal **65**. concrete and epoxy modified concrete. Delft University of Technology.

- Kulhawy, F.H., Mayne, P.W. (1990). Manual on Estimating Soil Properties for Foundation Design. Cornell University, Ithaca, New York.
- Kwak. H.G., Filippou, F.C. (1996). Nonlinear fe analysis of r/c structures under monotonic 67. loads. Computer and Structures, 65(1), 1-16.
- Laera, A., Brinkgreve, R.B.J. (2015). Liquefaction analysis with the use of the finite element 68. code plaxis. In 5th. Int. Conf. IAGIG. Roma.
- 69. Leroueil, S. (1977). Quelques considérations sur le comportement des argiles sensibles. Ph.d. thesis, Laval University, Québec.
- Li, X.S., Dafalias, Y.F. (2000). Dilatancy for cohesionless soils. Geotechnique, 50(4), 449-70. 460.
- Marinos, P., Hoek, E. (2001). Estimating the mechanical properties of heterogeneous rock 71. masses such as flysh. Bulletin of Engineering Geology, 92,60-85.
- Masing, G. (1926). Eigenspannungen und verfestigung beim messing. In In Proc. 2nd Int. **72.** Congr. Appl. Mech. Zurich.
- 73. Mayne, P.W. (2001). Keynote: Stress-strain-strength-flow parameters from enhanced insitu tests. In In-Situ Measurement of Soil Properties and Case Histories. Indonesia, 27-47.
- 74. Meschke, G., Kropik, C., Mang, H.A. (1996). Numerical analysis of tunnel linings by means of a viscoplastic material model for shotcrete. International Journal for Numerical Methods in Engineering, 39, 3145-62.
- Mesri, G., Godlewski, P.M. (1977). Time and stress-compressibility inter-relationship. **75**. Journal of the Geotechnical Engineering Division, ASCE, 103(GT5), 417-430.
- Muir Wood, D. (1990), Soil Behaviour and Critical State Soil Mechanics, Cambridge 76. University Press.1, 355-358.
- 77. Murayama, S., Shibata, T. (1966). Flow and stress relaxation of clays. In I.U.T.A.M. Symp. on Rheology and Soil Mechanics. Grenoble, 99-129.
- Naesgaard, E. (2011). A hybrid effective stress-total stress procedure for analysing soil 78. embankments subjected to potential liquefaction and flow. Ph.d. thesis, University of British Columbia.
- 79. Niemunis, A., Herle, I. (1997). I.: Hypoplastic model for cohesionless soils with elastic strain range. Mechanics of Cohesive Frictional Materials, 2(3), 279–299.
- 80. Ohta, H., Hata, S. (1973). Immediate and consolidation deformations of clay. In 8th. Int. Conf. S.M.F.E. volume 1, 193-196.
- Oluokun, F.A., Burdette, E.G., Deatherage, J.H. (1991). Splitting tensile strength and 81. compressive strength relationship at early ages. ACI Materials Journal, 88(2), 115–121.
- Petalas, A., Galavi, V. (2012). Plaxis liquefaction model ubc3d-plm. PLAXIS knowledge 82.
- Pipatpongsa, T., lizuka, A., Kobayashi, I., Ohta, H. (2002). Fem formulation for analysis 83. of soil constitutive model with a corner on the yield surface. Journal of Structural Engineering, 48, 185-194.
- 84. Polling, R. (2000). Eine praxisnahe, schÄd'digungsorientierte Materialbeschreibung von Stahlbeton fÄijr Strukturanalysen. Ph.d. thesis, Ruhr-Universität, Bochum.
- Prevost, J.H. (1976). Undrained stress-strain-time behaviour of clavs. Journal of the 85. Geotechnical Engineering Division, GT12, 1245-1259.
- Puebla, H., Byrne, M., Phillips, P. (1997). Analysis of canlex liquefaction embankments 86. prototype and centrifuce models. Canadian Geotechnical Journal, 34, 641-657.
- 87. Randolph, M., Gourvenec, S. (2011). Offshore Geotechnical Engineering. Spoon Press, New
- Roscoe, K.H., Burland, J.B. (1968). On the generalized stress-strain behaviour of "wet" 88. clay. In In: Heyman & Leckie, Engineering Plasticity, Cambridge University Press. 535-609.
- Roscoe, K.H., Schofield, A.N., Thurairajah, A. (1963). Yielding of clays in states wetter than critical. Geotechnique, 13(3), 211-240.
- 90. Rots, J.G. (1988). Computational modelling of concrete fracture. PhD Thesis. Delft University of Technology.

- 91. Rowe, P.W. (1962). The stress-dilatancy relation for static equilibrium of an assembly of particles in contact. In Proc. Roy. Soc. A., No. 269, 500-527.
- Santos, J.A., Correia, A.G. (2001), Reference threshold shear strain of soil, its application 92. to obtain a unique strain-dependent shear modulus curve for soil. In Proceedings 15th International Conference on Soil Mechanics and Geotechnical Engineering, Istanbul, Turkey, volume 1, 267-270.
- Schadlich, B., Schweiger, H.F. (2014). A new constitutive model for shotcrete. In T..F. 93. Group (ed.), Numerical Methods in Geotechnical Engineering, 103–108.
- 94. Schanz, T. (1998). Zur Modellierung des Mechanischen Verhaltens von Reibungsmaterialen. Habilitation, Stuttgart Universität.
- 95. Schanz, T., Vermeer, P.A. (1996), Angles of friction and dilatancy of sand, Géotechnique. 46. 145–151.
- 96. Schanz, T., Vermeer, P.A. (1998). Special issue on pre-failure deformation behaviour of geomaterials. Géotechnique, 48, 383-387.
- Schanz, T., Vermeer, P.A., Bonnier, P.G. (1999). The hardening-soil model: Formulation and 97. verification. In R.B.J. Brinkgreve, Beyond 2000 in Computational Geotechnics, Balkema, Rotterdam. 281-290.
- Schütz, R., Potts, D.M., Zdravkovi'c, L. (2011). Advanced constitutive modelling of 98. shotcrete: Model formulation and calibration. Computers and Geotechnics, 38(6), 834-845.
- 99. Schweiger, H.F. (2002). Results from numerical benchmark exercises in geotechnics. In P. Mestat (ed.), 5th European Conference Numerical Methods in Geotechnical Engineering. Numge 2002, Paris, volume 1, 305-314.
- 100. Sekiquchi, H. (1977). Rheological characteristics of clays. In Proceedings of the 9th ICSMFE. Tokyo, volume 1, 289-292.
- 101. Sekiguchi, H., Ohta, H. (1977). Induced anisotropy and time dependency in clays. In Proceedings of the 9th ICSMFE. Tokyo, volume 3, 542–544.
- 102. Simpson, B. (1992), "retaining structures; displacement and design", the 32nd rankine lecture. Geotechnique, 42(4), 541-576.
- 103. Sluis, J. (2012). Validation of embedded pile row in PLAXIS 2D. Master's thesis. Delft University of Technology.
- 104. Smith, I.M., Griffiths, D.V. (1982). Programming the Finite Element Method. John Wiley & Sons, Chisester, U.K., second edition.
- 105. Souliotis, C., Gerolymos, N. (2016). Seismic analysis of guay wall in liquefiable soil with the ubc3d-plm constitutive model: Calibration methodology and validation. In 1th International Conference on Natural Hazards & Infrastructure. Chania.
- 106. Stolle, D.F.E. (1991). An interpretation of initial stress and strain methods, and numerical stability. International Journal for Numerical and Analytical Methods in Geomechanics, 15, 399-416.
- 107. Stolle, D.F.E., Bonnier, P.G., Vermeer, P.A. (1997). A soft soil model and experiences with two integration schemes. In Numerical Models in Geomechanics. Numog 1997, 123-128.
- 108. Taiebat, H.A., Carter, J.P. (2008). Flow rule effects in the tresca model. Computers and Geotechnics, 35, 500-503.
- 109. Takeyama, T., Ohno, S., Pipatpongsa, T., Iizuka, A., Ohta, H. (2010). The stress update using implicit integration for the viscid version of sekiguchi-ohta model. Technical report, Technical report.
- 110. Tsegaye, A. (2010). Plaxis liquefaction model. external report. PLAXIS knowledge base.
- Ukritchon, B., Whittle, A.J., Sloan, S.W. (2003). Undrained stability of braced excavations in clay. Journal of Geotechnical and Geoenvironmental Engineering, 129(8), 738–755.
- 112. Vaid, Y., Campanella, R.G. (1977). Time-dependent behaviour of undisturbed clay. ASCE Journal of the Geotechnical Engineering Division, 103(GT7), 693-709.
- van Genuchten, M. (1980). A closed-form equation for predicting the hydraulic conductivity of unsaturated soils. Soil science society of America journal, 44(5), 892-898.

- 114. van Langen, H., Vermeer, P.A. (1990). Automatic step size correction for non-associated plasticity problems. Int. J. Num. Meth. Engng., 29, 579-598.
- 115. Vermeer, P.A., Borst, R. (1984). Non-associated plasticity for soils, concrete and rock. Heron, 29(3).
- 116. Vermeer, P.A., Neher, H. (1999). A soft soil model that accounts for creep. In R.B.J. Brinkgreve, Beyond 2000 in Computational Geotechnics, Balkema, Rotterdam. 249-261.
- Vermeer, P.A., Stolle, D.F.E., Bonnier, P.G. (1998). From the classical theory of secondary compression to modern creep analysis. Proc. 9th Int. Conf. Comp. Meth. and Adv. Geomech., Wuhan, China, 4, 2469-2478.
- 118. Vermeer, P.A., van Langen, H. (1989). Soil collapse computations with finite elements. In Ingenieur-Archive 59. 221-236.
- 119. von Mises, R. (1913). Mechanik der festen körper in plastisch deformablem zustand. Göttinger Nachrichten Math.-Phys. Klasse, 1, 582-592.
- 120. von Soos, P. (1990). Properties of soil and rock (in german). In In: Grundbautaschenbuch Part 4. Ernst & Sohn, Berlin.
- 121. Vucetic, M., Dobry, R. (1991). Effect of soil plasticity on cyclic response. Journal of Geotechnical Engineering, ASCE, 117(1), 89-107.
- 122. Wyllie, D.C., Mah, C. (2004). Rock slope engineering. CRC Press, Boca Raton.

Appendices

Symbols

A.1 General symbols

Symbol	Name
А	Cross section area
С	Cohesion
csp	Current stiffness parameter
С	Correction factor for SPT value
C_{α}	Creep index for secondary compression
C _c	Compression index
C _r	Ricompression index
C_s	Swelling index
C_u , S_u	Undrained shear-strength
d	Thickness
D	Disturbance factor
D^e	Elastic material matrix representing Hooke's law
е	Void ratio
Е	Young's modulus

Symbol	Name
E _{oed}	Oedometer modulus
f	Yield function
f _{dens}	Densification factor
<i>f</i> _{Epost}	Post-liquefaction factor
g	Plastic potential function
G	Shear modulus
GSI	Geological Strength Index
G _{ur}	Unloading/reloading shear modulus
I	Moment of inertia
k ^{*e} _B	Elastic bulk modulus factor
k ^{*e} _G	Elastic shear modulus factor
k ^{*p} _G	Plastic shear modulus factor
k ^{*p} _{G,secondary}	Secondary plastic shear modulus factor
К	Bulk modulus
K ₀	Coefficient of lateral earth pressure (initial stress state)
K_0^{nc}	Coefficient of lateral earth pressure for a normally consolidated stress state
me	Power in stress-dependent relation for elastic bulk modulus
m _i	Intact rock parameter
ne	Power in stress-dependent relation for elastic shear modulus
np	Power in stress-dependent relation for plastic shear modulus
М	Slope of critical state line in p'-q space
М	Bending moment
n _{rev}	Number of shear stress reversals
N	Normal force
N _{1,60}	Corrected SPT value
OCR	overconsolidation ratio
p	Isotropic stress or mean stress, negative for pressure; positive for tension
p_w	Pore pressure
ρ_p	Isotropic pre-consolidation stress, negative for pressure
POP	Pre overburden pressure, positive for (over)pressure
q	Equivalent shear stress or deviatoric stress

Symbol	Name			
Q	Shear force			
R_f	Failure ratio			
r _{u,σ'v}	Excess pore pressure ratio in terms of vertical effective stresses			
r _{u,p'}	Excess pore pressure ratio in terms of mean effective stresses			
RD	Relative density			
s ^a u	Undrained active shear strength			
s ^{c,TX} u	Undrained triaxial compressive shear strength			
s ^{DSS} u	Undrained direct simple shear strength			
s ^p u	Undrained passive shear strength			
t	Time			
\underline{u}	Vector with displacement components			
γ	Unit weight			
γ	Various types of shear strain			
α ₁	dip angle			
α_2	dip direction			
Δ	Increment			
<u>ε</u>	Vector with Cartesian strain components, normal components positive for extension; negative for compression			
$arepsilon_q$	Deviatoric strain (invariant)			
$\varepsilon_{\scriptscriptstyle V}$	Volumetric strain, negative for compression; positive for extension			
К	Cam-Clay swelling index			
К *	Modified swelling index			
λ	Plastic multiplier			
λ	Cam-Clay compression index			
λ *	Modified compression index			
μ *	Modified creep index			
ν	Poisson's ratio			
<u>σ</u>	Vector with Cartesian stress components, normal components positive for tension; negative for pressure			
σ_{ψ}	Confining pressure at which ψ = 0			
σ_{ci}	Uni-axial compressive strength			
σ_p	Vertical pre-consolidation stress, negative for pressure			
φ	Friction angle			

Symbol	Name
$arphi_{\scriptscriptstyle extsf{CV}}$	Costant volume friction angle
$arphi_{mob}$	Mobilised friction angle
φ_{p}	Peak friction angle
Ψ	Dilatancy angle
Ψ_m	Mobilised dilatancy angle
Ψ _{max}	Maximum dilatancy angle
× ^c	Denotes creep component
x ^e	Denotes elastic component
× ^p	Denotes plastic component
× ^{ref}	Denotes reference value (related to a reference stress)
× _u	Denotes undrained
× _{ur}	Denotes unloading and reloading
× _m	Denotes mobilised

A.2 Concrete Model symbols

Model symbol	Name
а	Increase of $arepsilon_{cp}$ with increase of p
f	Yield stress
f_{xxn}	Normalised strength
F	Yield function
G	Fracture energy
Н	Normalised hardening/softening
J	Shotcrete strength class
k_{σ}	Degree of concrete utilisation in compression
L _{eq}	Characteristic length of the finite element
s	Power in time-dependent strength/stiffness relations
t _{hydr}	Time of full curing
V _{fx}	Safety factor for strength
$arphi_{ m cr}$	Creep factor
$oldsymbol{arphi}_{max}$	Maximum friction angle
Ψ	Dilatancy angle

Model symbol	Name
× ^{cr}	denotes creep
× ^{shr}	denotes shrinkage
× _∞	Denotes a time $t = \infty$
× ₂₈	Denotes a value of cured concrete
×50	Denotes a time t when 50% of the phenomenon has occurred
× _{cp}	Denotes peak in uniaxial compression
× _{xf}	Denotes a uniaxial failure value

Applicability of the material models

B.1 Aplicability material models: Based on different materials

Considering different materials:

Model	Concrete	Rock	Gravel	Sand	Silt	OC clay	NC clay	Peat(org)
Linear Elastic Model	С	С						
Mohr- Coulomb model	В	В	С	С	С	С	С	С
Hardening soil model			В	В	В	В	В	
HS small model			А	А	А	А	В	
UBC3D- PLM model			В*	B*	B*			

Model	Concrete	Rock	Gravel	Sand	Silt	OC clay	NC clay	Peat(org)
Soft Soil creep model							A*	A*
Soft soil model							A*	A*
Jointed rock model		A**						
Modified Cam- Clay model							С	С
NGI-ADP model						A*	A*	A*
UDCAM- S model						A*	A*	A*
Hoek- Brown model		A**						
Concrete model	А							

A: The best standard model in PLAXIS for this application

B: Reasonable modelling

C: First order (crude) approximation

- *: Soft Soil Creep model in case time-dependent behaviour is important; UBC3D-PLM model for dynamics analysis of sandy soils involving liquefaction
- *: NGI-ADP model for short-term analysis and UDCAM-S model for cyclic analysis, in case only undrained strength is known
- ** : Jointed Rock model in case of anisotropy and stratification; Hoek-Brown model for rock in general

B.2 Aplicability material models: Based on different applications

Considering different types of applications(consider also type of soil!)

Model	Foun- dation	Exca- vation	Tunnel	Embank- ment	Slope	Dam	Offshore	Other
Linear Elastic model	С		С					

Model	Foun- dation	Exca- vation	Tunnel	Embank- ment	Slope	Dam	Offshore	Other
Mohr- Coulomb model	С	С	С	С	С	С	С	С
Hardening Soil model	В	В	В	В	В	В	В	В
HS small model	А	А	А	А	А	А	А	А
UBC3D- PLM model*	В	В	В	В	В	В	В	В
Soft Soil Creep model	В	В	В	А	А	В	В	В
Soft Soil model	В	В	В	А	А	В	В	В
Jointed Rock model	В	В	В	В	В	В	В	В
Modified Cam- Clay model	С	С	С	С	С	С	С	С
NGI-ADP model	В	В	В	А	А	В	А	В
UDCAM- S model*							А	
Hoek- Brown model	В	В	В	В	В	В	В	В
Concrete model	А	А	А	А	А	А	А	А

A: The best standard model in PLAXIS for this application

B: Reasonable modelling

C: First order (crude) approximation

st: UDCAM-S model for cyclic analysis, in case only undrained strength is known; UBC3D-PLM model for dynamics analysis of sandy soils involving undrained cyclic loading

*: As an alternative PM4Sand is available as a user-defined soil model under [GSE]

B.3 | Aplicability material models: Based on different type of loading and material

Considering different types of loading and soils (consider also type of soil!):

Model	Primary compression	Unloading/Reloading	Shear / Deviatoric Ioading	Undrained loading	Cyclic	Compression + Shear	Extension + Shear	
Linear Elastic model	O	၁						
Mohr-Coulomb model	၁	В	၁	၁		O	၁	
Hardening Soil model	٨	В	В	В	O	A	A	
HS small model	٨	A	A	В	В	A	A	
UBC3D-PLM model*	В	В	В	В	В	В	В	
Soft Soil Creep model	A	В	В	В	O	A	В	
Soft Soil model	A	В	В	В	0	A	В	
Jointed Rock model	В	В	В			В	В	
Modified Cam-Clay model	0	S	Э	S	O	O	Э	
NGL_ADP model	В	В	В	A	O	В	В	
UDCAM-S model*	В	В	В	A	*V	A	В	
Hoek-Brown model	В	В	В			В	В	
Concrete model**	A	A	A		O	A	٨	
A : The best standard m	A : The best standard model in PLAXIS for this application	olication						
B : Reasonable modelling	βι							
C : First order (crude) approximation	pproximation							
*: UDCAM-S model for	*: UDCAM-S model for cyclic analysis, in case only undrained strength is known; UBC3D-PLM model for dynamics analysis of sandy soils involving undrained cyclic loading	ly undrained strength is kn	iown; UBC3D-PLM model	for dynamics analysis of s	sandy soils involving undr	rained cyclic loading		
*: As an alternative PM.	st : As an alternative PM4Sand is available as a user-defined soil model upon request	er-defined soil model upon	request					



Modelling of embedded structures

C.1 Applicability of modelling techniques for embedded structures

In this appendix, an overview of the applicability of the different modelling techniques for embedded structures is given. In addition to displacement differences and shear forces in axial direction, the embedded structures can undergo transverse forces due to lateral displacements. The lateral displacements can be induced by a transverse force applied at the top of the pile (*Pile head loading*) or as a consequence of the transverse distributed load induced by the lateral displacement field of the surrounding soil (*Horizontal soil displacement*).

PLAXIS 2D	Axial behaviour			Lateral b Pile head		Lateral behaviour Lateral soil movement	
Approach	Wall behaviour	Pile row	Single pile	Pile row	Single pile	Pile row	Single Pile
Volume elements	В	С	-	-	-	-	-
Plate	Α	С	-	В	-	С	-
Node to node anchor	-	С	-	-	-	-	-

PLAXIS 2D	Ах	ial behavio	our	Lateral b		Lateral behaviour Lateral soil movement	
Approach	Wall behaviour	Pile row	Single pile	Pile row	Single pile	Pile row	Single Pile
embedded beam	-	В	С	В	-	В	-

A: The best modelling choice for the correspondent application

B : Reasonable modelling

C : First order (crude) approximation

-: Not recommended



Fortran subroutines for User-defined soil models

In this appendix, a listing is given of the subroutines and functions which are provided by PLAXIS in libraries and source code in the User-defined soil model directory. These can be called by the User_Mod subroutine:

D.1 Subroutines

Subroutine	Description
MZeroR(R,K)	To initialize K terms of double array R to zero.
MZerol(I, K)	To initialize K terms of integer array I to zero.
SetRVal(R, K, V)	To initialize K terms of double array R to V.
SetIVal(I, K, IV)	To initialize K terms of integer array I to IV.
CopylVec(I1, I2, K)	To copy K values from integer array I1 to I2.
CopyRVec(R1, R2, K)	To copy K values from double array R1 to R2.
MulVec(V, F, n)	To multiply a vector V by a factor F, n values.

Subroutine	Description	
MatVec(xMat, im, Vec, n, VecR)	 Matrix (xMat)-vector(Vec) operation. First dimension of matrix is im; resulting vector is VecR. 	
AddVec(Vec1, Vec2, R1, R2, n, VecR)	To add n terms of two vectors; result in VecR • VecRi = R1 · Vec1i + R2 · Vec2i	
MatMat(xMat1, id1, xMat2, id2, nR1,nC2, nC1, xMatR, idR)	 Matrix multiplication xMatRij = xMat1_{ik} ·xMat2_{kj} id1,id2, idR: first dimension of matrices nR1 number of rows in xMat1 and resulting xMatR nC2 number of column in xMat2 and resulting xMatR nC1 number of columns in xMat2 = rows in xMat2 	
MatMatSq(n, xMat1, xMat2, xMatR)	 Matrix multiplication xMatRij = xMat1_{ik} · xMat2_{kj} Fully filled square matrices with dimensions n 	
MatInvPiv(AOrig, B, n)	Matrix inversion of square matrices AOrig and B with dimensions n. • AOrig is NOT destroyed, B contains inverse matrix of AOrig. • Row-pivoting is used.	
WriVal(io, C, V)	To write a double value V to file unit io (when io > 0). • The value is preceded by the character string C.	
WriIVI(io, C, I)	As WriVal but for integer value I.	
WriVec(io, C, V, n)	As WriVal but for n values of double array V.	
WriIVc(io, C, iV, n)	As WriVal but for n values of integer array iV	
WriMat(io, C, V, nd, nr, nc)	As WriVal but for double matrix V. nd is first dimension of V, nr and nc are the number of rows and columns to print respectively.	
PrnSig(iOpt, S, xN1, xN2, xN3, S1, S2, S3, P, Q)	To determine principal stresses and (for i0pt=1) principal directions. • i0pt = 0 to obtain principal stresses without directions. • i0pt = 1 to obtain principal stresses and direction of the stress components (XX, YY, XY, YZ, ZX). • xN1, xN2, xN3 array containing 3 values of principal stresses (S1 ≤ S2 ≤ S2 + P isotropic stress (negative for compression). • Q deviatoric stress.	

Subroutine	Description
	To calculate Cartesian stresses from principal stresses and principal directions.
CarSig(S1, S2, S3, xN1, xN2, xN3, SNew)	 S1, S2, S3 principal stresses. xN1, xN2, xN3 arrays containing principal directions (from PrnSig). SNew contains 6 stress components (XX, YY, ZZ, XY, YZ, ZX).
CrossProd(xN1, xN2, xN3)	Cross product of vectors xN1 and xN2
SetVecLen(xN, n, xL)	To multiply the n components of vector $\times N$ such that the length of $\times N$ becomes $\times L$ (for example to normalize vector $\times N$ to unit length).

D.2 | Functions

Functions	Description
Logical Function LEqual(A, B, Eps)	Returns TRUE when two values A and B are almost equal, FALSE otherwise.
	• LEqual = $ A-B < \mathrm{Eps*}(A + B + \mathrm{Eps})/2$
Logical Function IsOArr(A, n)	Returns TRUE when all n values of real (double) array A are zero, FALSE otherwise.
Logical Function Is0IArr(IArr, n)	Returns TRUE when all n values of integer array IArr are zero, FALSE otherwise.
Double Precision Function DInProd(A, B, n)	Returns the dot product of two vectors with length n

Soil Models and License levels

E.1 Overview Soil Models and Licese Levels

In the table below, it is a summary of the different Soil Models Available in PLAXIS with their required licence level. To know more about PLAXIS licencing please visit the <u>General Information Manual</u>.

Table E-1: Available soil models in PLAXIS 2D

	Licence Level		
Soil Model	PLAXIS 2D	PLAXIS 2D Advanced [ADV]	PLAXIS 2DUItimate [ULT]
Mohr-Coulomb/ Linear Elastic	~	~	~
Hoek & Brown (rock behaviour)	~	~	~
Jointed Rock (anisotropy)	~	~	~
Hardening Soil (isotropic hardening)	~	~	~
Hardening Soil (Isotropic hardening)	~	~	~

	Licence Level			
Soil Model	PLAXIS 2D	PLAXIS 2D Advanced [ADV]	PLAXIS 2DUItimate [ULT]	
The Hardening Soil with small- strain stiffness	~	~	~	
Modified Cam-Clay	~	✓	~	
NGI-ADP (anisotropic undrained shear strength)	~	~	~	
Soft soil	-	~	~	
Soft Soil Creep	-	✓	~	
Sekiguchi-Ohta	-	✓	~	
UDCAM-S	-	~	~	
Concrete	-	~	~	
UBC3D-PLM	-	-	~	
User defined Soil Mode	els (UDSM)	•		
Barcelona Basic	-	✓ + [GSE]	✓ + [GSE]	
CASM	-	✓ + [GSE]	✓ + [GSE]	
Creep-SCLAY1S	-	✓ + [GSE]	✓ + [GSE]	
Fluid model	-	✓ + [GSE]	✓ + [GSE]	
Frozen and Unfrozen Soil	-	✓ + [GSE]	✓ + [GSE]	
Generalized Hardening Soil	-	✓ + [GSE]	✓ + [GSE]	
Hoek & Brown with softening	-	✓ + [GSE]	✓ + [GSE]	
Hypoplastic model with inter- granular strain	-	✓ + [GSE]	✓ + [GSE]	
Isotropic Jointed Rock with Mohr-Coulomb Failure Criterion	-	✓ + [GSE]	✓ + [GSE]	
Masonry	-	✓ + [GSE]	✓ + [GSE]	
NorSand		✓ + [GSE]	✓ + [GSE]	
N2PC-Salt	-	✓ + [GSE]	✓ + [GSE]	
OC-Clay	-	✓ + [GSE]	✓ + [GSE]	
PM4Sand	-	-	✓ + [GSE]	
PM4Silt		-	✓ + [GSE]	

	Licence Level		
Soil Model	PLAXIS 2D	PLAXIS 2D Advanced [ADV]	PLAXIS 2DUItimate [ULT]
SHANSEP Mohr Coulomb	-	✓ + [GSE]	✓ + [GSE]
SHANSEP NGI-ADP	-	✓ + [GSE]	✓ + [GSE]
Swelling Rock Model	-	✓ + [GSE]	✓ + [GSE]
Visco-elastic perfectly plastic	-	✓ + [GSE]	✓ + [GSE]

Note: For detailed information about the User Defined Soil Models please visit <u>Bentley Communities</u>. Some user-defined soil models have been developed and are supported by the PLAXIS team itself.